DYNAMICS IN THE CENTRAL PLANT CELL METABOLISM:

METABOLOME AND FLUXOME RESPONSE OF PLANT CELLS TO LOW OXYGEN STRESS

Jerry AMPOFO-ASIAMA

Supervisors:
Prof. B. Nicolai
Prof. A. Geeraerd
Prof. E. Waelkens

Members of the Examination Committee:
Prof. K. Bernaerts
Prof. J. van Dongen (RTWH Aachen University)
Dr. M. Hertog
Prof. W. Van den Ende
Prof. J. Van Impe

Chairman:
Prof. J. Buyse

Dissertation presented in partial fulfillment of the requirements for the degree of Doctor in Bioscience Engineering

July 2014

Doctoraatsproefschrift nr. 1196 aan de faculteit Bio-ingenieurswetenschappen van de KU Leuven

Uitgegeven in eigen beheer, W. de Croylaan 42, B-3001 Heverlee, Belgium

ISBN 978-90-8826-369-9
D/2014/11.109/37

Acknowledgment

I would like to say a special thank you to Prof. Nicolai, my promoter, for his vision and encouragement throughout the programme. My sincere appreciation goes to Dr. Hertog, Prof. Geeraerd and Prof. Waelkens for their advice, inspiration and daily support throughout my doctoral studies. I am also thankful to the members of my examination committee: Prof. Van Impe, Prof. Bernaerts, Prof. van Dongen, Prof. Van den Ende and Prof. Buyse for the time and effort they invested in reading the manuscript and coming up with useful suggestions to improve the content of the thesis.

I will like to thank all the staff of MeBioS and VCBT who helped me in one way or another to bring my PhD to completion. Especially, I would like to thank Elfie Dekempeneer for helping with the GC-MS work and Jeroen Tirry for his IT support.

I will also like to say a special thank you to Victor Baiye, Sunny-George, Darwish Hatoum, Elias Bekele, Dennis Cantre as well as all the members of the System Biology group and the GC-MS user group of MeBioS.

The Research Fund of the KU Leuven (DBOF/08/033, Jerry Ampofo-Asiama) is greatly acknowledged for financially supporting this research.

I will also like to thank the Ghanaian community in Leuven especially Pastor Seth and family, Lydia Owusu, Nana Ansu and family, Nana Akowuah and family, and the members of the Christ Centered Churh for the time spent together.

Also to my colleague Ghanaian students in Leuven: Francis Andoh, Esther Danso, Samuel Iddi, Jude Acolatse, Eden Kove, Dina Danso, Felix Boamah, Gladys Kontoh, Bobby Caiquo, Michael Amoafo and Abigail Forson, I say thank you for the time spent together.

I will like to express my special thanks to my Dad and Mum, as well as my sisters: Doreen, Wendy, Sharon and Mavis, and brother William for their prayers and support.

Finally, I would like to thank my wife, Adelaide, and daughter, Afua, for their support and patience during this long period.

God bless you all.

Jerry Ampofo-Asiama

July 2014

Abstract

As part of their development, plants have acquired adaptive mechanisms to cope with different stress situations they encounter in their environment. These adaptive mechanisms include the ability to alter their metabolism when faced with extreme environmental conditions such as low oxygen. In higher plants, oxygen (O_2) availability is important for energy production through respiratory metabolism. Under conditions where O_2 becomes limiting, respiratory metabolism can be impeded leading to impaired growth. Low O_2 conditions in plants can be created by environmental and man-made factors such as soil flooding and control atmosphere (CA) storage, respectively. In addition, anatomical arrangements can create uneven gas distribution leading to low O_2 conditions in cells located in the inner tissues of plants. The effect of low O_2 stress on plants include stunted growth of field crops and development of storage disorders in fruits stored under CA. Taking into account that plants serve as an important source of food, it is important to study and understand how plant metabolism cope with low O_2 stress.

The main objective of this thesis is to *study the effect of low O_2 on plants through metabolome and fluxome analysis*. Metabolome analysis involves the comprehensive quantitative analysis of all low molecular weight metabolites in an organism while fluxome analysis measures the rates at which metabolites are distributed through a reaction network. Together, these two techniques can be used to study and understand the response of plants to low O_2 stress.

Analysis of flux, especially using isotope labelling techniques, require feeding an organism with labelled substrate and measuring the incorporation of label in different metabolites. In whole plants, performing isotopic feeding experiments is limited by the long incubation times needed for metabolites to incorporate quantifiable amounts of label in their storage polymers like proteins and carbohydrates. To overcome this difficulty heterotrophic cell suspensions were used as a model system as they can be easily manipulated to grow on a defined medium, allowing a much faster incorporation of labelled substrate into their metabolome.

In the first part of this thesis, techniques were developed to establish cell suspension from tomato leaves. Subsequently, a gas chromatography-mass spectrometry (GC-MS) based protocol for separating, identifying and quantifying intracellular polar metabolites and their label accumulation during ^{13}C-label feeding experiments was developed. Finally, ^{13}C-label feeding experiments were carried out to determine the effect of low O_2 stress on the polar metabolic profile of tomato cell suspension and to analyse the changes in fluxes of the central carbon metabolism under both metabolic dynamic and steady-state conditions.

A cell suspension was established from dark grown friable callus of tomato leaves (*Lycopersicum esculentum* L. var cerasiforme). The growth of the cell suspension involved a lag period, a linear phase of growth and a stationary phase. Polar metabolites present in the cells were separated and detected on the GC-MS after methanol extraction and derivatisation using N,O-bis-(trimethylsilyl)trifluoroacetamide. A total of 70 polar metabolites could be identified and quantified with a GC-MS temperature programme of approximately 40 min duration. The polar metabolites present in the cells belonged to the functional groups of amino acids, organic acids, sugars and sugar alcohols. After performing feeding experiments, ^{13}C-label accumulation could be detected in 47 of the 70 metabolites measured.

The metabolic response of plant cells following the induction of low O_2 stress was studied by analysing the changes in polar metabolite after incubating cell suspension at different O_2 levels in a bioreactor. The cells were incubated at O_2 levels of 21, 1 and 0 kPa and cell samples taken every hour for a period of 12 h with a final sampling after 24 h of incubation. ^{13}C-glucose was added to the medium of the cells four hours after the start of the incubation. The changes in metabolite levels as well as the incorporation of ^{13}C-label was measured with GC-MS. Low O_2 altered the polar metabolic profile of the cells. There was a general reduction in the levels of most amino acids, organic acids and sugars and an increase in the intermediates of glycolysis, lactate and some sugar alcohols. The ^{13}C-label data showed reduced label accumulation in almost all metabolites except lactate and some sugar alcohols under low O_2 stress. The results indicated that low O_2 in plant cells activated fermentative metabolism and sugar alcohol synthesis while inhibiting the activity of the TCA cycle. Also, the levels of metabolites whose precursors are derived from the intermediates of the central carbon metabolism such as amino acids were reduced upon the induction of low O_2 stress.

To obtain a quantitative understanding of the response of the fluxome following the induction of low O_2 stress in plant cells, the changing metabolite levels and ^{13}C-label accumulation were

used to construct a dynamic model of the central carbon metabolism. A compartmentalised metabolic network model containing glycolysis in the cytosol and plastid, the TCA cycle in the mitochondria and the syntheses of alanine, aspartate, lactate, glutamate, serine, sucrose and valine was developed. The model contained differential equations describing both Michaelis-Menten and first-order kinetics and the model parameters were estimated using a non-linear least square optimisation approach. The dynamic modelling showed that incubating cell suspension under low O_2 lead to a significant reduction in glucose uptake rate. Low O_2 stress also caused a reduction in the activity of several enzymes involved in the TCA cycle resulting in the accumulation of intermediates of the glycolysis. An increase flux of lactate and ethanol synthesis was observed showing the enhanced role of fermentative metabolism in ensuring energy production under the low O_2 stress. Analysis of energy production and utilisation showed similar amounts of ATP production at the different O_2 levels even though the ATP produced under the low O_2 conditions came at a cost of high substrate usage. Metabolic control analysis of glycolysis, fermentation and the TCA cycle showed that the uptake of external glucose controls most of the fluxes in the central carbon metabolism while the transport of pyruvate into the mitochondria from the cytosol controls the activity of the TCA cycle. Also, enzymes which compete for a common substrate exerted negative control on each other.

Steady-state metabolic flux analysis was carried out using the ^{13}C-label incorporated into free intracellular metabolites instead of the conventional approach of utilising the label being incorporated in proteinogenic amino acids. This was done to avoid the long incubation times needed to achieve metabolic and isotopic steady-state in proteinogenic amino acids. For steady-state flux analyses, cell suspensions were incubated in a bioreactor at O_2 levels of 21, 8, 5 and 0 kPa until metabolic and isotopic steady-state was reached (24 h after the start of the experiment). Free intracellular metabolites were extracted with methanol, derivatised with N-(tert-butyldimethylsilyl)-trifluoroacetamide and analysed using GC-MS. ^{13}C-label present in metabolites of the central carbon metabolism, amino acids and sugars were determined for steady-state fluxes analyses. Fluxes were estimated using the 13CFLUX2 software. The steady-state response to low O_2 stress was similar to the observations made under dynamic conditions with a decrease in substrate uptake, an increase increased fermentative metabolism and a reduced TCA cycle activity and amino acid synthesis. Based on the similarity in fluxes through the central carbon metabolism, the dynamic and steady-state modelling approaches were compared. Dynamic modelling offers several advantages including providing more

detailed information on the structure and regulation of metabolic networks under different stress conditions and providing a time dependent response of an organism to stress. Steady-state flux analysis is, however, useful in obtaining a quick overview of the changes in metabolism upon stress induction especially in systems where metabolic and isotopic steady-state can be ascertained.

Samenvattting

Planten hebben, als onderdeel van hun ontwikkeling, aanpassingsmechanismen verworven om het hoofd te bieden aan voorkomende stress-situaties. Eén van deze mechanismen is het vermogen hun metabolisme aan te passen aan extreme condities zoals een lage zuurstofspanning. De beschikbaarheid van zuurstof (O_2) is voor hogere planten van belang voor hun energievoorziening via het ademhalingsmetabolisme. Wanneer O_2 beperkend wordt, kan het hierdoor onderdrukte ademhalingsmetabolisme leiden tot een verminderde groei. Lage O_2-condities kunnen optreden als gevolg van zowel omgevingsinvloeden (bv. overstroming) als ook menselijk ingrijpen (bv. tijdens bewaring van vruchten en groenten onder gecontroleerde atmosfeer (CA)). Verder kan de anatomische structuur van een plant aanleiding geven tot een ongelijke gasverdeling resulterend in lage zuurstofcondities in het binnenste weefsel van een plant. Lagezuurstofstress kan onder meer leiden tot een geremde groei van veldgewassen en de ontwikkeling van bewaargebreken tijdens CA-bewaring van fruit. Gezien het belang van plantaardige voeding, is het belangrijk inzicht te verkrijgen in hoe planten omgaan met lage zuurstof stress.

De hoofddoelstelling van deze thesis is het beter begrijpen *van het effect van lage O_2 op planten via analyses van het metaboloom en het fluxoom*. De metaboloomanalyse betreft een alomvattende analyse van alle metabolieten in een organisme met een laag molecuulgewicht terwijl de fluxoomanalyse inzicht geeft in de snelheid van omzettingen doorheen een reactienetwerk. Deze technieken kunnen samen gebruikt worden om de respons van planten op lagezuurstofstress te bestuderen en beter te begrijpen.

Fluxanalyse, gebruik makend van isotopen, vereist het voeden van een organisme met gelabelde substraten om vervolgens de inbouw van dit label in de verschillende metabolieten op te meten. In intacte planten is de toepassing van voedingsexperimenten beperkt door de lange incubatietijden die nodig zijn om meetbare hoeveelheden label in te bouwen in biopolymeren zoals eiwitten en koolhydraten. Om dit probleem te omzeilen werd gebruik

gemaakt van een modelsysteem van heterotrofe celsuspensieculturen die zich makkelijk laten vermeerderen en die veel sneller gelabeled substraat inbouwen in hun metaboloom.

In het eerste deel van deze thesis werden technieken ontwikkeld voor het maken van een celsuspensiecultuur vertrekkende van tomatenbladeren. Vervolgens is er een protocol op punt gesteld voor het scheiden, identificeren en kwantificeren van intracellulaire polaire metabolieten met behulp van gaschromatografie – massaspectrometrie en de accumulatie van het label tijdens ^{13}C-labelvoedingsexperimenten. Uiteindelijk werden er ^{13}C-label-voedingsexperimenten uitgevoerd om het effect van lage O_2 stress op het polaire metabolietprofiel en de veranderingen in de fluxen doorheen het centraal koolstofmetabolisme van de tomatencellen te kwantificeren. Dit werd gedaan onder zowel dynamische condities als tijdens stabiele evenwichtscondities.

De celsuspensiecultuur werd verkregen uit een in het donker gegenereerd los callus van tomatenbladeren (*Lycopersicum esculentum* L. var cerasiforme). De groeicurve van de celsuspensiecultuur omvat een incubatieperiode, een lineaire groeifase en een stationaire fase. De polaire celmetabolieten werden gescheiden en gedetecteerd op de GC-MS na een methanolextractie en derivatisatie met behulp van N,O-bis-(trimethylsilyl)trifluoroacetamide. In totaal werden 70 polaire metabolieten geïdentificeerd en gekwantificeerd tijdens een 40 minuten durend temperatuursprogramma. De polaire celmetabolieten omvatte aminozuren, organische zuren, suikers en suikeralcoholen. Na afloop van de voedingsexperimenten werd in 47 van de 70 metabolieten ^{13}C-label aangetroffen.

De metabole respons van plantencellen op lagezuurstofstress werd bestudeerd door de veranderingen in de polaire metabolieten te analyseren tijdens blootstelling in een bioreactor aan verschillende O_2-niveaus. De cellen werden geïncubeerd bij 21, 1 of 0 kPa O_2. Gedurende 12 uur werden er elk uur stalen genomen met een laatste staalname 24 uur na aanvang van de incubatie. Vier uur na de start van de incubatie werd er ^{13}C-gelabeld glucose toegevoegd aan het groeimedium. De veranderingen in metabolietniveaus en de inbouw van ^{13}C-label werd opgemeten met de GC-MS. Lagezuurstofstress wijzigde de samenstelling van het polair metabolietprofiel van de cellen. Er was een algemene reductie van de concentraties aan aminozuren, organische zuren en suikers en een toename van de intermediairen van de glycolyse, lactaat en een aantal suikeralcoholen. Veder veroorzaakt lagezuurstofstress voor nagenoeg alle metabolieten een reductie van de hoeveelheid ingebouwd label, uitgezonderd voor lactaat en sommige suikeralcoholen. Deze resultaten duiden erop dat lagezuurstofstress

in plantencellen leidt tot een activatie van het fermentatiemetabolisme en de synthese van suikeralcoholen terwijl de citroenzuurcyclus gereduceerd wordt. Tevens werden de concentraties van die metabolieten die zijn afgeleid van de intermediairen van het centraal koolstofmetabolisme, zoals aminozuren, gereduceerd onder lage O_2 stress.

Om kwantitatief inzicht te verkrijgen in de respons van het fluxoom op de blootstelling aan lagezuurstofstress in plantencellen werd er aan de hand van waargenomen veranderingen in metabolietniveaus en de inbouw van ^{13}C-label een wiskundig dynamisch model opgesteld van het centraal koolstofmetabolisme. Er werd een gecompartimentaliseerd metabolisch netwerkmodel opgesteld van de glycolyse (in het cytosol en de plastiden), de citroenzuurcyclus (in de mitochondriën) en de synthese van alanine, aspartaat, lactaat, glutamaat, serine, sucrose en valine. Het model omvat differentiaalvergelijkingen voor zowel Michaelis-Menten- als eerste-ordekinetiek. De modelparameters werden geschat met de niet-lineaire kleinstekwadratenmethode. Het dynamisch model toonde aan dat de incubatie onder lage O_2 leidde tot een significante reductie in de opnamesnelheid van glucose. Lagezuurstofstress veroorzaakte tevens een reductie in de activiteit van verschillende enzymen van de citroenzuurcyclus resulterend in een accumulatie van de intermediairen van de glycolyse. Een verhoogde flux van de lactaat- en ethanolsynthese weerspiegelde het toegenomen belang van het fermentatiemetabolisme voor de realisatie van een voldoende energieproductie tijdens lagezuurstofstress. Een analyse van de netto energieproductie toonde dat de hoeveelheid ATP geproduceerd bij de verschillende O_2 behandelingen gelijkaardig is, alhoewel de ATP-productie bij de lage O_2-conditie ten koste ging van een veel hoger substraatverbruik. Met behulp van een metabolecontrole-analyse van de glycolyse, de fermentatie en de citroenzuurcyclus werd duidelijk dat de opnameflux van extern glucose bepalend is voor de meeste fluxen van het centraal koolstofmetabolisme terwijl de opnameflux van pyruvaat naar de mitochondriën bepalend is voor de activiteit van de citroenzuurcyclus. Verder oefenen enzymen die concurreren om een gemeenschappelijk substraat een negatieve controle uit op elkaar.

Onder aanname van een stabiel evenwicht werd een fluxanalyse uitgevoerd gebruik makend van de ^{13}C-label die was ingebouwd in de vrije intracellulair metabolieten. Dit in plaats van een conventionele aanpak waarbij wordt vertrokken van de label ingebouwd in de eiwitgebonden aminozuren. Op deze manier konden lange incubatietijden nodig voor het bereiken van een stabiele evenwichtssituatie op het niveau van de concentraties en de labelinbouw in biopolymeren worden vermeden. Voor deze fluxanalyse werd de

celsuspensiecultuur geïncubeerd in een bioreactor bij O_2-niveaus van 21, 8, 5 of 0 kPa totdat er een stabiele evenwichtssituatie op het niveau van de concentraties en de labelinbouw werd bereikt (24 h na de start van het experiment). De celmetabolieten werden geëxtraheerd met methanol, gederivatiseerd met behulp van N-(tert-butyldimethylsilyl)-trifluoroacetamide en geanalyseerd met de GC-MS. De hoeveelheid ^{13}C-label ingebouwd in de metabolieten van het centraal koolstofmetabolisme, aminozuren en suikers werd bepaald. De fluxen werden geschat met behulp van de 13CFLUX2 software. De evenwichtsrespons op lagezuurstofstress was gelijkaardig aan hetgeen wat was waargenomen in het dynamische experiment: een afname in de substraat opname, een toename van het fermentatiemetabolisme en een gereduceerde citroenzuurcyclus en aminozuursynthese. Tenslotte werden op grond van de berekende fluxen de dynamische en de evenwichtsgebaseerde modelbenaderingen met elkaar vergeleken. De dynamische modelaanpak biedt een aantal voordelen, waaronder de meer gedetailleerde informatie die wordt verkregen ten aanzien van de structuur en de regulatie van het metabool netwerk onder de verschillende stresscondities en de tijdsafhankelijkheid van de stressrespons. De evenwichtsaanpak is echter geschikt voor het snel verkrijgen van een overzicht van de belangrijkste veranderingen in het metabolisme in response op stress in die systemen waar een stabiel evenwicht kan worden verondersteld op het niveau van metaboliet concentraties en de hoeveelheid ingebouwde label.

Abbreviations and Symbols

Abbreviations

ACoA	Acetyl coenzyme A
ADP-GLC	Adenosine diphosphate glucose
ATP	Adenosine triphosphate
BSTFA	N,O-Bis(trimethylsilyl)trifluoroacetamide
CA	Controlled Atmosphere
CCC	Concentration control coefficient
CE-MS	Capillary electrophoresis-mass spectrometry
CI	Confidence interval
EI	Electron ionisation
ETC	Electron transport chain
FBA	Flux balance analysis
$FADH_2$	Flavin adenine dinucleotide
FCC	Flux control coefficient
GC	Gas chromatography
GC-MS	Gas chromatography-mass spectrometry
INV	Invertase
LC-MS	Liquid chromatography-mass spectrometry
LV	Latent variables
MCA	Metabolic control analysis
METAFoR	Metabolic flux ratio
MFA	Metabolic flux analysis
MID	Mass isotopomer distribution
MS	Mass spectrometer
MSTFA	N-methyl-N-(trimethylsilyl) trifluoroacetamide
m/z	Mass-to-charge ratio

NAD^+/NADH	Nicotinamide adenine dinucleotide (reduced)
$NADP^+$/NADPH	Nicotinamide adenine dinucleotide phosphate (reduced)
NMR	Nuclear magnetic resonance
OPLS	Orthogonal partial least square
PAA	Proteinogenic amino acids
PC	Principal Component
PCA	Principal Component analysis
PLS	Partial least square
PLS-DA	Partial least square discriminate analysis
PPP	Pentose phosphate pathway
RNA	Ribonucleic acid
RTL	Retention time locked
sd	Standard deviation
sem	Standard error of the mean
SFL	Sum fractional labelling
SPP	Sucrose-phosphate phosphatase
SPS	Sucrose-phosphate synthase
SuSy	Sucrose synthase
TBDMS	N-(tert-butyldimethylsilyl)-trifluoroacetamide
TCA	Tricarboxylic acid
TIC	Total ion chromatogram
UDP-GLC	Uridine diphosphate glucose
VIP	Variable importance in projection

Symbols

K_M	Michaelis-Menten constant
V_{max}	Maximum reaction rate
v	Flux
t	Time
[X]	Concentration of metabolite X

Table of Content

Chapter 1

General Introduction

1.1 Low oxygen stress in plants

Oxygen (O_2) is involved in many biochemical reactions in plants (Babcock, 1999). A high percentage of the total O_2 level in plants is utilised during respiration for energy production (Babcock, 1999), but also less-O_2-demanding reactions such as double-bond introduction in fatty acyl chains (Rebeille et al., 1980) occur in the plant. Nevertheless, even though higher plants have the ability to produce O_2 through photosynthesis, they can experience low O_2 conditions both in the field and during the postharvest phase. In the field, low O_2 may occur due to flooding caused by poor drainage after rainfall (Drew, 1997). During flooding, water fills the air space in the soil reducing the exchange of O_2, carbon dioxide (CO_2) and other gases between the soil and the atmosphere (Drew, 1997). Due to slow diffusion rate of O_2 in air compared to water, the amount of O_2 available to the roots for metabolism can decrease significantly resulting in the induction of low O_2 stress (Bailey-Serres et al., 2012).

In the postharvest phase, fruit may be stored under controlled atmosphere (CA) conditions to prolong their shelf-life by reducing their respiration rate (Kader and Ben-Yehoshua, 2000). CA storage involves the reduction and increase in O_2 and CO_2 levels, respectively, combined with reduced temperatures. The temperature employed in CA storage is usually kept low to reduce the rate of metabolism while avoiding chilling and freeze injury. The CO_2 levels used in CA storage are increased to help maintain fruit colour, while O_2 levels are lowered with the aim to reduce respiration rate and avoid the induction of fermentative metabolism (Franck et al., 2007). For instance, pears are stored in an environment of 2.5-3 % O_2 and 0.7-1 % CO_2 at temperatures between -0.5-1 °C (VCBT, 2012). Deviation from this optimal gas conditions may induce low O_2 stress in the fruit (Franck et al., 2007). Flooding and CA storage, however,

are not the only causes of low O_2 in plants. Even under normal O_2 levels in the surrounding atmosphere, cells which are located in the inner tissues of plants can experience low O_2 due to the consumption of O_2 through respiration coupled with impeded gas transport towards the centre of the fruit (Geigenberger et al., 2000; Ho et al., 2010, 2008).

Low O_2 has been observed to have a detrimental effect on plants in the field and plants stored under CA. Wilting and leaf damage (Simova-Stoilova et al., 2012), reduction in photosynthetic ability (Mcfarlane et al., 2003) and destruction of agricultural crops have been observed in plants growing in the field under flooded conditions. Under CA storage, low O_2 conditions have been shown to induce browning and core breakdown in some fruits (Franck et al., 2007), leading to impaired quality. Obviously, low O_2 stress can cause huge reductions in the yield of agricultural crops both in the field and during storage.

1.2 Understanding plant response to low oxygen stress

The detrimental effect low O_2 stress can have on plants means that the response and adaptive mechanism plants employ when faced with low O_2 conditions needs to be investigated. The biochemical changes that occur in plants due to the effect of low O_2 can be studied at different cellular organisational levels such as the transcriptome and metabolome (Figure 1.1). This biochemical response which might start from the expression of new genes, through to the transcription of ribonucleic acid (RNA) and the translation of proteins is reflected finally in changes in the cell metabolism. It is therefore important to study and understand the response of plant cell metabolism to low O_2 stress.

Metabolism, which involves processes such as substrate uptake, transport and chemical transformations are enzyme-catalysed reactions which enable cells to survive, grow and multiply. Though the metabolism of plant cells is very complex, due to the presence of different compartments (Lunn, 2007; Plaxton, 1996) and their ability to synthesise a range of secondary metabolites (Nascimento and Fett-Neto, 2010), there is a need to study the changes in the metabolism of plants under stress conditions, such as low O_2. This is due to the fact that the survival, growth and phenotype of plants depend on the output of plant metabolism. An important aspect is to understand the role of the central carbon metabolism in the response of plant cells to low O_2 stress. This is because the central carbon metabolism is fundamental to the survival of all cells through its role in synthesising energy carriers and providing precursors to be used for other biosynthetic reactions (Rontein et al., 2002). The effect of

metabolism involves changes in the concentration of metabolites and fluxes through plant metabolic networks (Wiechert et al., 2007). To be able to study the metabolism of plant under low O_2 stress, there is the need to measure both the changes in metabolites and metabolite fluxes using metabolomics and fluxomics.

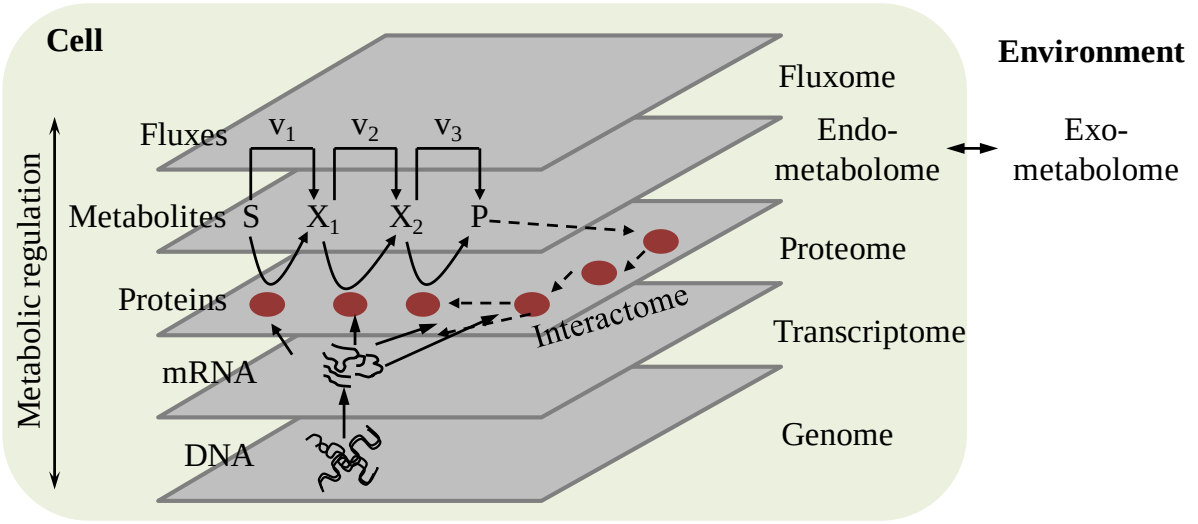

Figure 1.1: The different biochemical composition of cells at which the effect of low O_2 on plants can be studied (Nielsen and Oliver, 2005).

1.2.1 Metabolomics

Metabolomics is the comprehensive study of all low molecular weight compounds (less than 1 kDa) present in an organism under a given physiological and environmental condition (Fiehn, 2002; Hall et al., 2002). The application of metabolomics in order to study the response of plants to low O_2 stress can be carried out using three main procedures: metabolic profiling, metabolic fingerprinting and target metabolite analysis (Fiehn, 2002; Hall et al., 2002).

Metabolic profiling involves studying the changes in a group of metabolites such as sugars, organic acids and amino acids or those associated with a metabolic network (Fiehn, 2002; Hall et al., 2002; Kopka et al., 2004). Detecting, identifying and quantifying the changes in metabolites is an important component of metabolic profiling. In metabolic profiling, either the absolute concentration of metabolites or their relative changes can be measured. Metabolic fingerprinting involves studying the changes in metabolite patterns under a given physiological and environmental condition without necessarily identifying those metabolites (Kopka et al., 2004). Target metabolite analysis is carried out to determine the response of a few metabolites to a stress condition and usually involves the absolute quantification of

metabolites (Fiehn, 2002). Target metabolite analysis is the oldest and most used of the metabolomics approaches and it has been applied to study the response of some specific metabolites like lactate and ethanol to different low O_2 stress situations (Andrews et al., 1994; Thomson and Greenway, 1991).

Metabolic profiling provides the platform to be able to combine large scale metabolite identification with quantification needed for metabolic flux analysis (MFA). Among the available instruments for carrying out metabolic profiling is gas chromatography-mass spectrometry (GC-MS). GC-MS is currently the most employed instrument in the metabolic profiling of plants (Lisec et al., 2006). This is due to wide range of low weight compounds which can be measured with GC-MS. These low molecular weight compounds are mostly primary metabolites which are directly involved in the growth and development of plants. GC-MS can also be used in quantifying the ^{13}C-label accumulated in metabolites after performing ^{13}C-label feeding experiments (Wiechert et al., 2007), making it an essential instrument for both metabolic profiling and flux analysis.

1.2.2 Fluxomics

Fluxomics involves the measurement of metabolic fluxes which are the end result of the interplay of gene expression, changes in proteins and metabolites (Wiechert et al., 2007; Wittmann, 2007). Fluxomics measures how materials (metabolites) flow within a metabolic network, and it illustrates the contribution of individual reactions to the response of a metabolic network to a perturbation (Wiechert et al., 2007; Wittmann, 2007). Intracellular metabolic fluxes cannot be determined directly, and their analysis requires solving mass balance equations containing measured metabolite concentrations, substrate uptake and product secretion rate(s), and changes in biomass (Stephanopoulos, 1999). Metabolic fluxes can be determined under both steady-state or dynamic conditions (Morgan and Rhodes, 2002; Rios-Estepa and Lange, 2007).

Steady-state MFA is based on the assumption that the changes in intracellular metabolite levels with time is constant while under dynamic condition conditions the change in flux is estimated at several time points (Morgan and Rhodes, 2002; Rios-Estepa and Lange, 2007). Both steady-state and dynamic fluxes can be estimated by feeding plants with a labelled substrate (e.g., either radio or stable isotope) and following the incorporation of label within the different metabolites. Currently techniques based on feeding with ^{13}C-label are the most

popular approach in the estimation of metabolic fluxes (Kruger et al., 2012; Rios-Estepa and Lange, 2007).

1.3 Objectives of the thesis

Taking into account the detrimental effects of low O_2, it is important to study the metabolic response of plants to low O_2 stress to gain a better understanding of the adaptive strategies plants employ when face with low O_2 conditions. The main objective of this thesis is to *study the effect of low O_2 on plants through metabolome and fluxome analysis* with a focus on changes in the central carbon metabolism. The emphasis of this thesis is to understand the response of the metabolome and fluxome to low O_2 conditions as experienced by fruit stored under CA conditions. Studying the response to low O_2 on whole organs would require dealing with complexities such as tissue differentiation and O_2 gradients inside fruits. Therefore a simpler experimental system consisting of a tomato cell suspension was used for this work. Tomato cell suspension was chosen due to the fact tomato is cultivated and consumed worldwide making it an economically important model plant to study postharvest low O_2 stress response in plants.

To meet the main objective of this thesis, the following sub-objectives were defined:

- To characterise the changes in the metabolome of tomato cell suspension after the induction of low O_2 stress using GC-MS metabolic profiling,
- To construct a dynamic model of the central carbon metabolism and investigate how the control of the different pathways of the central carbon metabolism is affected by low O_2 stress,
- To estimate the effect of low O_2 stress on the central carbon metabolic fluxes of tomato cell suspension under steady-state conditions using ^{13}C-labelling.

To able to achieve the above sub-objectives, protocols were developed to establish and maintain cell suspension from tomato leaves and to identify and quantify intracellular metabolites and their ^{13}C-label accumulation after the induction of low O_2 stress using GC-MS.

1.4 Outline of the thesis

The outline of the thesis is shown in Figure 1.2. Chapter 2 will provide an overview of plant energy metabolism (respiration and fermentation) as well as the metabolism of sucrose, sugar alcohols and starch, compounds which play important roles in the response of plant to low O_2 stress. The principles of GC-MS based metabolic profiling will be discussed and its application to study the low O_2 stress response of plants will be highlighted. Other techniques available for plant metabolic profiling will also be presented.The analysis of flux under both steady-state and dynamic conditions as well as the principles of ^{13}C-label feeding experiments will be discussed.

Chapter 3 will provide a description of the procedure used to establish and maintain suspension cells from tomato leaves. In addition, a GC-MS based protocol used to separate, identify and quantify intracellular polar metabolites present in tomato cell suspension and their ^{13}C-label accumulation will be explained.

Chapter 4 will discuss the effect of low O_2 on the polar metabolite composition of tomato cell suspension after performing feeding experiments with a mixture of unlabelled and ^{13}C-labelled glucose at different O_2 levels.

The data obtained in Chapter 4 will be combined with mathematical modelling to determine the effect of low O_2 stress on plant cells. The principle of dynamic labelling will be applied to model the central carbon metabolism of plant cells and this will be described for the first time in Chapter 5. The estimated kinetic parameters and fluxes will be discussed and the principle of metabolic control analysis will be used to analyse how the control of fluxes in the cell suspension is affected by low O_2.

Due to the fact that the response of plants to low O_2 stress involves dynamic changes in metabolism before steady-state is attained, the result of the dynamic flux analysis will be presented first (Chapter 5). The result of the dynamic response will be used to assess the attainment of the subsequent steady-state metabolism in the cell suspension.

Chapter 6 will, therefore, describe the resulting steady-state fluxes of the central carbon metabolism in tomato suspension cells, differentiated according to different O_2 levels. Also a comparison will be made between the steady-state and dynamic approach of estimating metabolic fluxes in plants.

The last chapter of this thesis (Chapter 7) will provide some general conclusions and possible ideas for further research on this topic.

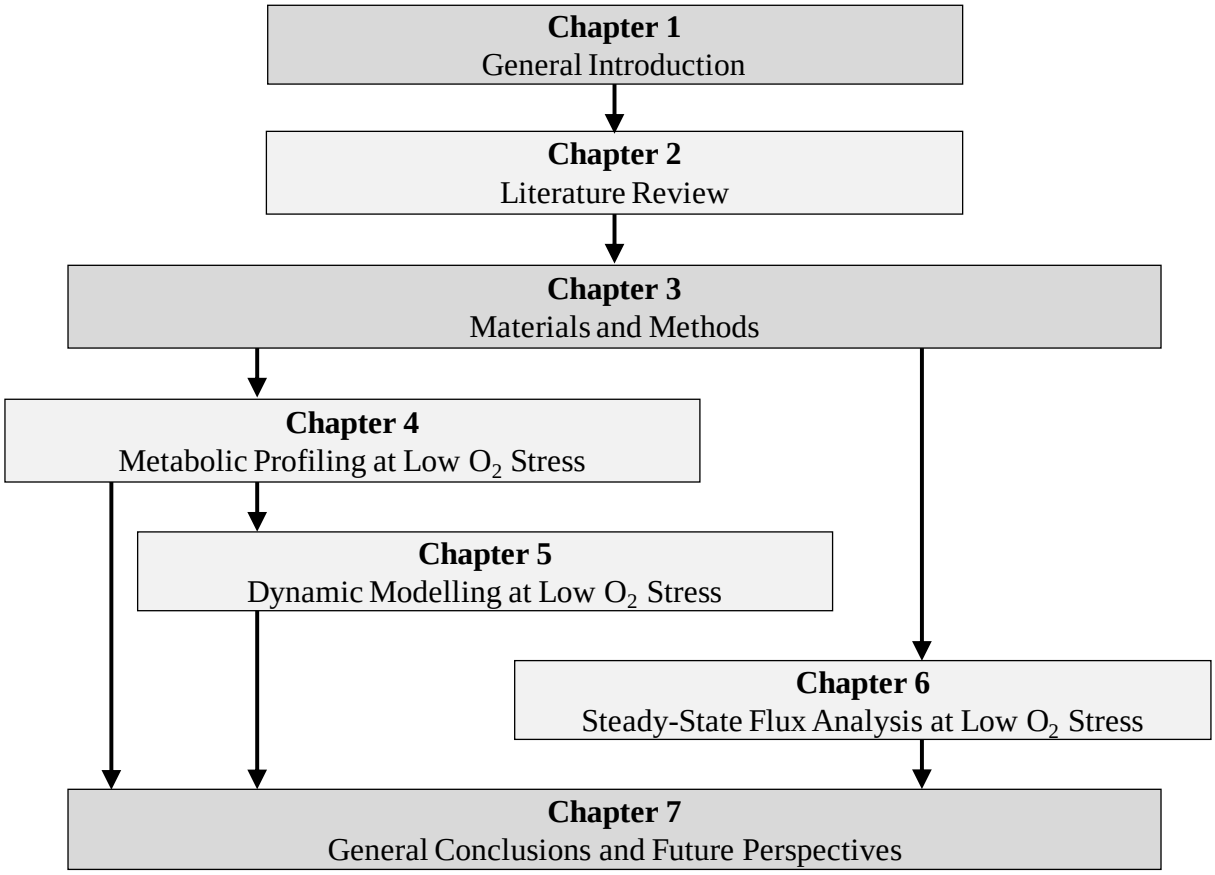

Figure 1.2: Outline of the PhD dissertation.

Chapter 2

Literature Review

2.1 Introduction

A thorough knowledge of the response of plants to low O_2 stress is crucial in understanding the adaptive mechanisms plants employ when faced with low O_2 conditions. Metabolic profiling and ^{13}C-MFA are two techniques that can be used to unravel the metabolic changes involved in the response of plants to low O_2 stress. In this chapter, an overview of plant energy metabolism at different O_2 levels will be given. The metabolism of sucrose, sugar alcohols and starch, metabolites which play important roles in the low O_2 response of plants will be discussed. A comprehensive review of the literature on plant metabolic profiling using GC-MS will be given. Also, other techniques that can be used for metabolic profiling in plants will be highlighted. Finally, the analysis of metabolic flux in plants will be discussed.

2.2 Plant metabolism at different oxygen conditions

2.2.1 The central carbon metabolism

The metabolic pathway used for energy production is dependent on the O_2 status of plants. When the amount of O_2 available to a plant is equal to the normal atmospheric O_2 level, the plant is said to be growing under normoxic conditions (Drew, 1997). Under normoxia, plants cells usually carry out respiratory metabolism. Under conditions when O_2 levels are limited (hypoxia), or O_2 is completely absent in the environment (anoxia), plants usually carry out fermentative metabolism (Drew, 1997).

Respiratory metabolism consists of the pathways of glycolysis, the pentose phosphate pathway (PPP), the tricarboxylic acid (TCA) cycle and the mitochondrial electron transport chain (ETC). Together, these pathways are referred to as the central carbon metabolism. The central carbon metabolism enables cells to survive and grow by providing energy and metabolic intermediates for use by other metabolic pathways. The activity of the central carbon metabolism starts with the breakdown of sugar to pyruvate through glycolysis. Among the sources of sugar which can be utilised for glycolysis in plants are glucose, fructose and sucrose. The breakdown of sugar involves the production and hydrolysis of adenosine triphosphate (ATP) as well as the reduction of nicotinamide adenine dinucleotide (NAD^+) (Figure 2.1). Glycolysis can be broken-down into two main phases. The first, which require ATP hydrolysis, involves the conversion of sugar to fructose-1,6-biphosphate which is then split into triose-phosphate (glyceraldehyde-3-phosphate and dihydroxyacetone phosphate). The second phase involves ATP- and NADH-producing reactions which convert triose-phosphate to pyruvate (Figure 2.1). The net amount of ATP produced from glycolysis is 2, as there are two ATP-hydrolytic reactions and two-parallel ATP-producing reactions. In plant cells, glycolysis has been observed to occur in both the cytosol and with metabolite exchange possible between the two compartments. (Plaxton, 1996).

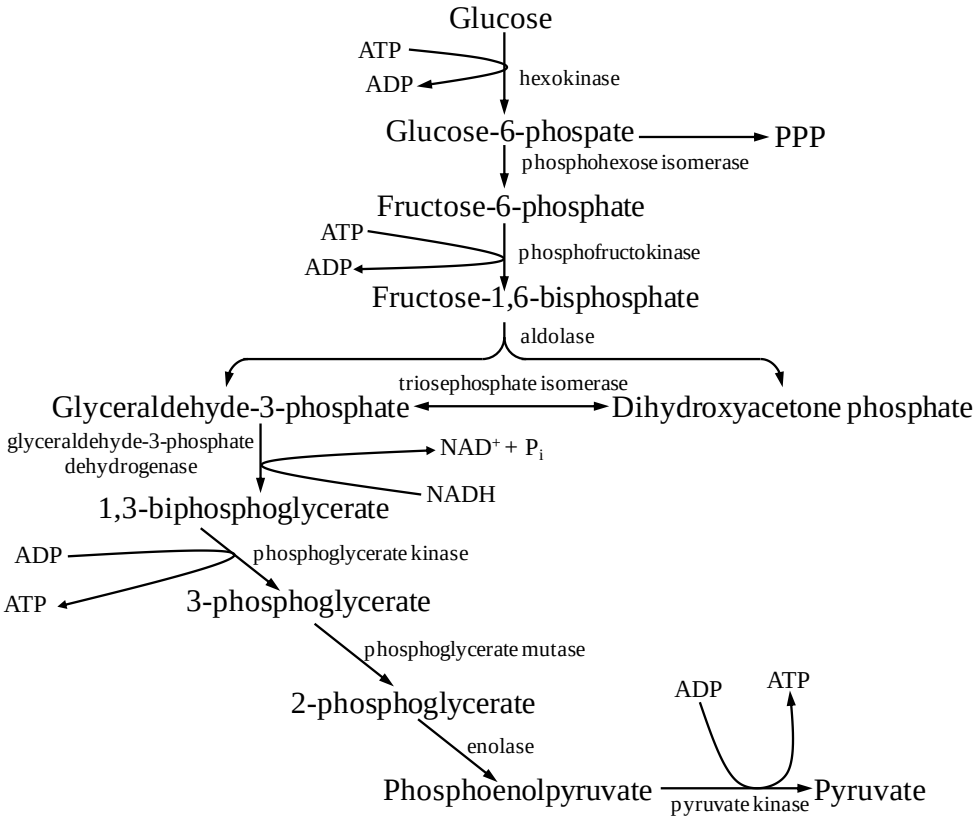

Figure 2.1: A schematic overview of the glycolysis.

The PPP provides another route for the oxidation of sugars in plant cells. The reactions of the PPP have been shown to occur in the cytosol and plastid, even though the pathways present in the plastid dominates that of the cytosol (Ampofo-Asiama et al., 2014). The PPP can be split into two main phases; an oxidative and reductive phase. In the oxidative phase, glucose-6-phosphate is converted to ribulose-5-phosphate with the release of CO_2 and the production of reduced nicotinamide adenine dinucleotide phosphate (NADPH). During the reductive phase, ribulose-5-phosphate is converted to glyceraldehyde-3-phosphate and fructose-6-phosphate (Figure 2.2). Although both glycolysis and the PPP are involved in sugar oxidation, glycolysis accounts for between 80-90 % of total carbon flow in plant cells (ap Rees, 1980). However, the role of the PPP has been observed to increase during tissue growth and differentiation (ap Rees, 1980). This increase is probably due to the fact that NADPH produced from PPP plays an important role in biosynthetic reactions such as fatty acid synthesis while intermediates of the pathway such as ribose-5-phosphate is involved in the synthesis of RNA and deoxyribonucleic acid.

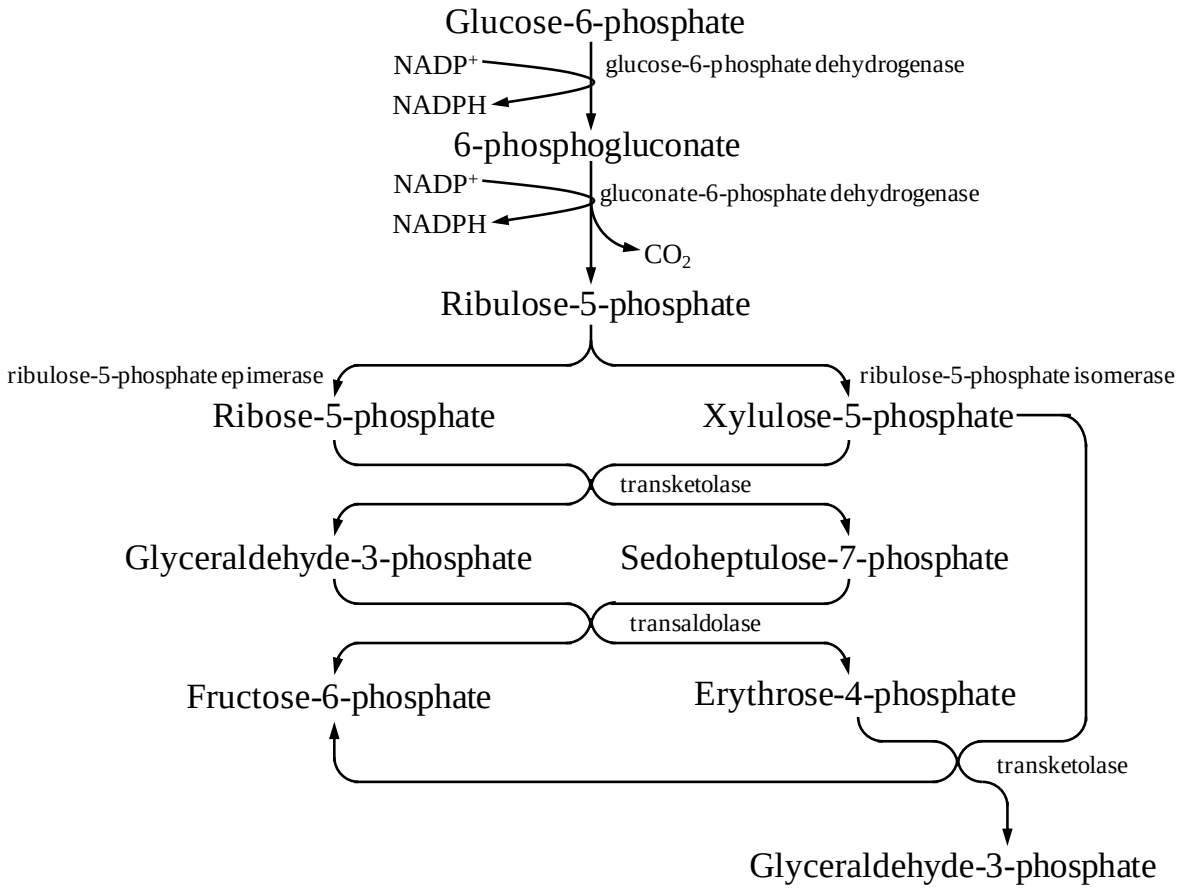

Figure 2.2: The reactions of the PPP in plants.

In the presence of O_2, the product of glycolysis (pyruvate) is utilised as a substrate in the TCA cycle. The reactions of the TCA cycle begin with the decarboxylation of pyruvate to acetyl coenzyme A (ACoA) which then combines with oxaloacetate to form citrate (Figure 2.3). The TCA cycle can be broken into three distinct but related phases. The first phase involves the reactions of 6 carbon (citrate and isocitrate) metabolites, the second phase involves 5-carbon (2-ketoglutarate and succinyl-coA and succinate) reactions and the final phase involves 4-carbon (malate, fumarate, succinate and oxaloacetate) reactions (Figure 2.3). The end result of the TCA cycle is the production of ATP and reducing equivalents in the form of NADH and $FADH_2$ (flavin adenine dinucleotide). In addition, the intermediates of the TCA cycle serve as substrates in the biosynthesis of amino acids, nucleic acids and cell wall components needed for plant growth.

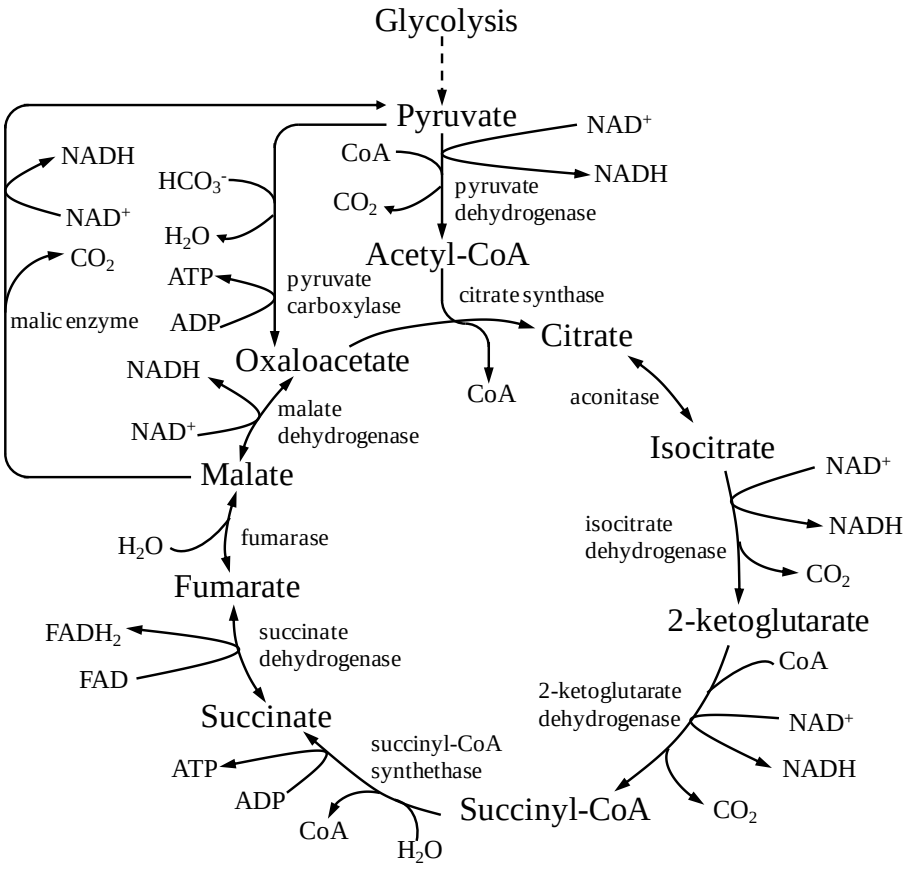

Figure 2.3: A schematic representation of the reactions of the TCA cycle in plants.

To enable glycolysis and the TCA cycle to function for the production of ATP, the NADH and $FADH_2$ produced have to be oxidised. This oxidation process occurs in the mitochondria ETC. In the ETC, the electrons present on NADH and $FADH_2$ are transferred to O_2 through protein complexes. This transfer causes protons to be translocated creating a membrane

potential which drives the synthesis of ATP. The oxidation of NADH and $FADH_2$ results in the production of 3 and 2 ATP molecules, respectively. Taking together the ATP and NADH produced from glycolysis and the TCA cycle, a net amount of 36 ATP molecules is produced when plants utilised respiratory metabolism.

Under hypoxia and anoxia, the reduction in O_2 levels affects the activity of the mitochondria ETC. This results in a restricted operation of the TCA cycle leading to the accumulation of pyruvate. The lack of O_2 decreases the regeneration of NADH produced though glycolysis. To ensure the availability of NAD^+ for continuous ATP production through glycolysis, plants cells oxidise NADH through fermentation. The main substrate for fermentation is pyruvate, which is oxidised to lactate, acetaldehyde and ethanol (Figure 2.4). These fermentative reactions ensure the availability of NAD^+ for use in glycolysis even though fermentation is accompanied by a lowered ATP production.

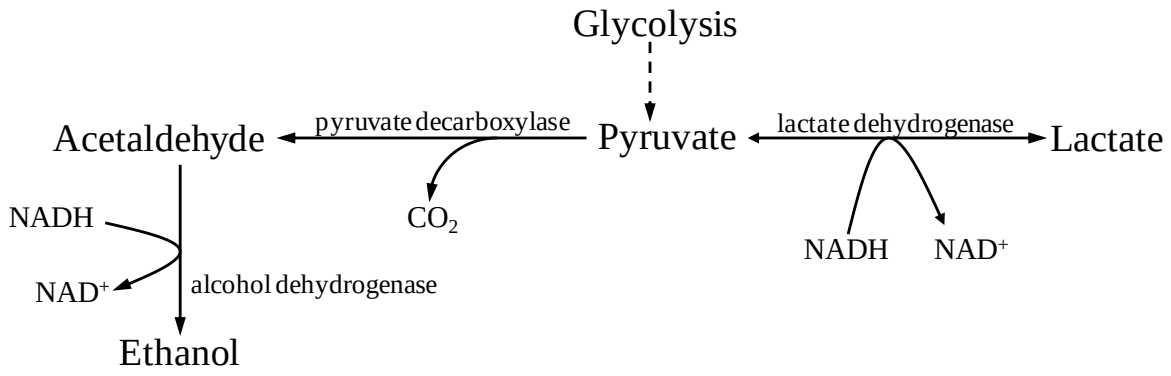

Figure 2.4: The ethanol and lactate fermentation pathway utilised by plants under low O_2 conditions.

The production of lactate through fermentation may lower the cell pH causing acidosis. Also, ethanol which is a gas may escape from cells leading to the loss of carbon units. To avoid this detrimental effect, certain plant species utilise alanine fermentation instead of ethanol/lactate fermentation (Bailey-Serres et al., 2012; Rocha et al., 2010). In alanine fermentation, pyruvate is converted to alanine instead of ethanol (Figure 2.5). Alanine production from pyruvate, however, does not lead to the regeneration of NADH. To ensure NADH regeneration, the reversal activity of malate dehydrogenase increases (Rocha et al., 2010). In addition, the extra 2-ketoglutarate produced through alanine formation can be converted to succinate with the production of ATP (Figure 2.5). These reactions can lead to the accumulation of succinate and GABA, as has been observed in *Arabidopsis* (van Dongen et al., 2009) and pears (Pedreschi et al., 2009).

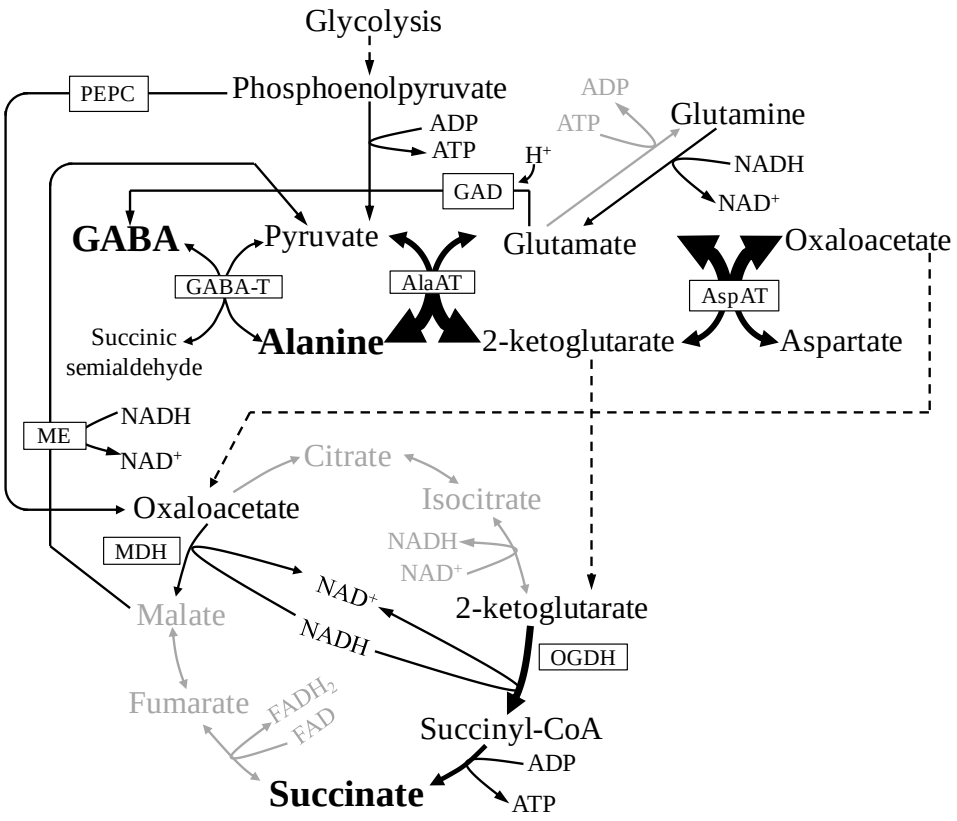

Figure 2.5: The alanine fermentation pathway utilised by plants under low O_2 conditions (Rocha et al., 2010). When plants utilise this pathway, alanine, succinate and GABA (shown in bold) accumulate. Pathways which are shown in bold are activated while those in gray are inactivated under low O_2 stress. Abbreviations: AlaAT, alanine amino transferase; AspAT, aspartate amino transferase; GABA-T, γ-aminobutyric acid transaminase; GAD, glutamate decarboxylase; MDH, malate dehydrogenase; ME, malic enzyme; OGDH, 2-oxoglutarate dehydrogenase; PEPC, phosphoenolpyruvate carboxylase.

2.2.2 Metabolism of sucrose

The disaccharide, sucrose, is an important plant metabolite which can serve as substrate for respiratory metabolism. In addition, sucrose has been observed to play a role in the transport of sugars in higher plants, as well as acting as a compatible solute and a signal compound (Lunn and MacRae, 2003). The synthesis of sucrose in plants can occur via the action sucrose-phosphate synthase (SPS) and sucrose synthase (SuSy). SPS uses uridine diphosphate glucose (UDP-GLC) and fructose-6-phosphate as substrates to synthesise sucrose-6-phosphate. A phosphatase, sucrose-phosphate phosphatase (SPP), releases orthophosphate (Pi) from sucrose-6-phosphate yielding sucrose. The action of the phosphatase ensures the rapid removal of sucrose-6-phosphate from the cytosol making the reaction irreversible. In plant cells, sucrose synthesis is mainly considered to be catalysed by SPS along with SPP

with SuSy playing only a minor role (Huber and Huber, 1996). The reaction catalysed by SuSy, which is reversible, utilises UDP-GLC and fructose yielding sucrose and uridine diphosphate (Figure 2.6). The synthesised sucrose can be utilised in the cytosol or transported to other plant organelles such as the vacuole.

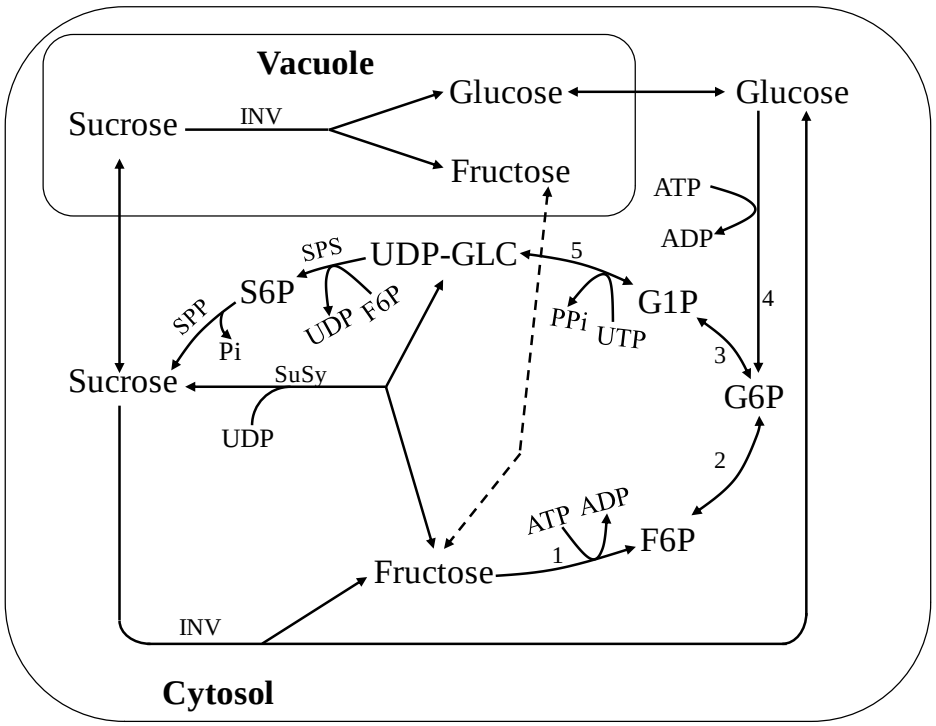

Figure 2.6: The pathway for the synthesis and degradation of sucrose in plant cells (Nguyen-Quoc and Foyer, 2001). Sucrose synthesis can occur via the action of SPS and SPP. Sucrose breakdown in the cytosol can occur via the action of SuSy and/or INV. Sucrose breakdown via INV is also possible in the vacuole, cell wall and mitochondria. Other enzymes involved in the sucrose pathway are fructose kinase and hexose kinase (1), phosphohexose isomerase (2), phosphogluco mutase (3), glucokinase and hexose kinase (4) and UDP-GLC pyrophosphorylase (5). Abbreviations: F6P, fructose-6-phosphate; G1P, glucose-1-phosphate; G6P, glucose-6-phosphate; S6P, sucrose-6-phosphate.

The use of sucrose in energy metabolism requires its hydrolysis into monomer units. The enzymes invertase (INV) and SuSy are involved in sucrose breakdown in plant cells. The hydrolysis of sucrose by INV yields glucose and fructose while the activity of SuSy results in the release of fructose and UDP-GLC. In higher plants, INV activity has been observed in the cytosol, vacuole and cell walls (Lunn and MacRae, 2003; Ruan, 2014). INV activity has also been discovered in the mitochondria (Xiang et al., 2011). When subjected to low O_2 conditions, plant cells favour the hydrolysis of sucrose via SuSy compared to INV (Drew, 1997; van Dongen et al., 2003). This is due to the fact that the energy cost associated with

sucrose degradation via either enzyme is different. While the breakdown of sucrose by INV requires the hydrolysis of two ATP molecules, the action of SuSy uses only one inorganic pyrophosphate (PPi). Indeed, studies on maize (Zeng et al., 1999) and peach fruit (Lara et al., 2010) have shown an increase in the activity of SuSy while INV activity declined under low O_2 conditions.

2.2.3 Metabolism of sugar alcohols

Sugar alcohols are produced from the chemical reduction of aldose and ketose sugars. Among the sugar alcohols found in plants are mannitol, sorbitol, maltitol and glycerol. Mannitol which is produced by the reduction of mannose by mannose-6-phosphate reductase is the most common sugar alcohol in plants (Williamson et al., 2002). Sorbitol is synthesised from glucose through the action of aldose-6-phosphate reductase. In plants the enzymes involved in sugar alcohols synthesis are localised in the cytosol and require NADPH as a co-factor. Sugar alcohols have been observed to play essential roles in the survival of plants under different abiotic stress conditions (Moing, 2000). Sugar alcohol levels have been observed to increase in pears (Pedreschi et al., 2009), apples (Lee et al., 2012) and *Arabidopsis* (van Dongen et al., 2009) subjected to various low O_2 conditions.

Among the roles assigned for the accumulation of sugar alcohols in response to stress is the ability to act as compatible solutes due to the fact that they can accumulate to high levels without interfering in cellular metabolism. Also, plants can utilise sugar alcohols as carbohydrates storage reserves when faced with extreme stress conditions by reducing their sugars to sugar alcohols (Moing, 2000). The oxidation of sugar alcohols to their precursor molecules has been observed in plants. An NAD^+-dependent sorbitol dehydrogenase which oxidises sorbitol to fructose has been detected in apple and pear callus while a sorbitol oxidase which can convert sorbitol to glucose has also been isolated in apple (Loescher, 1987). The conversion of mannitol to mannose is also possible through the action of the NAD^+-dependent mannitol-1-phosphate dehydrogenase (Loescher, 1987). The availability of these enzymes shows that sugar alcohols can be re-used by plants for cellular metabolism under ambient conditions.

The production of sugar alcohols under stress can be a strategy employed by plants to ensure the recycling of NADPH produced in the PPP (Loescher, 1987). Sugar alcohols also

contribute to the scavenging of free radicals in plant cells (Williamson et al., 2002) like many other sugars (Peshev et al., 2013; Stoyanova et al., 2011).

2.2.4 Metabolism of starch

The most abundant storage carbohydrate of plants is starch. Starch, which exists mainly as granules, is made up of two glucose polymers- amylose and amylopectin. Amylose consists mainly of linear glucose units while amylopectin is highly branched. The synthesis of starch occurs in the plastid in both photosynthetic and non-photosynthetic tissues. The substrate for the synthesis of starch is adenosine diphosphate glucose (ADP-GLC). The first committed step in starch synthesis involves the production of ADP-GLC from glucose-1-phosphate and ATP, catalysed by the enzyme ADP-GLC pyrophosphorylase (Figure 2.7) (Martin and Smith, 1995). ADP-GLC acts as a donor of glucosyl units for use by starch synthase to elongate the α-1,4-linked glucan chains of amylose and amylopectin (Geigenberger, 2011). Branching occurs at the same time as starch chain elongation. Branching is introduced by starch-branching enzymes (α-1,4-glucan-6-glycosyltransferase), which breaks α-1,4-linked glucan chains and introduces six or more glucose units to the sixth position of a glucosyl residue of the same or another chain (Smith et al., 1997). Also, starch debranching enzymes (α-1,6-glucan 6-glucanohydrolase) which cleave the branch point of amylopectin play an important role in determining the structure of starch (Zeeman et al., 2010).

The breakdown of starch yields two main end products, glucose and maltose (Figure 2.7). These breakdown products can be exported from the plastid for use in other cell organelles. The breakdown of the linear starch chain is catalysed by β-amylases (α-1,4-glucan maltohydrolase) that release maltose from the non-reducing end of the starch chain. Due to the fact that β-amylases cannot breakdown the α-1,6-branch points, the complete hydrolysis of starch also requires the action of starch debranching enzymes (Zeeman et al., 2010). In addition to glucose and maltose, glucose-1-phosphate can also be generated from the hydrolysis of starch by the action of starch phosphorylase (Figure 2.7). Starch phosphorylase can also catalyse the reversible formation of starch from glucose-1-phosphate (Green and Stumpf, 1942; Hanes, 1940). However, the low concentration of glucose-1-phosphate and the high ratio of Pi to glucose-1-phosphate in most plant tissues implies that starch phosphorylase mainly catalyses the degradation of starch (Schupp and Ziegler, 2004). The main enzymes involved in the synthesis of starch are, therefore, considered to be ADP-GLC pyrophosphorylase and starch synthase.

The availability of O_2 plays an important role in the production of starch by plants (Geigenberger, 2003). In potato tuber disks incubated with ^{14}C-sucrose at varying O_2 levels, a decrease in ^{14}C-label accumulation in starch was detected when the O_2 concentration was below 8 kPa with the lowest ^{14}C-label accumulated into starch at 0 kPa O_2 (Geigenberger et al., 2000). In a similar study on *Arabidopsis* seeds, a decrease in ^{14}C-label accumulation was observed with lowered O_2 levels (Gibon et al., 2002). This indicates that starch synthesis declines under conditions of low O_2 availability.

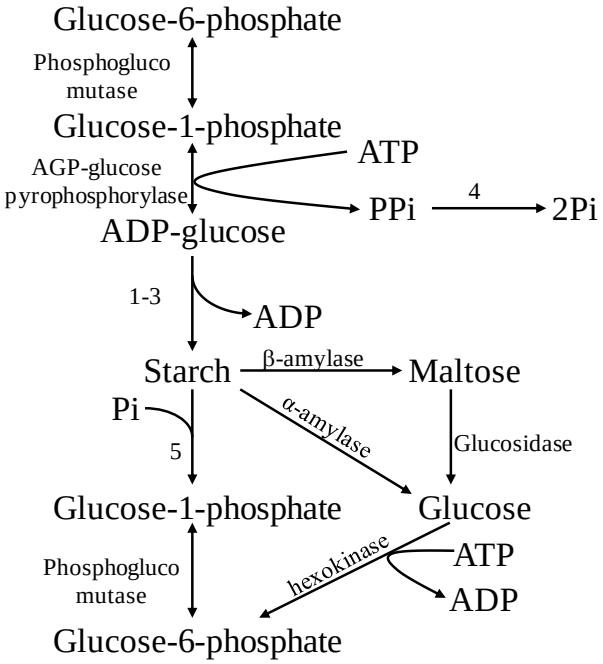

Figure 2.7: A schematic representation of the pathway for the synthesis and hydrolysis of starch in the plastid of heterotrophic tissues (Geigenberger, 2011). The pathway for starch synthesis also involves the action of starch synthase (1), starch branching enzymes (2), starch debranching enzyme (3), inorganic phosphatase (4) and starch phosphorylase (5).

2.3 Metabolic profiling of plants

A typical metabolic profiling analysis consists of three distinct but interlinked stages which include (1) sample preparation, (2) metabolite detection and quantification, and (3) data analysis and interpretation (Figure 2.8).

2.3.1 Sample preparation

The successful application of metabolomics requires careful sample preparation. Sample preparation is performed in several steps. Harvesting is the first and most critical step as the

sample should not change before analysis starts. All biochemical process such as enzymatic and oxidation reactions should be stopped (quenched) immediately after harvesting (Kim and Verpoorte, 2010; Lisec et al., 2006). The most widely used quenching technique in metabolomics is freezing in liquid nitrogen. Other available quenching procedures include denaturation of proteins using acids or solvents such as cold methanol (Kim and Verpoorte, 2010; Lisec et al., 2006).

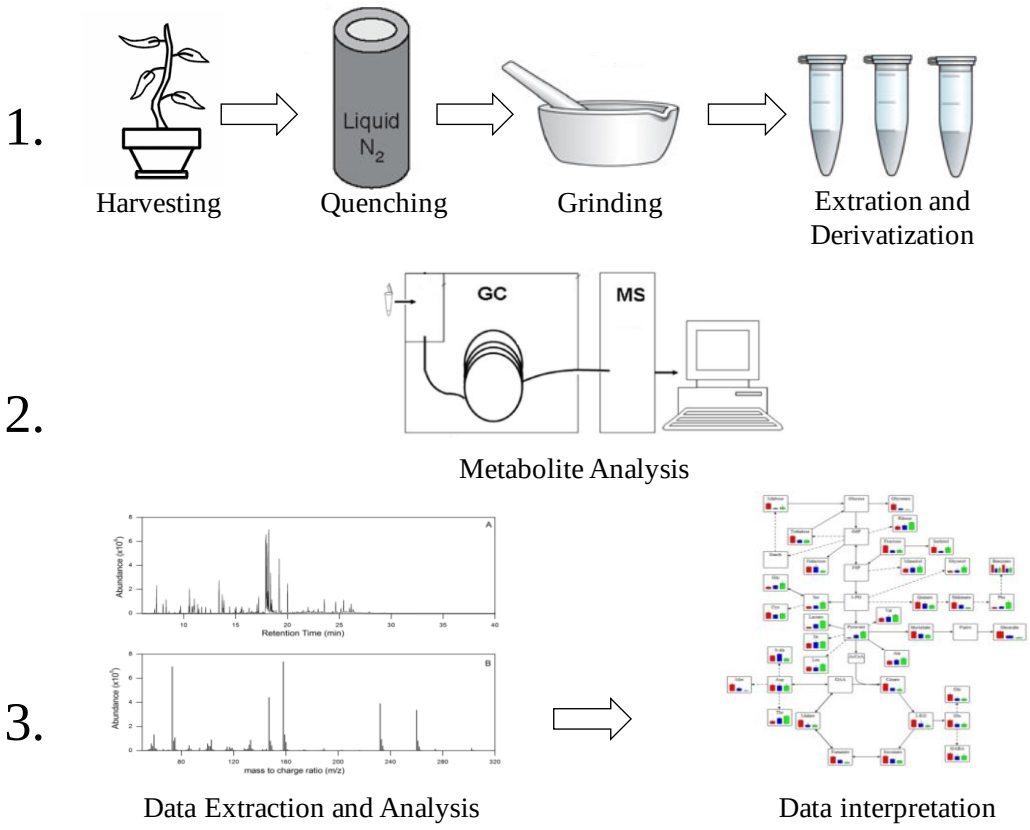

Figure 2.8: A schematic scheme for performing metabolic profiling of plants involving the steps of sample preparation (1.), metabolite detection and quantification with GC-MS (2.), data analysis and interpretation (3.).

After harvesting, the samples are dried to remove water. This water might cause variations in the weight of samples which will lead to erroneous quantification of metabolites. Drying is also carried out to remove excess water which might serve as medium for enzyme-catalysed reactions during sample processing (Kim and Verpoorte, 2010; Lisec et al., 2006). The most popular drying method is lyophilisation (freeze-drying), even though other drying techniques, for example oven-drying, are employed. Homogenisation of samples is usually carried out before drying to increase drying efficiency and to enhance the efficiency of metabolite extraction (Kim and Verpoorte, 2010; Lisec et al., 2006).

Extraction involves the separation of metabolites from undesired components. Among the most important factors in metabolite extraction are the type and amount of extraction solvent, the extraction temperature and the duration of extraction. Liquid-liquid extraction, which involves dissolving metabolites in appropriate solvent(s), is the most commonly used procedure for extracting both polar and non-polar metabolites. The most commonly used solvent for polar metabolite extraction is methanol, which can be used alone or as part of a mixture of methanol/water or methanol/water/chloroform (Kim and Verpoorte, 2010; Lisec et al., 2006; Roessner et al., 2000). Other solvents which can be used for extracting polar metabolites are ethanol and acetonitrile. Metabolite extraction using methanol is usually carried out at either high (70 °C) or low temperatures (-4 °C).

Samples for GC–MS analysis are routinely derivatised to increase their volatility and stability (Halket et al., 2005). Derivatisation is carried out to replace active hydrogen on polar functional groups with less polar trimethylsilyl groups. The most widely used derivatisation reagents in polar metabolite analysis are N-methyl-N-(trimethylsilyl) trifluoroacetamide (MSTFA) and N,O-bis(trimethylsilyl)trifluoroacetamide (BSTFA) (Halket et al., 2005). Derivatisation is usually preceded by oximation (usually with methoxyamine hydrochloride dissolved in pyridine) of keto-groups to improve their stability and prevent keto-enol tautamerisation which can lead to several derivatised products from a single metabolite (Halket et al., 2005).

2.3.2 Metabolite detection and quantification through GC-MS analysis

GC-MS based metabolic profiling is based on the separation of metabolites in a gas chromatography (GC) and subsequent identification and quantification in a mass spectrometer (MS). GC is an analytical technique used to separate a mixture of components based on their volatility and thermal stability. In GC, separation is achieved by partitioning a volatilised mixture between a stationary phase (column) and a mobile phase (carrier gas) (Grob, 2004). The affinity of the different volatilised components for the column will determine the rate of elution. Components that interact strongly with the column will leave the column later than components that interact less with the column (Grob, 2004). The main components of a GC are the inlet, the column, the mobile phase or carrier gas, oven and a detector.

Samples are introduced into the GC through the inlet. Vaporisation of the sample and its introduction into the column occurs in the inlet (Snow, 2004). Samples can be introduced into

the column in either a split or splitless mode. In the split mode the samples after been vaporised is mixed homogenously with carrier gas. The sample-gas mixture flows with a high velocity past the column where a small fraction is introduced into the column and the rest is carried away via the split outlet (Figure 2.9). Even though the small amount of samples entering the column makes the detection of metabolites with very low concentration impossible, split injections reduces the residence-time of the sample in the liner, lowering sample degradation. Also the reduced amount of sample entering the column ensures that the volume of sample matches the column capacity preventing column overload (Snow, 2004). Among the most common used split ratios used in GC-MS metabolite analysis is 10:1 where only a tenth of the injected sample reaches the column.

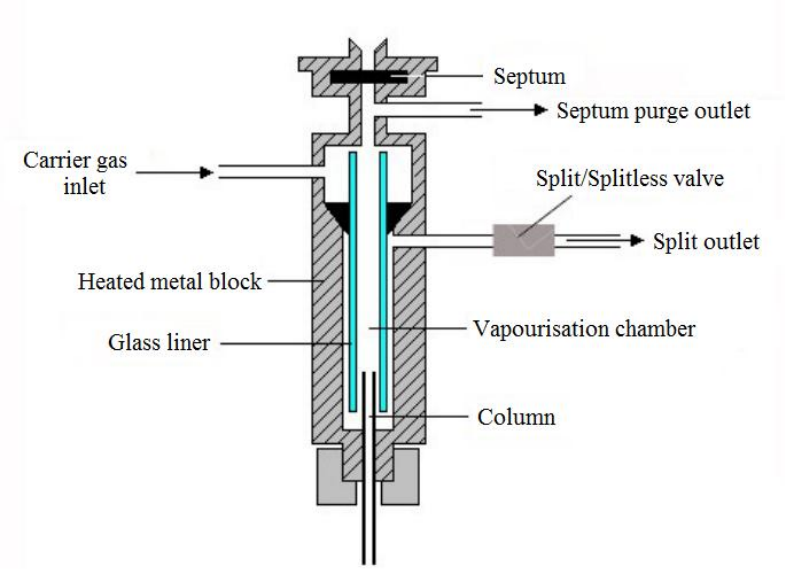

Figure 2.9: A schematic overview of a split-splitless injection technique used in GC (Snow, 2004).

In splitless injection, the sample is heated in the liner and transported to the column, but the outlet valve line is usually closed ensuring that a large part of the sample is introduced to the column (Snow, 2004). Due to the long time needed to force the entire sample through the column, thermal degradation of samples is more pronounced in splitless injection. Splitless injection is, however, suitable for the analysis of metabolites with low abundance (Snow, 2004). Other sample introductions available for GC analysis are on-column injection and programmed-temperature vaporisation. Both split and splitless injection are applied in metabolome analysis depending on the tissue been analysed, the concentration metabolite(s) of interest and the signal-to-noise ratios of the chromatogram(s) (Fiehn, 2006).

In a GC system, separation of metabolites occurs in the column. Two main types of columns are available for GC analysis, packed and capillary columns. For comprehensive metabolomics experiments, samples are analysed in capillary columns because they offer better separations with high resolution (Dettmer et al., 2007). In addition, capillary columns are more sensitive requiring small sample volumes and have short analysis times (Lei et al., 2011). GC analysis is achieved by regulating the temperature of the column so that compounds with different volatilities can be separated. The temperature of the column is regulated by an oven which can be operated isothermally or with a temperature programme (Hinshaw, 2004). Isothermal temperature programmes are usually used for target metabolite analysis since only a few metabolites can be separated at the set temperature. Almost all metabolomics experiments are carried out using oven temperature programmes in which the temperature of the column is increased linearly. Oven temperature programmes results in better separations and short analysis time (Hinshaw, 2004).

Carrier gasses are responsible for carrying the volatised compounds through the column. The most common gasses available for GC analysis are helium, nitrogen and hydrogen. The choice of appropriate carrier gas is dependent on the diffusivity which determines the speed of chromatography. Helium and hydrogen have similar diffusivities while nitrogen has a much slower diffusion speed (Bartram, 2004). Hence the use of nitrogen as carrier gas will lead to long chromatographic times. Helium is the most commonly used carrier gas in GC systems due to the high explosive behaviour of hydrogen (Bartram, 2004).

The coupling of GC to MS enables the detection and quantification of large number of compounds due to the sensitivity of MS and the ability to identify unknown compounds using mass spectral data generated from MS analysis (Villas-Bôas et al., 2005). The identification of compounds in MS is based on the fragments created when metabolites are ionised. These fragments which contain portions of the compound travel with different paths when placed in an electric or magnetic field due to differences in their mass-to-charge (m/z) ratio. The main components of an MS are an ion source where ionisation/fragmentation of compounds occur and a mass analyser where the fragments are separated. The most commonly used ion source in GC-MS analysis of metabolites is the electron ionisation (EI) ((Dettmer et al., 2007; Villas-Bôas et al., 2005).

EI occurs when compounds, in the gas phase, interact with high energy electrons produced by thermionic emission from a wire filament heated at a high electric current (Figure 2.10).

Through this interaction, some of the energy from the electrons is transferred to the gaseous compound causing it to be ionised leading to the production of fragments (de Hoffmann and Stroobant, 2007). EI produces single-charged ions from the parent compound which can be further ionised to produce several fragments. EI is one of the predominantly used ionisation methods in metabolomics. This is due to the fact that ionisation of compounds follows known chemical reactions that can be used to identify unknown compounds. Also the availability of commercial mass spectral libraries of most compounds has made EI the most popular ionisation method in GC-MS metabolome analysis (Dettmer et al., 2007; Villas-Bôas et al., 2005)

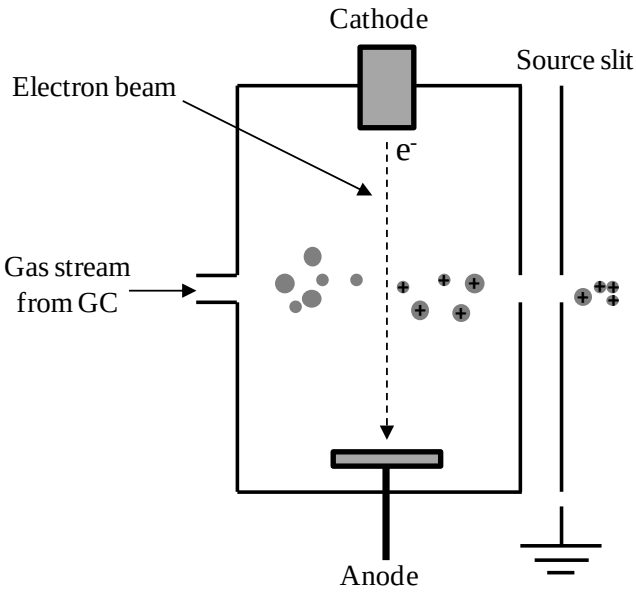

Figure 2.10: A schematic overview of the ionisation of compounds in EI.

The separation of compound fragments produced after ionisation takes place in the mass analyser. The most commonly used mass analyser in GC-MS metabolome analysis is the quadrupole mass analysers. A quadrupole mass analyser consists of four electrified cylindrical rods set parallel to each other with adjacent rods having opposite voltage polarity (Figure 2.11). When an ionised fragment enters the quadrupole, their motion depends on their charge, mass, the voltage on the quadruple and the radio frequency. At any given voltage of the quadrupole, only ions with a certain m/z will reach the detector, allowing ions with different m/z to be separated (de Hoffmann and Stroobant, 2007).

The attractiveness of using GC-MS in metabolome analysis is related to the reproducibility of results generated and its cost. GC-MS is highly sensitive and accurate in analysing

metabolites. The availability of commercial libraries such as NIST (National Institute of Standards and Technologies, (Babushok et al., 2007) and FiehnLib (The Fiehn Metabolomics Library (Kind et al., 2009) for comparison of chromatograms and mass spectra makes GC-MS an excellent tool for plant metabolic profiling. GC-MS has been used to study the effect of low O_2 stress in different plant species. Pedreschi et al. (2009) and Lee et al. (2012) used GC-MS to study the changes in the metabolome of pears and apples, respectively, under CA storage. GC-MS based metabolomics has also been used to study the effects of flooding (Kreuzwieser et al., 2009) and varying levels of O_2 on the metabolome of plant tissues (Shingaki-Wells et al., 2011; van Dongen et al., 2009). GC-MS has also been employed in other low O_2 stress response studies in plant (Biais et al., 2010; Kontunen-Soppela et al., 2007; Narsai et al., 2009).

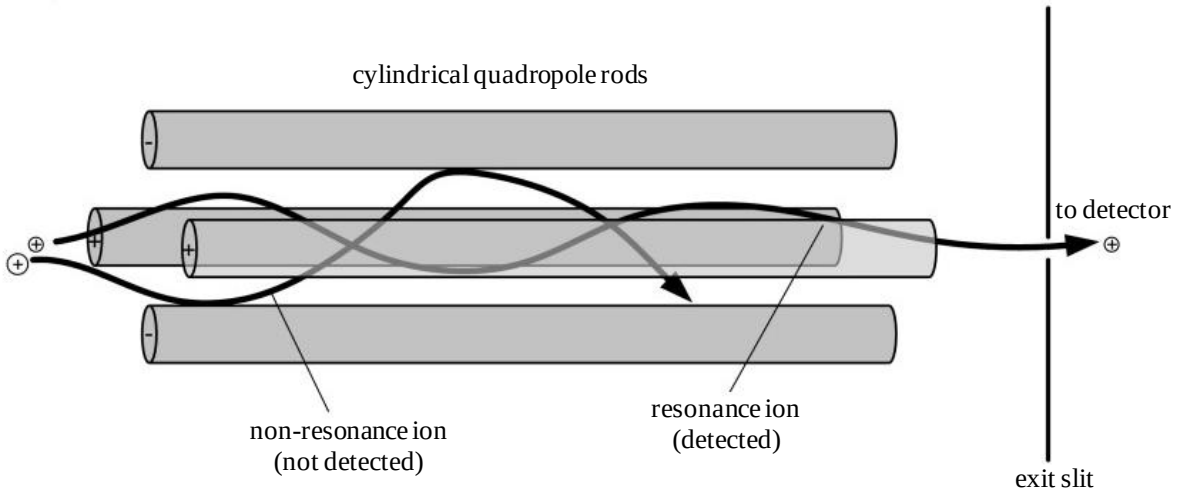

Figure 2.11: A schematic overview of quadrupole mass analyser.

GC-MS can be used for the detection of volatile metabolites like ketones, aldehydes and alcohols as well as metabolites which can be rendered volatile after derivatisation like amino acids, organic acids, sugars and lipids. However, the need for samples to be volatile or derivatised to make them volatile has limited the use of GC-MS, making it unsuitable for the analysis of highly polar compounds like secondary metabolites (Dettmer et al., 2007; Lei et al., 2011; Villas-Bôas et al., 2005).

2.3.3 Analysis and interpretation of metabolomics data

Extraction and statistical analysis of the large amount of data generated through metabolite analysis is important in obtaining useful biological information from metabolomics experiments. Metabolome data analysis involves three main procedures - raw data extraction

and processing, comparative data analysis between replicates and across treatments and data integration with other metabolomics results (Hur et al., 2013).

2.3.3.1 Data extraction and processing

The raw data generated from metabolome analysis are usually extracted and semi-manually processed using software designed by the instrument manufacturers. Among the available software's are Chemstation (Agilent Technologies Inc., Wilmington, USA) which has been developed to process GC-MS data.

Different forms of variation can be introduced into the raw data obtained from metabolomics experiments. These variations might come from both biological and experimental sources (De Livera et al., 2012). Experimental variations might be introduced during sample preparation and analysis. In addition, sample degradation with time and difference between instruments might contribute to experimental variation. Biological variations are introduced during sampling. These sources of variation can get confounded with the observed response been studied making the interpretation of metabolomics data difficult. Normalisation is, therefore, required to remove both known and unknown sources of variation from metabolomics data (van den Berg et al., 2006).

The first form of normalisation carried out to minimise experimental variation is to randomise the order in which the samples are analysed. In addition, internal and external standards can be analysed along with the samples to help reduce experimental variation (De Livera et al., 2012). The most commonly used internal standards are compounds which do not occur naturally in the tissues been analysed. Ribitol and phenyl-β-D-glucopyranoside are two of the most common compounds used as internal standards in metabolome analysis (Lisec et al., 2006). The use of multiple compounds and labelled internal standards like ^{13}C-palmitate is also gaining prominent attention (Sysi-Aho et al., 2007). Internal standards can be added to the tissue before and after extraction, depending on their solubility, to help reduce the variation in sample processing and analysis (Sysi-Aho et al., 2007).

Statistical normalisation methods have also been developed to help reduce both experimental and biological variation in metabolomics data. The most commonly employed statistical normalisation procedures include total-sum normalisation, mean normalisation, median normalisation and logarithmic transformation (De Livera et al., 2012). When performing total-sum normalisation, the total sum-of-squares of all metabolite is expressed as unity by

scaling all the samples. In median normalisation, all metabolite levels are scaled relative to the median of the sample. In mean normalisation, the metabolite abundance is expressed relative to the mean of the sample. Median normalisation is usually preferred to mean normalisation as the median of samples is usually more robust to outliers compared to the mean (De Livera et al., 2012). Logarithmic transformation is carried out to minimise the effect of outliers and to highlight increases and decreases in the observed data. In a time-series and comparative experiments, the metabolome data can be normalised respectively by expressing the metabolite levels relative to the initial value (measurement at time zero) or the control sample (De Livera et al., 2012).

2.3.3.2 Comparative data analysis

The huge dataset generated from metabolomics experiments and the high sensitivity of analytical instruments used in metabolite analysis means that subtle changes in metabolite levels can be overlooked (Steuer, 2006). To be able to obtain useful information from metabolomics experiments, multivariate statistical (chemometrics) methods have been developed. The application of chemometrics in the analysis of metabolomics data fall into three main categories: exploratory analysis where the data is analysed to detect trends, classification analysis where samples are grouped into classes and regression analysis which is used for quantitative and predictive purposes (Steuer, 2006). The most common chemometrics approaches use in metabolomics are correlation analysis, cluster analysis, principal component analysis (PCA) and partial least square (PLS) regression analysis (Steuer, 2006).

Correlation analysis is performed to determine how the changes in metabolite levels are linked between the different metabolites in an organism. In correlation analysis, the changes in the metabolome of an organism induced through the imposed stressed conditions are observed through changes in metabolite levels. Correlation analysis is based on the assumption that metabolites are produced from other metabolites which creates a correlation between these metabolites such that changes in one metabolite will affect the level of other metabolites producing or consuming this metabolite (Steuer, 2006). Correlation coefficients are estimated to determine how the different metabolites affect each other. The most commonly used correlation analysis approach in metabolomics is the Pearson correlation analysis, which calculates correlation coefficients by dividing the covariance of two elements by the product of their respective standard deviation (sd) (Steuer, 2006).

Cluster analysis is performed to group objects of similar kind into subgroups to make visualisation easy. The results of cluster analysis are usually visualised through dendrograms. The objective of cluster analysis is to organise a dataset into groups so that objects in the same group are similar while objects within different groups are dissimilar (Grafahrend-Belau et al., 2009a). In cluster analysis, groups are created within a dataset. Given a set of measurements, the distance between each pair of measurements, such as Euclidean distance, is calculated and measurements with smaller distances grouped together (Grafahrend-Belau et al., 2009a). Grouping can be created under supervised or non-supervised conditions. In supervised clustering, a certain number of groups are inferred and the dataset grouped accordingly while in non-supervised clustering, the number of groups is created by iteratively grouping the data until all datasets become part of a group (Grafahrend-Belau et al., 2009a). The most common clustering approach used in metabolomics is hierarchical clustering (Grafahrend-Belau et al., 2009a). In hierarchical clustering, a dendrogram is created such that objects in the leaves are similar while objects in different leaves are dissimilar. The dendrogram can be cut at any level to yield different clusters of the dataset.

Large scale metabolomics experiments are carried out by measuring the effect of an environmental or genetic perturbation on the metabolic composition of an organism. Metabolomics data can be obtained at a specific time-point or the changes in the metabolites can be monitored over time. To have an overview of which metabolites are affected by the treatment, PCA can be carried out. In PCA, a high dimensional dataset is reduced so that the observed variation in the variables due to the treatment can be explained with a few factors called principal components (PC). PCA is performed in such a way that a dataset containing *n* variables (metabolites) is replaced with *n* new PC's. The amount of explained variance decreases as one move to higher PC's. By plotting the first two or three PC's against each other, the dataset can be visualised in either a two- or three-dimensional space. PC1 is estimated by searching for the direction of maximum variance within the dataset. PC2 is calculated by searching for the maximum variance in the dataset in a direction orthogonal to PC1. PC3 is then calculated by searching for the maximum variance in the dataset in a direction orthogonal to both PC1 and PC2. Therefore, all PCs are constructed such that they are pair-wise orthogonal (un-correlated) to each other and ordered by the amount of variance they explain. PCA can be interpreted as linear mixture model, where the data matrix is factorised into two matrices: a score matrix, which contains the positions of the observations in a new, rotated coordinate system and a loading matrix, which contains the weights for the

original variables to transform them into the scores. Because of its applicability in dimensionality reduction, sample group discrimination, data visualisation and clustering, PCA is often used as a starting point for most metabolome data analysis.

The ability to model one or several dependent variables or responses (treatments: environmental or genetic perturbations), Y, by means of a set of predictor variables (metabolic composition: metabolome), X, is one of the most common data-analytical problems in metabolomics. In PCA, the PCs' are chosen to explain maximal variation in X with a minimum number of PCs. There is, however, no guarantee that these PC's contain most information on the relation between X and Y. PCA, therefore, maybe suboptimal for prediction purposes. To solve this problem, PLS can be performed instead of PCA. PLS is similar to PCA in that latent variables (LV), which are similar to PC's, are estimated PLS models are constructed to explain as much variation in the Y-variables based on the observed changes in X-variables.

PLS is sometimes subdivided into regression analysis and discriminant analysis (PLS-DA). In classification or PLS-DA, the samples are allocated into the appropriate discrete classes. PLS is a method for relating two data matrices, X and Y, by a linear multivariate model, but goes beyond traditional regression in that it models also the structure of X and Y. PLS derives its usefulness from its ability to analyse data with many, noisy, collinear, and even incomplete variables in both X and Y. The advantage of PLS over PCA is that unlike PCA, PLS has predictive capabilities. However, without caution, PLS modelling can be prone to over-fitting. A recent extension to the supervised PLS regression method is the orthogonal-PLS (OPLS) method, which has drawn attention in metabolomics research recently. The main difference between OPLS and classical PLS analysis is that OPLS splits up the data variation into the variance of interest, which is related to the response, and an orthogonal (noise) part, which is unrelated to the response. This leads to a simplified interpretability of the resulting components allowing to additionally asses within- and between-group variance (Bylesjö et al., 2006; Trygg and Wold, 2002).

2.3.4 Metabolite detection and quantification through other metabolite profiling techniques

Besides GC-MS, other techniques are available for the separation and detection of metabolites in plants. These include liquid chromatography-mass spectrometry (LC-MS), capillary

electrophoresis-mass spectrometry (CE-MS) and nuclear magnetic resonance spectrometry (NMR).

2.3.4.1 Liquid chromatography-mass spectrometry

Similar to gas chromatography, separation in liquid chromatography is based on the affinity of compounds for either a stationary or mobile phase. In contrast, the mobile phase in a liquid chromatography is a liquid. In liquid chromatography, the mobile phase (solvent) is pumped through a filter and passes through an injection valve where it is mixed with the injected sample. The sample and solvent are then filtered before being sent to a column for separation. Separation of compounds on an liquid chromatography can be carried out based on polarity, molecular weight or charge (Dettmer et al., 2007; Lei et al., 2011). The application of LC-MS in metabolome analysis involves separation of the metabolites in the liquid chromatography and the introduction of the separated mixture into an MS for ionisation and detection. The introduction of the separated metabolites into the MS requires their conversion to the gaseous phase since, unlike GC, metabolites leave the liquid chromatography as intact solutes (Dettmer et al., 2007; Lei et al., 2011).

Compared with GC-MS, the advantages of LC-MS in metabolite analysis include minimal sample preparation and the possibility to analyse samples without the need for derivatisation. LC-MS can also be used to separate large molecular weight compounds like plant secondary metabolites which are not amenable to GC (de Vos et al., 2007). The major drawback in using LC-MS is the lack of publicly available mass spectral libraries thus requiring the need to develop mass spectra libraries under the LC-MS conditions been employed (Dettmer et al., 2007; Lei et al., 2011).

The application of LC-MS to low O_2 stress studies in plants is limited even though it has been applied in other plant metabolomics studies. LC-MS has been used to compare the secondary metabolite profile of roots and leaves of wild-type and mutant *Arabidopsis* plants (von Roepenack-Lahaye et al., 2004) and to study metabolic alterations in the fruits of light-hypersensitive mutants of tomatoes (Bino et al., 2005). LC-MS has also been used to compare the metabolome of potato tubers with different genetic origin and developmental stages (Vorst et al., 2005), as well as to determine the tissue specificity of metabolic pathways in tomato fruits (Moco et al., 2006) and to establish gene-to-metabolite networks in *Catharanthus roseus* (Rischer et al., 2006).

2.3.4.2 Capillary electrophoresis-mass spectrometry

Capillary electrophoresis is an instrument that can be used to efficiently separate and identify compounds. When coupled to MS (CE-MS), it can be used for metabolite fingerprinting, profiling and target analysis. Compounds are separated in a capillary electrophoresis based on their electrophoretic mobility when an external voltage is applied. The mobility of metabolites is in turn dependent on their charge, size and viscosity of the solvent (Ramautar et al., 2006). Compared to LC-MS, CE-MS separations are faster, consume less solvent and are more suitable for the separation of low molecular weight compounds (Ramautar et al., 2006). The major drawback which has restricted the use of CE-MS in metabolome analysis is that only charged metabolites or those which can be charged through pH adjustment can be analysed (Dettmer et al., 2007; Lei et al., 2011; Ramautar et al., 2006). Despite its limitation, CE-MS has been used in both targeted and non-targeted metabolite analysis of plants. In the field of low O_2 stress, CE-MS has been used to study the effect of flooding on the mitochondria of roots and hypocotyls of soybeans (Komatsu et al., 2011) as well as to investigate the metabolic response of rice cell suspension to cell-death-inducible oxidative stress (Ishikawa et al., 2010) and to study the response of the leaves of rice seedlings to ozone treatment (Cho et al., 2008).

2.3.4.3 Nuclear magnetic resonance spectrometry

NMR has been used extensively for both target analysis and profiling of metabolites in plants. NMR can be used to identify and quantify metabolites of different sizes, volatility and charge (Dunn and Ellis, 2005). Metabolite analysis using NMR is based on the energy emitted when nuclei with charge and spin are placed in a static magnetic field and exposed to an oscillating magnetic field (pulse frequency) (Kim et al., 2010; Ratcliffe and Shachar-Hill, 2001). Nuclei of atoms with odd masses like ^{1}H, ^{13}C and ^{31}P have the ability to spin which may not be present in even numbered nuclei like ^{12}C and ^{14}N. These odd mass nuclei, when placed in external magnetic field, will spin with a frequency unique to each nucleus which is also proportional to the strength of the external magnetic field. Due to the difficulty in measuring the spin frequency, a pulse frequency is applied perpendicular to the external magnetic field and the energy emitted, in the form of a radiation, when the nuclei returns to it ground state is recorded. This energy is characteristic of each compound and can be used to identify it (Dunn and Ellis, 2005).

The main advantage of NMR compared to the MS-based metabolite analysis techniques is that NMR can be used to measure the levels of *in vivo* metabolites without the need for sample destruction (Kim et al., 2010; Ratcliffe and Shachar-Hill, 2001). NMR is suitable for the identification of compounds with different functional and chemical groups, like the simultaneous analysis of primary and secondary metabolites. Also, NMR can be used to accurately determine the absolute concentrations of metabolites (Ratcliffe and Shachar-Hill, 2001). NMR, however, is less sensitive and requires large amounts of sample for accurate detection and quantification (Kim et al., 2010). The low sensitivity of NMR is caused by comparative small difference in energy states between excited and ground nuclei of atoms, hence requiring large amount of samples to record detectable signals (Kim et al., 2011).

NMR has been applied extensively to study abiotic and biotic response in plants. NMR has been used to monitor the metabolic response of several plant tissues to anoxia (Ratcliffe, 1997). It has been applied to study metabolic changes induced in different plants by measuring the response of 20 metabolites from unfractionated tissue extracts exposed to anoxia (Fan et al., 1986) and to investigate metabolite gradients in melon fruits induced by hypoxia (Biais et al., 2010). NMR has also been used to investigate the changes in metabolites in relation to browing in apples (Vandendriessche et al., 2013) and to study the metabolic response of *Arabidopsis* cell suspension incubated under different O_2 levels (Branco-Price et al., 2008).

2.4 Metabolic flux analysis in plants

Metabolic flux analysis (MFA) involves measuring intracellular *in vivo* fluxes. The metabolic flux represents the rate of production or consumption of a metabolite, showing how materials flow within a network and reflecting the function of a pathway under a given physiological and environmental condition (Ratcliffe and Shachar-Hill, 2006, 2005; Stephanopoulos, 1999).

Intracellular metabolic fluxes cannot be determined directly, and their analysis requires solving mass balance equations containing measured metabolite concentrations, substrate uptake and product secretion rate(s), changes in biomass as well as accounting for dilution of metabolites due to growth of the organism (Stephanopoulos et al., 1998). Considering a metabolic pathway consisting of J intracellular reactions occurring via K pathway metabolites, the changes in metabolite concentration with time can be expressed as Eq. (2.1):

$$\frac{d\mathbf{X}_{met}}{dt} = \mathbf{v}_{met} - \mu\mathbf{X}_{met} \quad \text{(Eq. 2.1)}$$

where $\mathbf{X}_{met}$ is metabolite concentration vector for all intracellular metabolites (the intermediates in the different pathways), μ is the specific growth rate of the organism and $\mathbf{v}_{met}$ is a vector containing the net rate of formation (fluxes) of the intracellular metabolite in the *J* reactions. Eq. 2.1 can be solved to determine fluxes under both steady-state and dynamic conditions (Morgan and Rhodes, 2002; Rios-Estepa and Lange, 2007; Stephanopoulos, 1999).

2.4.1 Steady-state metabolic flux analysis

In most cells the turnover of metabolites is high, therefore, the concentration of metabolites quickly adjusts to new levels even upon changes in the environment. This means that metabolites present in a pathway can be assumed to be in (pseudo) steady-state, hence metabolite accumulation can be considered negligible and Eq. 2.1 can be written as:

$$0 = \mathbf{v}_{met} - \mu\mathbf{X}_{met} \quad \text{(Eq. 2.2)}$$

With the term $\mathbf{v}_{met}$ describing the sum of fluxes producing and consuming a metabolite and $\mu\mathbf{X}_{met}$ describing the dilution of metabolite pool due to cellular (biomass) growth.

However, due to the fact that the levels of most intracellular metabolites are low, dilution of metabolites due to cellular (biomass) growth is small in comparison to the fluxes producing and consuming the metabolite. Hence Eq. 2.2 can be written as:

$$0 = \mathbf{v}_{met} \quad \text{Eq. 2.3}$$

which can be written as:

$$\mathbf{v}_{met} = \mathbf{S}\mathbf{v} = 0 \quad \text{Eq. 2.4}$$

where **S** is a stoichiometric matrix with fluxes in columns and the stoichiometric coefficients of metabolites in each of the fluxes in rows, and **v** is a column vector of fluxes. The matrix equation contains *K* linear balances for *K* metabolites contributing to *J* reactions giving the degrees of freedom of *K*-*J*. In solving Eq. 2.4, when the number of measurements is the same as the fluxes to be estimated, an exactly determined system is obtained. It is also possible that there are more measurements than the degrees of freedom, yielding an overdetermined

system. However, in most cases there are less metabolites than reactions in a metabolic network and the number of measurements is less than the degrees of freedom, yielding an underdetermined system (Stephanopoulos et al., 1998). In an underdetermined system, fluxes can be determined using a constraint based approach such as flux balance analysis (FBA). Also, isotope labels can be fed to cells to determine intracellular fluxes (Reed and Palsson, 2003).

2.4.1.1 Flux balance analysis

Flux balance analysis (FBA) involves the application of constraints to restrict the possible flux estimates from Eq. 2.3 for an underdetermined system. This involves placing boundaries on the possible flux estimates with the view to optimise an objective function (Reed and Palsson, 2003). Among the available objective functions is to the option to optimise the production of biomass. To further reduce the solution space, additional constraints based on reaction thermodynamics, transcription and extracellular metabolome data can be included (Edwards and Palsson, 2000; Reed and Palsson, 2003; Terzer et al., 2009).

The application of FBA in the elucidation of metabolic fluxes has been limited by the complexity of the plant metabolic network. The presence of parallel and alternative pathways as well as substrate cycles and bidirectional fluxes in plants, for instance, has restricted the use of FBA since these fluxes are poorly estimated using FBA (Gombert and Nielsen, 2000). Also, choosing a suitable objective function is difficult when applying FBA. To be able to overcome the limitations of FBA, steady-state MFA analysis can be estimated using isotope-labelling techniques (Kruger and Ratcliffe, 2009; Libourel and Shachar-Hill, 2008; Morgan and Rhodes, 2002; Rios-Estepa and Lange, 2007). Both radio- and stable- isotopes can be used for the elucidation of metabolic fluxes (Rios-Estepa and Lange, 2007; Voit et al., 2004).

2.4.1.2 ^{13}C-metabolic flux analysis

The application of stable isotopes especially carbon-13 (^{13}C-isotope) for MFA have gained prominent attention. This is due to the fact that metabolism involves the making and breaking of mainly carbon-carbon bonds, making ^{13}C an ideal tracer to steady metabolism (Tang et al., 2009). Also, advances in analytical techniques for quantifying ^{13}C-labelled metabolites and the development of computational approaches to estimate fluxes from ^{13}C-labelled data have contributed to the popularity of ^{13}C-label MFA. ^{13}C is a stable isotope of carbon with a natural abundance of 1.1 %.

The advantage of steady-state ^{13}C-MFA over FBA is that it can be used to estimate bi-directional and parallel fluxes since different enzymes cleave the carbon-backbone of metabolites differently. Hence, by measuring the distribution of ^{13}C-label within a metabolite, fluxes producing and consuming that metabolite can be elucidated (Schwender and Ohlrogge, 2002). Also, the availability of commercial compounds with ^{13}C-label in different positions means that experiments can be carried out with a mixture of ^{13}C-labelled substrates to determine specific metabolic fluxes. Despite these advantages the application of ^{13}C-MFA to elucidate steady-state fluxes is restricted by the need to supply plants with an external ^{13}C-labelled precursor(s), hence limiting the technique to heterotrophic plant systems (Sweetlove and Ratcliffe, 2011).

Steady-state ^{13}C-MFA has been applied to estimate the central metabolic flux in *Arabidopsis* cell suspension under different O_2 conditions (Williams et al., 2008) and to study the metabolic adaptation following menadione-induced oxidative stress (Williams et al., 2010). Steady-state ^{13}C-MFA has also been used to estimate the effect of hypoxia on substrate cycles involved in sucrose metabolism (Alonso et al., 2007b). The procedure has also been used in estimating the central metabolic fluxes in other plant tissues such as *Arabidopsis* (Masakapalli et al., 2010) and tomato (Rontein et al., 2002) cell suspension. The estimation of fluxes using ^{13}C-labels is carried out by performing a ^{13}C-isotope labelling experiment.

A ^{13}C-isotope labelling experiment is performed by feeding an organism with a ^{13}C-labelled substrate, such as ^{13}C-glucose, under defined experimental conditions. Upon uptake, the labelled substrate is metabolised and the ^{13}C-label is distributed throughout the metabolites of the organism (Figure 2.12). The distribution of ^{13}C-label is proportional to the flux through each metabolite (Wolfgang and Wiechert, 2001). Label is first incorporated into free intracellular metabolites, and upon prolonged incubation label can accumulate in macromolecules and storage metabolites (Zamboni et al., 2009).

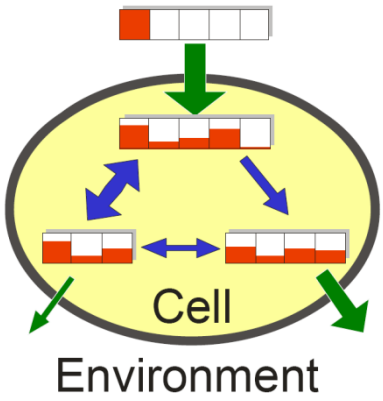

Figure 2.12: The principle of ^{13}C-MFA. An organism is feed with a labelled substrate, with the labelled being metabolised and incorporated into different metabolites. The amount of label incorporated into each metabolite depends on the flux through that pathway. The label accumulated by the metabolites can therefore be measured and used to estimate intracellular fluxes (Wolfgang and Wiechert, 2001).

The analysis of fluxes under steady-state conditions using ^{13}C-MFA analysis requires the achievement of both isotopic and metabolic steady-state. Isotopic steady-state is attained when the distribution of label within a metabolic network reaches stationary levels, while under metabolic steady-state the rate of formation of a metabolite is equal to its breakdown (Rios-Estepa and Lange, 2007). A typical steady-state ^{13}C-MFA experiment is carried out by determining the appropriate choice of ^{13}C-label substrate, feeding an organism with the substrate, quantifying the accumulated ^{13}C-label in the different metabolites and computing fluxes using the ^{13}C-label data and any other extracellular flux measurements (Figure 2.13).

2.4.1.2.1 Choice of ^{13}C-labelled substrate

The choice of labelled substrate is important in determining how fluxes in a metabolic network can be accurately estimated (Schwender, 2009). The choice of label is dependent on the objectives of the experiment as certain fluxes can be predicted more accurately than others with a label or label-combination. In addition, cost also influences the decision on which label will be used for ^{13}C-MFA (Antoniewicz, 2013; Schwender, 2009). Two main types of labels can be utilised in the estimation of fluxes when carrying out ^{13}C-MFA: uniform and positional labels. When using a uniformly labelled substrate, all the carbon atoms present in the substrate contain ^{13}C-label. Uniform labels are usually utilised in combination with unlabelled substrates to be able to differentiate the labelling incorporated into different metabolites.

Positional labels, which contain ^{13}C in specific carbon position or positions of the substrate, can be used alone or in combination with other unlabelled substrates to elucidate fluxes.

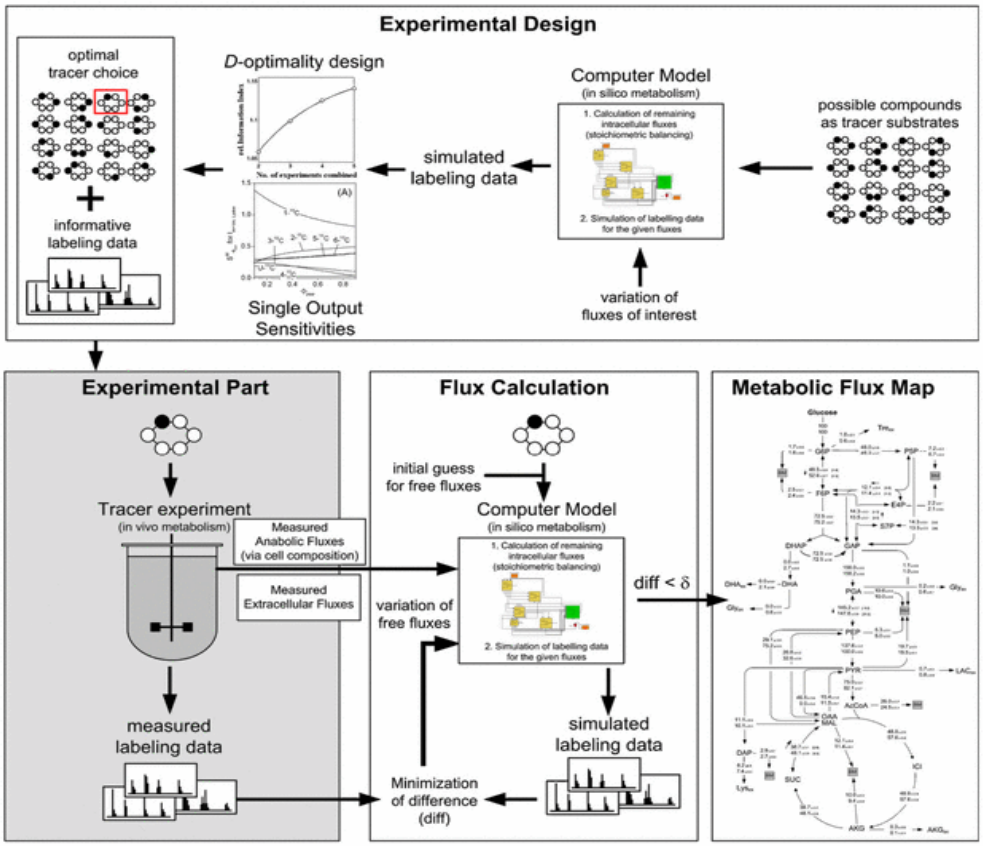

Figure 2.13: A schematic overview of a typical ^{13}C-MFA experiment involving determining the appropriate labelled substrate, feeding an organism with the substrate, quantifying the amount of label within different metabolites, measuring extracellular fluxes and computing intracellular fluxes (Kohlstedt et al., 2010).

The most popular labelling substrate used in ^{13}C-MFA is glucose. Both 1-^{13}C-glucose and a mixture of uniformly labelled (U-^{13}C-glucose) and unlabelled-glucose have been used extensively in ^{13}C-MFA (Schwender, 2009). While 1-^{13}C-glucose is able to resolve accurately the split between glycolysis and PPP, a mixture of U-^{13}C- and unlabelled-glucose provides better prediction of fluxes of pathways downstream of glycolysis. A decision on the appropriate choice of label for ^{13}C-MFA can be made by using the techniques of optimal experimental design (Antoniewicz, 2013). Prior to the actual experiment, in-silico modelling of the effects of different label or label combination can be performed to determine which label is appropriate to answer the experimental question under consideration (Antoniewicz,

2013). The best label is the one that is able to resolve metabolic fluxes accurately at a minimum cost (Schwender, 2009).

2.4.1.2.2 ^{13}C-label analysis

The accurate determination of ^{13}C-label is an important requirement in ^{13}C-MFA. NMR and MS are the available techniques for quantification of ^{13}C-label. NMR and MS estimate ^{13}C-label differently even though they can be used as complementary tools in ^{13}C-MFA. MS, however, has a higher sensitivity compared to NMR. GC-MS is the most popular MS analysis approach for the estimation of label after performing ^{13}C-label experiments (Wiechert et al., 2007). Among the factors that influence the choice of instrument are sample size, experimental cost, instrument availability and desired ^{13}C-label information. The analysis of ^{13}C-label using NMR results in the determination of positional isotopomers (Szyperski, 1998). Positional isotopomers are isotopes which differ in the position of the carbon atom at which ^{13}C-label is incorporated. For a metabolite containing n carbon atoms, 2^n positional isotopomers can be estimated.

MS measures the difference in mass due to the incorporation of label. MS cannot distinguish molecules having the same mass but with label incorporated into different carbon positions (Zamboni et al., 2009). Analysis of ^{13}C-labelled using MS results in the estimation of mass isotopomer distributions (MID). MID differ in the number of ^{13}C-label incorporated into the carbon backbone of the metabolite (Szyperski, 1998). For any metabolite fragment containing n carbon atoms, n+1 MID can be estimated (Figure 2.14). For metabolites containing a few carbon atoms such as glycine, positional isotopomers can be estimated in addition to mass isotopomers. Positional isotopomers can be estimated for metabolites having more than two carbon atoms, when the MID of several ion-fragments containing different carbon backbones are detected in the MS.

The main factors influencing the accuracy of label estimation using MS are the effectiveness of chromatographic separation and the ability to correct the obtained MID for the presence of naturally occurring isotopes of carbon and other elements (Allen and Ratcliffe, 2009). Due to the fact that MS is not able to distinguish between the ^{13}C-label coming from the supplied substrate and the natural abundance of the ^{13}C-label present in metabolites, it is important to correct MID for natural abundance isotopes (Wittmann and Heinzle, 1999). The correction involves multiplying the experimentally determined MID with a correction matrix containing

the natural abundance distribution of the isotopes of all elements present in the ion-fragment being analysed (van Winden et al., 2002b).

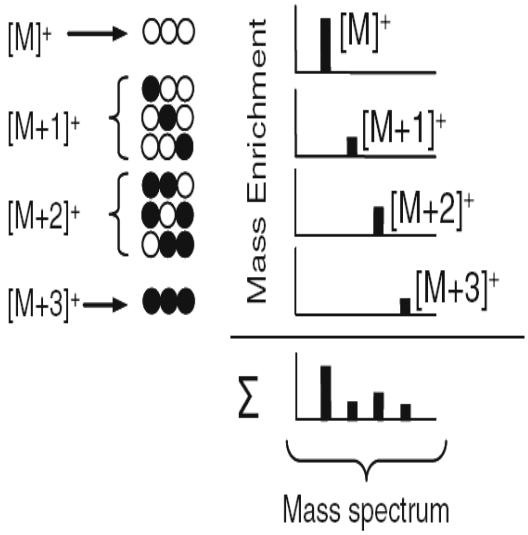

Figure 2.14: The estimation of ^{13}C-label in a three-carbon metabolite using MS. MS can be used to determine mass isotopomer as well as positional isotopomers when other ion fragments are available (^{12}C, open circles; ^{13}C, closed circles) (Allen and Ratcliffe, 2009).

Steady-state ^{13}C-MFA is usually carried using the ^{13}C-label accumulated by proteinogenic amino acids (PAA). This is because PAA are abundant in cells, are easy to extract and their ^{13}C-label data can be determined accurately (Dauner and Sauer, 2000). Also, the steady-state ^{13}C-label of PAA is a good reflection of metabolic fluxes since most PAA are synthesised from intermediates of the central carbon metabolism (Dauner and Sauer, 2000). The major drawback of using PAA for MFA is the long incubation times needed to attain isotopic steady-state in PAA. When the ^{13}C-label present in the intermediates of the central carbon metabolism and other free intracellular metabolites can be estimated accurately, these can be used to estimate fluxes instead of PAA (Mori et al., 2011)

2.4.1.2.3 Estimation of fluxes from ^{13}C-label data

The conversion of measured ^{13}C-label data into fluxes requires mathematical modelling and statistical analysis of the computed fluxes. A metabolic network map containing the transfer of atoms between metabolites needs to be constructed for flux estimation. Two main approaches are available for the estimation of metabolic fluxes from ^{13}C-label data: a global iterative fitting and metabolic flux ratio analysis (METAFoR) (Zamboni et al., 2009).

2.4.1.2.3.1 Global iterative fitting

In global iterative fitting, the propagation of label is followed by constructing a mass balance model for the transfer of ^{13}C-label between the different metabolites of the metabolic network under consideration. Balance equations are therefore setup for each metabolite isotopomers resulting in a high number of isotopomers equations. Iteration is then performed to search for the best fit between the observed and simulated ^{13}C-label data (Wolfgang and Wiechert, 2001). Iterations are usually initiated from an initial random (guessed) flux distribution and are continued until a minimum difference between the simulated and measured ^{13}C-label pattern is obtained. At the end of the iteration, a single flux distribution is obtained (Zamboni et al., 2009).

When estimating fluxes using isotopomers the high number of equations that may be obtained may be computionally demanding to solve. This has led to the development of other approaches such as cumomers and bondomers analysis. Cumomers consists of sums of isotopomers containing both positional and isotopomer data. By transforming isotopomers to cumomers, linear and reduced analytical equations can be obtained for estimating metabolic fluxes (Wiechert et al., 1999). The analysis of flux using bondomers is based on tracing the fate of carbon-carbon bonds that remain unbroken in a metabolic network. Due to the breaking and rearrangement of carbon-carbon bonds during metabolism, the number of bondomers remains few leading to a reduction in the equations to be solved. Bondomer analysis is, however, limited to the use of uniformly labelled substrates (van Winden et al., 2002a). Among the computer programmes available for performing global iterative fitting are 13CFLUX2 (Weitzel et al., 2013), OpenFLUX (Quek et al., 2009) and *influx_s* (Sokol et al., 2012). Almost all steady-state ^{13}C-MFA in plants have been performed using global iterative fitting (Kruger et al., 2012).

2.4.1.2.3.2 Metabolic flux ratio analysis

METAFoR makes use of ^{13}C-labelling data to estimate the ratio of converging fluxes from ^{13}C-label accumulated by PAA (Nanchen et al., 2007). When using METAFoR, errors associated the data and the construction of large metabolic networks are minimised (Zamboni et al., 2009) since only branched pathways are studied. The ability to estimate flux ratios from ^{13}C-label in PAA is possible due to the fact that the carbon backbone of the intermediates of the central carbon metabolism are conserved during the synthesis of PAA. Therefore the ^{13}C-

label in PAA can be propagated back to the metabolite intermediates enabling flux ratios to be estimated (Nanchen et al., 2007). METAFoR, for example, can be used to estimate the fraction of serine produced from 3-phosphoglycerate derived from either glycolysis or the PPP in the plastid (Nanchen et al., 2007).

The flux ratios obtained from METAFoR analysis can be used as constraints in global iterative fitting and FBA (Nanchen et al., 2007). Flux ratios determined from ^{13}C-labelled data have been used as constraints to estimate central metabolic fluxes in microorganisms (Nanchen et al., 2007). METAFoR in combination with constraint based flux analysis have been applied in the estimation of fluxes in *Escherichia coli* (Fischer et al., 2004) and *Pichia anomala* (Fredlund et al., 2004). To ensure faster calculation of flux ratios from ^{13}C-glucose experiments, FiatFlux a software which runs in MatLab has been developed (Zamboni et al., 2005). The main input substrates for FiatFlux are U-^{13}C-glucose combined with unlabelled glucose and 1-^{13}C-glucose. Compared to global iterative fitting, METAFoR is a simple flux estimation procedure that can be used to access alterations in metabolic fluxes upon growing an organism under different conditions.

2.4.2 Dynamic modelling of plant metabolic networks

To improve our understanding of the metabolic behaviour of plants under low O_2 stress, steady-state metabolic fluxes can be supplemented with dynamic flux measurements. Dynamic models can be constructed by measuring the changes in metabolite concentrations with time (Rios-Estepa and Lange, 2007). This approach can be coupled with kinetic modelling to determine the *in vivo* kinetic response of plants to low O_2 stress (Rios-Estepa and Lange, 2007). Dynamic fluxes can also be estimated using the dynamic labelling approach. The procedure for performing dynamic labelling experiments is similar to steady-state flux analysis, in that an organism is supplied with a labelled substrate and the distribution of label within the different metabolites is measured in addition to the concentration of the metabolite (Fernie and Morgan, 2013; Voit et al., 2004). Unlike steady-state flux analysis, however, the metabolite concentration and label accumulation are measured at several time points (Fernie and Morgan, 2013; Voit et al., 2004). Mathematical equations are then formulated to explain the changes in the labelled and unlabelled fraction of each metabolite.

For example, in the dynamic label modelling approach a partially labelled substrate (A) can be is supplied to an organism which is metabolised using an enzyme with a rate constant *k* to produce B. Due to the fact that the enzyme is not able to distinguish between the labelled and unlabelled fraction of the substrate, both fractions are converted to the product with the same rate constant. Mass balances equations can be written to depict the changes in the total (Eq. 2.5), labelled (Eq. 2.6) and unlabelled (Eq. 2.7) concentration of the metabolite based on the same rate constant, *k* (Voit et al., 2004).

$$\frac{d\left[\mathrm{B_T}\right]}{dt} = k \cdot \left[\mathrm{A_T}\right] \qquad \text{(Eq. 2.5)}$$

$$\frac{d\left[\mathrm{B_L}\right]}{dt} = k \cdot \left[\mathrm{A_L}\right] \qquad \text{(Eq. 2.6)}$$

$$\frac{d\left[\mathrm{B_U}\right]}{dt} = \left[\mathrm{A_T}\right] - \left[\mathrm{A_L}\right] \qquad \text{(Eq. 2.7)}$$

where $[A_T]$, $[A_L]$ and $[A_U]$ are the concentrations of total, labelled and unlaballed substrate A, and $[B_T]$, $[B_L]$ and $[B_U]$ are the concentrations of total, labelled and unlaballed product B, respectively.

Dynamic labelling offers some advantages over steady-state flux analysis in that attaining metabolic and isotopic steady-state, an important component in steady-state flux analysis, is not required, making dynamic labelling amenable to different tissue types and experimental conditions (Fernie and Morgan, 2013; Voit et al., 2004). Dynamic labelling, however, is unsuitable for the analysis of large metabolic networks, as following the time-course of a label becomes more difficult as the label moves away from the point of supply (Fernie and Morgan, 2013; Ratcliffe and Shachar-Hill, 2006)

2.4.3 Metabolic control analysis

An in-depth quantitative knowledge of the mechanisms employed by living organisms to regulate their metabolism under different conditions can only be gained by analysing how the control of fluxes and metabolites is shared among the different enzymes in a metabolic network (Heinrich and Rapoport, 1974; Kacser and Burns, 1995). This regulatory information can be obtained through metabolic control analysis (MCA). In MCA, an organism is

perturbed, and the effect of the perturbation on metabolic pathways is measured after steady-state is attained (Kacser and Burns, 1995). The magnitude of change caused by the perturbation is expressed as a control coefficient (Fell, 1996; Heinrich and Rapoport, 1974; Kacser and Burns, 1995). Both flux and concentration control coefficients can be estimated. Flux control coefficient (FCC) measures the relative change in steady-state flux of a pathway caused by an infinitesimal change in the activity of an enzyme (Figure 2.16) (Fell, 1996; Kacser and Burns, 1995) while concentration control coefficient (CCC) measures the relative change in steady-state flux caused by an infinitesimal change in the concentration of a metabolite (Fell, 1996; Kacser and Burns, 1995).

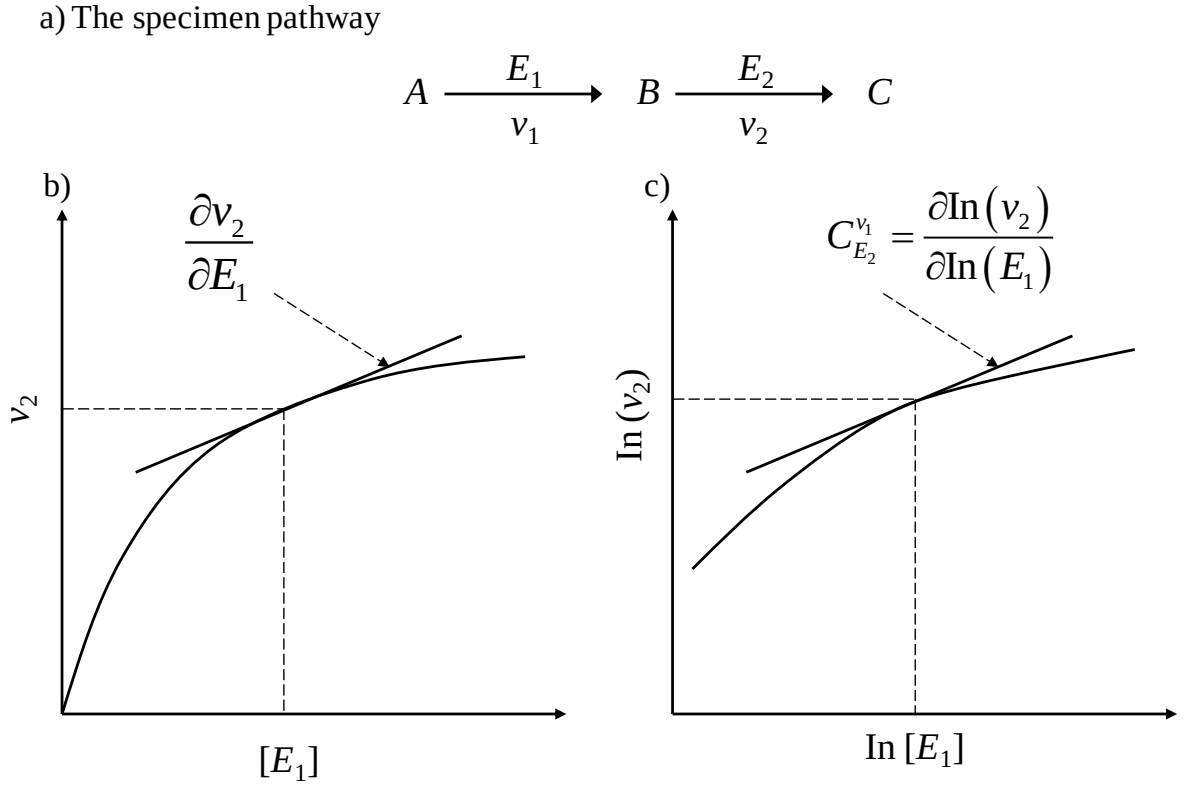

Figure 2.16: A procedure for estimating FCC. (a) A hypothetical metabolic pathway (metabolite A is converted to B by an enzyme E_1 which is further metabolised to C by enzyme E_2.). (b) The variation of flux v_2 upon changes in enzyme E_1. (c) On a double-logarithmic plot, the slope is the FCC ($C_{E_1}^{v_2}$) of enzyme E_1 on flux v_2.

Control coefficients are system wide properties which can change under different conditions (ap Rees and Hill, 1994; Fell, 1996). This means that the enzymes or metabolites that exert major control on a metabolic pathway can change when an organism is moved from one condition to another. In the control of a given pathway, the enzymes with the highest FCC

exert major control on that pathway. The contribution of each enzyme within a metabolic network on the control of a pathway can be assessed using the summation theory, which states that the sum of all FCC of metabolic flux should be unity (Sauro et al., 1987).

Both dynamic models and MCA have been applied to study respiration and other metabolic pathways in plants. Dynamic modelling has been used to study plant mitochondrial respiration (Affourtit et al., 2001) and the regulation of central metabolic enzymes in maize root tips under hypoxia (Roscher et al., 1998). MCA have been applied to investigate the control of photosynthesis by Rubisco (Stitt et al., 1991) and to study the conversion of sucrose to starch in potato tubers (Geigenberger et al., 2004). A combination of dynamic modelling and MCA have been used to study phenylpropanoid metabolism in potato tuber disks (Heinzle et al., 2007) and *Petunia hybrid* (Colón et al., 2010).

2.5 Conclusions

The critical role metabolism plays in the survival of plants requires that the two main end products of metabolism, namely metabolites and fluxes, be studied to understand the response of plants to low O_2 stress. GC-MS based metabolic profiling, which offers the opportunity to identify and quantify a wide range of compounds, will be used to study the response of plant cells to low O_2 stress in this thesis. ^{13}C-MFA which offers the opportunity to determine pathways that are (de)activated will be used later in this thesis to determine the metabolic flux response of tomato cell suspension to low O_2 stress under both dynamic and steady-state conditions.

Chapter 3

Materials and Methods

3.1 Introduction

Metabolome studies on the effect of low O_2 on plants can be carried out by storing fruits and vegetables under CA. However, when carrying out fluxomics studies using ^{13}C-labelling techniques, there is the need to feed the fruits with ^{13}C-labelled substrate. Taking into account that the incorporation of a ^{13}C-label into intact fruits and the quantification of the label accumulation is a non-trivial task, due to the abundance of storage sugars and polymers and the long times needed for these polymers to turn-over and incorporate quantifiable amounts of ^{13}C-label into their metabolite pools (Alonso et al., 2007b), it is important to use model systems which can be easily manipulated to take-up ^{13}C-label.

To reduce the complexity of the experimental system and make it amenable to manipulations, cell suspension can be used as a model system. Cell suspension consists of relatively homogeneous cell population growing on a defined media (Mathur and Koncz, 1998). Cell suspension offer several benefits when used in plant research. Firstly, the growth conditions such as the supplied carbon source and other nutrients as well as temperature, pH and dissolved O_2 levels can be easily controlled (Mustafa et al., 2011). Secondly, by incubating cell suspension under standardised and controlled conditions, in a bioreactor for example,

---

The content of this part of the thesis is based on

Ampofo-Asiama, J., Baiye, V.M.., Hertog, M.L.A.T.M., Waelkens, E., Geeraerd, A.H., Nicolai, B.M., 2014. The metabolic response of cultured tomato cells to low oxygen stress. Plant Biology, 16, 594–606.

biological variation within different batches of cells can be minimised. In addition, by using cell suspensions, diffusion barriers within fruits and plants which can create low O_2 conditions, can be eliminated ensuring that any response measured is due to a uniform and known low O_2 condition.

Metabolite identification and quantification is an important aspect in studying the metabolomics and fluxomics response of plants to low O_2 stress. Metabolite analysis with GC-MS provides the opportunity to measure the response of the metabolome to low O_2 stress. Especially techniques utilising GC-EI-MS have been developed to characterise the primary metabolite fraction of different plants tissues (Lisec et al., 2006). GC-EI-MS is also one of the most employed instruments in MFA due to its capacity for quantifying ^{13}C-label accumulated in both free intracellular metabolites and PAA (Wittmann, 2007).

In this chapter, a protocol for separating, identifying and quantifying intracellular polar metabolites in tomato cell suspension using GC-EI-MS will be discussed. Prior to that, a detailed procedure for establishing and maintaining cell suspension from tomato leaves will be explained and the process for estimating the ^{13}C-label accumulated by polar metabolites will be discussed.

3.2 Establishment of tomato cell suspension

3.2.1 Induction of tomato cell suspension

The starting explant used for the establishment of callus was tomato leaves (*Lycopersicum esculentum* L. var cerasiforme). The leaves, cut from the stem of the tomato plant, were used within an hour of picking. The leaves were washed with water to remove soil particles and other surface contaminants and sterilised in 10 % sodium hypochlorite (NaOCl) solution (containing 1-1.4% available Cl_2) containing a few drops of Tween 20. Sterilisation was carried out twice for duration of 15 min each. The leaves were washed with sterile distilled water after sterilisation (Evans et al., 2003; Mustroph and Albrecht, 2003). The sterilised leaves were cut into pieces of approximately equal size (about 1 cm length) and placed on a callus agar medium. Small incisions were made on the leaves to serve as sites for callus growth. The agar medium with the leaves was sealed with Parafilm and incubated in the dark at 25 °C.

The agar medium for callus initiation was prepared from sucrose, Murashige and Skoog Basal Salt Mixture, Nitsch's Vitamin Mixture (1000x) (Duchefa, The Netherlands) and the plant growth hormones, 2,4-dichlorophenoxyacetic acid (Sigma, Belgium) and benzylaminopurine (Sigma, Belgium) (Table 3.1). A 25 mL stock solution each of the growth hormones and the vitamin mixture was prepared by dissolving a weighed amount in either 1 mL ethanol or sodium hydroxide (NaOH) and adding distilled water to obtain the required volume (Table 3.2). The Murashige and Skoog Basal Salt Mixture contained trace elements such as cobalt and molybdenum as well as nitrogen source (ammonium nitrate) while the Nitsch's Vitamin Mixture contained essential vitamins such as biotin, folic acid and nicotinic acid needed for cell growth (Table 3.3).

Table 3.1: Composition of media used for the growth of callus and suspension cells (values reported per litre of media).

Media constituent	**Callus**	**Cell suspension**
Murashige and Skoog basal salts (g)	4.3	4.3
Glucose (g)	30	30
1000x Nitsch's vitamin mixture (mL)	1	1
2,4-dichlorophenoxyacetic acid (μM)	9	9
Benzylaminopurine (μM)	11.4	11.4
Plant agar (g)	7	-
pH	5.8	6.0

Table 3.2: Composition of the growth hormones used in callus and cell suspension media preparation.

Media component	**Amount (g)**	**Solvent**
2,4-dichlorophenoxyacetic acid	0.025	ethanol
Benzylaminopurine	0.0125	NaOH (1 N)
Nitsch's Vitamin Mixture	2.713	water

Table 3.3: Composition of the Murashige and Skoog Basal Salt Mixture and Nitsch's Vitamin Mixture (1000x) used for culturing tomato callus and cell suspension (Murashige and Skoog, 1962).

MS basal Salt		**Nitsch vitamin mixture**	
Component	**Amount (mg/L)**	**Component**	**Amount (mg/L)**
Calcium chloride dihydrate	440	Myo - Inositol	100000
Cobalt chloride hexahydrate	0.025	Thiamine hydrochloride	500
Cupric sulfate pentahydrate	0.025	Pyridoxine hydrochloride	500
Ferrous sulfate hepta hydrate	27.8	Nicotinic acid	5000
Boric acid	6.2	Folic acid	500
Potassium phosphate (mono)	170	Biotin	50
Potassium iodide	0.83	Glycine	2000
Potassium nitrate	1900		
Manganese sulfate heptahydrate	370		
Magnesium sulfate (anhydrous)	16.9		
EDTA disodium dihydrate	37.3		
Molybdic acid dihydrate	0.25		
Sodium phosphate dihydrate	170		
Ammonium nitrate	1650		
Zinc sulfate heptahydrate	8.6		

In the preparation of the callus media, the powdered components (sucrose and Murashige and Skoog Basal Salt Mixture) were dissolved to 900 mL distilled water, after which the vitamin mixture and growth hormones were added and the solution adjusted to the desired pH (Table 3.2). Plant agar was added before adjusting the pH. Distilled water was then added to obtain the required volume of 1 L. The media were dispensed into glass bottles and autoclaved at 121 °C for 15 min. The callus growth media was transferred to Petri dishes (60 mm × 15 mm) and sealed with Parafilm (Evans et al., 2003; Mustafa et al., 2011) until further use.

Callus formation was observed within two weeks following the incubation of tomato leaves on an agar media in the dark. Subculturing was carried out after three weeks to remove the leaves which did not form callus and to transfer the callus to a new medium. Subsequent subculturing of the callus was carried out every three weeks to remove dead callus and separate out homogenous callus to ensure faster growth. By the first four subculturing, loose, friable callus could be observed.

Cell suspension was initiated by transferring 1-2 g of friable callus into a 100 mL culture flask containing 25 mL sterilised culture medium (Table 3.1). The composition of the culture medium was the same as the callus medium but without agar (Table 3.1). The culture was incubated in the dark on a rotary shaker at 100 rpm at 25 °C. Every six days the cell suspension was subcultured by removing dead cells as well as two-thirds of the old medium and replaced with new medium while keeping the ratio of medium to cells at approximately 3:1. To promote faster growth, the cell suspension was either transferred to larger culture flasks (250 mL) or distributed between several 100 mL culture flasks after every three subcultures. All cell culture techniques including the induction of callus were performed under sterile conditions in a laminar flow cabinet. A schematic overview of the procedure used to establish and maintain cell suspension from tomato leaves is shown in Figure 3.1.

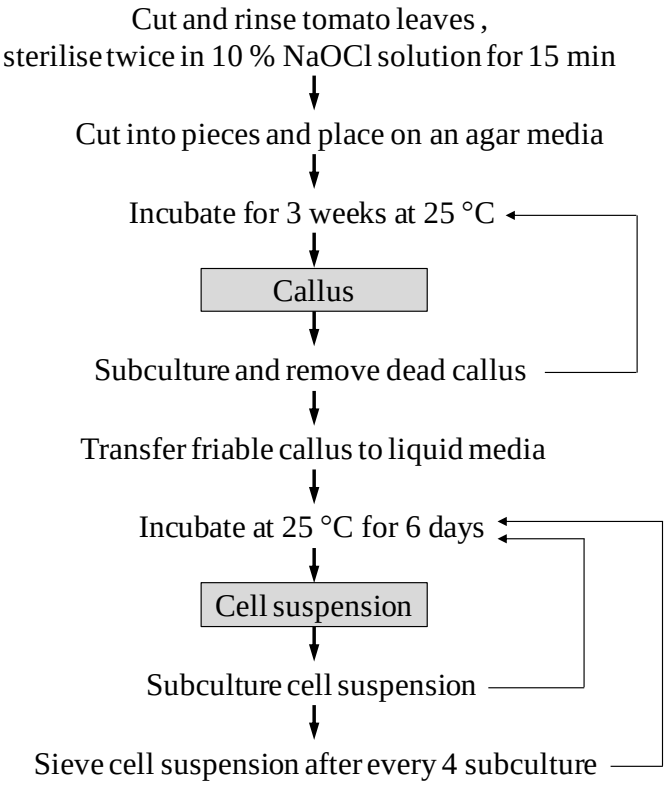

Figure 3.1: A schematic overview of the procedure used to extract and derivatise polar metabolites present in tomato cell suspension.

The growth of the cell suspension was characterised by the release of fine cells into the liquid medium and the formation of cell clumps and aggregates (Evans et al., 2003). To ensure that the cells continued to survive and growth, the medium of the cell suspension was replaced after every six days. To promote faster growth, reproduction and homogeneity, the cell

suspension was sieved with sterile metal sieves of diameters 100, 500 and 900 µm (Saulas, France) after every three subcultures to separate out large clumps.

3.2.2 Characterisation of tomato cell suspension

The growth characteristic of the cell suspension was determined to know the time at which the cell suspension could be harvested for low O_2 studies and to determine the frequency of sub-culturing. For growth analysis, a subcultured 250 mL cell suspension was divided between 25 mL flasks and incubated simultaneously. Every 24 h one 25 mL cell suspension was harvested and analysed for dry weight and counted for the number of cells present.

Dry weight was determined by collecting cells on Buchner vacuum filter containing a pre-weighed filter paper dried to constant weight at 50 °C. After filtration, the filter containing the cells was dried to constant weight at 50 °C and the difference in weight considered the dry weigh of the cells (Evans et al., 2003; Mustafa et al., 2011). Cell counting was determined by hydrolysing 1 mL of cell suspension in an enzymatic solution containing 0.5 mL of 10 % cellulase and 0.5 mL of 1 % pectinase. Cell counting was carried out with a haemocytometer under a microscope after 30 min of incubation at 25 °C (Evans et al., 2003).

The growth behaviour of the cells determined through dry weight and cell counting is shown in Figure 3.2. The cell suspension exhibited a lag phase of between two to three days before cell density started to increase. The stationary phase of growth was reached after about ten days of incubation. The tomato cell suspension had a growth pattern similar to what has been observed in most cell culture studies of tomatoes (Felix et al., 1991; Robertson et al., 1995) and other plants like carrots (Kanabus et al., 1986) and *Arabidopsis* (Tjellström et al., 2012). The cell suspension growth was characterised by a distinct lag phase, followed by linear period of growth and a slowing down of growth (stationary phase).

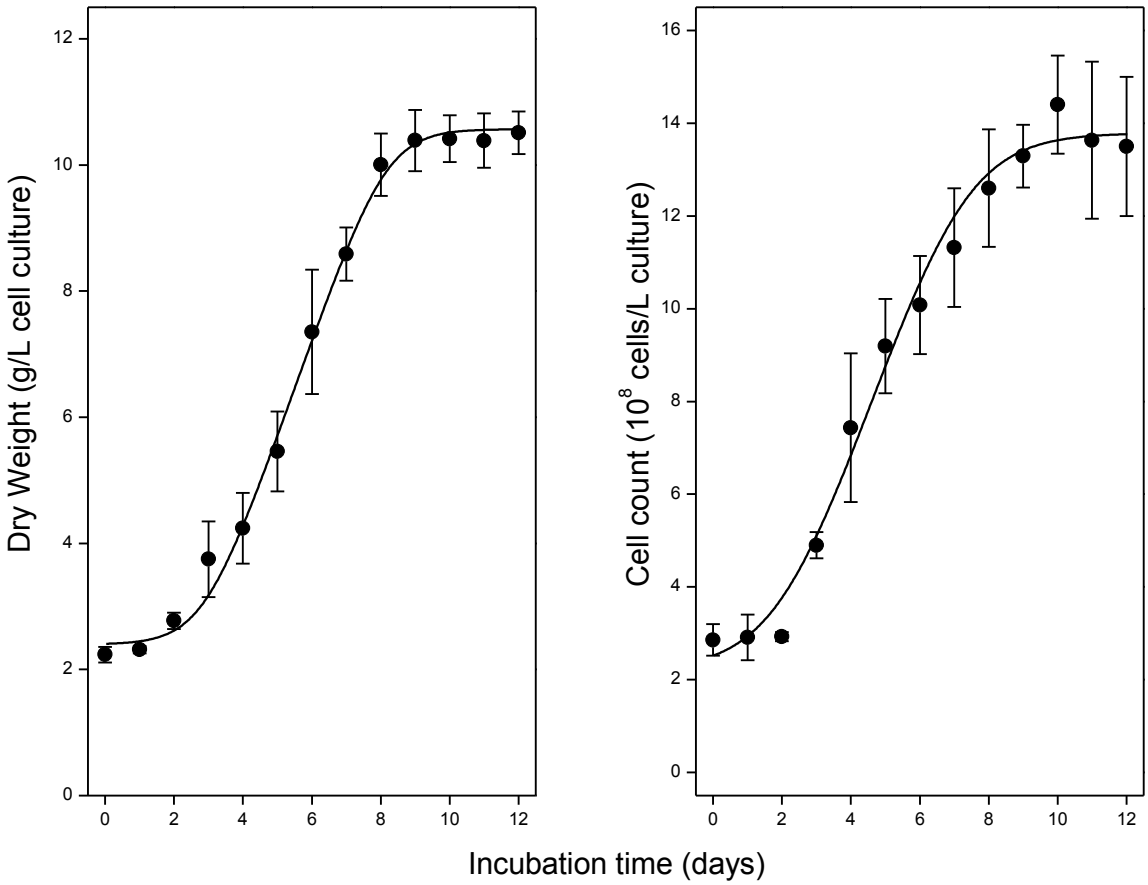

Figures 3.2: Growth of tomato cell suspension determined through dry weight and cell count analysis. Measurement is the mean of three independent biological experiments ± sd. The growth curve was obtained by fitting the data points with the growth model of Baranyi and Roberts (1994).

To further characterise the cell suspension, the biomass (proteins, lipids, soluble metabolites, and starch) composition of the cells was determined in the linear phase of growth. Before biomass analysis, cells were washed with glucose free medium, quenched with liquid nitrogen and lyophilised (Duratop and Duradry, FTS Systems Inc., Stone Ridge, NY, USA) for 24 h and dried for further 24 h in an oven at 50 °C. The soluble metabolite content was determined by extracting 10 mg dried cells with methanol at 70 °C for 15 min. After extraction, the methanol was dried off under a stream of nitrogen gas. The pellet was further dried to a constant weight in an oven at 50 °C and the weight of the pellet considered the soluble metabolite content of the cells (Williams et al., 2008). The lipid fraction of the cells was determined by weighing 10 mg dried cells into a dried filter paper and extracting the lipids present in the cells with hexane at 60 °C for an hour. The lipid content of the cells was expressed as the difference in weight of the cells after extraction and drying the to a constant weight at 50 °C (Sriram et al., 2006). The starch content of the cells was determined by enzymatic hydrolysis of starch with α-amylase and amyloglucosidase to glucose. The glucose

present in the cells before and after the enzymatic hydrolysis was analysed and the difference used to determine starch content (Rontein et al., 2002). Total protein was extracted with a phosphate buffer and analysed using the Bio-Rad DC (detergent compatible) protein assay with bovine serum albumin as standard (Amoako-Andoh et al., 2014). The amount of cell wall material present in the cell suspension was calculated from the difference in other biomass measurements. Figure 3.3 shows the biomass composition of the cells. The cells had a lipid, starch, protein and soluble metabolite content of 10.4, 2.8, 20 and 14 %, respectively.

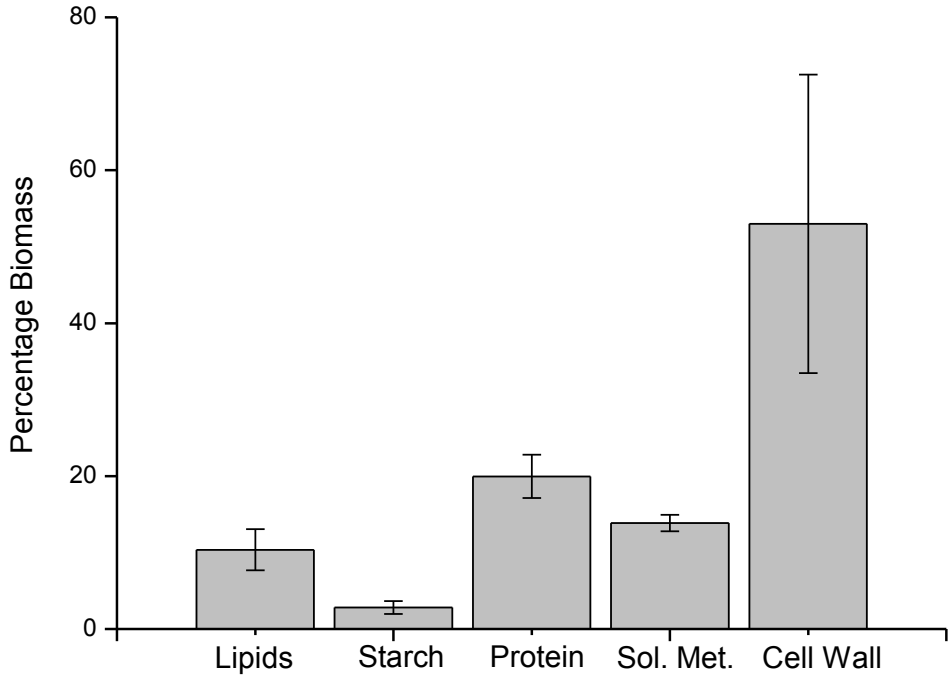

Figure 3.3: Biomass composition of the tomato cell suspension used for low O_2 stress studies. The error bars represent the standard deviation of three independent biological replicate experiments. Sol. Met.: soluble metabolites.

3.2.3 Cell suspension for low oxygen stress studies

For low O_2 studies and ^{13}C-labelling experiments, the substrate for the growth of the cell suspension was changed from sucrose to glucose. This change in substrate was performed at least four residence times (one residence time is the period between two subcultures) before the low O_2 experiment. This change in substrate was necessary due to the fact that autoclaving the glucose media resulted in the breakdown of glucose, leading to its inability to support the growth of the cells.

Sterilisation of glucose culture media was, therefore, carried out by preparing 900 mL of the medium without glucose and autoclaving in glass bottles at 121 °C for 15 min. 30 g of

glucose was dissolved in 100 mL of sterile distilled water and sterilised by filtration (Millex syringe filter unit with 0.2 µm pore size and 25 mm diameter). The sterilised glucose solution was added to the autoclaved glucose-free medium at room temperature under sterile conditions.

Low O_2 stress experiments were carried out in the Lambda Minifor bench-top laboratory bioreactor (Lambda Laboratory Instruments, Czech Republic) (Figure 3.4). The bioreactor had a base dimension of 22 x 40 cm with an incubation vessel made from Pyrex glass with a working volume of 35-400 mL. The base of the vessel consisted of double-jacketed glass enabling temperature to be controlled with a constant stream of water from a water-bath. The vessel could be sterilised in an autoclave. Agitation in the bioreactor was achieved using a "vibromixer", which moves one or more stirring disk up and down ensuring efficient mixing and aeration. The bioreactor was equipped with an automatic pH control unit. Deviations from set pH values were corrected by the action of peristaltic pumps which added either acid or base to restore the pH to the set value.

Figure 3.4: The Lambda Minifor bench-top laboratory bioreactor (Lambda Laboratory Instruments, Czech Republic) used for carrying out low O_2 stress experiments.

The O_2 level used for low O_2 experiments was achieved by bubbling gas through the cell suspension medium at a constant flow rate with gas from a mixing panel. The gas mixing panel was set to deliver the desired percentage O_2 level with the remainder being nitrogen. The error associated with the set gas level was usually less than one-hundredth of the gas concentration specified in the gas mixing panel. The level of dissolved O_2 in the medium was monitored using a sterilisable Clark-type electrode. A dissolved O_2 level of 8.35 mg/L was

measured when delivering 21 kPa O_2 from the gas mixing panel into the cell suspension maintained at 25 °C.

3.3 Analysis of polar metabolites in tomato cell suspension

3.3.1 Extraction and derivatisation

Cell suspension used for polar metabolite analysis were washed with glucose-free suspension cell media immediately after sampling, snap frozen in liquid nitrogen and stored at -80 °C. The samples were lyophilised (Duratop and Duradry, FTS Systems Inc., Stone Ridge, NY, USA) for 24 h and dried for further 24 h in an oven at 50 °C.

10 mg of the dried cells was extracted at 70 °C in a thermomixer (Eppendorf, Belgium) for 15 min after adding 700 µL methanol in a 2 mL Eppendorf tube. After extraction, an equal volume of water (700 µL) was added and vortexed for 10 s. 325 µL chloroform was added to separate the non-polar fraction and the mixture centrifuged at 14 000 rpm for 5 min. 500 µL of the upper methanol/water mixture was pipetted and 45 µL of 291 ng/µL internal standard (phenyl-β-D-glucopyranoside) was added and dried under a stream of nitrogen gas at 50 °C (Oms-Oliu et al., 2011; Roessner et al., 2000).

For metabolic profiling (*Chapter 4*), the dried cell pellets were derivatised using BSTFA. Prior to derivatisation, oximation was carried at 37 °C by adding 40 µL of 20 mg/mL methoxyamine hydrochloride dissolved in pyridine and incubating for 90 min. Derivatisation was carried out by adding 60 µL of BSFTA and incubating at 37 °C for 30 min (Oms-Oliu et al., 2011; Roessner et al., 2000).

For ^{13}C-MFA (*Chapter 6*), the dried cell pellet was dissolved in 60 µL of 20 mg/mL methoxyamine hydrochloride dissolved in pyridine and incubated at 37 °C for 90 min. 90 µL of N-(tert-butyldimethylsilyl)-trifluoroacetamide (TBDMS) containing 1 % tert-butyldimethylchlorosilane (Sigma, Belgium) was added and samples incubated at 55 °C for 60 min (Metallo et al., 2009). Table 3.4 provides a summary of the conditions used for extraction and derivatisation of polar metabolites in tomato cell suspension.

Table 3.4: Summary of the protocol used for extracting and derivatising intracellular polar metabolites in tomato cell suspension culture. Method 1 was used for analysing metabolites for metabolic profiling while Method 2 was used for metabolites for steady-state MFA.

	Units	Method 1	Method 2
Extraction			
Solvent		Methanol	Methanol
Amount	mL	700	700
Temperature	°C	70	70
Duration	min	15	15
Derivatisation			
Solvent		BSTFA	TBDMS
Amount	µL	60	90
Temperature	°C	37	55
Duration	min	30	60

3.3.2 GC-MS analysis of polar metabolites

Metabolite separation and quantification was carried out on a GC-MS system consisting of a 7890A GC (Agilent Technologies, Palo Alto, CA, USA) and 5975C VL-MSD with triple-axis detector (Agilent Technologies, Palo Alto, CA, USA) equipped with a 9852C automatic liquid sampler (Agilent Technologies, Palo Alto, CA, USA).

Chromatographic separations were carried out on a 30 m DB-5ms capillary column with 0.25 mm internal diameter and 0.25 µm film thickness (Agilent Technologies, Palo Alto, CA, USA) with helium as the carrier gas at a constant flow rate of 1 mL/min. Metabolites eluting from the GC were ionised in an EI at 70 eV. Tuning of the MS was performed using tris-(perfluorobutyl)-amine (CF43), as recommended by the manufacturer. Mass spectra were acquired in the scan mode at 2 scans/s.

The separation of both BSTFA and TBDMS derivatised samples was performed by injecting 1 µL sample into the GC in a split mode with a ratio of 10:1. The sample inlet and interface temperatures were set at 230 °C and 250 °C, respectively, while the ionisation source was adjusted to 230 °C. The GC oven temperature programme consisted of 1 min isothermal

heating at 50 °C followed by a ramp of 10 °C/min to a final temperature of 310 °C with further holding of 13 min. The system was then temperature equilibrated for 5 min at 70 °C before injection of the next sample (Oms-Oliu et al., 2011; Roessner et al., 2000). For the separation of the BSTFA derivatised samples, the GC-MS programme was retention time locked (RTL) to tetracosane (Agilent Technologies Inc., Wilmington, USA). Table 3.5 gives an overview of the parameters used for analysing polar metabolite in the GC-MS. A schematic overview for the GC-MS analysis of polar metabolite in tomato cell suspension using BSTFA derivatisation is shown in Figure 3.5.

Table 3.5: Summary of the GC-MS parameters used for the analysis of polar metabolites in tomato cell suspension.

	Units	**Parameter**
GC		
Carrier gas		He
Flow rate		1
Split ratio	mL/L	10:1
Injection temperature	°C	230
Interface temperature	°C	250
MS		
Ionisation energy	eV	70
Ion source temperature	°C	230
Quadruple temperature	°C	150
Scanning range	m/z	50-600
Scan rate	scan/s	2

3.3.3 Identification and quantification of metabolites

GC-MS chromatograms and mass spectra were evaluated and deconvoluted using the Chemstation (Agilent Technologies Inc., Wilmington, USA) and AMDIS (automated mass spectral deconvolution and identification system) software. Metabolites were identified by comparing their retention times and mass spectra with an in-house library. The library was developed by injecting commercial standards using the same derivation and GC-MS conditions as described above and confirmed with the Agilent Fiehn GC-MS Metabolomics

RTL library (Agilent Technologies Inc., Wilmington, USA). Metabolite abundance was calculated using the manual integration method in Chemstation. The abundance of each metabolite was expressed in relative terms by correcting with the area of the internal standard and the sample weight.

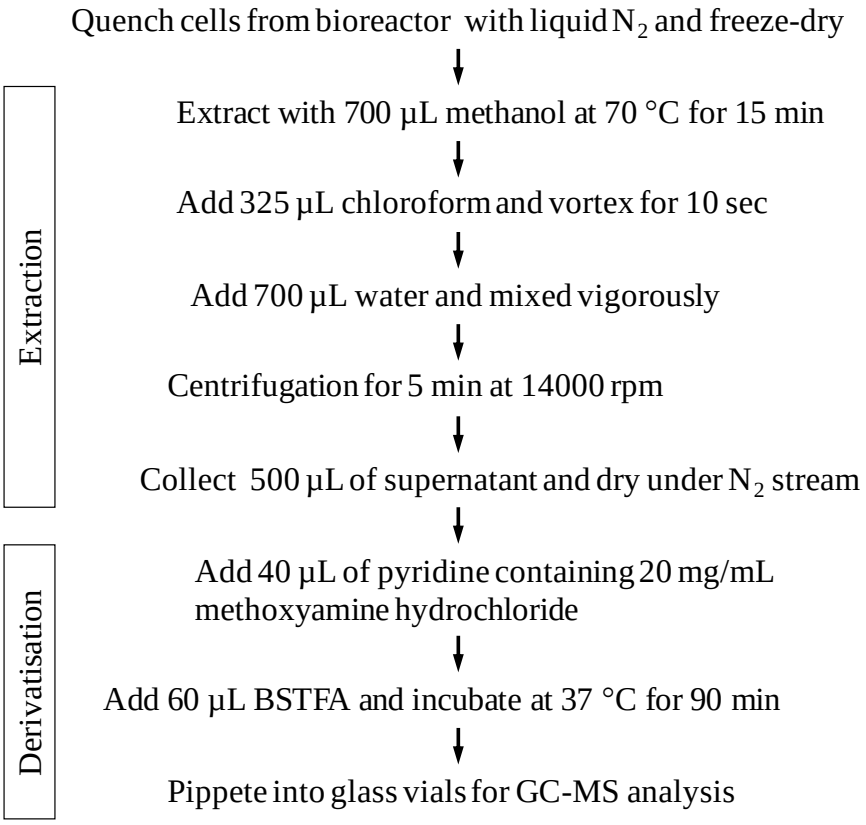

Figure 3.5: A schematic overview of the procedure used to extract and derivatise polar metabolites present in tomato cell suspension.

The absolute abundance of selected metabolites used for MFA (*Chapter 5 and 6*) was determined by establishing calibration graphs using commercial standards. 50 µL solutions of the commercial standards with concentrations of 1, 5, 8, 10, 50, 80 and 100 µg/mL containing 45 µL of 291 ng/µL internal standard (phenyl-β-D-glucopyranoside) were dried under a stream of nitrogen gas, derivatised and analysed using the GC-MS protocol explained in *Section 3.3.1* and *3.3.2*. The absolute concentrations of the metabolites were estimated from the calibration graphs (Appendix 1) based on the standards.

The analysis of tomato cell suspension in the GC-MS based on the conditions described in Table 3.5 took approximately 40 min. The total ion chromatogram (TIC) (Figure 3.6) upon deconvolution revealed patterns in the separation of the metabolites. Metabolites were

separated based on their polarity and molecular weight after the derivation. The less polar metabolites eluted faster than the highly polar metabolites which had high molecular weights.

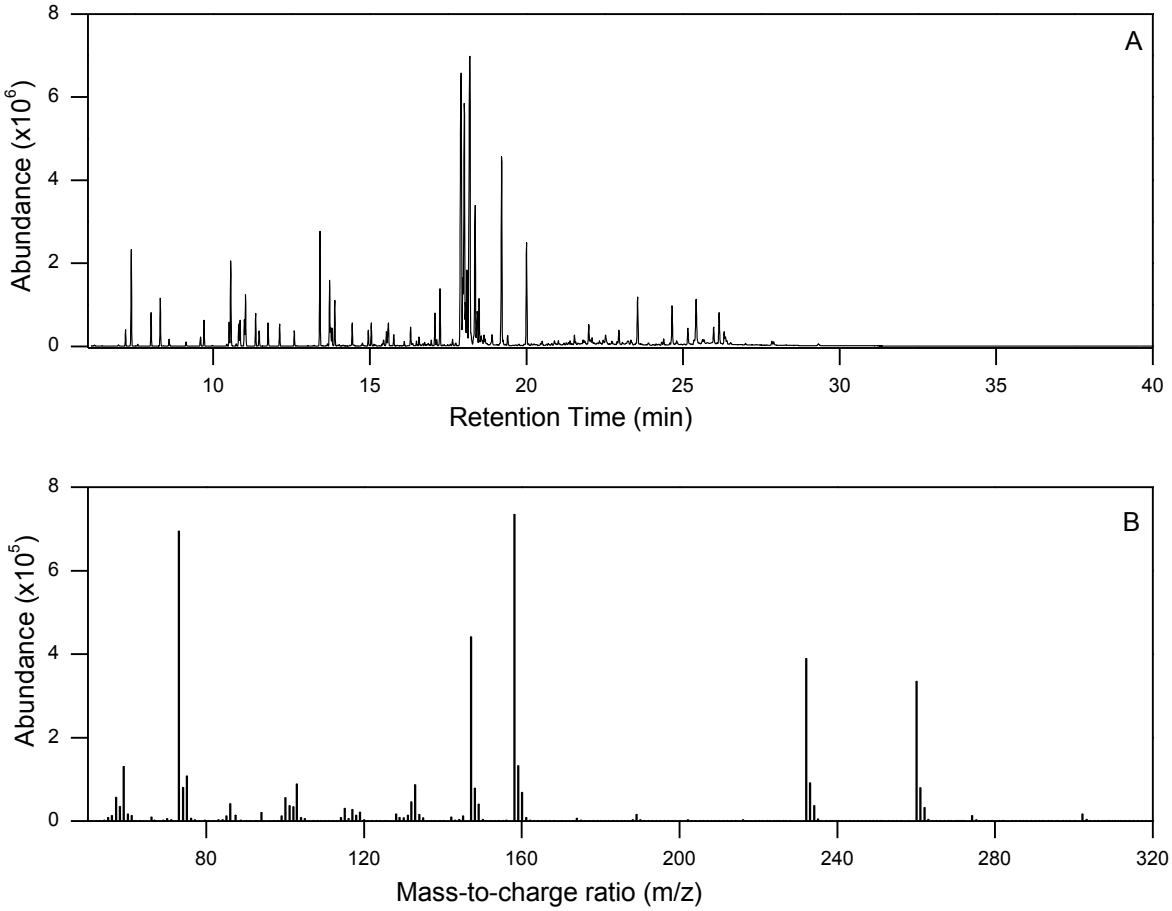

Figure 3.6: A TIC of BSTFA derivatised samples (A) and a representative mass spectrum of alanine (B) obtained by separating polar metabolites present in tomato cell suspension using GC-MS.

In general, two-to-four carbon metabolites like glycine, alanine, serine, GABA, and malate eluted within the 7-18 min time window (Figure 3.7A), while five- and six-carbon sugars like ribose, glucose, fructose, mannose and galactose eluted within the 18-19 min time window. Disaccharides such as sucrose, maltose and trehalose as well as highly polar metabolites such as chlorogenate eluted within the 19-30 min time window (Figure 3.7B). The phosphorylated six-carbon sugars such as fructose-6-phosphate and glucose-6-phosphate also eluted within the 19-30 min time window (Figure 3.7B).

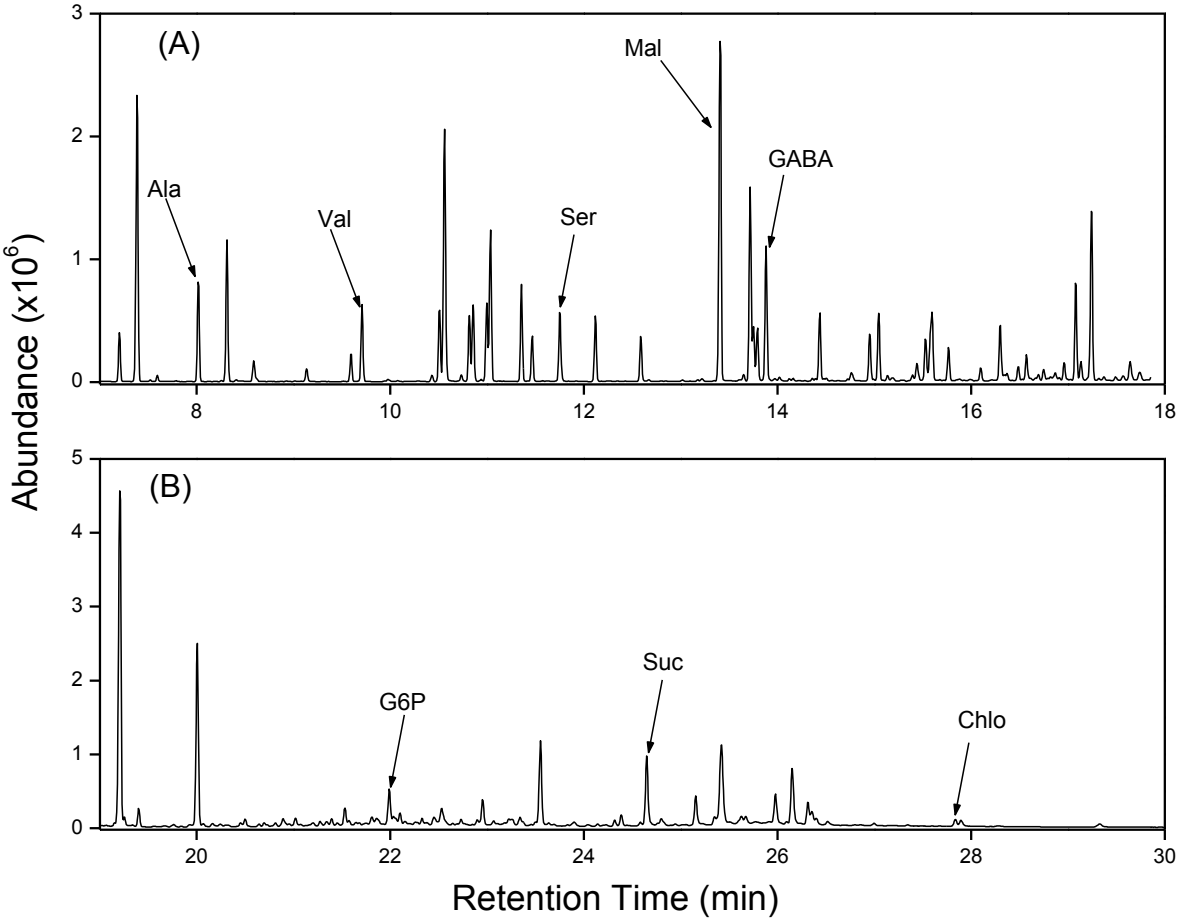

Figure 3.7: An expanded TIC of tomato cell suspension showing the separation of peaks from 7-18 min (A) and 19-30 min (B) with some selected metabolites shown within the specified time window (Ala, alanine; Chlo, chlorogenate; GABA, γ-aminobutyric acid; G6P, glucose-6-phosphate; Mal, malate; Ser, serine; Suc, sucrose; Val, valine).

A total of 70 polar metabolites could be identified and their abundance estimated in the tomato cell suspension (Table 3.6). The 70 identified metabolites included 22 amino acids, 26 organic acids including 5 fatty acids, 19 sugars including 6 sugar alcohols and 3 other compounds. The total number of metabolites which were detected in the cell suspension is comparable to the 52 compounds identified in tomato fruits (Oms-Oliu et al., 2011) and 64 metabolites analysed in tomato leaves (Schauer et al., 2005) using similar extraction and derivatisation protocols. GC-MS metabolite analysis of different plant cell suspensions has also revealed similar metabolites identified with this protocol. Baxter et al. (2007) detected 50 polar metabolites in cell suspension of *Arabidopsis* (ecotype *Landsberg erecta*) while 68 polar metabolites were detected in *Arabidopsis* T87 cultured cells (Fukusaki et al., 2006). GC-MS polar metabolite analysis of cell suspension of *Taxus cuspidata* resulted in the identification of 65 polar metabolites (Han and Yuan, 2009).

Table 3.6: Polar metabolites determined in tomato cell suspension.

Amino acids	Organic acdis	Sugars	Others
β-alanine	2-ketoglutarate	Erythritol	Glycerol-3-phosphate
Alanine	2-ketogulonate	Fructose	Putrescine
Aspartate	3-phosphoglycerate	Fructose-6-phosphate	Urea
Cysteine	Benzoate	Galactose	
Glutamate	Chlorogenate	Glucose-6-phosphate	
Glutamine	Citramalate	Glycerol	
Glycine	Citrate	Inositol	
Histidine	Dehydroascorbate	Lyxose	
Homoserine	Fumarate	Maltitol	
Isoleucine	GABA	Maltose	
Leucine	Glucarate	Maltose	
Lysine	Gluconate	Mannitol	
Methionine	Glycerate	Mannose	
Norleucine	Lactate	Raffinose	
Ornithine	Laurate	Ribose	
Phenylalanine	Malate	Sorbitol	
Proline	Maleate	Sucrose	
Pyroglutamate	Malonate	Tagatose	
Serine	Myristate	Trehalose	
Threonine	Palmitate		
Tyrosine	Phosphate		
Valine	Pyruvate		
	Quinate		
	Shikimate		
	Stearate		
	Succinnate		

The effectiveness of the GC-MS protocol in analysing polar metabolites present in tomato cell suspension was assessed by analysing the efficiency of the extraction process, the reproducibility of the method, the linearity of the GC-MS range and the carryover of metabolites between subsequent GC-MS runs. The reproducibility of the GC-MS method was

tested by extracting, derivatising and injecting six samples, each weighing 10 mg from a batch of tomato cell suspension and estimating the variation between the metabolite abundance (Table 3.7). The linearity of the GC-MS response was assessed by injecting a dilution series of commercial standards within a concentration range of 1-100 µg/mL. The peak area of each metabolite was calculated and linear correlation coefficients estimated in the analysed concentration interval (Table 3.7).

To assess the efficiency of the extraction process, a known concentration (250 µg/mL) of commercial standards was added to 10 mg tissue sample. After extraction and GC-MS analysis, extraction efficiency was calculated using the abundance of the metabolites in both spiked and un-spiked samples. The carryover of metabolites between subsequent GC-MS runs was assessed by injecting sample blanks between GC-MS runs.

The efficiency of the extraction and derivation process which was determined through recovery experiments showed that more than 85 % of the polar metabolites within tomato cell suspension were extracted and analysed with the protocol developed. Similar extraction efficiencies have been reported when using GC-MS to analyse polar metabolites in plants (Roessner et al., 2000; Shepherd et al., 2007). The reproducibility of the GC-MS method, which was assessed based on the variation in the peak area upon the analysis of a batch of cell suspension showed the variation introduced by the extraction, derivations and GC-MS analysis was less than 8 %. When analysing polar (Roessner et al., 2000) and non-polar metabolites (Lytovchenko et al., 2009) present in potato tubers using similar extraction and derivatisation protocols, similar variations were introduced by the experimental procedure.

The analysis of blank samples revealed that the carryover of samples between subsequent GC-MS runs was not present as metabolite peaks could not be detected in the TIC. With respect to the linearity range of the GC-MS, distorted peaks were observed when metabolite standards of concentration above 100 µg/mL were injected. The linearity range was therefore estimated within the metabolite concentration of 1-100 µg/mL. Within the range linearity range, high correlation coefficients were estimated after the injection of standards (Table 3.7).

To determine whether the cells released metabolites into the medium during their growth, 10 mL of the growth media was analysed with the GC-MS after derivatisation. No peaks were detected in the GC-MS chromatogram after analysis showing that the cells did not secrete metabolites into medium.

Table 3.7 Validation of the GC-MS method- linearity, reproducibly and recovery of some selected metabolites

Metabolite	Linearity (R^2)	Reproducibility (% Variance)	Extraction efficiency (%)
2-ketoglutarate	0.99	5.85	85
3-phosphoglycerate	1.00	5.65	96
Alanine	0.98	4.59	98
Aspartate	0.98	2.65	92
Citrate	0.94	5.55	94
Fructose-6-phosphate	0.95	6.25	86
Fumarate	0.97	3.25	95
Glucose-6-phosphate	0.94	7.54	94
Glutamate	0.98	4.55	98
Lactate	0.98	6.25	94
Malate	0.98	3.65	96
Pyruvate	1.00	7.25	89
Serine	0.95	4.65	94
Succinate	1.00	7.55	93
Sucrose	0.98	6.88	89
Valine	0.95	5.69	93

3.3.4 Quantification of ^{13}C-label in polar metabolites

Under conditions that the cell suspension was incubated on a media containing ^{13}C-glucose, the ^{13}C-label accumulated by the different metabolites was quantified in addition to the metabolite abundance. From a mass spectrum (Figure 3.8), the total amount of ^{13}C-label accumulated by a metabolite fragment, also termed sum fractional labelling (SFL), as well as its MID could be estimated.

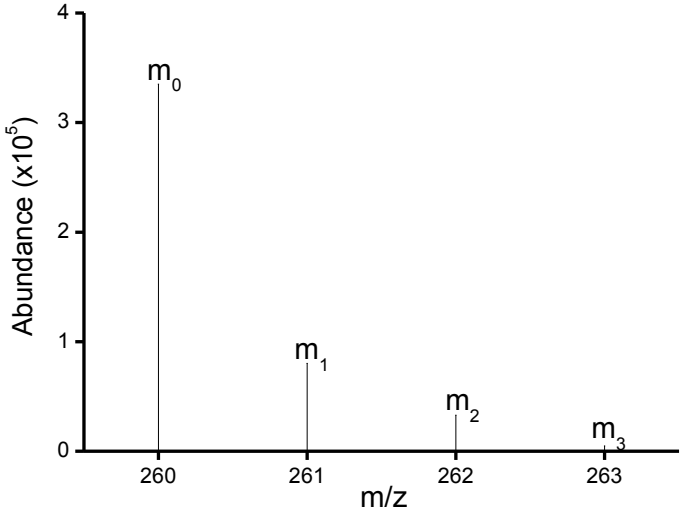

Figure 3.8: A portion of a mass spectrum of a three-carbon metabolite used to demonstrate the procedure for estimating MID and SFL.

MID was estimated by exporting the mass spectral data and calculating the ratios of the molecular ion peak and/or any other ion fragment of the carbon skeleton of the metabolite (Eq. 3.1). The mass spectrum was integrated over the full peak range of the metabolite and the SFL was estimated based on isotopic ratios (Eq. 3.2).

$$MID = \frac{m_i}{\sum_{0}^{3} m_i} \qquad \text{(Eq. 3.1)}$$

$$SFL = \frac{0 \cdot m_0 + 1 \cdot m_1 + 2 \cdot m_2 + 3 \cdot m_3}{m_0 + m_1 + m_2 + m_3} \qquad \text{(Eq. 3.2)}$$

The estimated MID was corrected for the presence of naturally occurring isotopes of carbon and other elements (Wahl et al., 2004). The calculation of MID and correcting MID for the presence of naturally abundant isotopes was performed in the MSTool, a MatLab based isotope correction software (Wahl et al., 2004). The label accumulated by 47 polar metabolites could be estimated after performing ^{13}C-label feeding experiments and derivatisation of the extracted metabolites with BSTFA. The inability to estimate ^{13}C-label in other metabolites besides the 47, was due to the fact that the molecular ion peak associated with these metabolites could not be detected in the mass spectrum due to complete

fragmentation in the MS. Also, the other ions produced upon fragmentation did not contain the carbon backbone of the metabolite making the quantification ^{13}C-label impossible.

The analysis of polar metabolites in tomato cell suspension in this thesis was carried out using two GC-MS based derivatisation methods. This was done in order to achieve the objectives of measuring the metabolomics and fluxomics response of the tomato cell suspension to low O_2 stress. BSTFA was used to derivatise for metabolic profiling while TBDMS was the preferred derivatisation method for steady-state MFA. BSTFA is a broad spectrum derivatisation agent which can be used to derivatise and identify metabolites belonging to different chemical groups. BSTFA is, therefore, suitable for performing metabolic profiling as metabolites belonging to the functional groups of organic acids, amino acids and sugars can be derivatised. BSTFA is, however, unsuitable for the quantification of ^{13}C-label for MFA especially under steady-state conditions due to the need to measure multiple ion fragments to ensure the elucidation of the complete isotopomer distribution. To overcome this limitation, TBDMS, which is more specific for derivatising amino acids and organic acids which occur in high concentrations, was used. TBDMS produces ion fragments which are much easier to identify and quantify making it suitable for the analysis of isotopomers needed for MFA after performing ^{13}C-label feeding experiment.

3.4 Conclusions

A protocol for the analysis of polar metabolites, as well as an in-depth methodology for the establishment of tomato cell suspension has been described. The formation of cell suspension started from the induction of callus from leaves of tomato. The callus formed was used to initiate cell suspension. Polar metabolites present in the cells were separated and detected on the GC-MS after methanolic extraction and derivatisation. A method for the quantification of ^{13}C-label present in the polar metabolites was also developed. The established GC-MS method could reliably detect and quantify over 70 polar metabolites in tomato suspension including amino acids, organic acids, sugars and other hydrophilic metabolites.

Chapter 4

Metabolic Profiling of the Response of Tomato Cells to Low Oxygen

4.1 Introduction

Measuring the biochemical changes in plants is important in understanding their response to low O_2. Among the observed responses that have been noted in plants subjected to different low O_2 conditions include decrease in protein synthesis (Bailey-Serres and Freeling, 1990; Drew, 1997), dissociation of polysomes (Bailey-Serres and Freeling, 1990) and an increase in the activity of enzymes involved in anaerobiosis like alcohol dehydrogenase and pyruvate dehydrogenase complex (Andrews et al., 1994; Sachs et al., 1996). In addition, low O_2 conditions have been shown to increase the activities of malic enzyme and pyruvate-phosphate dikinase (Lara et al., 2010) while decreasing the expression levels of proteins involved in energy and antioxidant metabolism (Pedreschi et al., 2007).

Metabolome analysis of the response of plants to low O_2 has shown that some metabolites accumulate, while others deplete under low O_2. Among the metabolites which have been found to accumulate under low O_2 in several plant species are proline, alanine and GABA (Geigenberger et al., 2000; Rocha et al., 2010; van Dongen et al., 2009). Most metabolites

---

The content of this part of the thesis is based on:

Ampofo-Asiama, J., Baiye, V.M.., Hertog, M.L.A.T.M., Waelkens, E., Geeraerd, A.H., Nicolai, B.M., 2014. The metabolic response of cultured tomato cells to low oxygen stress. Plant Biology, 16, 594–606.

involved in radical O_2 scavenging (Franck et al., 2007) and respiratory metabolism (Pedreschi et al., 2009) have been observed to decrease under low O_2. These metabolome studies, however, were limited by the lack of complementary label experiments, making it impossible to determine which pathways are up or down-regulated to account for the observed accumulation and depletion of metabolites. However, considering the deleterious effect of low O_2 stress on plants, it is important to combine metabolome analysis with ^{13}C-label information to give a better insight to the response of plants to low O_2.

The objective of this part of the thesis is to study the metabolome changes that occur in tomato cell suspension when exposed to low O_2 conditions, similar to the conditions experienced by food crops stored under CA. Metabolomics data is complemented with ^{13}C-labelling incorporation making it possible to recognise which pathways are being up-or down-regulated under low O_2. By monitoring the fast changes in metabolite levels and ^{13}C-label incorporation as a function of time, insight is created in the metabolic flexibility of plant cells in adapting to the externally imposed low O_2 condition.

4.2 Experimental procedure

4.2.1 Defining experimental conditions

The O_2 levels used in this experiment were chosen so as to limit respiration in the tomato cell suspension. The Michaelis-Menten constant (K_M) of respiration was used as a guide to select the appropriate O_2 levels. The K_M of respiration was determined by measuring the depletion of O_2 within a biological oxygen monitor and calculating the O_2 uptake rate using Eq. 4.1:

$$\frac{d[O_2]}{dt} = V_{max}\frac{n\times[O_2]}{K_M + [O_2]} \qquad \text{(Eq. 4.1)}$$

where V_{max} [µg/(L x s x 10^6 cells)] is the maximum O_2 uptake rate and n (10^6 cells) is the number of cells placed in the BOM. Using three independent O_2 depletion experiments (Figure 4.1), the rate of consumption of O_2 by the cells was estimated along with the K_M of respiration (Figure 4.2). A K_M of 0.64 (sd of 0.0306) µM corresponding to an O_2 concentration of 0.045 kPa and a V_{max} of 1.805 (sd of 0.0006) µg/(L x s x10^6 cells) was obtained through non-linear least squares parameter estimation. Based on the K_M of respiration, three O_2 levels were chosen for this part of the thesis: an O_2 concentration below

the K_M (0 kPa), an O_2 concentration slightly above the K_M (1 kPa) and 21 kPa O_2 which served as the control.

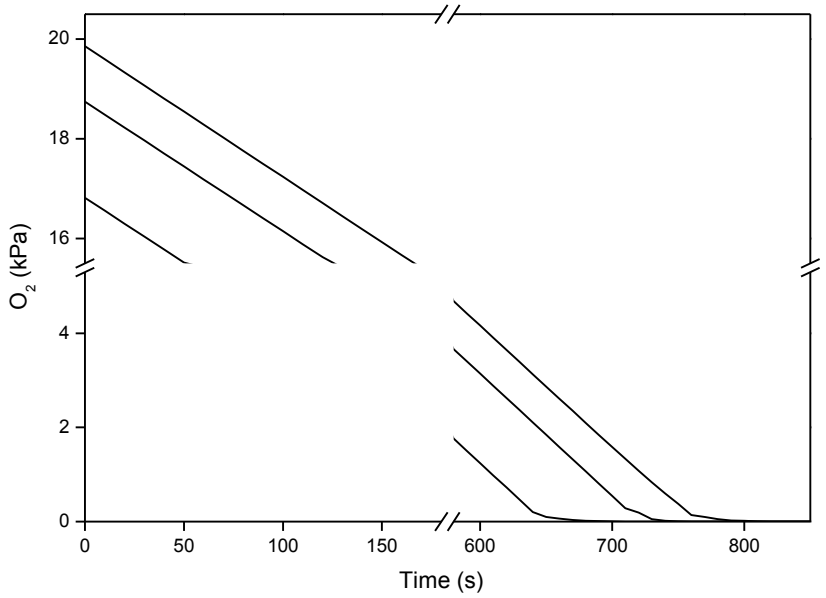

Figure 4.1: Depletion of O_2 within the biological oxygen monitor after bubbling the medium in which the cells were growing with gas containing 21 kPa O_2. The three lines represent the data points of three independent replicate experiments (O_2 levels were recorded within 5 s intervals).

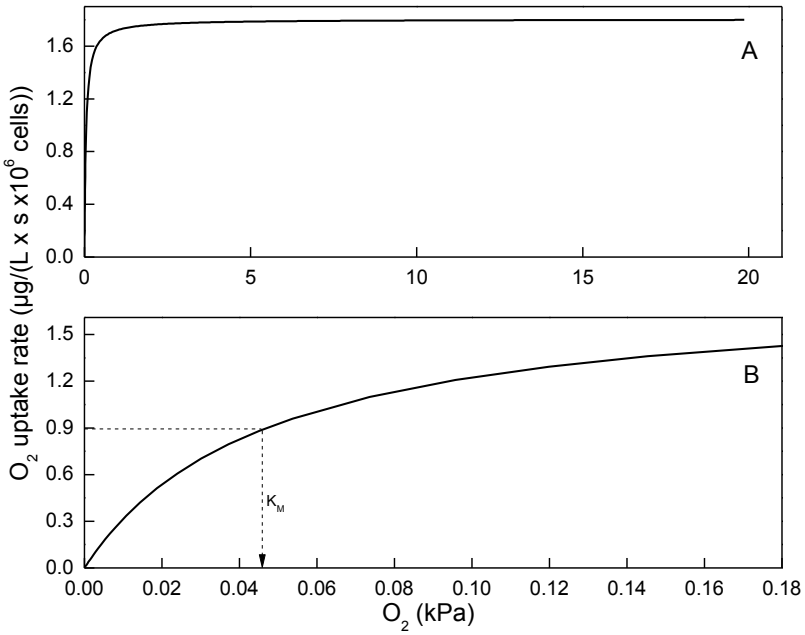

Figure 4.2: Estimation of the respiration kinetics of cell suspension culture of *Lycopersicum esculentum* (A) Uptake rate of O_2 by tomato cells as a function of O_2 partial pressure (B) A magnified portion of the uptake rate to show the K_M of respiration.

4.2.2 Bioreactor experiments

To determine the effect of low O_2 on the metabolome of the cell suspension, 250 mL cell suspension in the linear phase of growth (five days after sub-culture, Figure 3.2), were transferred to the bioreactor maintained at a temperature of 25 °C. The concentration of glucose in the medium at the time of transfer was 85 mM. The pH of the medium was kept at 6 throughout the experiment and low O_2 was achieved by bubbling gas through the medium at a rate of 10 L/h for the entire duration of the experiment. Four independent replicate experiments per condition were carried out. The cells were allowed to adapt to the prevailing O_2 condition during the first four hours, after which a substrate pulse (10 mL volume) containing ^{13}C-label was added to bring the concentration of glucose to 166 mM without significantly changing the ratio of medium to cells (3:1).

The concentration of ^{13}C-label was adjusted to ensure that 50 % of the total glucose in the medium was U-^{13}C-glucose (uniformly labelled ^{13}C-glucose). Cell samples were taken every hour for the next eight hours and a final sample taken 24 hours from the start of the experiment. Sampling was carried out by withdrawing 15 mL of medium containing cells from the bioreactor. The samples were washed with glucose free medium, frozen in liquid nitrogen and stored at -80 °C. The samples were lyophilised (Duratop and Duradry, FTS Systems Inc., Stone Ridge, NY, USA) for 24 h and dried for further 24 h in an oven at 50 °C.

4.2.3 Metabolite determination and statistical analysis

Polar metabolites present in the cell suspension and ^{13}C-label accumulation were quantified using *Method 1* of the GC-MS protocol explained in *Chapter 3*. Univariate statistical analysis was performed to identify the difference between the levels of metabolites under the three O_2 levels at the different time points using Origin 8 (v 8.0725, OriginLab Corporation, Northampton, USA). The difference among means was identified using the t-test with a significance level of $p = 0.05$. Multivariate statistical analysis was performed in The Unscrambler (v.10.2, CAMO A/S, Trondheim, Norway) using PLS-DA (Pedreschi et al., 2009) to identify which metabolites change significantly in response to low O_2. In PLS-DA, the different O_2 growth conditions were considered categorical Y-variables with the metabolite abundance as X-variables. The data was mean centered and the variables given equal variance.

4.3 Results

4.3.1 Early changes in response to low oxygen

The metabolome of cultured tomato cells was affected by the induction of low O_2. Different concentrations of dissolved O_2 in the growth medium of cultured tomato cells clearly lead to different levels for most primary metabolites (Figure 4.3 and Appendix 2A). Sharp increases (more than two fold increase compared to the control) were observed in the levels of fructose-6-phosphate, glucose-6-phosphate, lactate and pyruvate with seemingly steep reduction (about 50 %) in maltose, L-dehydroascorbate and tyrosine within the first hour of cells incubated at 1 and 0 kPa O_2 levels (Figure 4.3). Increases in glucose-6-phosphate and fructose-6-phosphate also occurred in cells incubated under control conditions, yet these were significantly less than those observed at the low O_2 conditions. Mannitol and sorbitol also increased significantly within the first hour under both low O_2 conditions (Figure 4.3). With the exception of erythritol and glycerol-3-phosphate (Appendix 2A) which did not change significantly within the first hour under low O_2, almost all the other metabolites decreased. From the second to the fourth hour, all the metabolites continued either their increasing or decreasing trend under low O_2, with the exception of 3-phosphoglycerate and gluconate that started to increase after the third and second hour, respectively.

4.3.2 Effect of adding ^{13}C-glucose

The addition of a small amount of media saturated with ^{13}C-glucose (at 4 h) changed the levels of metabolites in both the control and the low O_2 cells (Figure 4.3 and Appendix 2A). In the control cells, the levels of most metabolites started to increase and, after 12 hours of incubation, reached levels higher than the starting point (Appendix 2A). However, the levels of β-alanine, benzoate, L-dehydroascorbate and homoserine decreased within one hour after the addition of ^{13}C-labelled glucose (so at 5 h). Some metabolites (benzoate, chlorogenate, erythritol, GABA, galactose, gluconate, glycerol, glycerol-3-phosphate, isoleucine, lactate, maltitol, maltose, mannitol, proline, quinate, ribose, sorbitol, stearate and urea) were less abundant after 12 h of incubation compared to 0 h. In the low O_2 cells, the response to the extra glucose included a reduction in the rate of decline of those metabolites which were already decreasing within the first four hours of low O_2. Small increases in the levels of some metabolites (alanine, cysteine, galactose, glutamate, glutamine, isoleucine, leucine, phenylalanine, succinate, stearate, trehalose and urea) were observed between 5 h and 6 h,

even though these metabolites started to decrease thereafter (Appendix 2A). The levels of metabolites like norleucine, and mannose seem not to be affected by either the induction of low O_2 or the addition of ^{13}C-glucose.

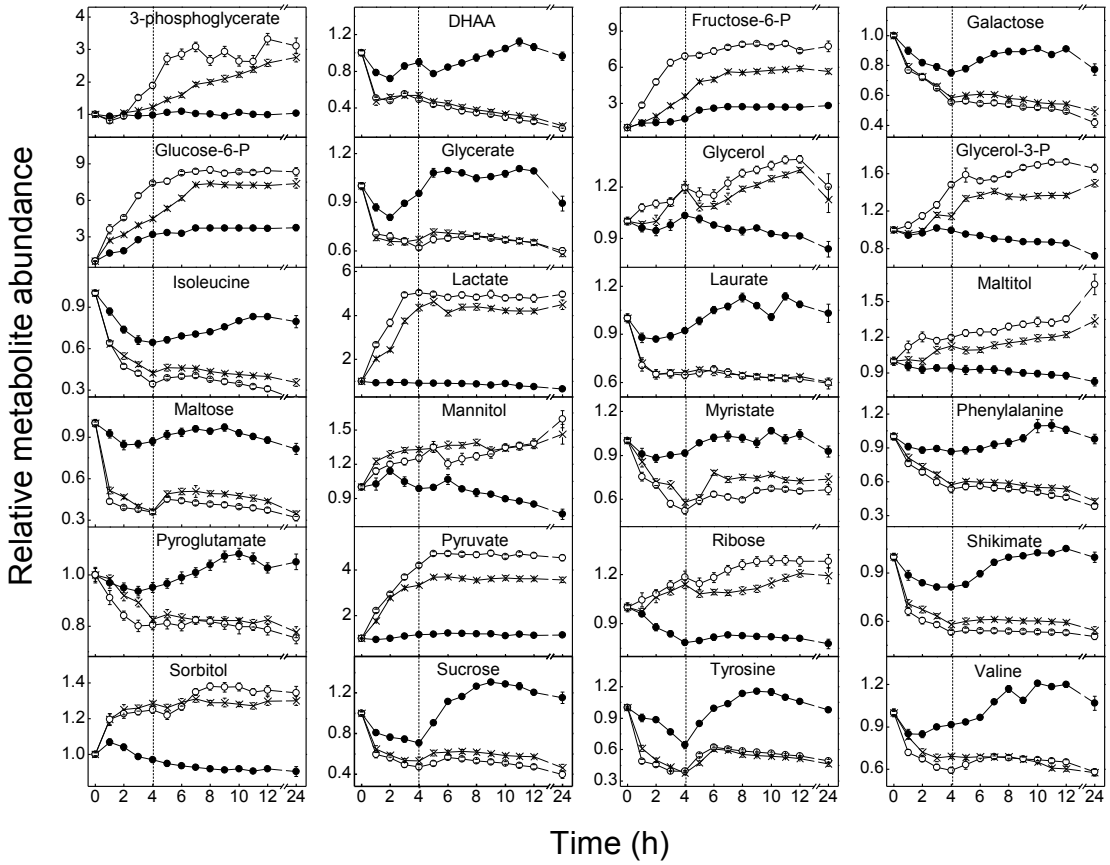

Figure 4.3: A plot of the 24 most altered metabolites out of the total of 63 reported in Appendix 2A following the incubation of tomato cell suspension cultures under different O_2 levels [21 kPa (●), 1 kPa (x) and 0 kPa (○)]. Metabolites are ordered alphabetically (DHAA, L-dehydroascorbate; Fructose-6-P, fructose-6-phosphate; glucose-6-P, glucose-6-phosphate). All values are means of four independent biological replicates expressed relative to starting value. Error bars indicate the standard error of the mean (sem). The dashed lines indicate the time point where ^{13}C-labelled glucose was added.

4.3.3 Fast ^{13}C-label incorporation

^{13}C-label was incorporated into the different metabolites after the addition of ^{13}C-glucose at 4 h (Figure 4.4 and Appendix 2B). In the control cells, ^{13}C-label could be detected in the metabolites one hour after the addition. For the metabolites involved in glycolysis, a fast build-up of ^{13}C label was observed, reaching steady-state labelling levels after a few hours. ^{13}C-label accumulation by other metabolites occurred more slowly often not reaching steady-

state levels within the time frame of the experiment. The rate of ^{13}C-label accumulation into the different metabolites was dependent on the metabolic proximity to the supplied substrate and the need for the cell to synthesise or utilise the metabolites involved. For instance, glucose-6-phosphate and fructose-6-phosphate (Figure 4.4) were labelled close to the maximum level of 50 % within three hours after the label addition while isoleucine apparently even had not reached its maximum labelling eight hours after the addition. Low O_2 affected the accumulation of ^{13}C-label by the cells. Compared to the control, the accumulation of ^{13}C-label in most metabolites was low under both low O_2 conditions. Metabolites which, compared to the control, accumulated more or about the same ^{13}C-label under both low O_2 conditions included glycerate, glycerol, glycerol-3-phosphate, lactate, mannitol, ribose and sorbitol (Figure 4.4).

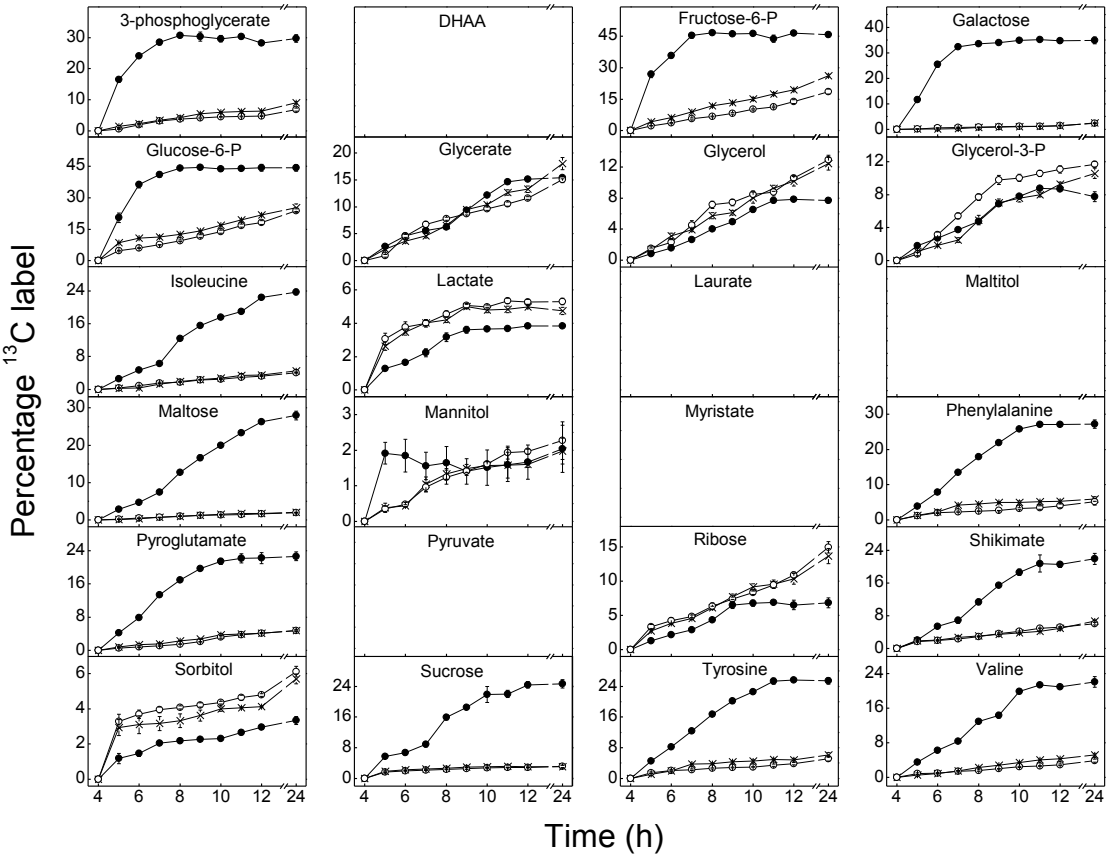

Figure 4.4: Accumulation of ^{13}C-label by the metabolites shown in Figure 4.3 with the exception of DHAA, laurate, maltitol, myristate and pyruvate whose ^{13}C-label data could not be obtained. All values are means of four independent replicates. Error bars indicate the sem. Labels are 21 kPa (●), 1 kPa (x) and 0 kPa (○). The time axes starts from 4 hours, the point at which ^{13}C-labelled glucose was introduced.

Comparing the two low O_2 conditions, the metabolites which were more abundant under 0 kPa O_2 compared to 1 kPa O_2 in more than seven sampling time points before and after the addition U-^{13}C-glucose included 3-phosphoglycerate, fructose-6-phosphate, glucose-6-phosphate, glycerol, glycerol-3-phosphate, lactate, maltitol, pyruvate and ribose (Figure 4.3). In contrast, 2-oxoglutarate, citrate, chlorogenate, isoleucine, leucine, malonate, succinate, serine and shikimate were more abundant in 1 kPa than 0 kPa O_2 in more than seven sampling time points (Appendix 2A). No metabolite accumulated significantly higher ^{13}C-label under 0 kPa O_2 compared to 1 kPa O_2 in more than seven time points (Appendix 2B). Only GABA, glutamate, fructose-6-phosphate and glucose-6-phosphate accumulated more ^{13}C-label under 1 kPa O_2 compared to 0 kPa in more than seven sampling time points (Appendix 2B).

4.3.4 Changes after 24 hours of low oxygen induction

The metabolites continued to change when incubated for a further 12 hours under low O_2 (Figure 4.3 and Appendix 2A). With the exception of the intermediates of glycolysis, glycerol-3-phosphate, lactate, maltitol, mannitol, sorbitol and ribose which increased and reached peak levels within the first twelve hours (Figure 4.3), all other metabolites continued to decline under low O_2 stress. With respect to ^{13}C-label accumulation, cells exposed to low O_2 continued to increase their ^{13}C-label content, albeit slowly except for sucrose, lactate and urea (Figure 4.4 and Appendix 2B). Under 21 kPa O_2, no further increase in ^{13}C-label was observed in the metabolites involved in the central carbon metabolism (3-phosphoglycerate, citrate, fructose-6-phosphate, fumarate, glucose-6-phosphate, malate and succinate), indicating that isotopic steady-state had been reached within 24 hours of incubation. The ongoing accumulation of ^{13}C-label by cells exposed to the two low O_2 conditions shows that isotopic steady-state was not reached within the experimental duration. A metabolic network map showing the effects of low O_2 on the central carbon metabolism and associated pathways in cultured tomato cells after 24 hours of incubation can be seen in Figure 4.5.

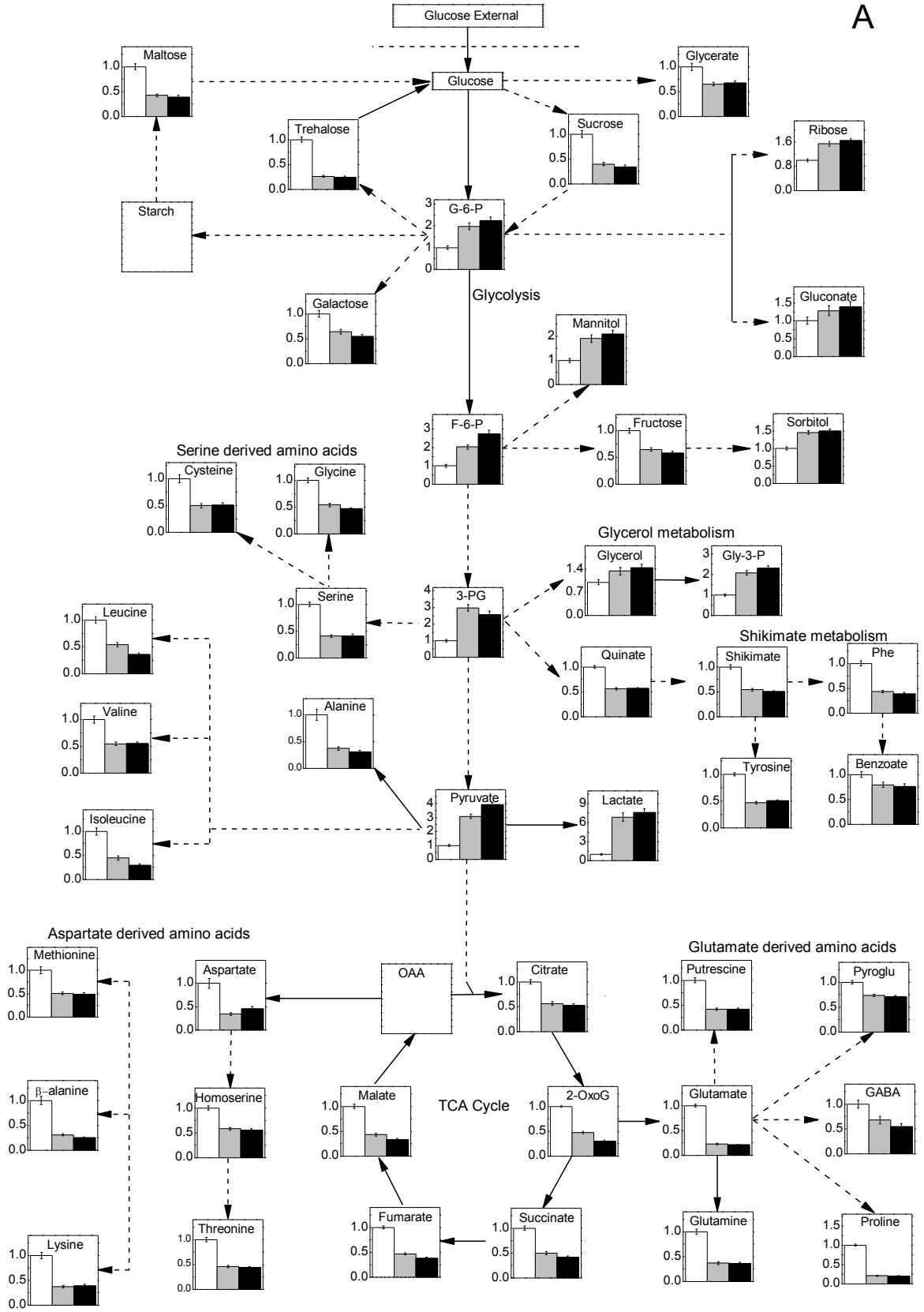
A
Glucose External
Maltose
Glucose
Glycerate
Trehalose
Sucrose
Ribose
Starch
G-6-P
Glycolysis
Galactose
Mannitol
Gluconate
F-6-P
Fructose
Sorbitol
Serine derived amino acids
Cysteine
Glycine
Glycerol metabolism
Glycerol
Gly-3-P
Serine
3-PG
Leucine
Quinate
Shikimate metabolism
Shikimate
Phe
Valine
Alanine
Tyrosine
Benzoate
Pyruvate
Lactate
Isoleucine
Aspartate derived amino acids
Glutamate derived amino acids
Methionine
Aspartate
OAA
Citrate
Putrescine
Pyroglu
β-alanine
Homoserine
Malate
TCA Cycle
2-OxoG
Glutamate
GABA
Fumarate
Succinate
Glutamine
Proline
Threonine
Lysine

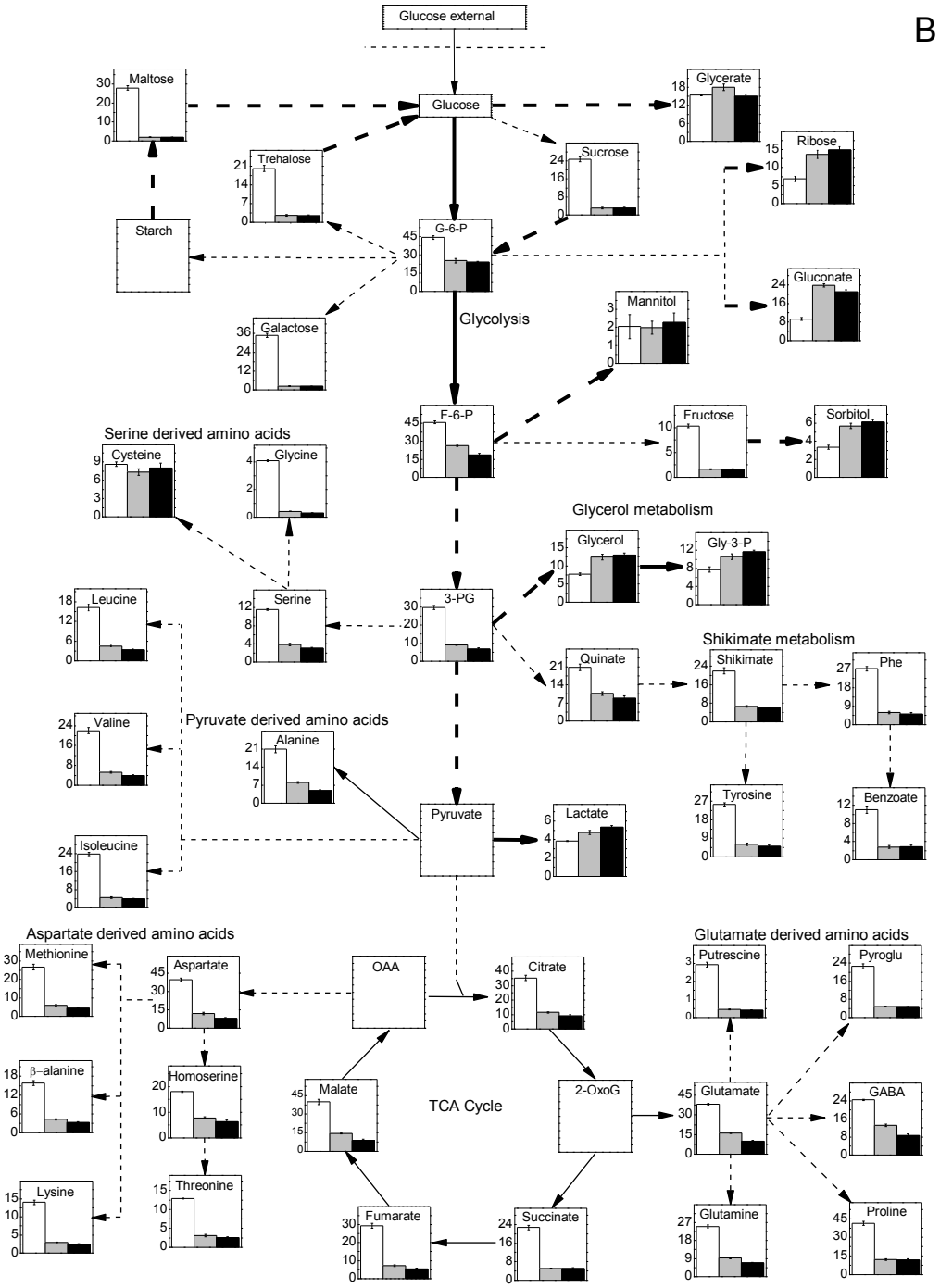

Figure 4.5 (A) Metabolic network map showing the changes in relative abundance after 24 h of incubating tomato cell culture under different O_2 levels. (B) Metabolic network map showing the accumulation of ^{13}C-label by the different metabolites with the thickness of the arrows increased for pathways which are up-regulated under low O_2. The white, gray and dark bars represent 21 kPa, 1 kPa and 0 kPa O_2 levels, respectively. All values are means of four independent replicates expressed relative to starting value. Error bars indicate sem. Abbreviations: 2-OxoG, 2-oxoglutarate; 3-PG, 3-phosphoglycerate; OAA, oxaloacetate; Phe, phenylalanine; Pyroglu, pyroglutamate.

4.3.5 Global metabolomic changes in tomato cells due to low oxygen

The relationship between metabolite abundance, O_2 level and incubation time was evaluated to identify those metabolites that change significantly in the low O_2 response using PLS-DA. A plot of metabolite and treatment correlation loadings superimposed on the sample scores can be found in Figure 4.6. PLS-DA aims to reduce the multivariate metabolite space into a low dimensional space of LV (the axes in Figure 4.6) while regressing these on the treatment variables (O_2 level and time) thus facilitating interpretation of the data. The positions of the individual samples in this new space are represented by the colored symbols. Their position can be interpreted both in relation to the position of the metabolites (the open symbols) and in relation to the direction of time and the three O_2 levels applied (represented by the four arrows).

Figure 4.6A is a plot of LV1 vs. LV2 while Figure 4.6B is a plot of LV1 vs. LV3 for the same PLS-DA analysis. These first three LVs cover about 82 % of the observed variation in metabolite levels with the regression explaining 81 % of the variation in the treatment variables. Figure 4.6 therefore provides a good overview of the changes occurring in the 63 dimensional metabolite space. Metabolites oriented in Figure 4.6 in the same direction are positively correlated and show similar response in time to a given O_2 treatment or incubation time, while those in opposite directions are defined as negatively correlated showing opposite response to a given O_2 treatment or incubation time (in terms of an increase or decrease). PLS-DA revealed a divergence of tomato cell metabolome with increasing incubation time in response to low O_2. Separation between the control (21 kPa O_2) and the two low O_2 conditions could be achieved using the first two LV (Figure 4.6A). Together these two LV accounted for 78 and 47 % of the explained X and Y-variance, respectively. A third LV (Figure 4.6B) was needed to achieve a clear separation between the two low O_2 conditions (1 and 0 kPa). Using the first three LV the difference between the control and the two low O_2 conditions could be explained with a total X and Y-variance of 82 and 81 %, respectively.

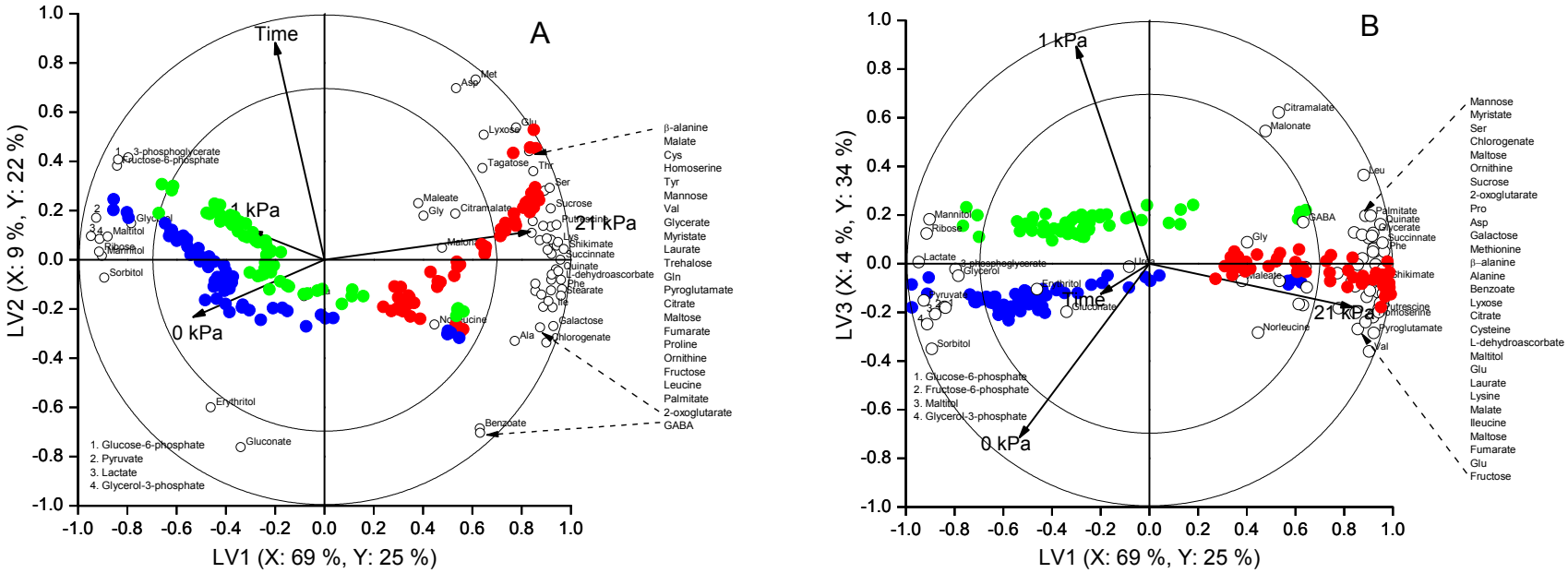

Figure 4.6: PLS-DA bi-plot showing tomato cells samples taken from the O_2 conditions at different time points. Figures (A) and (B) show a plot of LV1 vs. LV2 and LV1 vs. LV3 respectively. The percentage explained variance (X and Y representing the O_2 level and metabolite abundance respectively) are inserted next to the LV. The samples scores (closed circles: red, 21 kPa; green, 1 kPa; blue 0 kPa) are superimposed on the metabolite loadings (open circles). The line arrows indicate the position of the treatments (O_2 levels and incubation time) in the new parameter space. Amino acids are represented by their three letter symbols.

The arrows in Figure 4.6 show how the experimental conditions (O_2 level and incubation time) correlate with the metabolites in the new parameter space. Metabolites which are found around a given O_2 level indicate a close association with that O_2 condition. The metabolites which were closely associated with the low O_2 conditions included 3-phosphoglycerate, fructose-6-phosphate, glucose-6-phosphate, glycerol, glycerol-3-phosphate, lactate, mannitol, maltitol, pyruvate, ribose and sorbitol (Figure 4.6A). All these metabolites increased with the induction of low O_2. With respect to time (Figure 4.6A) metabolites above the horizontal axis increased with incubation time while those below decreased with incubation. For example, 3-phosphoglycerate and methionine, associated with the low O_2 levels and the control respectively, increased with incubation time while benzoate and gluconate which are located opposite the time arrow but associated with the control and the low O_2 levels respectively, decreased with incubation time. In Figure 4.6B, the direction of the time arrow shows that the changing levels of the metabolites under the different O_2 levels is largely independent of time and mainly a direct result of the O_2 level applied.

The variable importance in projection scores (VIPs) were calculated and used to assess the contribution of each metabolite in explaining the effects of incubation time and the different O_2 levels and thus being responsible for the observed separation in Figure 4.6. Metabolites with VIP close to or greater than one are considered important in given model while those with significantly less than one are less important and can be excluded from the model. Table 1 shows a list of the ten highest VIP for each O_2 treatment and incubation time. The VIP scores showed that benzoate, citramalate, fructose, glycerol-3-phosphate, gluconate, homoserine, leucine, norleucine pyroglutamate, sorbitol, tyrosine and valine were the major metabolites which explained the difference between the control and the low O_2 levels. These metabolites, with the exception of glycerol-3-phosphate, were present in higher amounts in the control compared to the low O_2 incubated cells. Gluconate which decreased in abundance under the three O_2 levels had the highest VIP for incubation time.

Table 4.1: VIP scores of the top 10 metabolites under the different O_2 conditions and incubation time. VIP's were calculated from the correlation loadings after PLS-DA analysis as explained in materials and method ([a]Pyroglutamate, [b]Glycerol-3-phosphate, [c]3-phosphoglycerate).

0 kPa		1 kPa		21 kPa		Time	
Metabolite	**VIP**	**Metabolite**	**VIP**	**Metabolite**	**VIP**	**Metabolite**	**VIP**
Citramalate	6.92	Citramalate	10.11	Pyroglu	1.56	Gluconate	9.52
Valine	2.69	Valine	3.49	Mannose	1.55	Benzoate	5.73
Sorbitol	2.63	Leucine	3.37	Ribose	1.48	GABA	5.64
Leucine	2.58	Sorbitol	3.33	Stearate	1.47	Aspartate	5.62
Pyroglu[a]	2.16	Pyroglu	2.59	Lactate	1.44	Methionine	5.04
Fructose	1.49	Fructose	1.72	Laurate	1.42	Erythritol	3.32
Tyrosine	1.47	Tyrosine	1.66	Sorbitol	1.42	Glutamate	2.49
Gluconate	1.46	Homoserine	1.49	Maltose	1.40	Lyxose	2.23
Benzoate	1.43	Norleucine	1.47	Shikimate	1.39	β-alanine	2.12
Glycerol-3-P[b]	1.34	Glycerol-3-P	1.47	Malate	1.39	3-PG[c]	1.99
Homoserine	1.33	Maltitol	1.42	Glycerate	1.36	Alanine	1.80

4.4 Discussion

4.4.1 Studying cell suspension cultures allows highly repeatable results to be generated

In this study cultured tomato cells were taken as the model system thus to exclude diffusion barriers, as would be encountered in intact tissue, and to enable the direct manipulation of substrate levels (both ^{13}C-glucose and O_2). By taking away these diffusion barriers, any variation related to the typical fruit-to-fruit variation in tissue porosity has been cancelled out. In addition, biological variations between cell suspensions are assumed to be relatively small as the culturing conditions are tightly controlled. This is mirrored by the small error bars in Figure 4.3 and 4.4, representing the variation based on 4 independent replicate experiments, and also by the tight clustering of the replicate observations in Figure 4.6.

4.4.2 Low oxygen changes the overall metabolism of plant cells

Low O_2 was accompanied by an increase in the levels of some metabolites (3-phosphoglycerate, fructose-6-phosphate, glucose-6-phosphate, glycerol, glycerol-3-phosphate,

lactate, mannitol, pyruvate, ribose and sorbitol) while other metabolites decreased. The increase in the level of glycerol, glycerol-3-phosphate, lactate and the sugar alcohols (with the exception of mannitol) was accompanied by an increase in ^{13}C-label accumulation, which indicates an increased flux due to an increased synthesis. Among the metabolites which decreased under low O_2 were some within the general group of sugars (except ribose and the sugar phosphates), amino acids and organic acids (except lactate). In addition to their decreased levels, these metabolites accumulated less ^{13}C-label which suggests a general reduction of their synthesis. The up and down regulation of the various metabolite levels, in combination with the differential accumulation of ^{13}C-label shows that the response of the plants to low O_2 is not limited to a particular pathway but involves changes in the overall metabolism of cells.

4.4.3 Low oxygen activates fermentation and decrease TCA cycle activity

Low O_2 in cultured tomatoes cells resulted in the accumulation of the intermediates of glycolysis, which suggests an inhibition of pathways downstream of glycolysis. The accumulation of glycolytic intermediates with low O_2 has also been observed in other plant systems (Galili, 2011; Miyashita and Good, 2008a). The increased levels of glycolytic intermediates under low O_2 without a corresponding increase in ^{13}C-label (Figure 4.5) suggests a reduction of the uptake rate of labelled substrate by the cells and an increased release from unlabelled intracellular sources. Suppression of substrate uptake by cells could be a strategy to reduce energy expenditure since substrate uptake is an active transport process which consumes cellular energy. The ability of plants to reduce energy consumption in the form of ATP is an important requirement to ensure their survival under low O_2 conditions (Drew, 1997; Geigenberger, 2003; Geigenberger et al., 2000). In potato tubers incubated under ^{14}C sucrose, a reduction in substrate uptake was observed within 2 h of incubation when the level of dissolved O_2 was reduced below 12 kPa (Geigenberger et al., 2000). In *Arabidopsis* roots grown under O_2 limiting conditions, a reduction in the transcripts encoding for proteins involved in energy consuming processes like transport and biosynthesis was observed (van Dongen et al., 2009).

The response of the intermediates of the TCA cycle to low O_2 involved a general decrease in levels accompanied by low ^{13}C-label accumulation (Appendices 2A and B), which indicates a reduced activity of the TCA cycle. The decrease in TCA cycle activity under low O_2 could be due to a general inhibition of oxidative phosphorylation due to the unavailability of O_2.

Taking into account that O_2 serves as an electron acceptor in the oxidation of reduced cofactors, NADH and $FADH_2$, produced from the TCA cycle, the absence of O_2 will impede the regeneration of these cofactors eventually leading to an inhibition of the TCA cycle. The increase in gluconate (Appendix 2A) during the early stages of low O_2 could be due to increases in the activity of the PPP. Considering that PPP activity results in the synthesis of reducing equivalents required to ensure the redox balance of the cell and to produce electrons for the reduction of reactive O_2 species, its activation under low O_2 is likely. Increases in the activity of PPP have been noted in cell cultures (Baxter et al., 2007; Ishikawa et al., 2010) and roots (Lehmann et al., 2009) subjected to oxidative stress.

The build-up of lactate (Figure 4.3) in the cells due to low O_2 indicates a possible shift in energy metabolism from respiration to fermentation. The activation of fermentative metabolism under low O_2 is important for producing ATP to ensure the survival of cells due to the inhibition of the TCA cycle. The accumulation of pyruvate (Figure 4.3) has been observed when plants switch from respiratory to fermentative metabolism because of the inefficiency of fermentation to utilise the intermediates of glycolysis (Geigenberger et al., 2000; Miyashita et al., 2007; van Dongen et al., 2009). The induction of fermentation as a response to low O_2 is not only restricted to changes in the metabolome, as studies in maize roots have shown increases in the levels and expressions of anaerobic proteins and genes (Sachs et al., 1996). Increase in the expression profile of anaerobic proteins with low O_2 have also been observed in *Arabidopsis* roots (Klok et al., 2002).

4.4.4 Decrease in the biosynthesis of sugars, amino acids and organic acids

The response to low O_2 involved a general reduction in the levels of free amino acids and organic acids (Appendix 2A). This decrease could be due to the need to reduce energy consumption by limiting biosynthetic reactions which consumes energy. A general decrease in the levels of some amino acids have also been observed in *Arabidopsis* cells subjected to menadione-induced oxidative stress (Baxter et al., 2007) and in pears (Franck et al., 2005) and apples (Lee et al., 2012) under CA storage. In contrast, the metabolic response of anoxia-intolerant plant tissues like maize roots (Aloni and Rosenshtein, 1982) and anoxia-tolerant species like rice seedlings (Magneschi and Perata, 2009) and cell suspension (Ishikawa et al., 2010) is characterised by increasing levels of some amino acids. Also, differences in the response of amino acids have been observed between the root and shoot of rice seedlings (Lee et al., 2014), while a comparative analysis between species and tissues has shown differences

in the response of various metabolites including amino acids to low O_2 stress (Narsai et al., 2011). The different response of amino acids might suggest a possible role in the adaptive response of plants to low O_2 even though this might depend on the tissue under study and the mode of low O_2 induction. Below 1 kPa O_2, glutamate, among the different amino acids, accumulated the highest ^{13}C-labelling. This high accumulation of ^{13}C-label by glutamate might be related to its role in the synthesis of nucleotides, chlorophylls, polyamines and alkaloids as well as its involvement in the synthesis of other amino acids like glutamine, proline, putrescine and GABA.

Marked reductions were noted in the levels of most sugars with an increase in sugar alcohols under low O_2 (Figure 4.5). The decrease in levels of sucrose, maltose and trehalose with low O_2 could be related to the suppressed substrate uptake requiring alternative, intracellular sources to generate energy. Reductions in sucrose levels with the induction of low O_2 stress has been observed in other plant species (Geigenberger et al., 2000; Lee et al., 2012; Pedreschi et al., 2009). This is usually accompanied by an increase in the activity of SuSy with a reduction of INV activity (Lara et al., 2010; Zeng et al., 1999). This shows that plants cells utilise less energy costly pathways to ensure their survival under low O_2 stress (Drew, 1997; Geigenberger, 2003).

The incorporation of ^{13}C-label into maltose shows that the synthesis and hydrolysis of starch occurs very rapidly in a tomato cell suspension. In *Arabidopsis* cells incubated with ^{13}C-glucose, labelling of maltose occurred rapidly as the label was detected within an hour of incubation even though lowered label levels were detected in the oxidative stressed cells (Baxter et al., 2007). The high amount of ^{13}C-label in maltose at 21 kPa O_2 compared to 1 and 0 kPa O_2 shows that starch synthesis could be decreased under low O_2 conditions, as has been observed in other plant species incubated under low O_2 conditions (Geigenberger et al., 2000; Gibon et al., 2002).

The only sugar which increased with low O_2, ribose, has also been observed to accumulate in pears (Lee et al., 2012), cell cultures (Baxter et al., 2007) and roots (van Dongen et al., 2009) subjected to different oxidative stress conditions. Even though the precise role of ribose in the response of plants to low O_2 is unknown, it has been shown to enhance the regeneration of ATP in mammalians cells under anoxia (St Cyr et al., 1989). It is possible that ribose might play a similar role in plant cells subjected to low O_2. The increase in the levels of sugar alcohols was accompanied by an increase in ^{13}C-label (Figure 4.4), suggesting an increased

synthesis. Sugar alcohol accumulation has been observed as one of the by-products of the low O_2 response of plants (Baxter et al., 2007; Ishikawa et al., 2010; Lee et al., 2012; Pedreschi et al., 2009; van Dongen et al., 2009). Sugar alcohol accumulation has also been reported in plant subjected to other abiotic stress conditions (Moing, 2000). Sugar alcohol accumulation in response to low O_2 might be related to their role in complementing carbon storage reserves during sugar deprivation (Moing, 2000).

Organic acids have been noted to play crucial roles in the adaptive response of plants to low O_2. In potato tissues, stepwise decrease in the concentration of O_2 caused changes in the levels of most organic acids (Geigenberger et al., 2000), while the response of culture cells to oxidative stress involved decreases in the levels of some organic acids (Baxter et al., 2007; Ishikawa et al., 2010). In our study, low O_2 was characterised by a general decrease in the levels of most organic and fatty acids (Appendix 2A). The observed decrease in glycerate levels even though it accumulated about the same amount of ^{13}C-label compared to control (Appendix 2B) indicates a rather constant synthesis but an increased breakdown. The general reduction in amino and organic acids appears to be in agreement with the survival strategy employed by plants under low O_2 which involves reducing anabolic reactions along with nitrogen metabolism to make more substrate available for glycolysis (Drew, 1997; Geigenberger, 2003).

4.4.5 Reduction in the levels of other nitrogen containing metabolites

β-alanine, GABA and putrescine all decreased and accumulated less ^{13}C-label showing a decrease in their synthesis in response to low O_2. The role of putrescine in the biosynthesis of polyamines is well documented (Van de Poel et al., 2013; Ye et al., 1997), showing that a decrease in putrescine synthesis leads to a reduction in the biosynthesis of polyamines. In *Arabidopsis* cells under oxidative stress, decreases in the levels of transcripts related to putrescine were observed along with decreases in concentration (Baxter et al., 2007). In fruits (Pedreschi et al., 2009) and other plant parts (Ye et al., 1997), putrescine has been revealed to increase due to low O_2. The accumulation of putrescine in this species under low O_2 might help in the maintenance of ionic balance to counter the increase in the levels of some organic acids like GABA (Reggiani et al., 1993). The role of β-alanine, a polyamine product, implicated in the adaptive response of plants to various stressors, including low O_2 response is unclear. In Empire apples, low O_2 was accompanied by an increase in β-alanine (Lee et al.,

2012) even though β-alanine reduction was observed in *Arabidopsis* cells (Baxter et al., 2007).

The response of GABA to low O_2 was opposite to that observed in some studies on fruits where GABA has been shown to accumulate (Franck et al., 2005; Lee et al., 2012; Magneschi and Perata, 2009; Pedreschi et al., 2009). In *Arabidopsis* cell suspension grown under normal and elevated O_2 conditions, the levels of GABA were found to be higher under the elevated O_2 condition (Williams et al., 2008). In *Arabidopsis* cell cultures subjected to menadione induced oxidative stress, there was no significant change in the levels of GABA (Baxter et al., 2007) while a similar treatment on *Arabidopsis* roots resulted in a marked reduction in the levels of GABA (Reggiani et al., 1993). Considering that GABA synthesis is activated when cytosolic pH is decreased (Carroll et al., 1994), the production of GABA could be linked to the synthesis and/or degradation of other organic acids in cells, a situation which could be both tissue and treatment specific.

4.5 Conclusions

By combining metabolome data with ^{13}C-label information, clear patterns in the response of the cells to low O_2 emerged. Low O_2 inhibited the biosynthesis of amino acids, organic acids and other nitrogen containing compounds. Under low O_2, accumulation of the intermediates of glycolysis, some sugar alcohols and lactate was observed. The lower the O_2 level, the higher this accumulation. The accumulation of glycolytic intermediates went hand-in-hand with a decreased ^{13}C-labelling, indicating a reduced overall flux through glycolysis and not an up-regulation. The accumulation of lactate under low O_2 signaled the induction of fermentative metabolism providing an escape for the accumulating pyruvate levels. The fact that not every intermediate was labelled up to the same steady-state level indicates that the various intermediates also received unlabelled inputs from other pathways. The ^{13}C- label accumulated by the different metabolites showed that for the control cells (21 kPa O_2) isotopic steady-state of the central carbon metabolism was reached within 12 h while, under low O_2, this took more than 24 h, mirroring the suppressed metabolic rates at low O_2 levels.

Chapter 5

Kinetic Modelling of the Response of Tomato Cells to Low Oxygen

5.1 Introduction

Metabolic profiling, even though useful in giving an overview of the changes in metabolites levels needs to be combined with mathematical models to fully understand the response of plants to low O_2 stress. Mathematical methods such as dynamic modelling can be used to reconstruct the changes in metabolites levels with time (Rios-Estepa and Lange, 2007; Schallau and Junker, 2010). To facilitate the calibration of dynamic models and improve their accuracy, experimental data on the uptake of labelled substrates (either radio- or stable-isotope labelled) can be adopted to monitor the distribution of the label within the different metabolites in addition to the plain metabolite levels (Morgan and Rhodes, 2002; Voit et al., 2004).

The mathematical modelling of dynamic labelling data to the central carbon metabolism of plants has received limited attention. Dynamic label modelling have been applied to study the effect of nutrition on plants (Cloutier et al., 2009) and the photosynthetic incorporation of ^{13}C-labelled CO_2 into *Arabidopsis* leaves (Szecowka et al., 2013). However, despite the potential

---

The content of this part of the thesis is based on

Ampofo-Asiama, J., Baiye, V.M.M., van Dongen, J.T., Waelkens, E., Geeraerd, A.H., Nicolai, B.M., Hertog, M.L.A.T.M., 2014. Kinetic modelling of the central metabolism of *Lycopersicum esculentum* cell suspension incubated at different oxygen levels. In preparation.

detrimental effect of low O_2 stress, the use of dynamic label modelling to unravel the response of plants to low O_2 stress has yet to be carried out. Though dynamic modelling with label incorporation is experimentally and computationally demanding, they are invaluable in improving our understanding of the response of plant metabolism to low O_2 stress. Although the effect of low O_2 stress on plants can also be studied using FBA, FBA do not provide information on kinetic properties and control mechanisms underlying the response; knowledge which can be gained when applying dynamic models. Dynamic models can be used to predict the levels of unmeasured metabolites (Morgan and Rhodes, 2002; Rios-Estepa and Lange, 2007) as well as estimate the impact of changing kinetic parameters on metabolic pathways through MCA (ap Rees and Hill, 1994; Fell and Sauro, 1985).

To study the metabolic effect of low O_2 stress at the whole organ level during postharvest CA storage of fruit one eventually has to deal, not only with the metabolic complexity at the cellular level (including subcellular compartmentalisation), but also with the additional complexity coming with tissue differentiation and O_2 gradients inside the product (Ho et al., 2014). As a first step towards the long term goal of unravelling the metabolic response of intact fruit to low O_2 stress during postharvest CA storage, the simpler experimental system of tomato cell suspension is chosen with the objective to determine the effect of low O_2 on the kinetic parameters and fluxes of the central carbon metabolism in this simplified higher plant cell system. The aim is to determine which enzymes play significant roles in switching the central carbon metabolism from aerobic respiration to anaerobic fermentation when exposed to low O_2. In relation to this, metabolic control as affected by low O_2 will be assessed.

To this end, the metabolite levels and ^{13}C-label accumulated by tomato cell suspension incubated at O_2 levels of 21, 1 or 0 kPa as explained in *Chapter 4*, was used for the first time to construct and calibrate a dynamic model of the compartmentalised central carbon metabolism, to interpret the effect of low O_2 on the relevant metabolites and their fluxes through plant cells. Using this approach, a combination of Michaelis-Menten and first-order kinetics was used to describe the changes in both the labelled and unlabelled fraction of each metabolite. The estimated kinetic parameters were used to estimate FCC to determine how the induction of low O_2 at 1 and 0 kPa affected the control of the central carbon metabolism.

5.2 Model development

5.2.1 Kinetic model development: the underlying kinetics

In this work two types of kinetics were considered, either Michelis-Menten kinetics or simple first order reactions. Working from the principle that the model should not be more complex than can be warranted for by the data, Michaelis-Menten kinetics was limited to those reactions where the data showed the substrate saturation typical for Michaelis-Menten kinetics. This selection process was based on a preliminary analysis of the data.

For these cases the change in metabolite concentration was defined as:

$$\frac{d[\mathrm{C}]}{dt} = V_{\max} \frac{[\mathrm{C}]}{K_M + [\mathrm{C}]} \qquad \text{(Eq. 5.1)}$$

describing the rate of formation of some product from metabolite [C], and V_{max} and K_M are the maximum reaction rate and Michaelis-Menten constant, respectively.

For most reactions where no substrate saturation was observed, the simpler first order kinetics was applied which can be considered a simplification of Michaelis-Menten kinetics for the case where substrate levels are around or below the governing K_M value. In these cases the change in metabolite concentration was expressed as:

$$\frac{d[C_x]}{dt} = \sum_{i=1}^{n} k_i \prod_{j=1}^{m} C_{ij} \qquad \text{(Eq. 5.2)}$$

where Π is the product of all metabolite concentrations [C_{ij}] (with the index j=1,…,m referring to the different species) involved in the formation or consumption of C_x through the multiple reactions indexed by i (i=1,…,n) with k_i being the rate constant (either positive or negative) of each contributing reaction i.

The production of lactate from pyruvate under low O_2 conditions was assumed to be prone to competitive product inhibition following the form:

$$\frac{d[\mathrm{LAC}]}{dt} = V_{\max} \frac{[\mathrm{PYR}]}{K_M \cdot \left[1 + \frac{[\mathrm{LAC}]}{K}\right] + [\mathrm{PYR}]} \qquad \text{(Eq. 5.3)}$$

where K is the product inhibition constant and V_{max} and K_M are the maximum reaction rate and Michaelis-Menten constant, respectively.

The three approaches were combined in constructing the overall ordinary differential equations describing the dynamic changes in metabolite concentrations.

5.2.2 Kinetic model development: labelled versus unlabelled fractions

Model equations had to be formulated for the metabolites of the central carbon metabolism based on the changes in both labelled and non-labelled fraction of each metabolite (Voit et al., 2004). As soon as multiple reactants are involved in a synthesis reaction, labelling of the product becomes a combinatorial problem which is not always straightforward to write out in full detail as it depends on the labelling status of the reactants. What is straightforward is to determine the reaction path leading to unlabelled products as for this all carbon contributing reactants should be unlabelled. Furthermore, the reaction path responsible for the total product (regardless of labelling) is also unambiguous as the labelling state of the reactants plays no role in this. Having these two at hand, the change in labelled metabolites can be calculated as the difference between the two.

As an illustration of this procedure, the change in the total concentration of citrate (Figure 5.1) in the mitochondria was modelled using first-order kinetics (Eq. 5.2) and was defined as:

$$\frac{d\left[\mathrm{CIT}_{\mathrm{T},M}\right]}{dt} = \left[\mathrm{PYR}_{\mathrm{T},M}\right]\left[\mathrm{OAA}_{\mathrm{T},M}\right]\cdot k_{\mathrm{CIT},M} - \left[\mathrm{CIT}_{\mathrm{T},M}\right]\cdot k_{\mathrm{TKG},M} - \left[\mathrm{CIT}_{\mathrm{T},M}\right]\cdot k_{\mathrm{CLYS},M}$$

(Eq. 5.4)

where $[\mathrm{CIT}_{\mathrm{T},M}]$, $[\mathrm{PYR}_{\mathrm{T},M}]$ and $[\mathrm{OAA}_{\mathrm{T},M}]$ are the total concentrations in the mitochondrion of citrate, pyruvate and oxaloacetate respectively, and $k_{\mathrm{CIT},M}$ and $k_{\mathrm{2KG},M}$ are the first-order rate constants associated with the formation of citrate and 2-ketoglutarate, respectively. The constant $k_{\mathrm{CLYS},M}$ is the rate of citrate breakdown.

Due to the fact that labelled citrate can be formed from different combinations of labelled and unlabelled pyruvate and oxaloacetate, unlabelled citrate can only be formed from unlabelled pyruvate and unlabelled citrate, model equations were written for the change in concentration of unlabelled citrate:

$$\frac{d\left[\mathrm{CIT}_{\mathrm{U},M}\right]}{dt} = \left[\mathrm{PYR}_{\mathrm{U},M}\right]\left[\mathrm{OAA}_{\mathrm{U},M}\right]\cdot k_{\mathrm{CIT},M} - \left[\mathrm{CIT}_{\mathrm{U},M}\right]\cdot k_{\mathrm{TKG},M} - \left[\mathrm{CIT}_{\mathrm{U},M}\right]\cdot k_{\mathrm{CLYS},M}$$

(Eq. 5.5)

where $[\mathrm{CIT}_{\mathrm{U},M}]$, $[\mathrm{PYR}_{\mathrm{U},M}]$ and $[\mathrm{OAA}_{\mathrm{U},M}]$ are the concentrations in the mitochondria of unlabelled citrate, pyruvate and oxaloacetate, respectively. The change in labelled citrate concentration was defined as the difference between the change in total (Eq. 5.4) and unlabelled (Eq. 5.5) metabolite concentrations:

$$\frac{d\left[\mathrm{CIT}_{\mathrm{L},M}\right]}{dt} = \frac{d\left[\mathrm{CIT}_{\mathrm{T},M}\right]}{dt} - \frac{d\left[\mathrm{CIT}_{\mathrm{U},M}\right]}{dt} \qquad \text{(Eq. 5.6)}$$

with $[\mathrm{CIT}_{\mathrm{L},M}]$ being the concentration of labelled citrate in the mitochondrion. Eventually, the fraction (R) of labelled citrate in the mitochondrion was calculated by dividing the concentration of labelled metabolite by the total metabolite concentration:

$$R_{\mathrm{CIT},M} = \frac{\left[\mathrm{CIT}_{\mathrm{L},M}\right]}{\left[\mathrm{CIT}_{\mathrm{T},M}\right]}. \qquad \text{(Eq. 5.7)}$$

Although multiple differential equations are needed to describe the changes in total citrate concentration, unlabelled citrate and the fraction labelled, no additional model parameters are required under the assumption that the metabolism does not discriminate between the labelled and unlabelled fractions. In this way a more detailed model structure can be defined facilitating model calibration.

In the case of Michaelis-Menten kinetics it is the total metabolite concentration that is assumed to obey Michaelis-Menten kinetics. For example, the change in total concentration of cytosolic 3-phosphoglycerate (Figure 5.1) can be defined as:

$$\begin{aligned}\frac{d\left[\mathrm{3PG}_{\mathrm{T},C}\right]}{dt} = {} & 2\cdot V_{\mathrm{max,3PG},C}\,\frac{\left[\mathrm{F6P}_{\mathrm{T},C}\right]}{K_{M,\mathrm{3PG},C} + \left[\mathrm{F6P}_{\mathrm{T},C}\right]} \\ & - V_{\mathrm{max,PYR},C}\,\frac{\left[\mathrm{3PG}_{\mathrm{T,C}}\right]}{K_{M,\mathrm{PYR},C} + \left[\mathrm{3PG}_{\mathrm{T},C}\right]}\end{aligned} \qquad \text{(Eq. 5.8)}$$

where $[3PG_{T,C}]$ and $[F6P_{T,C}]$ are the total concentration of 3-phosphoglycerate and fructose-6-phosphate in the cytosol, respectively. $V_{max,3PG,C}$ and $V_{max,PYR,C}$ are maximum reaction rates while $K_{M,3PG,C}$ and $K_{M,PYR,C}$ are the Michaelis-Menten constants associated with the formation of 3-phosphoglycerate and pyruvate in the cytosol, respectively. The factor 2 indicates the fact that a single F6P molecule provides the carbon skeleton for two 3PG molecules.

Given a certain fraction of labelling of the substrate, the available enzyme capacity (given by V_{max}) will be divided over the two fractions accordingly. For this reason the fraction of labelled metabolite was used to calculate the changes in unlabelled metabolite concentration from the change in total concentration. The change in unlabelled 3-phosphoglycerate could thus be defined as:

$$\begin{aligned}\frac{d\left[3PG_{U,C}\right]}{dt} = {} & 2\cdot\left(1-R_{F6P,C}\right)\cdot V_{max,3PG,C}\,\frac{\left[F6P_{T,C}\right]}{K_{M,3PG,C}+\left[F6P_{T,C}\right]} \\ & -\left(1-R_{3PG,C}\right)\cdot V_{max,3PG,C}\,\frac{\left[3PG_{T,C}\right]}{K_{M,PYR,C}+\left[3PG_{T,C}\right]}\end{aligned} \qquad \text{(Eq. 5.9)}$$

where $R_{F6P,C}$ and $R_{3PG,C}$ are the fractions of labelled fructose-6-phosphate and 3-phosphoglycerate in the cytosol, respectively. The change in labelled 3-phosphoglycerate was finally calculated as the difference between the changes in the total (Eq. 5.8) and unlabelled (Eq. 5.9) metabolite concentrations.

5.2.3 Kinetic model development: Compartmentalisation

The various metabolites considered were partitioned over the different cellular compartments. For this reason transport terms were introduced to account for the exchange of metabolites between the different compartments. In the case of G6P the change in cytosolic ($[G6P_{T,C}]$) and plastidial ($[G6P_{T,P}]$) total concentrations due to the exchange between the two compartments was described by:

$$\begin{cases}\dfrac{d\left[G6P_{T,C}\right]}{dt} = -\left[G6P_{T,C}\right]\cdot\dfrac{k_{G6P,C\to P}}{V_C}+\left[G6P_{T,P}\right]\cdot\dfrac{k_{G6P,P\to C}}{V_C} \\ \dfrac{d\left[G6P_{T,P}\right]}{dt} = +\left[G6P_{T,C}\right]\cdot\dfrac{k_{G6P,C\to P}}{V_P}-\left[G6P_{T,P}\right]\cdot\dfrac{k_{G6P,P\to C}}{V_P}\end{cases} \qquad \text{(Eq. 5.10)}$$

with $k_{G6P,C\rightarrow P}$ and $k_{G6P,C\rightarrow P}$ being the transport rates from cytosol (with relative volume V_C) to plastid (with volume V_P) and from plastid to cytosol, respectively. Corrections for compartmental volumes were carried out for all metabolites transported, to incorporate the effect mass transport of single molecules has on the concentration in the compartment considered depending on the volume of that compartment.

Metabolite concentrations at the cellular level were calculated taking into account the contributions of the individual compartments. In the case of glucose-6-phosphate (G6P) the total cellular concentration [$G6P_T$] was calculated following:

$$\left[\mathrm{G6P_T}\right] = \left[\mathrm{G6P_{T,C}}\right]\cdot V_C + \left[\mathrm{G6P_{T,P}}\right]\cdot V_P + \left[\mathrm{G6P_{T,V}}\right]\cdot V_V + \left[\mathrm{G6P_{T,M}}\right]\cdot V_M \quad \text{(Eq. 5.11)}$$

where the volume of the cell was considered to be unity and V_C, V_P, V_V and V_M are the relative volumes of the cytosol, plastid, vacuole and mitochondria respectively. [$G6P_{T,C}$], [$G6P_{T,P}$], [$G6P_{T,V}$] and [$G6P_{T,M}$] are the total concentration of glucose-6-phosphate in cytosol, plastid, vacuole and mitochondria respectively. Similar equations were used to calculate labelled and unlabelled metabolite concentrations at the cell level from the different compartments.

Approximate numbers for the relative volume of the cytosol (V_C = 0.6962), plastid (V_P = 0.003), vacuole (V_V = 0.3) and mitochondria (V_M = 0.0008) were obtained from literature combining different sources of plant cell histological data (Gestel and Verbelen, 2002; Langbecker et al., 2004; Owens and Poole, 1979; Wang et al., 2010).

5.2.4 Model calibration

The model parameters were estimated using a non-linear least squares optimisation interface Optipa (Hertog et al., 2007), which can be used in combination with MATLAB® (MathWorks). The differential equations and other model calculations (Appendix 3F) were written and implemented in OptiPa. The model parameters were estimated after normal transformation of the metabolite concentration and ^{13}C-label data. All variables were given equal weight during the optimisation. The coupled differential equations were solved using the MATLAB solver ode15s and the non-linear optimisation algorithm was used for optimisation.

A total of 105 differential equations (representing changes in both labelled and unlabelled species of each metabolite in the different compartments) containing 19 Michaelis-Menten

parameters (K_M and V_{max}), 33 first-order rate constants and 16 first-order transport terms (Appendix 3F) were estimated per O_2 level. In addition, the initial concentrations of 18 metabolites in the different cell compartments were estimated in common for the three O_2 conditions. In total, 5304 experimental data points on metabolite concentrations and their fractional labelling distributed over the three O_2 levels were used to estimate all the model parameters.

With respect to the compartmentalised metabolites, simulations were initiated by distributing the metabolites equally between the different compartments. The initial value for the uptake rate of substrate was estimated from the depletion of glucose within the culture medium of the cell suspension while the initial values of all other parameters were selected randomly.

The complexity of the metabolic model caused by the large amount of differential equations and model parameters necessitated the decomposition of the estimation procedure which was carried out in four steps. The first two steps were carried out to estimate the model parameters of the glycolysis and the TCA cycle, respectively, and associated metabolic pathways. In the first step, the parameters describing the changes in glycolytic intermediates- glucose-6-phosphate, fructose-6-phosphate, 3-phosphosglycerate and pyruvate- in the cytosol and plastid as well as alanine, lactate, serine, sucrose and valine were estimated per O_2 condition. During this estimation step, the K_M values of cytosolic glycolysis were considered equal to that of the plastid and the $K_{M,\mathrm{UPT}}$ was kept at 83000 µmol/mg DW.

The obtained parameter values were used as starting values for the next estimation step. In the second estimation step, the parameters describing the changes in the intermediates of the TCA cycle (citrate, 2-ketoglutarate, succinate, fumarate, malate and oxaloacetate) as well as aspartate, GABA and glutamate were estimated per O_2 condition. In a third round, the results of the first and second estimation procedure were used as starting values to estimate the parameters of the central metabolic network model but still separated per O_2 condition.

In the final fourth optimisation run the data of the three O_2 conditions were combined allowing for the concurrent estimation of both the initial metabolite concentration (valid for the three O_2 levels combined) and all the kinetic parameter copies (one value per O_2 level for each kinetic parameter) starting from the parameter values obtained during the third optimisation run. The results presented are based on this final optimisation.

Confidence intervals (CI) of all model parameters were determined using an error based bootstrap resampling technique. By bootstrapping the complete dataset 50 times, the model was fitted to the obtained bootstrap datasets thus providing 50 estimated values for each individual model parameter. From these obtained parameter distributions, CI of the individual parameters were calculated and presented in Appendix 3A-D.

5.2.5 Metabolic control analysis

FCC – Flux Control Coefficients- were estimated using the principles of MCA (Heinrich and Rapoport, 1974; Kacser and Burns, 1995). FCC, which estimate the effect of an enzyme (E_i) on a pathway flux (v_j), were defined by the general formula (Eq. 5.12):

$$C_{E_i}^{v_j} = \frac{\partial v_j}{\partial E_i} \cdot \frac{E_i}{v_j} \qquad \text{(Eq. 5.12)}$$

where v represent the steady-state flux through reaction j, and E the activity of enzyme i. Under conditions where enzymatic measurements are not available, the rate constant can be considered a good approximation of the enzyme activity. FCC were therefore redefined as:

$$C_{E_i}^{v_j} = \frac{\partial v_j}{\partial k_i} \cdot \frac{k_i}{v_j} \qquad \text{(Eq. 5.13)}$$

where k is the estimated first-order rate constant or maximum Michaelis-Menten reaction rate (V_{max}) of enzyme E.

5.3 Results

To enable fully integrated quantitative analyses of the experimental data, a metabolic network model of the compartmentalised central carbon metabolism was developed. During the construction of the metabolic network a stepwise model extension approach was applied by including the different reactions taking into account the destiny of both ^{13}C-labelled and unlabelled metabolites.

5.3.1 Selection and reduction of model components

The first step in developing the metabolic network was the construction of the compartmentalised pathway of glycolysis as the reactions of glycolysis are distributed

between the plastid and cytosol (Plaxton, 1996). In addition, the main metabolites synthesised from the intermediates of glycolysis were included in the model. Serine, which is synthesised from 3-phosphoglycerate, as well as alanine, lactate and valine, all being synthesised from pyruvate (Umbarger, 1978), were included in the metabolic network. Pathways were introduced to account for the use of these metabolites in other metabolic reactions (Figure 5.1).

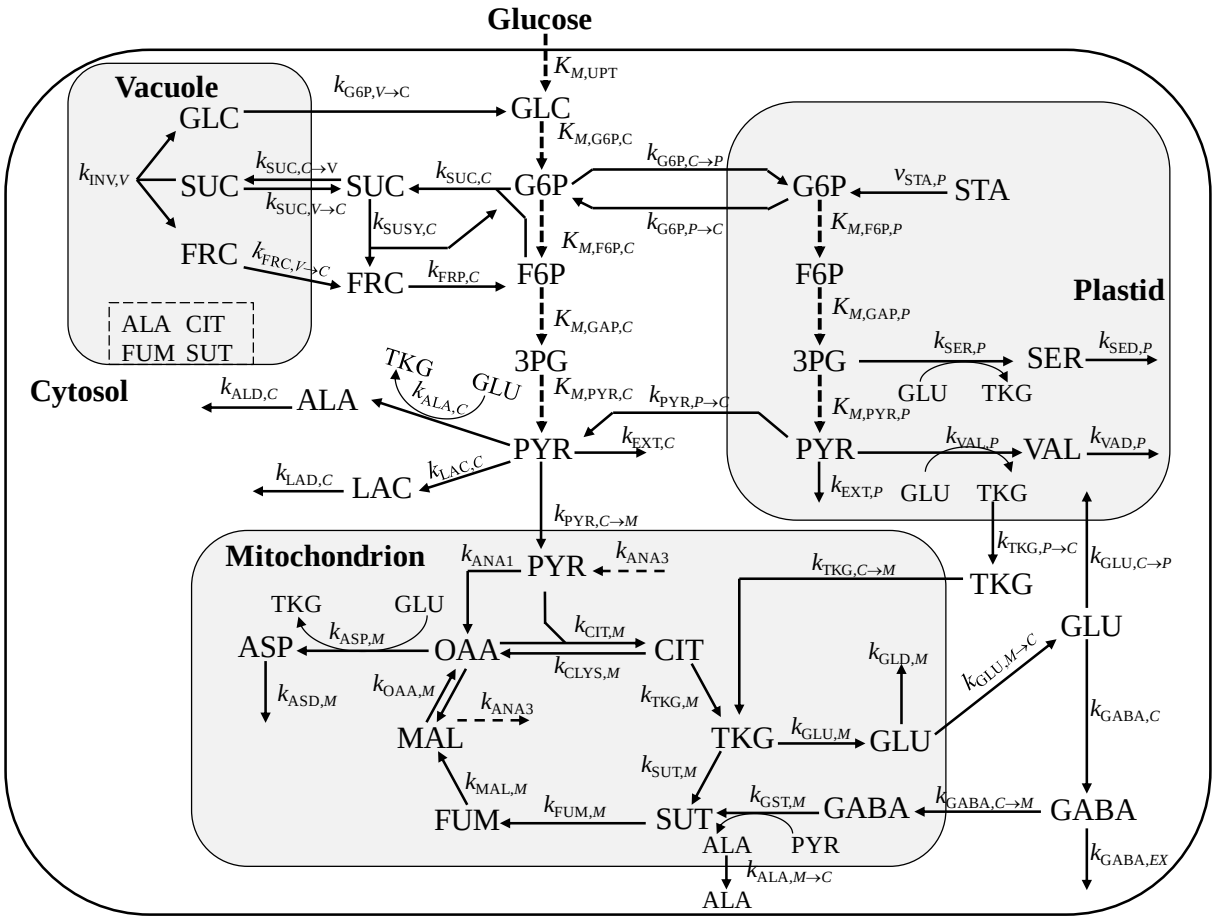

Figure 5.1: A schematic overview of the compartmentalised metabolic network used for dynamic label modelling of the central carbon metabolism in tomato cell suspension. The arrows indicate metabolite production and consumption with either a Michaelis-Menten constant (K_M, dash arrows) or first order rate constant (k, line arrows). The estimated K_M and k values can be found in Appendix 3A-D. Unlabelled fractions of ALA, CIT, FUM and SUT were maintain in the vacuole as explained in Section 5.3.1. Abbreviations: 2KG, 2-ketoglutarate; 3PG, 3-phosphoglycerate; ALA, alanine; ASP, aspartate; CIT, citrate; FRC, fructose; F6P, fructose-6-phosphate; FUM, fumarate; GABA, γ-amino butyric acid; GLC, glucose; G6P, glucose-6-phosphate; GLU, glutamate; LAC, lactate; MAL, malate; OAA, oxaloacetate; SER, serine; STA, starch; SUC, sucrose; SUT, succinate; PYR, pyruvate; VAL, valine.

The synthesis of valine and serine were localised in the plastid (Williams et al., 2008), while that of alanine (Miyashita et al., 2007; Williams et al., 2008) and lactate were restricted to the cytosol (Figure 5.1). To ensure availability of substrate for the metabolic reactions in the plastid, transport terms were introduced to exchange glucose-6-phophate between the cytosol and plastid. Similar transport terms were introduced to transport pyruvate from the cytosol to the mitochondria for use in the TCA cycle and to transport hexose from the vacuole to the cytosol. Corrections for the effect of differences in compartmental volumes were carried out for all metabolites transported. The deamination of glutamate resulting in the release of 2-ketoglutarate was included in the synthesis of amino acids.

To reduce the number of model parameters without significantly changing the structure of the metabolic network, some reactions of the glycolysis (both in the cytosol and plastid) were lumped. Firstly, fructose-1,6-bisphophate was removed from the network so that fructose-6-phosphate is directly cleaved to triose-phosphate. Secondly, all triose-phosphate reactions were lumped towards the formation and degradation of 3-phosphoglycerate (3PG), which was then used for the formation of pyruvate. Cytosolic pyruvate was either transported to the mitochondria or used in alanine, lactate and ethanol synthesis (Figure 5.1).

For the purpose of modelling, a simplified sucrose metabolic pathway was considered. First, due to inability to measure UDP-GLC, sucrose was considered to be synthesised from fructose-6-phosphate and glucose-6-phosphate (instead of UDP-GLC). Also, the reactions of sucrose-6-phosphate synthase and sucrose-6-phosphate phosphatase were considered a single reaction with the rate constant $k_{\mathrm{SUC},C}$ (Figure 5.1). The synthesised sucrose could be exchanged with the vacuole ($k_{SUC,C\rightarrow V}$ for the forward reaction and $k_{\mathrm{SUC},V\rightarrow C}$ for the backward). Vacuolar sucrose could be hydrolysed ($k_{\mathrm{INV},V}$) with the products transported to the cytosol (glucose ($k_{\mathrm{GLC},V\rightarrow C}$), fructose ($k_{\mathrm{FRC},V\rightarrow C}$)). To help reduce the number of model parameters to ensure accurate estimates, the action of cytosolic INV was omitted from the model. The degradation of sucrose in the cytosol was made to occur via the action of SuSy ($k_{\mathrm{SUSY},C}$). The product of SuSy reaction was considered to be fructose and glucose-6-phosphate (instead of UDP-GLC) (Figure 5.1).

The second part of the central carbon metabolism, the TCA cycle, was constructed based on information from literature and its activity was restricted to the mitochondria (Bowsher and Tobin, 2001; Lunn, 2007). The TCA cycle reactions start from pyruvate transported from the cytosol to the mitochondria (Figure 5.1). As no experimental data was available on ACoA,

citrate was assumed to be synthesised from pyruvate and oxaloacetate. The biosynthesis of glutamate, aspartate and GABA and their use in other reactions were also included.

Although most TCA cycle reactions occur at near-equilibrium conditions, only the reactions catalysed by malate dehydrogenase and citrate lyase were considered reversible for the purpose of this work. These assumptions were made to help reduce the number of model parameters, and also due to the role the reversal flux of malate dehydrogenase has been observed to play in the response of plants to low O_2 stress (Grafahrend-Belau et al., 2009b; Rocha et al., 2010). In the metabolic network model, transamination reactions were considered as one-directional reactions, even though the deamination of glutamate to 2-ketoglutarate occurs in plants. This deamination reaction was included as a separate reaction in the scheme.

Though the cell suspension was supplied with 50 % U-^{13}C-labelled glucose, none of the measured metabolites attained this maximum labelling. Even though metabolites in the upper part of glycolysis attained isotopic steady-state within the experimental duration, they were not labelled to the maximum level of 50 %, implying that a fraction of the metabolites remained unlabelled. For modelling purposes, this fraction was assumed to be stored inside the vacuole, since in plant cells the vacuole serves as storage compartment for a range of metabolites (Marty, 1999). Thus a constant pool of some metabolites (alanine, citrate, fumarate and succinate) was created inside the vacuole, responsible for diluting the accumulated ^{13}C-label and preventing it from reaching maximum labelling.

Initial analyses using the glycolytic network showed a prominent lack of fit at low O_2 conditions resulting in an underestimation of the hexose-phosphates levels. Since these increased hexose-phosphate levels showed a lower than expected ^{13}C-labelling, it was assumed that, under these conditions, the cells were using their own sugars in addition to the external supplied glucose to carry out glycolysis. To account for the usage of the cells energy pools, the flux $v_{STA,P}$ (starch breakdown) was introduced into the model. The pathway for the production of starch was not modelled due to the reduced synthesis of starch, especially under low O_2 conditions (Geigenberger, 2003), while the degradation of starch was simplified to the formation of glucose-6-phosphate. This assumption was made to reduce the number of model parameters to ensure accurate parameter estimation and also due to the fact that the breakdown products of starch (glucose, maltose and glucose-1-phosphate) can enter glycolysis by being converted to glucose-6-phosphate.

5.3.2 The effect of oxygen on the pathway kinetics

The metabolic network model from Figure 5.1 was used to analyse the changes in both the ^{13}C-label and metabolite levels at each O_2 level. For each condition a set of kinetic parameter values was obtained. The simulations could explain 93 % of the measured ^{13}C-label and metabolite concentration data of all the O_2 levels.

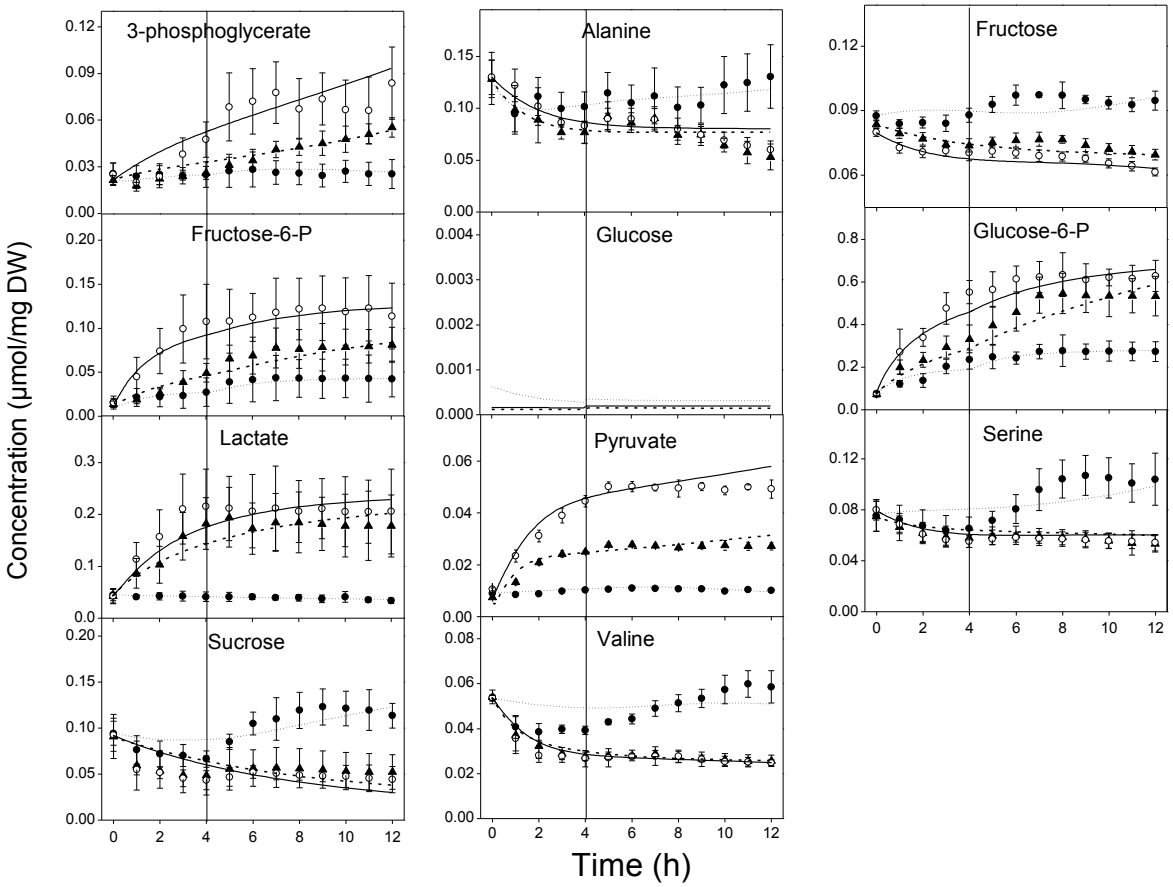

Figure 5.2: The simulated changes in total concentration of metabolites of glycolysis and associated pathways. The simulated metabolite concentrations (21 kPa, dotted line; 1 kPa, dashed lines; 0 kPa, solid lines) are plotted along with the experimentally determined values in the cell suspension (21 kPa, ●; 1 kPa, ▲; 0 kPa, ○). The measured data points are the average of 4 biological replicates ± 95 % CI. The vertical lines at 4 h indicate the time point labelled substrate was added.

Figure 5.2 and 5.3 shows the combined experimental and simulated data on the changes in total concentration of metabolites of the glycolysis (Figure 5.2), the TCA cycle (Figure 5.3) and their associated pathways. Experimental data on oxaloacetate, which was not observed during the GC-MS analyses, is missing (Figure 5.3). At 21 kPa O_2 levels, there was an initial decrease in the levels of alanine, sucrose, valine, serine within the first 2 h after which an

increase in levels was observed (Figure 5.2). However, some metabolites like glucose-6-phophate, fructose-6-phophate, pyruvate and 3-phosphoglycerate started to increase and reached peak levels after 5 h of incubation (Figure 5.2). The response of the intermediates of the TCA cycle at 21 kPa O_2 involved a general decrease within the first few hours and a subsequent increase in levels to those above that of time zero (Figure 5.3). At the low O_2 conditions, all metabolites except 3-phosphoglycerate, fructose-6-phophate, glucose-6-phophate, lactate and pyruvate decreased over the course of the experiment.

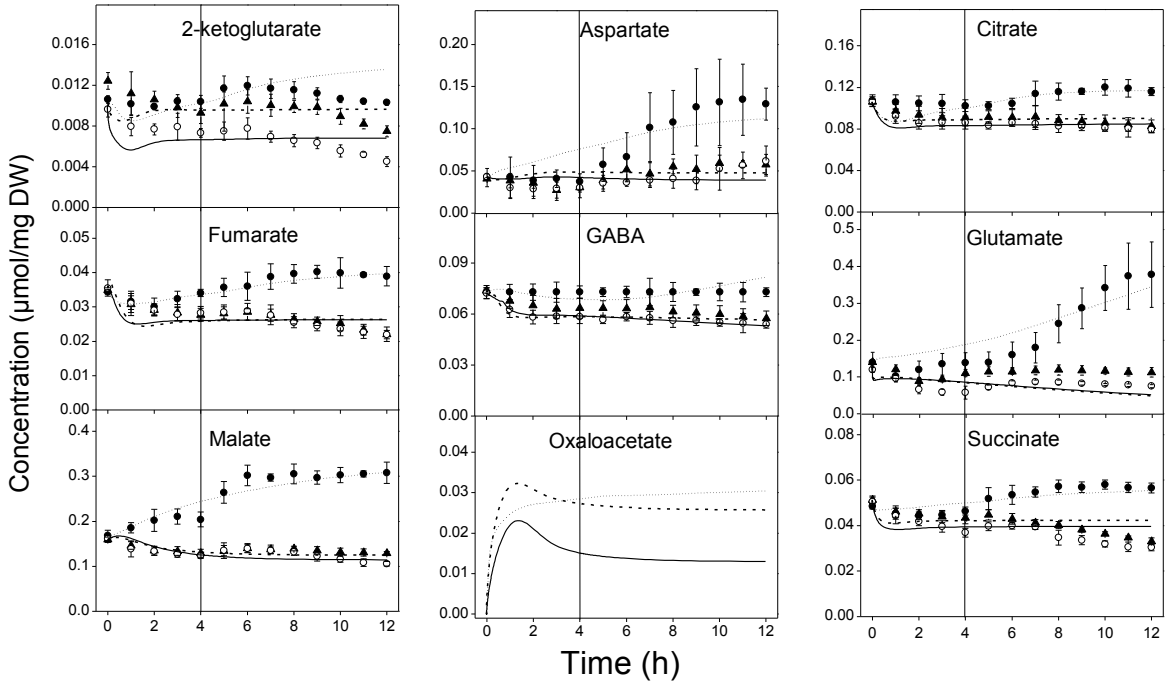

Figure 5.3: The simulated changes in total concentration of metabolites of the TCA cycle and associated pathways. The simulated metabolite levels (21 kPa, dotted line; 1 kPa, dashed lines; 0 kPa, solid lines) are plotted along with the experimentally determined values in the cell suspension (21 kPa, ●; 1 kPa, ▲; 0 kPa ○,) with the exception of oxaloacetate (which was not observed during the GC-MS analyses). The measured data points are the average of 4 biological replicates ± 95 % CI. The vertical lines at 4 h indicate the time point labelled substrate was added.

Figure 5.4 and 5.5 shows the fraction of ^{13}C-label accumulated by the metabolites of the glycolysis (Figure 5.4), the TCA cycle (Figure 5.5) and associated pathways, superimposing the simulated model values on the experimental values. Experimental data on pyruvate (Figure 5.4), 2-ketoglutarate (Figure 5.5) and oxaloacetate (Figure 5.5) labelling is missing as this information could not be reliably retrieved. The build-up of ^{13}C-label could be detected in all metabolites after 1 h of adding ^{13}C-glucose at the different O_2 levels. While metabolites in

the upper part of the central carbon metabolism like glucose-6-phosphate (Figure 5.4) accumulated high levels of ^{13}C within a few hours, it took some time for those downstream like succinate (Figure 5.5). With the exception of lactate (Figure 5.4), all the other metabolites accumulated high ^{13}C-label levels at 21 kPa compared to the low O_2 conditions. Some metabolites like glucose-6-phosphate, fructose-6-phosphate and 3-phosphoglycerate attained isotopic steady-state within the experimental duration when incubated at 21 kPa O_2 (Figure 5.4) but others did not. For some metabolites discrepancies between the simulated and measured data of the ^{13}C-label and metabolite concentrations could be observed. Considering the complexity of the central carbon metabolism and the use of its intermediates in various metabolic pathways in plants, a certain degree of discrepancy between the simulated and measured data is to be expected.

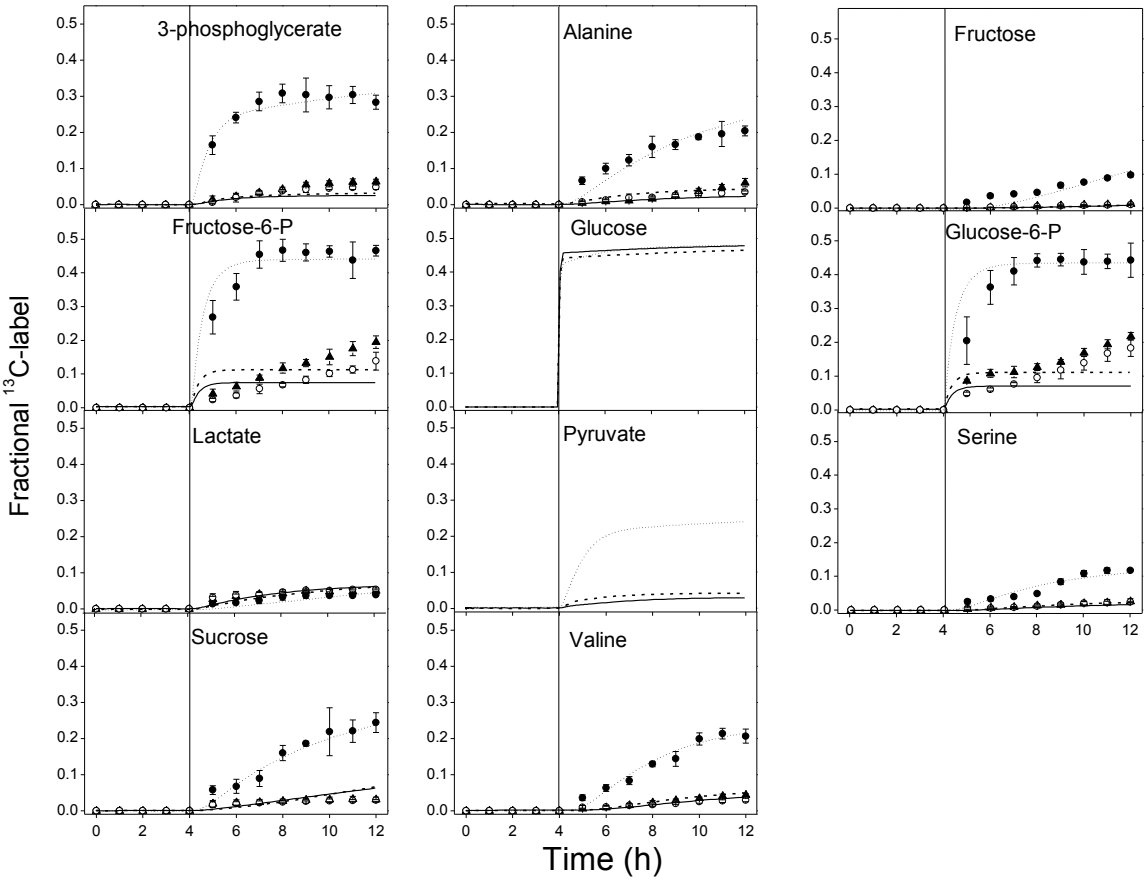

Figure 5.4: Simulated ^{13}C-label accumulated by the intermediates of glycolysis and associated pathways. The simulated ^{13}C-label changes (21 kPa, dotted line; 1 kPa, dashed lines; 0 kPa, solid lines) are plotted along with the experimentally determined values in the cell suspension culture (21 kPa, ●; 1 kPa, ▲; 0 kPa, ○) with the exception of pyruvate and glucose for which no experimental labelling data could be reliably obtained. The measured data points are the average of 4 biological replicates ± 95 % CI. The vertical lines at 4 h indicate the time point labelled substrate was added.

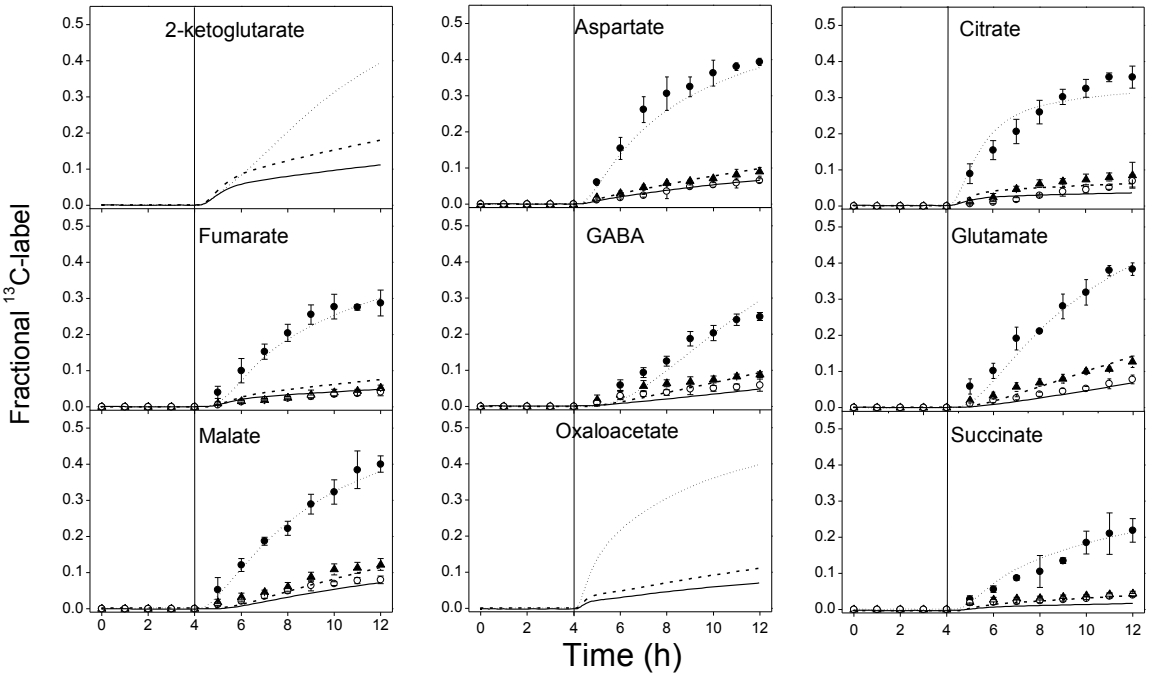

Figure 5.5: The simulated ^{13}C-label accumulated by the intermediates of the TCA cycle and associated pathways. The simulated ^{13}C-label changes (21 kPa, dotted line; 1 kPa, dashed lines; 0 kPa, solid lines) are plotted along with the experimentally determined values in the cell suspension culture (21 kPa, ●; 1 kPa, ▲; 0 kPa, ○) with the exception of 2-ketoglutarate (for which no experimental labelling data could be reliably obtained) and oxaloacetate (which was not observed during the GC-MS analyses). The measured data points are the average of 4 biological replicates ± 95 % CI. The vertical lines at 4 h indicate the time point labelled substrate was added.

The modelled changes in the ^{13}C-label and concentrations of glucose-6-phosphate and 2-ketoglutarate, examples of metabolites occurring in more than one subcellular compartment, are shown in Figure 5.6 and 5.7, respectively. Glucose-6-phosphate in the cytosol was labelled to higher levels compared to the plastid (Figure 5.6). The labelling in the cytosolic glucose-6-phosphate was achieved much faster (in about 4 h after label addition) compared to that of the plastidic one. With respect to the 2-ketoglutarate, a higher label accumulation was predicted in the mitochondria compared to the cytosol and plastid. The distribution of the metabolites and their rate of change also varied within the different compartments (Figure 5.7). Higher levels of glucose-6-phosphate were observed in the cytosol compared to those in the plastid. With respect to 2-ketoglutarate, the levels in the mitochondria was higher than observed in the other compartments (Figure 5.7).

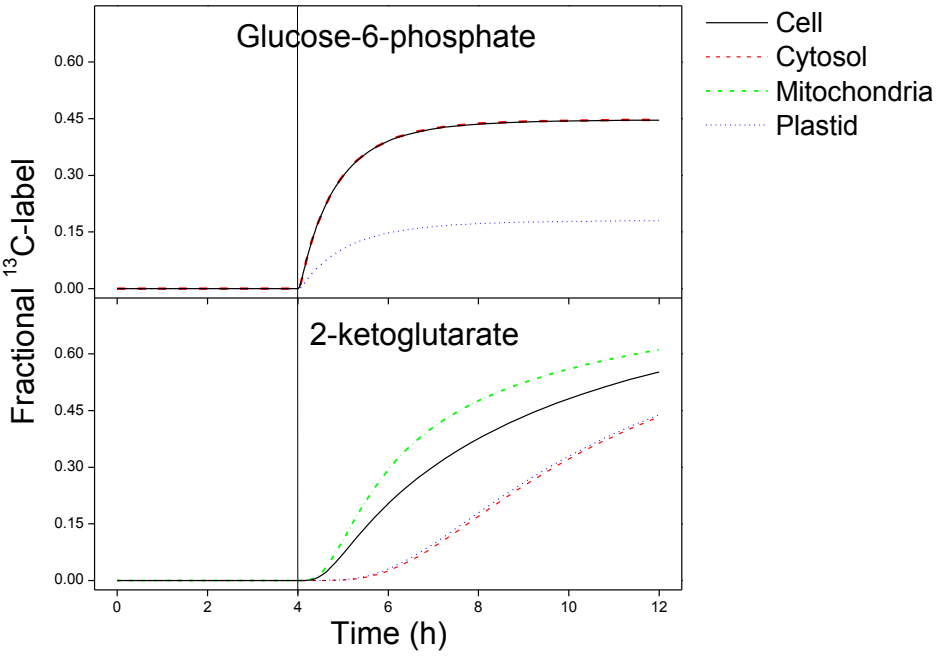

Figure 5.6: The modelled distribution of ^{13}C-label of glucose-6-phosphate and 2-ketoglutarate between the different compartments of the cell suspension in comparison to that of the whole cell ^{13}C-labelling at 21kPa O_2. The vertical lines at 4 h indicate the time point labelled substrate was added.

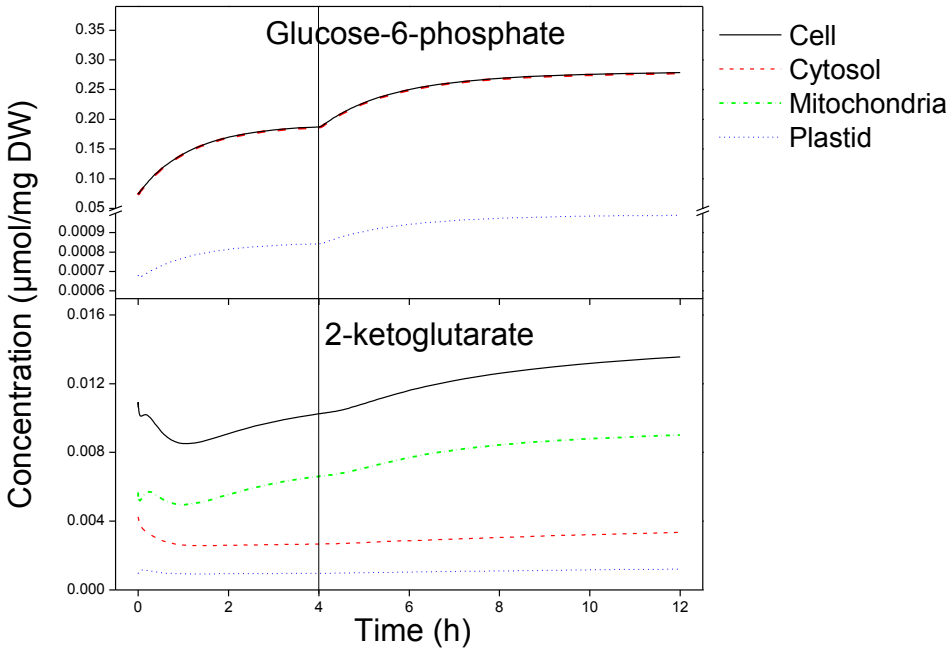

Figure 5.7: The distribution of metabolite levels of glucose-6-phosphate and 2-ketoglutarate between the different compartments of the cell suspension in comparison to that of the whole cell metabolite concentration at 21kPa O_2. The vertical lines at 4 h indicate the time point labelled substrate was added.

The estimated V_{max} values for the linear part of the glycolysis in both the cytosol and plastid are shown in Figure 5.8. At 21 kPa O_2 higher V_{max} values were obtained for the glycolytic reactions in the plastid as compared to corresponding reaction in the cytosol with the exception of the formation of pyruvate in the cytosol. Comparing the different O_2 levels, $V_{max,\mathrm{UPT}}$ was higher at 21 kPa as compared to low O_2 conditions (1 and 0 kPa). Both $V_{max,\mathrm{F6P},C}$ and $V_{max,\mathrm{3PG},C}$ were higher at both low O_2 conditions as compared to 21 kPa O_2 with the values at 0 kPa being higher than at 1 kPa.

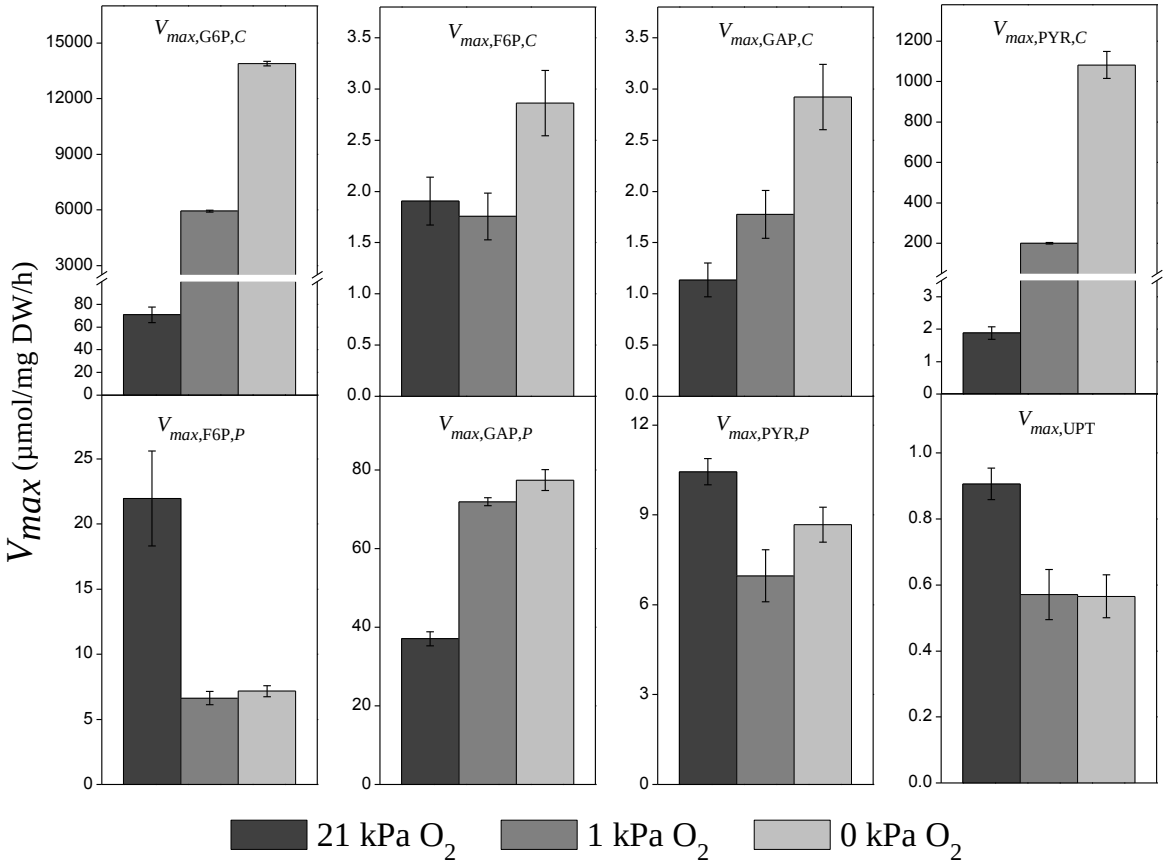

Figure 5.8: The effect of different O_2 levels on the V_{max} of glycolysis in both the cytosol (upper row) and plastid (lower row). The error bars are the standard deviations obtained from an error based bootstrap resampling technique.

Figure 5.9 shows the estimated rate constants for the transport reactions and some of the most affected first-order kinetic parameters of the central metabolism. There was an increase in the rate constant involved in the transport of glucose to the plastid ($k_{\mathrm{G6P},C\rightarrow P}$) and the synthesis of ethanol from pyruvate ($k_{\mathrm{EXT},C}$) while a decrease in the rate constant for the transport of pyruvate from the cytosol to the mitochondria ($k_{\mathrm{PYR,C}\rightarrow M}$) was observed when comparing high to low O_2 conditions. Among the other rate constants which decreased significantly at low O_2

were $k_{SUT,M}$, $k_{OAA,M}$, $k_{SER,P}$ $k_{VAL,P}$ and $k_{SUC,V}$. A full list of all model parameters can be found in Appenndix 3A-D.

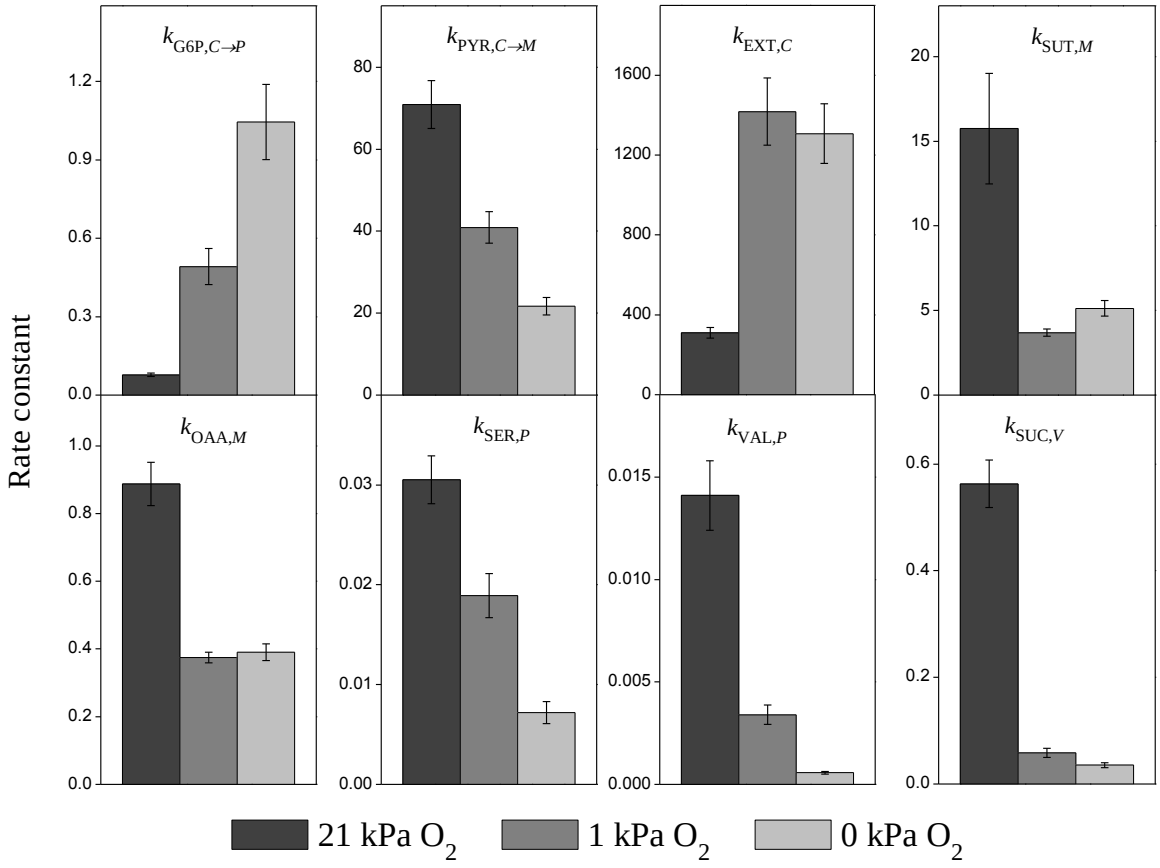

Figure 5.9: The effect of different O_2 levels on some selected first-order rate constants and transport terms of the central metabolism. All rate constants have the unit of h^{-1}, except $k_{SER,P}$, $k_{VAL,P}$ and $k_{SUC,V}$ which have units of mg DW/µmol/h. The error bars are the standard deviations obtained from an error based bootstrap resampling technique.

5.3.3 Fluxes through the central carbon metabolism at the different oxygen levels

The effect of O_2 on the flux distribution within the central carbon metabolism after 12 h of incubation is shown in Figure 5.10A-C. Low O_2 had a profound effect on the central carbon metabolism of the tomato cells as represented by the different thicknesses and colors of the flux arrows for the different O_2 levels.

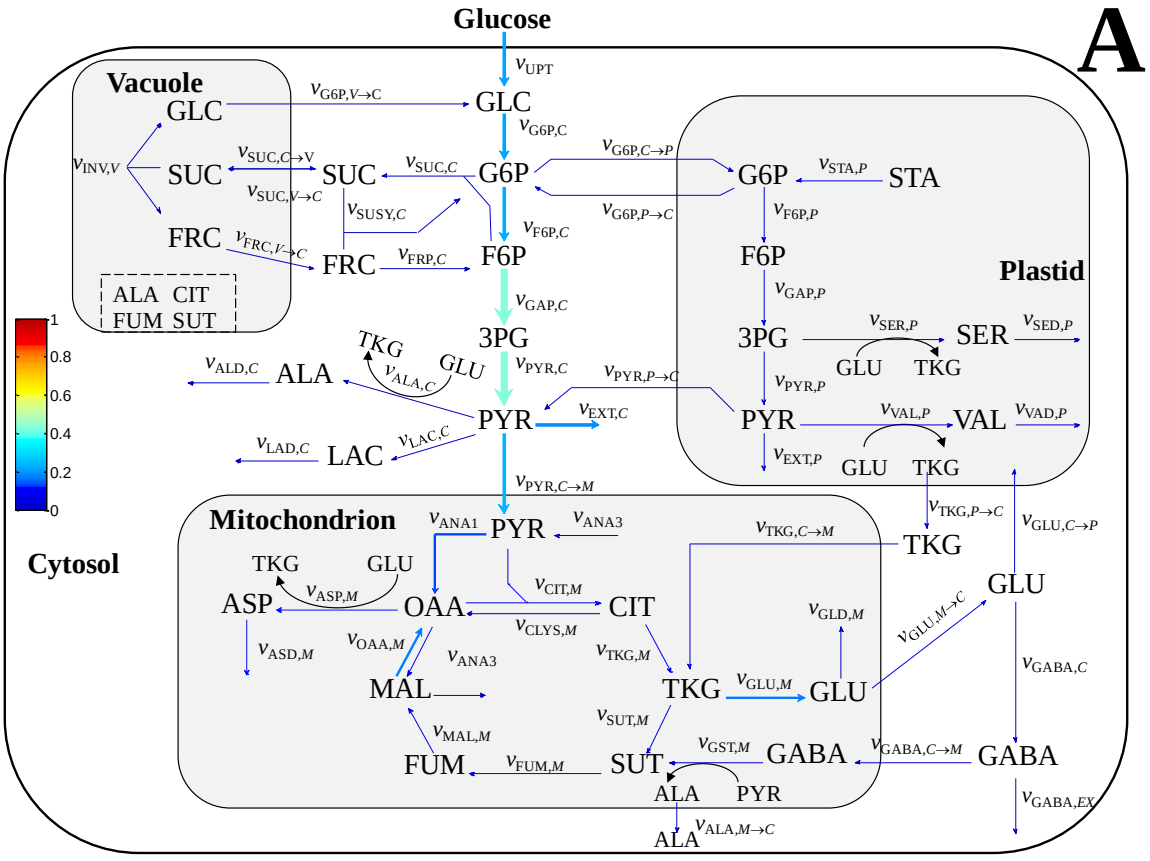
A
Glucose
Vacuole
GLC
SUC
FRC
ALA CIT
FUM SUT
Cytosol
Plastid
Mitochondrion
STA
SER
VAL
GABA
TKG
GLU
ASP
OAA
CIT
MAL
FUM
SUT
PYR
LAC
ALA
3PG
F6P
G6P
GLC
SUC
FRC

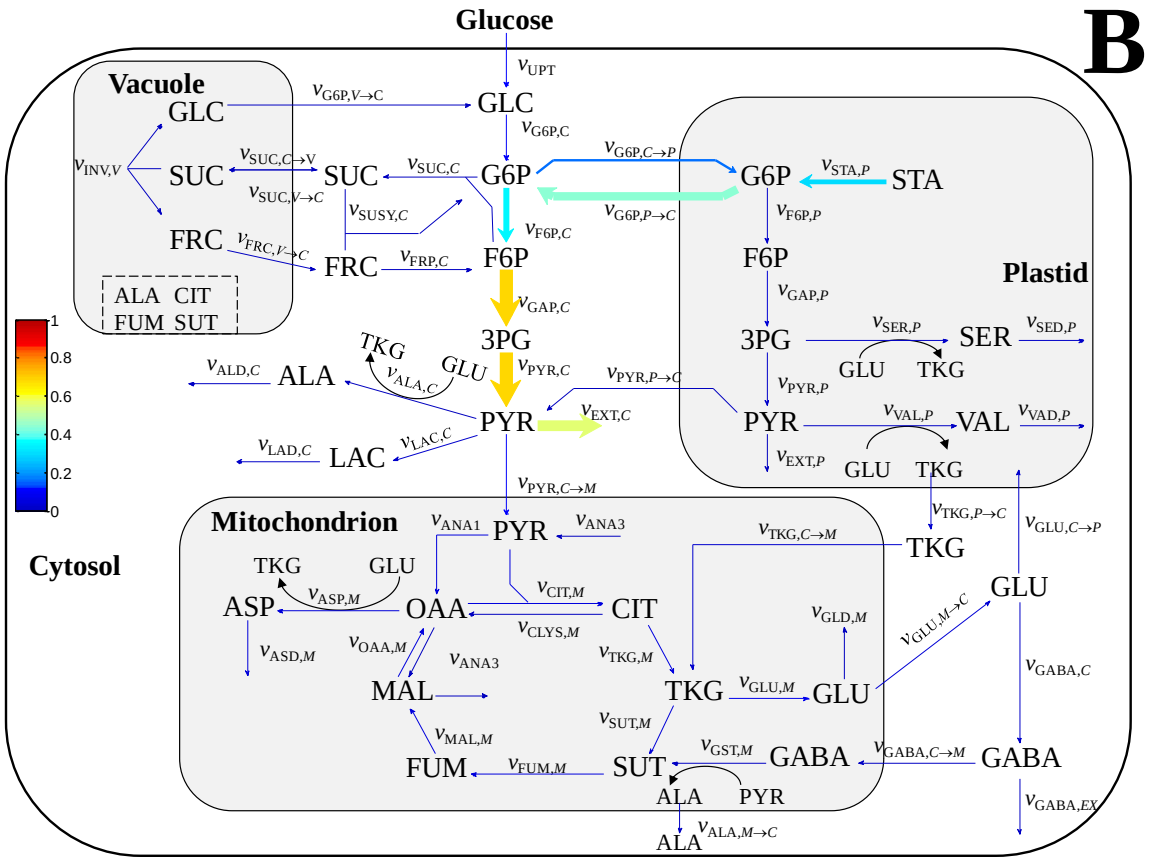
B
Glucose
Vacuole
GLC
SUC
FRC
ALA CIT
FUM SUT
Cytosol
Plastid
Mitochondrion
STA
SER
VAL
GABA
TKG
GLU
ASP
OAA
CIT
MAL
FUM
SUT
PYR
LAC
ALA
3PG
F6P
G6P
GLC
SUC
FRC

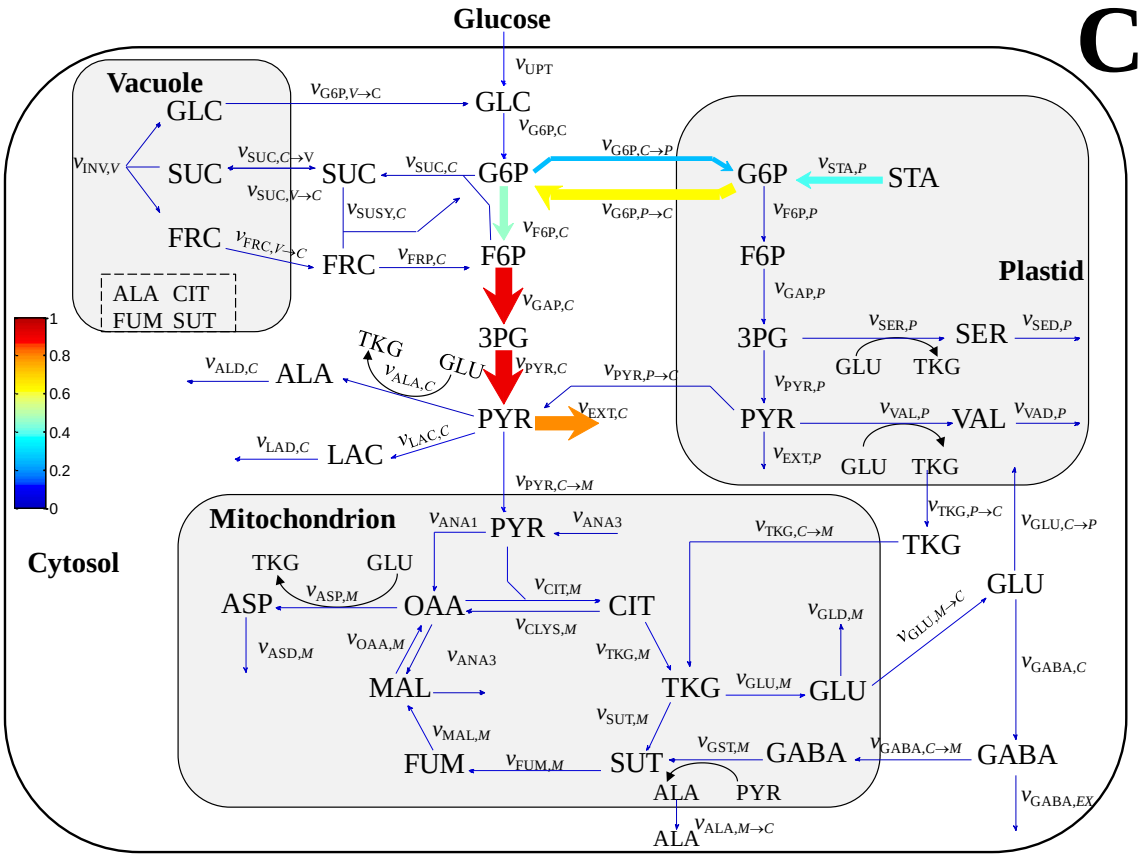

Figure 5.10: The effect of different O_2 level (A, 21 kPa; B, 1 kPa; C, 0 kPa) on the fluxes (µmol/mgDW/h) through the central metabolism of tomato cell suspension after 12 h of incubation. The thickness of an arrow and its colour is a measure of the flux through that pathway.

The effect of O_2 on some selected fluxes of the central carbon metabolism is shown in more detail in Figure 5.11. Comparing v_{UPT} and $v_{STA,P}$ between 21 kPa and 1 kPa O_2, it can be observed that, v_{UPT} reduced by more than 45 %, while $v_{STA,P}$ increased. Although a reduction in v_{UPT} with an increase in $v_{STA,P}$ was observed between the 1 and 0 kPa O_2 levels, these were not significantly different from each other.

The induction of low O_2 had a large effect on glycolytic activity both in the plastid and the cytosol (Figure 5.11B). At 21 kPa O_2, higher glycolytic activity was observed in the cytosol as compared to the plastid. Reducing the levels of dissolved O_2 led to an increase in pyruvate formation in the cytosol ($v_{PYR,C}$) while the plastidial pyruvate formation ($v_{PYR,P}$) was unchanged (Figure 5.11B). Coupled to the increase in cytosolic glycolytic flux under low O_2 conditions was an increase in lactate synthesis ($v_{LAC,C}$) with a corresponding increase in the use of pyruvate for other reactions ($v_{EXT,C}$) (Figure 5.11D).

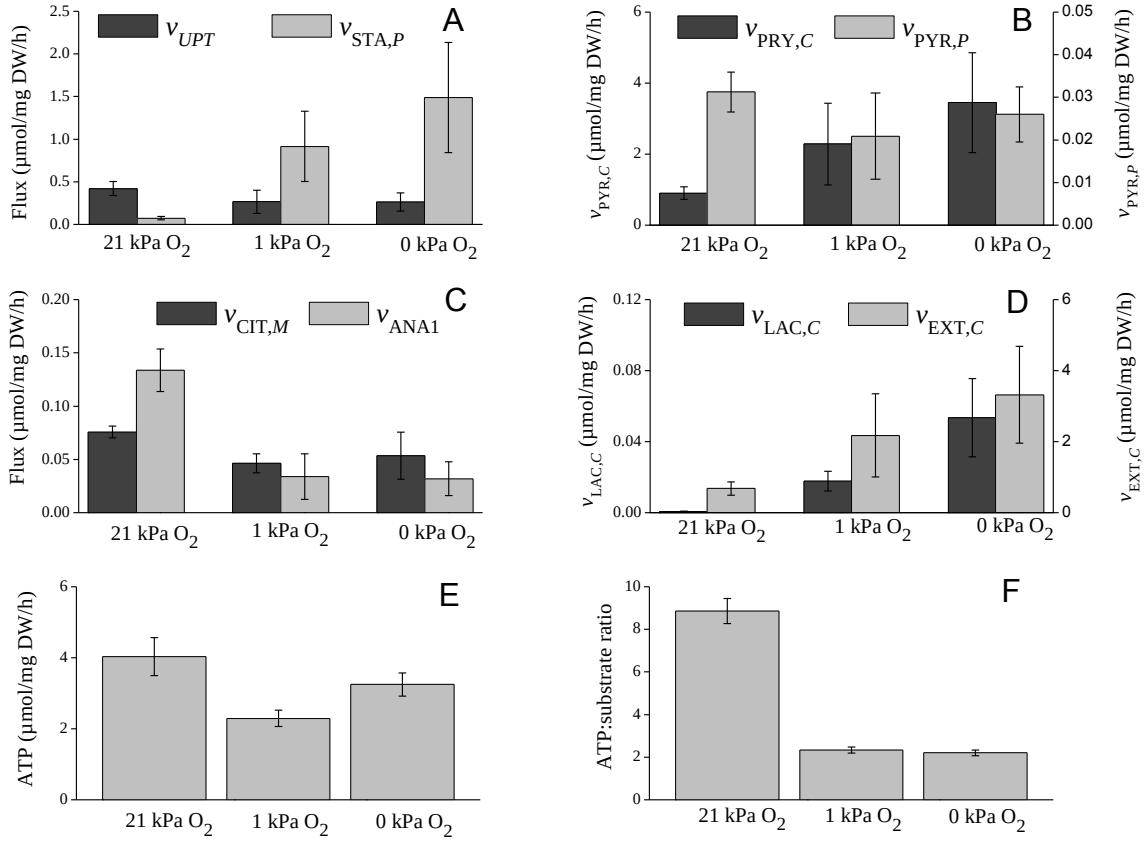

Figure 5.11. The effect of different O_2 levels on some central metabolic fluxes and ATP/substrate ratio of tomato cell suspension after 12 h of incubation. See Figure 1 for the position of the fluxes within the metabolic network model. The full list of the estimated fluxes can be found in Appedix 3E. Subheadings: A, energy source for the cell suspension from the uptake of external glucose (v_{UPT}) and starch hydrolysis ($v_{STA,P}$); B, fluxes towards pyruvate production in the cytsol ($v_{PYR,C}$) and plastid ($v_{PYR,P}$); C, entry of carbon into the TCA cycle from the synthesis of citrate ($v_{CIT,M}$) and the anaplerotic pathway (v_{ANA1}); D, synthesis of lactate ($v_{LAC,C}$) and ethanol ($v_{EXT,C}$); E; ATP production rate; F, ATP:substrate ratio.

Low O_2 resulted in a general reduction in the activity of the TCA cycle (Figure 5.11C). The net amount of ATP produced by the cells per unit of substrate utilised (ATP/substrate ratio) was calculated for the different O_2 levels. This was carried out by summing all fluxes producing ATP and subtracting fluxes consuming ATP and expressing this per amount of substrate consumed by the cells (sum of v_{UPT} and $v_{STA,P}$). ATP synthesised from the reducing equivalents, NADH and $FADH_2$, was included in the calculations. Also the amount of ATP produced by the cells was calculated by summing all fluxes producing ATP. Figure 5.11E and Figure 11F shows the ATP production rate and ATP/substrate ratios estimated under the different O_2 levels, respectively.

5.3.4 Flux control coefficient glycolysis, fermentation and the TCA cycle

The kinetic model was used to determine the control of the central carbon metabolism under the different O_2 levels. MCA was used to estimate the FCC associated with glycolysis in the cytosol and plastid, the synthesis of citrate (TCA cycle) and lactate (fermentative metabolism). For assessing the control of glycolysis in the cytosol and plastid, MCA was performed on the conversion of 3-phosphoglycerate to pyruvate in both the cytosol ($v_{PYR,C}$) and plastid ($v_{PYR,C}$).

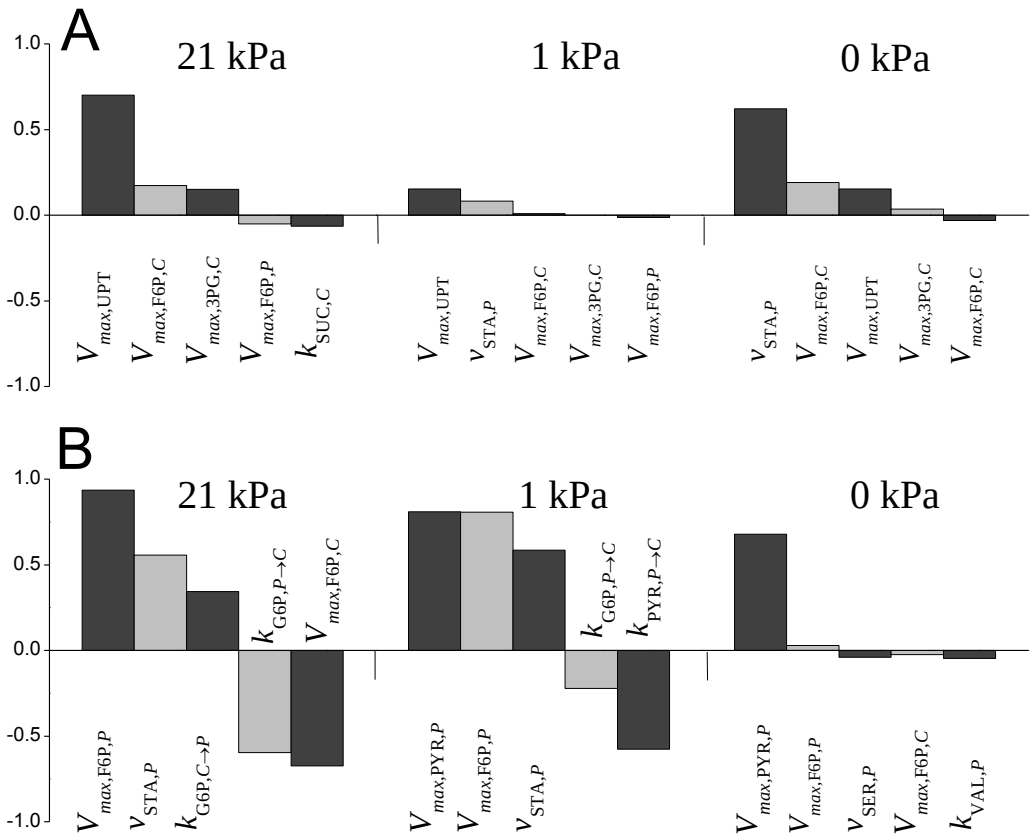

Figure 5.12: Flux control coefficients calculated for the production of pyruvate in the cytosol (A) and plastid (B) under the three O_2 levels studied.

Figure 5.12A shows the five highest FCCs involved in the cytosolic control of $v_{PYR,C}$. At 21 kPa O_2, $v_{PYR,C}$ was mainly controlled by $V_{max,UPT}$, $V_{max,F6P,C}$, $V_{max,3PG,C}$, $V_{max,F6P,P}$ and $k_{SUC,C}$. While $V_{max,UPT}$, $V_{max,F6P,C}$ and $V_{max,3PG,C}$ exerted a positive control, $V_{max,F6P,P}$ and $k_{SUC,C}$ exerted a negative control on $v_{PYR,C}$. At 1 and 0 kPa O_2, $v_{STA,P}$ was involved in the positive control of $v_{PYR,C}$ (Figure 5.12A). The FCC's associated with the plastidial control of $v_{PYR,P}$ is shown in Figure 12B. The main kinetic parameters which positively control $v_{PYR,P}$ at 21 kPa O_2 were

$v_{STA,P}$, $V_{max,F6P,P}$, and $k_{G6P,C\rightarrow P}$, while negative control was exerted by $k_{G6P,P\rightarrow C}$ and $V_{max,F6P,C}$. At the low O_2 conditions both $V_{max,PYR,P}$ and $V_{max,F6P,P}$ became important in the control of $v_{PYR,P}$ by exerting positive control (Figure 5.12B).

The kinetic parameters involved in the mitochondrial control of $v_{CIT,M}$ and the cytosolic control of $v_{LAC,C}$ are shown in Figure 5.13. Both $k_{EXT,C}$ and $k_{GLU,M}$ exerted negative control on $v_{CIT,M}$ under all O_2 levels while $V_{max,UPT}$ exerted positive control under 21 and 1 kPa O_2 levels (Figure 5.13A). The control of $v_{LAC,C}$ was strongly positively influenced by $k_{LAC,C}$ and $V_{max,LAC,C}$ at 21 kPa and the low O_2 levels, respectively, while $k_{EXT,C}$ exerted a strong negative control at all O_2 levels.

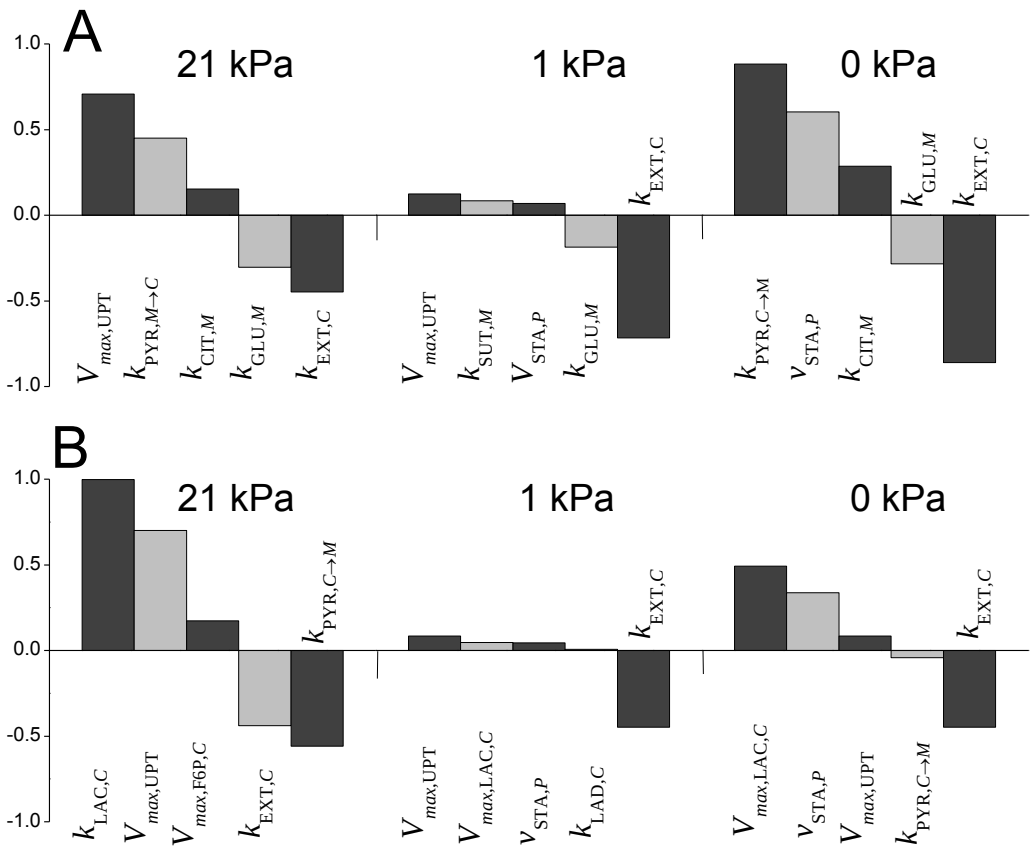

Figure 5.13: Flux control coefficients calculated for the production of citrate (A) and lactate (B) under the three O_2 levels studied.

5.3.5 Validity of the established model

The accuracy of the established model was determined by comparing the estimated fluxes and kinetic parameters with data from the literature. Even though published work from dynamic analysis for comparative purposes are limited, a good agreement was found between the 12 h

flux maps (Figure 5.10) and steady-state fluxes determined in tomato (Rontein et al., 2002), rice (Lakshmanan et al., 2013) and *Arabidopsis* (Williams et al., 2010, 2008) cell suspensions incubated at different O_2 levels. Also, the small CI of the estimated model parameters obtained through bootstrap analysis (Appendix 3A-D) shows the uniqueness and robustness of the model in its ability to converge to similar estimates. Starting from a model-based error resampling technique, 50 bootstrap datasets were obtained. Based on the parameter distributions, confidence intervals for each parameter was estimated. Despite the size of the experimental error on the data, a thorough replication of the best model could be obtained with 50 bootstrap, resulting in reproducible parameter estimates with relatively small confidence intervals.

Additionally, the ability of the cells to support the estimated flux from their own sugar pools ($v_{STA,P}$) was determined. In the analysis of biomass composition of the cell suspension (*Chapter 3*), the total starch content of the cells was determined to be around 3 % on dry weight basis. Based on the calculated $v_{STA,P}$ under 0 kPa O_2, over the 12 hours of the experiment, a reduction in the total starch content of 10 % can be expected. Therefore, excluding the use of other sugar sources in the cell suspension, the cells could rely on their starch content alone to survive the period of low O_2 stress. This shows that the estimated $v_{STA,P}$ and other fluxes were within a physiological feasible range. Finally, the estimated fluxes were compared to the maximum catalytic activity of some enzymes determined *in vitro* in plant tissues. The fluxes estimated by the model were lower then published maximal catalytic activities of plant enzymes.

5.4 Discussion

5.4.1 Dynamic modelling of plant metabolism

In this chapter, the effect of low O_2 stress on plant cells was studied using dynamic modelling. Although other mathematical models such as FBA (Grafahrend-Belau et al., 2009b; Lakshmanan et al., 2013) and steady-state ^{13}C-MFA analysis (Alonso et al., 2007b), have been used to study the effect of low O_2 stress on plants, these approaches do not provide information on kinetic properties and control mechanisms underlying the response to low O_2 stress. For instance, FBA has been used to obtain a phase resolved flux map of the central carbon metabolism in the endosperm of barley (Grafahrend-Belau et al., 2009b) without providing information on the kinetic response and the control mechanism underlying the

response to low O_2 stress. Such information, can however be gained when applying dynamic models.

5.4.2 The consequence of subcellular compartmentalisation

Compartmentalisation is an important and unique feature which enables plant cells to alter their metabolism in response to different stress conditions (Bowsher and Tobin, 2001; Lunn, 2007). The observed low ^{13}C-labelling levels of sucrose, amino acids associated with glycolysis and some organic acids of the TCA cycle confirmed the existence of compartmentalised metabolism in the cells. The ability to distinguish between parallel fluxes of glycolysis was made possible by their linkage to amino acids synthesised in the cytosol and plastid which were labelled to different levels.

The distribution of ^{13}C-label (Figure 5.6) and metabolites (Figure 5.7) within the different compartments showed that subcellular compartmentalisation turned out to be relevant in the dynamic label modelling of plant cells. For the same metabolite, the accumulated ^{13}C-label was found to differ within different compartments. While the ^{13}C-label accumulation of glucose-6-phosphate in the cytosol reached a maximum level of 45 %, the plastidial pool was only labelled to a maximum of 18 % after 12 hours of incubation at 21 kPa O_2 (Figure 5.6). This shows that the pathways which use glucose-6-phosphate in the plastid did not turn over sufficiently to incorporate the maximum label levels while, at the same time, the presence of unlabelled carbon storage pools contributed to lowering the plastidial glucose-6-phosphate ^{13}C-label accumulation. Very low levels of glucose-6-phosphate and 2-ketoglutarate were predicted in the plastid (Figure 5.7). This is related to correcting the concentration of the metabolites with the volumes of the different subcellular compartments. The very small volume of the plastid (assumed to account for only 0.3 % of the total cell volume) compared to the cytosol in non-photosynthetic tissues means such corrections will lower the concentration in the plastid. The high concentration of 2-ketoglurate in the mitochondria shows that the concentration of this metabolite in the mitochondria is 1000 times more than in the cytosol.

The cyclic nature of the TCA cycle implies that the involved metabolites can be expected to get labelled to levels above 50 % at 21 kPa O_2. This is due to fact that as metabolites turn over in the cycle, carbon atoms will be lost (through the release of CO_2 by the action of isocitrate dehydrogenase and 2-ketoglutarate dehydrogenase), and additional carbon from ACoA will be

added during the formation of citrate. The loss and gain of carbon atoms and the turnover of metabolites in the cycle can lead to ^{13}C-labelling levels exceeding the theoretical maximum of 50 %. This observation was made in the ^{13}C-labelled levels of 2-ketoglutarate in the mitochondria (Figure 5.6). As the ^{13}C-labelling levels of citrate, fumarate and succinate stayed at much lower levels, unlabelled pools of these metabolites must have existed. This motivated the decision to introduce constant and unlabelled pools of these metabolites in the vacuole as shown in Figure 5.1.

5.4.3 Complexity by simplicity

Reducing the complexity of the central carbon metabolism meant that most reversible pathways of glycolysis and the TCA cycle had to be modelled as forward reactions. Only the most relevant reversible pathways based on prior knowledge of their biological roles were modelled in this work. For example the reversible reaction catalysed by phosphoglucoisomerase in both the cytosol ($v_{\mathrm{F6P},C)}$ and plastid ($v_{\mathrm{F6P},P}$) could be modelled with only a forward reaction without significantly changing the model estimation while the transport of glucose-6-phosphate between the cytosol and plastid ($v_{\mathrm{G6P},C\rightarrow P}$) had to be made reversible to ensure the exchange of metabolites between the two compartments (Figure 5.1).

In the process of model development, various other aspects of the central carbon metabolism were considered such as the malate-aspartate shuttle and the PPP. The malate-aspartate shuttle could not be modelled to high degree of accuracy because it needed aspartate to be transported to the cytosol from the mitochondria to drive cytosolic oxaloacetate and malate synthesis. This situation is similar to the operation of plastidial glycolysis, which required glucose-6-phosphate to be transported from the cytosol to the plastid. The use of glycolytic intermediates for the synthesis of amino acids (serine and valine) played an important role in estimating plastidial glycolytic flux. In the malate-aspartate shuttle, however, the intermediates of the pathway are not used for the synthesis of amino acids or other metabolites meaning that there was no metabolite to drive the fluxes through this pathway making it completely unbalanced. Concerning the PPP, the lack of measured data on the metabolites of this pathway left it completely undefined disabling its proper calibration. Considering the cyclic nature of the PPP, feeding back into the glycolysis, it is impossible to quantify accurately any of the fluxes without measurement of its intermediates.

Although growth of the cell suspension was measured during the culture phase (Figure 3.3), the relatively short incubation time in the bioreactor meant that changes in biomass due to cell growth could be considered negligible and were omitted from the model. Also, data on the uptake of glucose from the media was not provided as prior analysis showed that the glucose uptake by the cells over the course of the incubation period did not have a detectable effect on the glucose concentration of the medium probably due to the relative small uptake as compared to the concentration levels in the medium.

The uptake of external glucose by the cell suspension and the reactions of glycolysis in both the cytosol and plastid were modelled with simple Michaelis-Menten kinetics. This assumption was made based on the observation that even though the amount of substrate available to the cell suspension was doubled after the fourth hour of incubation by adding ^{13}C-glucose, the concentration of metabolites in the glycolytic pathway did not increase accordingly. This implied that the uptake of external glucose and the reactions of glycolysis did not follow first-order kinetics. The other reactions of the central carbon metabolism were modelled with first-order kinetics in order to limit the number of model parameters.

The accumulation of lactate in the cell suspension under the low O_2 conditions was modelled with competitive Michaelis-Menten inhibition kinetics. The inhibitor was considered to be the product of the reaction, lactate. This assumption was made based on the observation that lactate levels peaked during the early stages of low O_2 induction and did not change thereafter, a phenomenon which has been observed in other low O_2 studies (Drew, 1997) and has been attributed to the inhibition of lactate dehydrogenase due to the lowering of pH caused by the synthesis of lactate and other organic acids (O'Carra and Mulcahy, 1997; Roberts et al., 1989).

5.4.4 Dynamics in reaching steady-state

Changes in the levels of metabolites were observed within an hour of their transfer to the bioreactor (Figure 5.2 and 5.3). At 21 kPa O_2, the change in metabolites could be due to the need for the cells to adapt to a new environment after transfer from the cell culture flask to well defined growth conditions in the bioreactor. This indicates that the cells were not growing under steady-state conditions before their transfer to the bioreactor. At 1 and 0 kPa O_2, however, the changes in metabolite levels at the first hours depict an adaptation not only to a new environment but also to the reduced O_2 levels. The effect of low O_2 on metabolites of the central carbon metabolism could be observed within the first few hours (Figure 5.4 and

5.5) showing a direct regulatory effect of O_2 on the activities of enzymes from time zero onwards.

Though metabolites in the upper part of glycolysis attained both metabolic (Figure 5.2) and isotopic steady-state (Figure 5.4), other metabolites in the central carbon metabolism did not attain steady-state. The flux maps of Figure 5.10 (calculated at 12 h, which was the last sampling point), which provide a clear overview of the effect of low O_2 on the central carbon metabolism, illustrate the closest steady-state could be approached under the experimental conditions studied. Interpretation of the flux maps, however, has to be carried out with a degree of caution since the unsteady-state conditions could create unequal mass balances around some metabolites. From Figure 5.10, it can be observed that low O_2 had a pronounced effect on the central carbon metabolism of the cells. The most significant difference was observed between 21 and 1 kPa O_2, with only minor additional changes when comparing 1 to 0 kPa O_2.

5.4.5 Effect of oxygen on the central carbon metabolism

At 21 kPa O_2, the flux model shows a behaviour characteristic of aerobic respiratory metabolism under optimal O_2 conditions (Grafahrend-Belau et al., 2009b; van Dongen et al., 2004) such as an active glycolysis, feeding of pyruvate into the TCA cycle, operation of the TCA cycle, high fluxes to production of anabolic metabolites including glutamate and aspartate, and a high energy status.

Low O_2 treatment was marked by a significant decrease in the uptake of external glucose by the cells (Figure 5.11A). Similar decreases in substrate uptake have been observed in other plant tissues subjected to low O_2 conditions (Geigenberger et al., 2000; Gout et al., 2001). The ability of the cells to reduce the uptake of externally supplied substrate is important in maintaining the energy status, since substrate uptake by plant cell suspensions comes with an additional energy cost. Indeed, the dependence of substrate uptake on ATP hydrolysis has been shown in cells of tobacco (Verstappen et al., 1991), suspension cells of *Olea europaea* (Oliveira et al., 2002) and *Daucus carota* (Krook et al., 2000), and protoplasts of *Pisum sativum* (Ritte et al., 1999) where the electrochemical gradient produced by the action of H^+-ATPase drives solute transport across the plasma membrane of cells. Coupled to the reduction in v_{UPT} was an increase usage of endogenous sugars ($v_{STA,P}$). This demonstrated that under low O_2 condition endogenous carbohydrates serve as an important substrate for glycolysis in heterotrophic plant cells.

The breakdown of starch is important in providing substrates for glycolysis under low O_2 stress. In rice seeds (Perata et al., 1992) and coleoptiles (Lasanthi-Kudahettige et al., 2007) as well as tomato fruit (Horchani et al., 2010) reductions in starch levels were observed under low O_2 stress. In the rice coleoptiles, a 60 % decrease in starch content was observed within 24 h after the induction of low O_2 stress. This decreased was accompanied by an increase activity of α-amylase showing the important role starch breakdown plays in the response of plant cells to low O_2 stress (Lasanthi-Kudahettige et al., 2007). When utilising the breakdown-products of starch (and sucrose) for glycolysis, plant cells can produce more ATP compared to using free glucose and fructose. The hydrolysis of starch and sucrose by starch phosphorylase and SuSy can yield 3 and 2.5 ATP molecules, respectively. This gain in ATP yield is related to the fact that glucose-1-phosphate and UDP-GLC produced from starch phosphorylase and SuSy do not need to be phosphorylated to enter glycolysis. This gain in ATP yield, though marginal, can be crucial for plant cells to survive low O_2 stress.

In addition to a reduced v_{UPT}, the translocation of pyruvate from the cytosol to the mitochondria ($v_{PYR,C\rightarrow M}$) and the ATP requiring synthesis of sucrose ($v_{SUC,V}$) were also reduced under low O_2 conditions (Appendix 3E). Reductions in the flux of the cytosolic to mitochondria pyruvate transport, an ATP dependent reaction (Weber and Bräutigam, 2013) , has also been observed in rice seedlings (Lakshmanan et al., 2013) and endosperm of barley (Grafahrend-Belau et al., 2009b) under low O_2 stress.This emphasises the need for plant cells to reduce energy usage when subjected to low O_2 conditions to ensure enough ATP for survival (Geigenberger, 2003). Indeed, in *Arabidopsis* roots a general reduction in the transcript levels of anabolic and transport proteins was observed at low O_2 (van Dongen et al., 2009).

At low O_2 an increased flux was observed through glycolysis in both cytosol (Figure 5.10B) resulting in an increased synthesis of pyruvate (Figure 5.11B). Comparing the fate of cytosolic pyruvate at the different O_2 levels, it was observed that about 26 and 2 % was transported to the mitochondria ($v_{PYR,C\rightarrow M}$) for use in the TCA cycle under 21 and 0 kPa O_2 respectively. However, the use of pyruvate for lactate ($v_{LAC,C}$) and ethanol (incorporated in $v_{EXT,C}$) production accounted for 73 and 97 % of cytosolic pyruvate at 21 and 0 kPa O_2 levels, respectively. This observation is in line with the behaviour of plants cells exposed to anaerobic conditions: up-regulation of glycolytic activity, inhibition of respiration and activation of the fermentative metabolism (Drew, 1997; Geigenberger, 2003). The ability of

plants to switch their metabolism from respiration to fermentation when faced with low O_2 conditions is important to ensure the continuous production of ATP.

Under the aerobic condition of 21 kPa O_2, a significant portion of cytosolic pyruvate (18 %) was still used for the synthesis of fermentative products (lactate and ethanol). This phenomenon has also been observed in other plant systems incubated under aerobic conditions (Edwards et al., 2012; Lakshmanan et al., 2013). A possible explanation for this observation is the availability of high amounts of substrate entering through glycolysis saturating the TCA cycle, hence requiring additional generation of NAD^+ by utilising pyruvate for fermentation.

Though mathematical modelling of different plant systems has shown that plastidial glycolytic fluxes occur at levels similar to or higher than that of the cytosol (Alonso et al., 2011; Grafahrend-Belau et al., 2009b; Rontein et al., 2002; Williams et al., 2010, 2008), the opposite was observed in this study (Figure 5.10). The high plastidial glycolytic fluxes observed in other plant tissues occur due to high anabolic fluxes in the plastid (including the synthesis of several amino acids and fatty acids) requiring more substrate as compared to the reactions in the cytosol. In the tomato cells used in this work and rice cell suspension (Lakshmanan et al., 2013), which were incubated under conditions of high substrate availability, the cytosolic glycolysis became more prominent due to the need to maximise the product of glycolysis (pyruvate) through the TCA cycle or fermentative pathways. It is assumed that the high amount of available substrate accounted for the high cytosolic glycolytic flux and the low transport of glucose-6-phosphate from the cytosol to the plastid ($v_{G6P,C\rightarrow P}$) as compared to the reversible transport flux ($v_{G6P,P\rightarrow C}$) at 21 kPa O_2.

The accumulation of the intermediates of glycolysis is one of the phenomena that have been observed in plants at low O_2 (Geigenberger et al., 2000; Miyashita and Good, 2008b). This accumulation is mainly caused by the inability of fermentation to utilise the intermediates synthesised from glycolysis due to the inhibition of the TCA cycle (Geigenberger et al., 2000; Miyashita and Good, 2008b; van Dongen et al., 2009). The accumulation of glycolytic intermediates is usually accompanied by an increase in the levels of other metabolites like alanine and succinate (Miyashita et al., 2007; Rocha et al., 2010). The accumulation of alanine in these plants systems has been attributed to the need for plants to avoid pyruvate accumulation due its activation effect on the alternative oxidase (Vanlerberghe et al., 1999) and the subsequent decline in respiratory ATP production under hypoxia (Gupta et al., 2009).

However, the main reason for cells to build-up alanine under anaerobic conditions is to avoid the production of ethanol, which can diffuse out of the cells leading to a loss of carbon (Bailey-Serres et al., 2012; Rocha et al., 2010). Plant cells, therefore, use the alanine production pathway to conserve their carbon reserves under low O_2. In the current work, no increased accumulation of alanine or any other amino acid was observed at low O_2 conditions. Maybe this was not the case due to the non-limiting supply of substrate, driving glycolysis and removing the need to conserve carbon. Hence, the cells could survive on fermentative metabolism through lactate and ethanol production without the need to conserve carbon by accumulation of alanine.

The lack of O_2 to regenerate the reducing equivalents generated by the TCA cycle meant that the ATP-dependent transport of pyruvate from the cytosol for use in the mitochondria (Weber and Braeutigam, 2013) had to be reduced since it occurs at a cost of ATP usage to the cells. This pyruvate transporter could, therefore, serve as an important control point in the operation of the TCA cycle in heterotrophic plant cells subjected to low O_2 stress.

Some phenomena such as the accumulation of succinate and the reversal of the TCA cycle, which have been detected in other low O_2 stress experiments (Grafahrend-Belau et al., 2009b) were not observed in this study. Reversing some reactions of the TCA cycle, especially the reaction catalysed by malate dehydrogenase, is important to oxidise the NADH produced from the conversion of 2-ketoglutarate to succinate via succinyl-CoA. This is important to ensure the redox balance of the cell. In heterotrophic plant cells at low O_2 conditions, reversing the activity of the TCA cycle might not be necessary since the accumulation of succinate and hence NADH does not occur.

Though the cells were able to produce ATP at O_2 levels (Figure 5.11E), the higher efficiency (expressed as ATP/substrate) at 21 kPa O_2 (Figure 5.11F) shows more ATP being produced per substrate utilised as compared to the low O_2 conditions. This is due to the reduced activity of the TCA cycle at low O_2, demonstrating the inefficiency of fermentative metabolism. The ATP/substrate ratio of 6 calculated for the low O_2 conditions is in agreement with the theoretical ATP levels produced when cells only utilise fermentative metabolism. The inability of the cells to produce, at 21 kPa O_2, anything close to the theoretical level of 36 ATP molecules per substrate utilised can be attributed to, on one hand, the use of ATP for substrate uptake (v_{UPT}) and on the other hand, use of pyruvate for other means like the biosynthesis of amino acids. Using the same principle, an ATP/substrate ratio of 7.8

(Williams et al., 2008) and 9.2 (Williams et al., 2010) was calculated for the central carbon metabolism of *Arabidopsis* cells growing under ambient O_2 levels, while a theoretical ATP/substrate ratio of 34 was obtained when all the glucose entering the cell was used for glycolysis and TCA cycle.

5.4.6 Control of the central carbon metabolism under different oxygen levels

The estimation of FCCs for cytosolic ($v_{PYR,C}$) and plastidial glycolysis ($v_{PYR,P}$), citrate ($v_{CIT,M}$) and lactate ($v_{LAC,C}$) production (Figure 5.12 and 5.13) showed that the control of metabolism is not restricted to a single enzyme, but is distributed over several enzymes. FCC, which are properties of metabolic networks, are not fixed parameters but can change under different environmental and genetic conditions (Fell, 1996). The sum of all FCC's acting on a specific pathway is unity with the enzyme having the highest FCC exerting a greater influence in the control of that pathway (Fell, 1996).

The FCC for $v_{PYR,C}$ and $v_{PYR,P}$ shows that v_{UPT} plays an important role in the control of glycolysis in both the cytosol and the plastid under the different O_2 levels. The control of glycolysis in the plastid is also strongly influenced by $v_{STA,P}$ for low O_2 levels. The control of glycolysis in plant systems have been found to depend on the tissue under investigation (Fothergill-Gilmore and Michels, 1993). In potato tubers, control of glycolysis was mainly exerted by pyruvate kinase (Thomas et al., 1997). In heterotrophic organisms like *Saccharomyces cerevisiae*, glycolytic activity has been found to be mainly influenced by the uptake of external sugar (Cortassa and Aon, 1994).

The entry of metabolites into the TCA cycle ($v_{CIT,M}$) was positively influenced by $k_{CIT,M}$ and $k_{PYR,C\rightarrow M}$ and negatively controlled by $k_{EXT,C}$, the pathway which competes with $v_{CIT,M}$ for substrate. To be able to increase TCA cycle activity under low O_2 conditions, plants need to increase the activity of enzyme(s) involved in transporting pyruvate from the cytosol to the mitochondria, to ensure the availability of substrate, and also to increase citrate production through activating citrate synthase.

The production of lactate under low O_2 conditions was controlled strongly by $k_{LAC,C}$ (and $V_{max,LAC,C}$ under the low O_2 levels) and by $k_{PYR,C\rightarrow M}$, meaning that efforts to reduce fermentative metabolism under low O_2 conditions should be geared towards reducing and increasing the activities of $k_{LAC,C}$ and $k_{PYR,C\rightarrow M}$ respectively, since these two enzymes exert activation and inhibitory effects on lactate production. Contrary to this observation, lactate

dehydrogenase was found to exert less than 2 % control on the production of lactate in tomato roots (Rivoal and Hanson, 1994), confirming that the control of metabolic pathways depends to a large extent on the tissue under study.

5.4.7 Metabolic versus genetic control

An important question that arises in the observed data is whether the regulation of plant metabolism within the initial period of low O_2 induction is under genetic or metabolic control. While both genetic and metabolic control will finally result in changed fluxes, genetic control starts from (de)-activation of genes, resulting in the expression of mRNA and the synthesis of proteins.

In the cell suspension studied, changes in metabolite levels were observed within an hour of their incubation under low O_2. This response to low O_2, even though fast, is likely to be controlled by changes in the expression of genes. This conclusion could be drawn based on observation made in other low O_2 stress studies. In *Arabidopsis* seedlings, changes in differential expression of transcripts and metabolite levels were observed within 0.5 h (van Dongen et al., 2009) and 2 h (Branco-Price et al., 2008) after induction of different levels of low O_2. Expression of anaerobic genes has also been observed within an hour of induction of hypoxia (Licausi et al., 2010). Even the expression of heat-related genes including heat shock proteins and heat shock factors which are induced by anoxia have been observed within an hour of low O_2 stress treatment (Banti et al., 2010). This shows that genetic control of the response of plants to low O_2 could occur fast enough to overrule metabolic control within the early stages of low O_2 induction.

Although genetic control might be responsible for the observed changes in the metabolism of the cells, this paper models the substrate-driven kinetics of the response to low O_2 as observed over the 12 h experimental period and does not explicitly model the kinetics of the genetic control. Implicitly, the impact of the genetic control is captured by the estimated rate constants that might differ between the different experimental O_2 conditions. Any observed difference in rate constants between the different O_2 levels is an indication of changes in enzymatic activity which might be caused by an increase or decrease in the amount of enzymes translated or a switch to a different iso-enzyme transcribed due to the induced low O_2 condition. Also regulation of metabolic reactions by enzyme co-factors was not explicitly

taken into account in this model and could be responsible for the differences in some of the estimated rate constants.

5.3.8 Cell suspension as a model system for studying fruit responses to low oxygen

The eventual objective of this study is to understand the metabolism of fruit stored under low O_2 conditions. In such conditions, the fruit should be stored at O_2 levels above the K_M of respiration in order avoid fermentation. Pears, for instance, are stored at low conditions of between 2.5-3 kPa O_2 (Pedreschi et al., 2009) well above the K_M of respiration of 0.68 kPa (de Wild et al., 1999) to avoid browning and other disorders caused by fermentation. However incubating plant cells at 1 kPa O_2, which is clearly above the K_M of respiration of 0.045 kPa (*Chapter 4*) lead to the activation of fermentative metabolism. The induction of fermentative metabolism has also been observed in other plants tissues incubated under low O_2 conditions above the K_M of respiration (Geigenberger et al., 2000; Narsai et al., 2009; Rocha et al., 2010; van Dongen et al., 2003). The difference between the low K_M of respiration of cell suspension and the high K_M values of intact fruits could be related to the presence of diffusion barriers within fruits which is absent in cell suspension.

The difference between the respiration kinetics of intact fruits stored under low O_2 conditions and cell suspension/tissues could be related to how metabolically active the cells are. Fruits under low O_2 conditions are kept at low temperatures (between -0.05 to -1°C for pears (Pedreschi et al., 2009)), while cell suspension/tissues are incubated at temperatures around 25 °C. The result is that fruits under CA storage are metabolically low active organs, while cell suspension/tissues are metabolically very active, meaning that they can respond readily to changes in O_2 levels. Despite these differences, cell suspension/tissues are suitable model systems to study and understand the metabolism of fruit low O_2 storage as they can incorporate ^{13}C-labelled and minimise gas diffusion barriers ensuring that the cells experience directly the experimentally induced low O_2 conditions.

5.5 Conclusions

The application of mathematical modelling to dynamic labelling data was crucial in understanding the changes in the metabolism of plant cells incubated at low O_2 conditions. Among the observed changes were a decrease in the uptake of external glucose, an increased hydrolysis of stored energy and a reduction in the activities of the TCA cycle, amino acid and sugar synthesis. In contrast, the activities of enzymes involved in the synthesis of lactate, and

the transport of glucose-6-phosphate from the plastid to the cytosol were enhanced under low O_2 as could be observed from the enhanced fluxes. The availability of high amounts of substrate ensured that the activation of alanine production from pyruvate and the reverse activity of malate dehydrogenase were not triggered, but an increased fermentative metabolism was able to sustain overall ATP production to ensure the survival of the cells. Though similar amounts of ATP were produced under all O_2 levels, this came at the cost of a reduced carbon use-efficiency. Analysis of metabolic control revealed that in heterotrophic cell suspension, the uptake of extracellular substrate controls most of the fluxes in the central carbon metabolism while the transport of pyruvate from the cytosol to the mitochondria controls the activity of the TCA cycle at low O_2 conditions. Also, enzymes which compete for a common substrate exert negative control on each other.

Chapter 6

Steady-State Flux Analysis of the Response of Tomato Cells to Low Oxygen

6.1 Introduction

The analysis of metabolic fluxes under steady-state conditions can be performed using ^{13}C-isotope labelling techniques by feeding an organism with a ^{13}C-label substrate and measuring the amount of label incorporated into different metabolites under steady-state conditions using MS or NMR (Rios-Estepa and Lange, 2007; Zamboni et al., 2009). Similar to this approach, fluxes can be measured under dynamic conditions by using dynamic label modelling approach described in *Chapter 5*. Between the two MFA approaches, fluxes measured under steady-state conditions is the most popular. This is partly related to the ease with which linear algebraic equations calculations can be solved for the steady-state situation compared to the more complex kinetic model equations that have to be solved for the dynamic case (Kruger et al., 2012; Rios-Estepa and Lange, 2007).

The analysis of steady-state fluxes using ^{13}C-MFA in plant cells is often based on the labelling information incorporated into PAA (Kruger et al., 2012). This procedure has been used to determine the flux distribution in different plant systems including *Arabidopsis* (Masakapalli et al., 2010; Williams et al., 2010, 2008), tomato cell suspension (Rontein et al., 2002), and maize seeds (Alonso et al., 2011) and to determine the role of the central carbon

---

The content of this part of the thesis is based on:

Ampofo-Asiama, J., Baiye, V.M.M., van Dongen, J.T., Waelkens, E., Geeraerd, A.H., Nicolai, B.M., Hertog, M.L.A.T.M., 2014. Kinetic modelling of the central metabolism of *Lycopersicum esculentum* cell suspension incubated at different oxygen levels. In preparation.

metabolism in lipid synthesis of sunflower embryos (Alonso et al., 2007a). However, to reduce the long incubation times needed to incorporate quantifiable amounts of ^{13}C-label into storage pools of plant cells including proteins, the focus of ^{13}C-labelling can be shifted to the free intracellular metabolites.

The objective of this chapter is to study the changes in the intermediate fluxes of the central carbon metabolism of tomato cell suspension following changes in the levels of dissolved O_2 in the culture medium. The aim is to investigate the changes in steady-state fluxes using the labelling of the free intracellular metabolites instead of the conventionally employed PAA and to compare the estimated steady-state fluxes with those determined from dynamic label modelling carried out in *Chapter 5*. Tomato cell suspensions were incubated in growth media equilibrated to air containing 21, 8, 5 and 0 kPa O_2. The cell suspensions were labelled to isotopic steady-state by feeding with a substrate mixture of U-^{13}C, 1-^{13}C and unlabelled glucose. The ^{13}C-label enrichment of the intermediates of the central carbon metabolism, free amino acids and sugars were measured with GC-MS. Using the mass isotopomer data of free intracellular metabolites, metabolic fluxes of the cell suspension equilibrated to different O_2 levels were estimated using the principle of steady-state ^{13}C-MFA.

6.2 Experimental procedure

6.2.1 Induction of low oxygen stress and metabolite analysis

Low O_2 stress experiments were carried out in the Lambda Minifor bench-top laboratory bioreactor (Lambda Laboratory Instruments, Czech Republic). The cell suspension in the linear phase of growth was transferred to the bioreactor, which was maintained at a temperature of 25 °C. The desired O_2 level (21, 8, 5 and 0 kPa) was achieved by flushing gas through the growth medium of the cells at a constant rate of 10 L/h throughout the experiment while the pH of the medium was maintained at a pH of 6.

The amount of glucose in the culture medium at the time of transfer to the bioreactor was around 85 mM. A concentrated glucose media containing U-^{13}C-glucose and 1-^{13}C-glucose was added to bring the concentration of glucose in the medium to 166 mM to achieve a ratio of 10:9:1 between the unlabelled, U-^{13}C and 1-^{13}C-glucose. The choice of label mixture was determined through the principles of optimal experimental design for ^{13}C-MFA (Antoniewicz, 2013; Metallo et al., 2009). Optimal experimental design selects the best input mixture for estimating the unknown network fluxes through maximisation of the information content of

the isotopomer measurements (Wiechert et al., 1999). The optimal mixture design was found by simulating different carbon labelling distributions starting from different mixtures of unlabelled, U-^{13}C and 1-^{13}C-glucose tracers. Simulations were done with the metabolic reaction network described in Appendix 4A, the software package 13CFLUX2 (Weitzel et al., 2013) and the measured labelling data. The performance of each mixture was evaluated based on the determinant of the Fisher Information Matrix, since this can be linked with the confidence regions of the unknown fluxes (Wiechert et al., 1999). A grid search considering all concentrations between 0 and 100 % was performed and the mixture (10:9:1) with the highest determinant value of the Fisher information matrix (or alternatively, the smallest determinant value of the variance-covariance matrix) was retained for experimental implementation (Bouvin and Cajot, 2012).

Cell samples were harvested under steady-state conditions (24 h after the start of the experiment where cells are in the stationary phase) by withdrawing 10 mL of medium, washing with glucose-free growth medium and immediately transferring to liquid nitrogen. The cells were assumed to be growing at steady-state when the percentage ^{13}C-label did not change significantly between subsequent sampling time points. A similar approach was used to determine metabolic steady-state in the cells. The harvested cells were lyophilised (Duratop and Duradry, FTS Systems Inc., Stone Ridge, NY, USA) for 24 h and dried for further 24 h in an oven at 50 °C. Free intracellular metabolites including organic acids, amino acids and sugars present in the cell suspension and ^{13}C-label accumulation were quantified using *Method 2* of the GC-MS protocol explained in *Chapter 3*.

6.2.2 Metabolic flux estimation using 13CFLUX2

Steady-state fluxes through the central carbon metabolism of the cells were estimated using 13CFLUX2, a high-performance software suite for ^{13}C-MFA (Weitzel et al., 2013). A compartmentalised metabolic network model consisting of the reactions of the glycolysis and TCA cycle was constructed for flux analysis. The metabolic network consisted of 50 reactions 6 of which were set as free fluxes and 8 were completely determined by constrained fluxes. All constrained fluxes were estimated as explained previously (Williams et al., 2010, 2008).

Metabolic fluxes were estimated using 99 mass isotopomer measurements of free intracellular polar metabolites. The values of free fluxes in the metabolic model were initiated randomly and 13CFLUX2 was used to minimise the sum of square error between the measured and

simulated mass isotopomer data. The *multifit* algorithm in 13CFLUX2 was used to initiate 1000 different combinations of free fluxes and the minimisation which gave the lowest error was chosen as the optimum solution. The sd of both dependent and free fluxes were determined using the 13CFLUX2 linearised statistical analysis algorithm. The estimated central metabolic fluxes were used to calculate the ATP production rate and ATP/substrate ratio of the cells as described in *Chapter 5*.

6.3 Results

6.3.1 Metabolic network for steady-state flux analysis

Steady-state MFA requires the construction of a network model that accurately depicts the governing metabolism and can also explain the measured ^{13}C-labelling data. In plant systems, a compartmentalised network model of the central carbon metabolism has been developed and used extensively for steady-state MFA (Kruger et al., 2012). In this work, however, a simpler network model of the central carbon metabolism was used (Figure 6.1). This was done to remove redundant pathways in the linear and cyclic part of the glycolysis and the TCA, respectively, as under steady-state condition these can be modelled with only a few reactions. Also, to ensure accurate flux estimates, most reversible reactions of the central carbon metabolism were modelled as forward reactions except for the transport reactions between cytosol and plastid, involving glucose-6-phosphate ($v_{G6P,C\rightarrow P}$) and pyruvate ($v_{PYR,P\rightarrow C}$), and the interconversion of malate and oxaloacetate (v_{OAA}).

In keeping with the key feature of compartmentalisation in plant metabolism, a compartmentalised network of glycolysis was implemented. The TCA cycle was included as well with its activity restricted to the mitochondria. The lack of measurements on the metabolites of the PPP lead to undefined flux estimates, hence the activity of the PPP was restricted to the production of ribose-5-phosphate which served the histidine synthesis.

Estimation of fluxes under steady-state conditions using ^{13}C-MFA requires attaining isotopic steady-state in the experimental system. Using the conventional approach of ^{13}C-label incorporated into PAA (Kruger et al., 2012), long incubation times are needed to achieve isotopic steady-state. In steady-state ^{13}C-MFA of *Arabidopsis* cell suspension (Williams et al., 2008) and sunflower embryos (Alonso et al., 2007a), isotopic steady-state in PAA was achieved after more than four days of incubation under ambient O_2 conditions. This implies that incubating tomato cell suspensions under low O_2 conditions, where cell growth can be

restricted, will require much longer incubation times to reach isotopic steady-state. To overcome this long incubation times, the ^{13}C-label incorporated into free intracellular metabolites, which can reach steady-state much faster, was used for steady-state MFA.

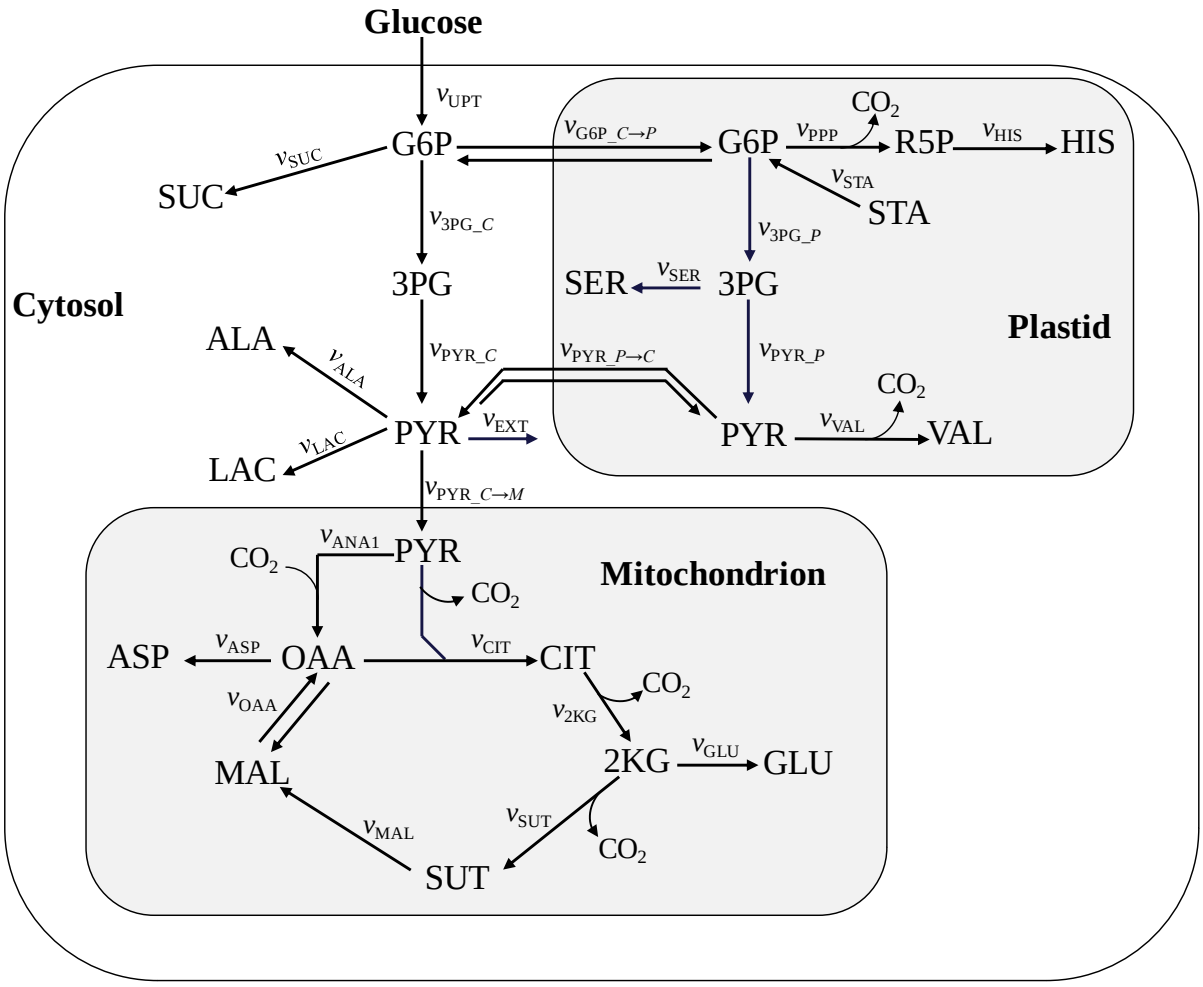

Figure 6.1: A schematic overview of the central metabolic network used to estimate the *in vivo* steady-state fluxes through tomato cell suspensions under different O_2 levels (2KG, 2-ketoglutarate; 3PG, 3-phosphoglycerate; ALA, alanine; ASP, aspartate; CIT, citrate; F6P, fructose-6-phosphate; G6P, glucose-6-phosphate; GLU, glutamate; LAC, lactate; HIS, histidine; MAL, malate; OAA, oxaloacetate; PYR, pyruvate; R5P, ribose-5-phosphate; STA, starch; SER, serine; SUC, sucrose; SUT, succinate; VAL, valine).

Considering that the key objective of this work was to focus on the free intracellular metabolites instead of PAA, biomass synthesis was considered negligible (due to that fact growth was assumed not to occur within the experimental duration) and excluded from the metabolic network model. A free flux, v_{EXT}, was introduced to account for the use of glycolytic intermediates, especially pyruvate, in pathways like fermentative metabolism at

low O_2 conditions (Figure 6.1). Intracellular amino acids (alanine, aspartate, glutamate, histidine, serine and valine), which are synthesised from the intermediates of the central carbon metabolism, were included in the model, and their activities were restricted to the different compartments as explained previously (Kruger et al., 2012). Although carbon dioxide (CO_2) released from the pathways of the central carbon metabolism is not incorporated into pyruvate for the formation of oxaloacetate (v_{ANA1}) as such, as the carbon source for this is bicarbonate, CO_2 was presented in Figure 6.1 for ease of interpretation. All carbon atom transitions in the metabolic network of Figure 6.1 were obtained from literature and can be found in Appendix 4A.

A smaller metabolic network model was used in the steady-state ^{13}C-MFA (Figure 6.1) compared to the dynamic label modelling (Figure 5.1) of *Chapter 5*. The difference in network model structure is due to the data used in both MFA approaches. The data used in the dynamic label modelling was based on the total ^{13}C-label incorporated into a metabolite. However, in the steady-state approach this data is not sufficient to provide accurate flux estimates as more ion fragments are needed to completely elucidate the isotopomer distribution of a metabolite. Hence, a different GC-MS derivatisation method (TDBMS, *Chapter 3*) which could provide more ion fragments from the intracellular metabolites was used in steady-state flux analysis. The result is that the information content of the available data in this steady-state approach, corresponds to a much smaller metabolite network in comparison with the dynamic approach.

6.3.2 Calibration of the metabolic network model on the experimental data

Based on the experimental data derived 24 h after the start of the incubation, steady-state fluxes were estimated using 13CFLUX2. Figure 6.2 shows the predicted versus measured labelling data. The simulated data could explain 91, 92, 97 and 98 % of the measured data at 21, 8, 5 and 0 kPa O_2 level respectively. The good agreement between the predicted and measured labelling data for all the O_2 treatments indicates that the constructed metabolic network model and the chosen free fluxes could adequately explain the measured mass isotopomer data set. Figure 6.2 also reveals the reduced label incorporation at 0 kPa as compared to 21 kPa O_2 which can be inferred from the predominant position of the data points at the two extremes of the line X=Y at 0 kPa as compared to 21 kPa O_2.

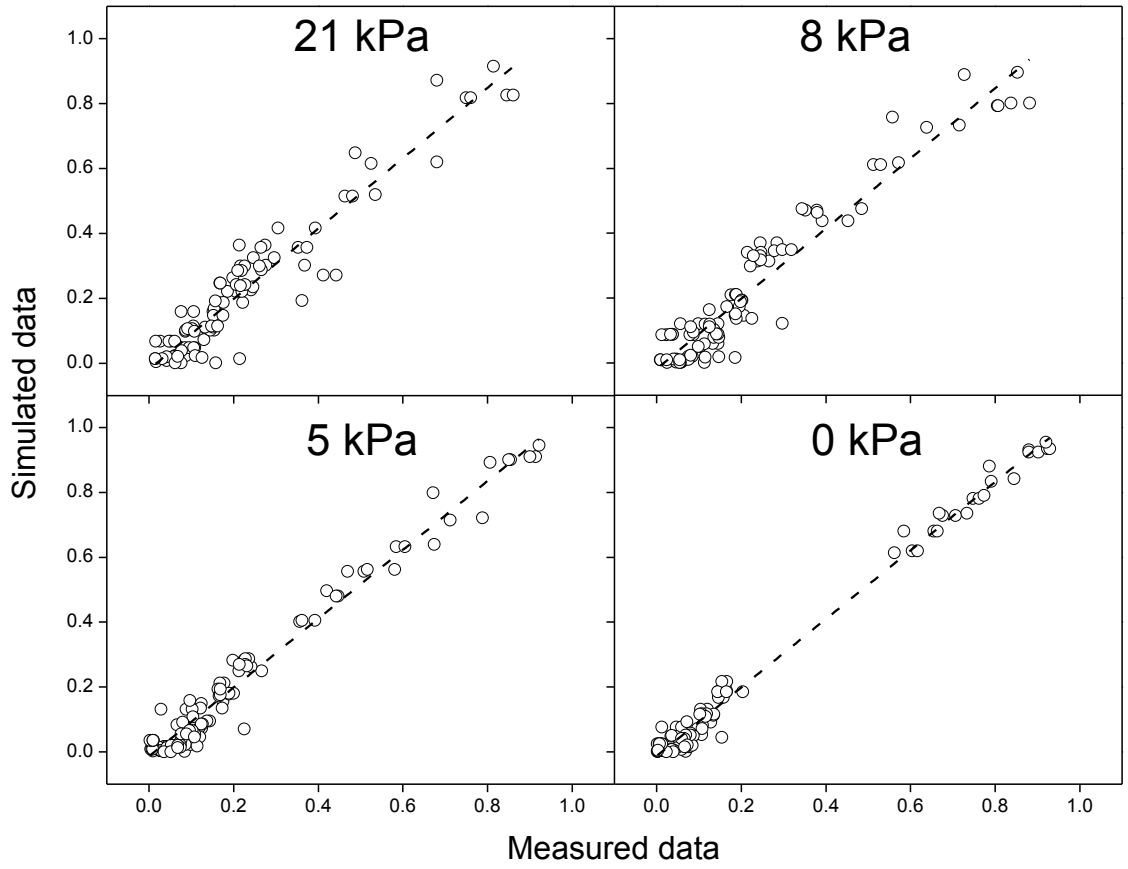

Figure 6.2: A plot of the simulated vs. measured ^{13}C-label data used for steady-state flux analysis at the different O_2 levels.

6.3.3 Fluxes through the central carbon metabolism at different oxygen levels

The estimated absolute fluxes through the central carbon metabolism and their sd can be found in Table 6.1. The fluxes thorugh the central carbon metabolism expressed relative to the glucose uptake rate (v_{UPT}) is shown in Appendix 4B.

The distribution of fluxes within the central carbon metabolism of the cells under the different experimental conditions as estimated using the fractional enrichment data is shown in Figure 6.3. Through Figures 6.3A-D, it can be observed that reducing the levels of dissolved O_2 in the growth medium of the cells had a pronounced effect on the fluxes through the central carbon metabolism. This is indicated by the colour and thickness of the arrows.

At 21 kPa O_2 level (Figure 6.3A), glucose taken up from the medium was mainly used as substrate for glycolysis. Starch hydrolysis (v_{STA}) was low as compared to the uptake of external glucose. The plastidial glycolytic flux was negligible as compared to the one in the cytosol. The doubling of the cytosolic flux around 3PG ($v_{PYR,C}$ as compared to $v_{3PG,C}$) resulted

from the breakdown of glucose-6-phosphate to give two molecules of 3-phosphoglycerate. About half of the cytosolic pyruvate was transported ($v_{PYR,C\rightarrow M}$) to the mitochondria and the remainder half was mainly used towards v_{EXT}. The fluxes towards amino acids, sucrose and PPP were very much lower compared to the fluxes through glycolysis and TCA cycle (Figure 6.3A).

Table 6.1: Absolute net fluxes (µmol/(mgDW·h)) and their standard deviation through the central carbon metabolism of tomato cell suspension at different O_2 levels estimated using 13CFLUX2.

Flux	**21 kPa**	**8 kPa**	**5 kPa**	**0kPa**
v_{ALA}	0.0049 ± 0.0008	0.0030 ± 0.0006	0.0029 ± 0.0003	0.0012 ± 0.0002
v_{ANA1}	0.0181 ± 0.0019	0.0102 ± 0.0012	0.0075 ± 0.0008	0.0049 ± 0.0006
v_{ASP}	0.0058 ± 0.0014	0.0035 ± 0.0006	0.0024 ± 0.0005	0.0015 ± 0.0003
v_{CIT}	0.1316 ± 0.0494	0.0519 ± 0.0116	0.0106 ± 0.0011	0.0068 ± 0.0014
v_{EXT}	0.2074 ± 0.0449	0.4172 ± 0.0251	0.3659 ± 0.0229	0.5801 ± 0.0542
$v_{G6P\_C\rightarrow P}$	0.0357 ± 0.0066	0.1112 ± 0.0099	0.0857 ± 0.0077	0.2110 ± 0.0256
v_{3PG_C}	0.1830 ± 0.0113	0.2420 ± 0.0143	0.1948 ± 0.0117	0.2973 ± 0.0276
v_{3PG_P}	0.0045 ± 0.0003	0.0034 ± 0.0004	0.0016 ± 0.0001	0.0008 ± 0.0001
v_{GLU}	0.0123 ± 0.0013	0.0067 ± 0.0010	0.0052 ± 0.0007	0.0034 ± 0.0005
v_{HIS}	0.0013 ± 0.00019	0.0008 ± 0.00008	0.0007 ± 0.00006	0.0002 ± 0.00003
v_{LAC}	0.0004 ± 0.00003	0.0007 ± 0.0001	0.0009 ± 0.0001	0.0009 ± 0.0001
v_{MAL}	0.1194 ± 0.0494	0.0452 ± 0.0116	0.0054 ± 0.0011	0.0034 ± 0.0014
v_{OAA}	0.1194 ± 0.0494	0.0452 ± 0.0116	0.0054 ± 0.0011	0.0034 ± 0.0014
v_{PPP}	0.0013 ± 0.0002	0.0008 ± 0.00008	0.0007 ± 0.00006	0.0002 ± 0.00003
v_{PYR_C}	0.3660 ± 0.0226	0.4841 ± 0.0286	0.3896 ± 0.0234	0.5947 ± 0.0553
$v_{PYR\_C\rightarrow M}$	0.1497 ± 0.0494	0.0621 ± 0.0116	0.0181 ± 0.0011	0.0117 ± 0.0014
v_{PYR_P}	0.0035 ± 0.0006	0.0035 ± 0.0008	0.0013 ± 0.0002	0.0007 ± 0.0003
v_{PYR_PC}	0.0037 ± 0.0006	0.0011 ± 0.0008	0.0018 ± 0.0002	0.0007 ± 0.0003
v_{SER}	0.0055 ± 0.0012	0.0032 ± 0.0004	0.0019 ± 0.0001	0.0009 ± 0.00002
v_{STA}	0.0415 ± 0.0065	0.1154 ± 0.0099	0.0879 ± 0.0077	0.2121 ± 0.0255
v_{SUC}	0.0012 ± 0.0002	0.0010 ± 0.0002	0.0008 ± 0.0002	0.0005 ± 0.00005
v_{SUT}	0.1194 ± 0.0494	0.0452 ± 0.0116	0.0054 ± 0.0011	0.0034 ± 0.0014
v_{2KG}	0.1316 ± 0.0494	0.0519 ± 0.0116	0.0106 ± 0.0011	0.0068 ± 0.0014
v_{UPT}	0.1485 ± 0.0074	0.1319 ± 0.0062	0.1099 ± 0.0055	0.0869 ± 0.0043
v_{VAL}	0.0036 ± 0.0004	0.0023 ± 0.0003	0.0015 ± 0.0003	0.0007 ± 0.0001

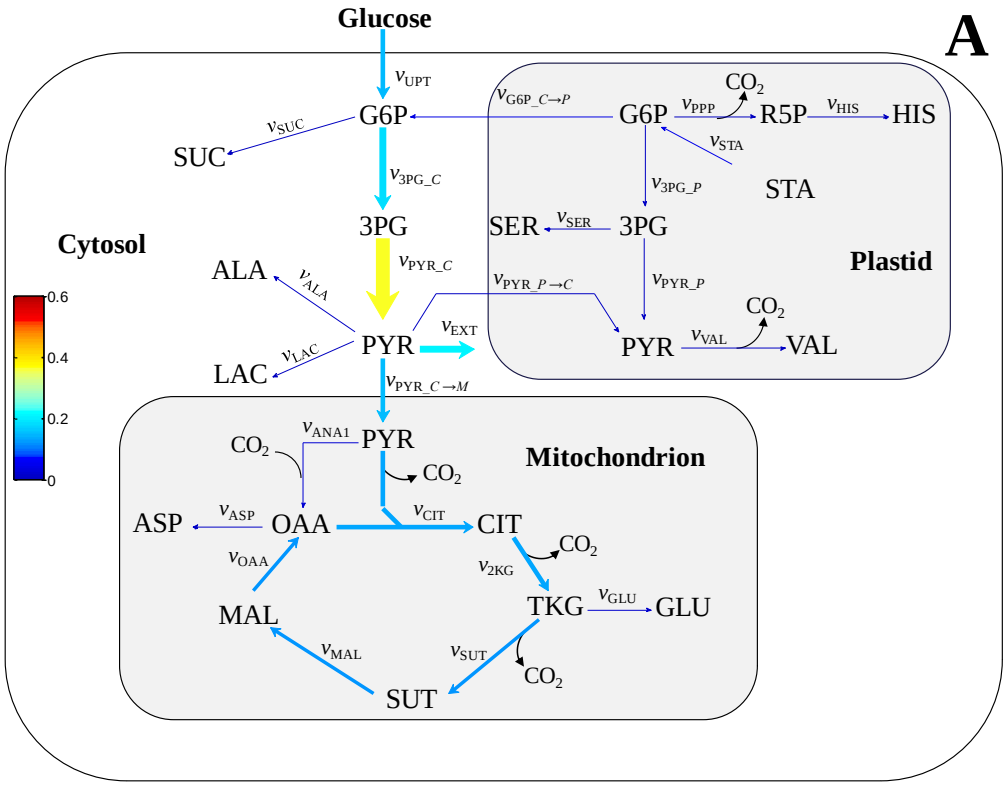
A
Glucose
v_{UPT}
G6P
v_{SUC}
SUC
v_{3PG_C}
3PG
Cytosol
ALA
v_{ALA}
LAC
v_{LAC}
PYR
v_{EXT}
v_{PYR_C}
$v_{PYR\_C \rightarrow M}$
0.6
0.4
0.2
0
$v_{G6P\_C \rightarrow P}$
G6P
v_{PPP}
CO_2
R5P
v_{HIS}
HIS
v_{STA}
STA
v_{3PG_P}
SER
v_{SER}
3PG
Plastid
$v_{PYR\_P \rightarrow C}$
v_{PYR_P}
PYR
v_{VAL}
CO_2
VAL
Mitochondrion
CO_2
v_{ANA1}
PYR
CO_2
ASP
v_{ASP}
OAA
v_{CIT}
CIT
CO_2
v_{OAA}
v_{2KG}
MAL
TKG
v_{GLU}
GLU
v_{MAL}
v_{SUT}
CO_2
SUT

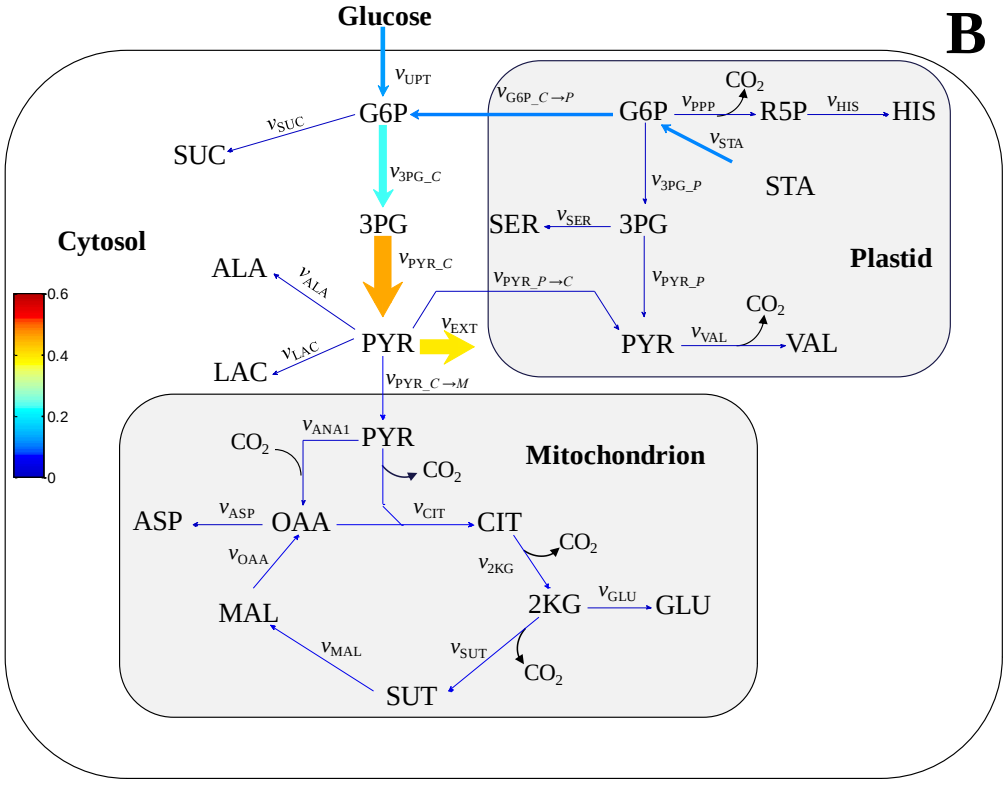
B
Glucose
v_{UPT}
G6P
v_{SUC}
SUC
v_{3PG_C}
3PG
Cytosol
ALA
v_{ALA}
LAC
v_{LAC}
PYR
v_{EXT}
v_{PYR_C}
$v_{PYR\_C \rightarrow M}$
0.6
0.4
0.2
0
$v_{G6P\_C \rightarrow P}$
G6P
v_{PPP}
CO_2
R5P
v_{HIS}
HIS
v_{STA}
STA
v_{3PG_P}
SER
v_{SER}
3PG
Plastid
$v_{PYR\_P \rightarrow C}$
v_{PYR_P}
PYR
v_{VAL}
CO_2
VAL
Mitochondrion
CO_2
v_{ANA1}
PYR
CO_2
ASP
v_{ASP}
OAA
v_{CIT}
CIT
CO_2
v_{OAA}
v_{2KG}
MAL
2KG
v_{GLU}
GLU
v_{MAL}
v_{SUT}
CO_2
SUT

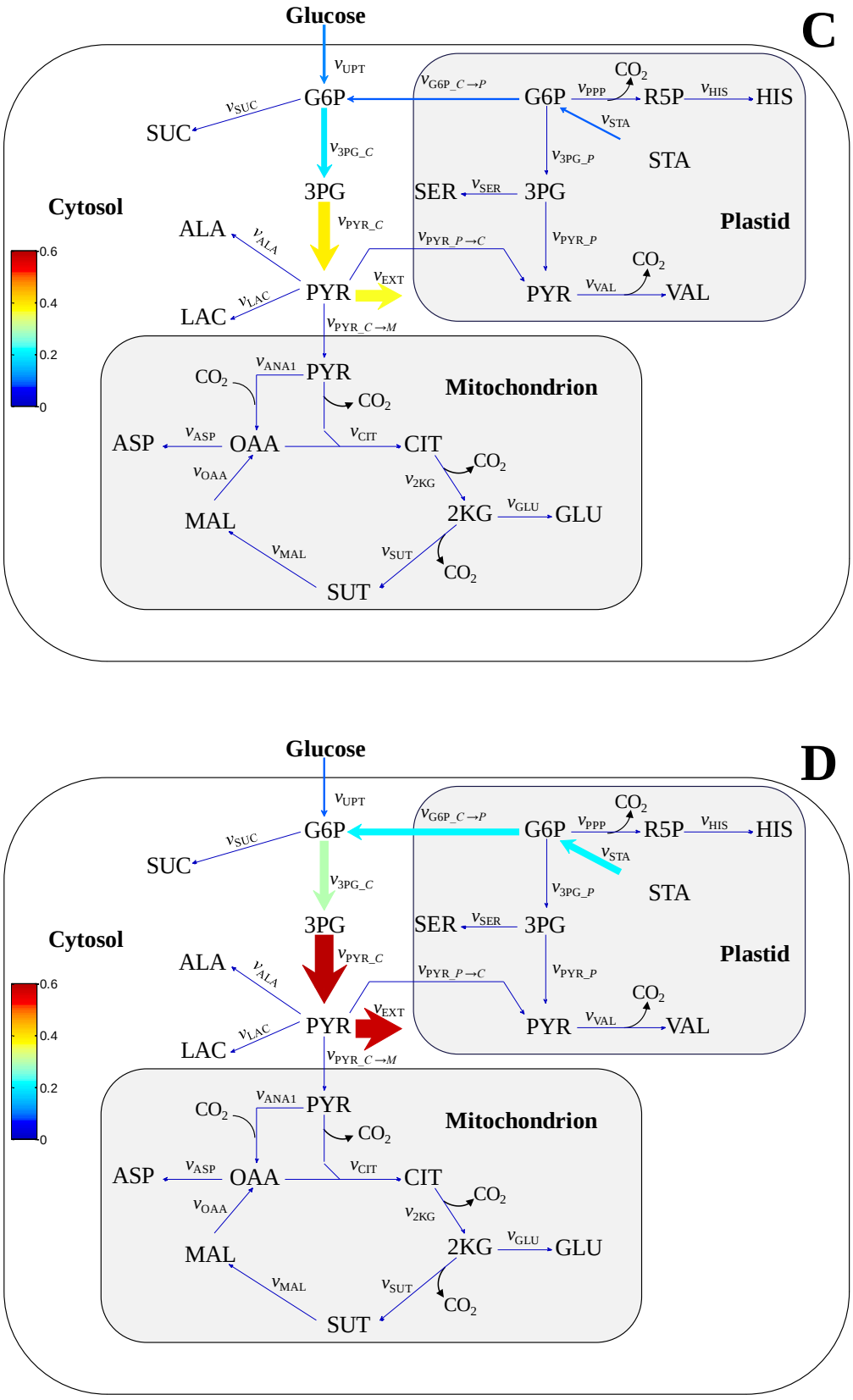

Figure 6.3: The effect of different O_2 levels (A, 21 kPa; B, 8 kPa; C, 5 kPa and D, 0 kPa) on the fluxes (µmol/(mgDW·h)) through the central carbon metabolism of tomato cells. The thickness and colour of an arrow is an indication of the flux through that pathway.

Lowering O_2 levels (Figure 6.3B-D) reduced the uptake of external glucose while an increased starch hydrolysis indicated an increase release of carbohydrates to sustain the meanwhile increased flux through glycolysis. Coupled to this was an increased flux of $v_{G6P,C\rightarrow P}$ with lowering O_2 levels. Another major effect of lowering O_2 levels was an increased diversion of the carbon flow from the TCA cycle towards fermentative metabolism (v_{EXT}). The reversible reactions involving glucose-6-phosphate ($v_{G6P,C\rightarrow P}$) and pyruvate ($v_{PYR,P\rightarrow C}$) as well as the interconversion of malate and oxaloacetate (v_{OAA}) retained the same net direction regardless the lowering O_2 levels.

The effect of different O_2 levels on some selected fluxes of the central carbon metabolism is shown in more detail in Figure 6.4. The uptake of external glucose (v_{UPT}) and the hydrolysis of stored carbon resources (v_{STA}) were both affected by the level of O_2 showing more than 40 % reduction in v_{UPT} while v_{STA} increased by more than 70 % when comparing 21 kPa to 0 kPa O_2 (Figure 6.4A).

Altering O_2 levels affected the operation of the glycolytic pathway in both the plastid and the cytosol. Taking the formation of pyruvate (v_{PYR_C} and v_{PYR_P}) as a measure of glycolytic activity, 100 times higher glycolytic fluxes were observed in the cytosol compared to the plastid (Figure 6.4B). While glycolytic fluxes through the cytosol increased with reducing O_2 levels, the opposite effect was observed in the plastid (Figure 6.4B).

Changes in the level of dissolved O_2 in the growth media of the cells had a profound impact on the operation of the TCA cycle (Figure 6.4C). There was a 50 % reduction in the activity of the TCA cycle (measured as the citrate formation flux, v_{CIT}) when the level of dissolved O_2 was changed from 21 to 8 kPa (Figure 6.4C). Between 8 and 5 kPa O_2, v_{CIT} decreased by another 20 %, while the flux at 0 kPa O_2 was not significantly different from the 5 kPa O_2 level (Figure 6.4C). The point of entry of carbon into the TCA cycle was also affected by the induction of low O_2 stress. While the anaplerotic flux (v_{ANA1}) accounted for about 10 % of carbon entering the TCA cycle at 21 kPa O_2 (Figure 6.4C), with lowering O_2 levels the relative contribution of v_{ANA1} increased to 16, 39 and 42 % of the total amount of carbon entering the TCA cycle under 8, 5 and 0 kPa O_2 levels respectively (Figure 6.4C). The formation of lactate (v_{LAC}) and the use of pyruvate for other reactions (v_{EXT}) were also affected by reducing O_2 levels (Figure 6.4D), even though v_{LAC} remained about 600 times lower than v_{EXT}.

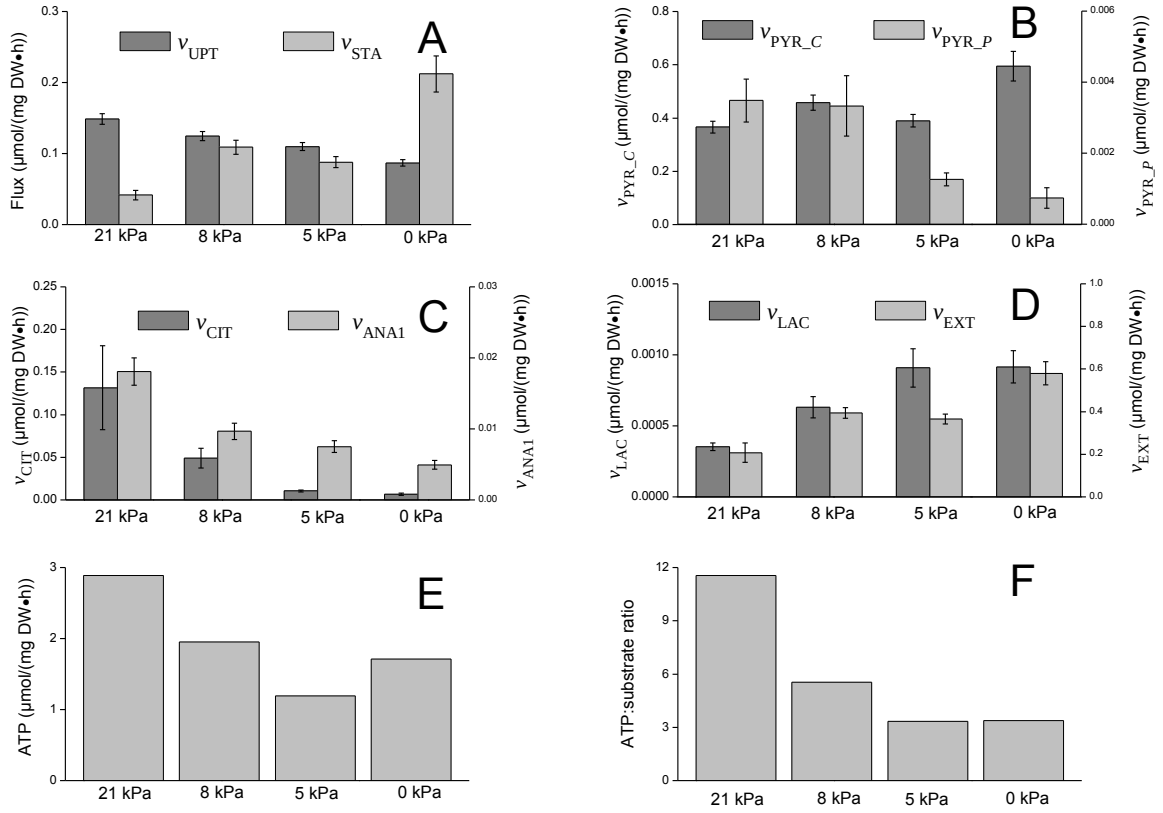

Figure 6.4: The effect of different O_2 levels on some selected fluxes through the central carbon metabolism of tomato cells as well as the ATP production rate and ATP/substrate ratio. The flux names are derived from Figure 6.1. The errors bars are sd derived from 13CFLUX2. Subheadings: A, energy source for the cell suspension from the uptake of external glucose (v_{UPT}) and starch hydrolysis ($v_{STA,P}$); B, fluxes towards pyruvate production in the cytsol ($v_{PYR,C}$) and plastid ($v_{PYR,P}$); C, entry of carbon into the TCA cycle from the synthesis of citrate ($v_{CIT,M}$) and the anaplerotic pathway (v_{ANA1}); D, synthesis of lactate ($v_{LAC,C}$) and ethanol ($v_{EXT,C}$); E; ATP production rate; F, ATP:substrate ratio.

The decrease in activity of the TCA cycle was accompanied by a significant reduction in the ATP/substrate ratio of the cells (Figure 6.4F) even though the total amount of ATP produced by the cells was less reduced (Figure 6.4E). Under 21 kPa O_2 level, an ATP/substrate ratio of 11.5 was estimated which reduced to 5.5 at 8 kPa O_2 (Figure 6.4F). An ATP/substrate of 3.4 was estimated for both 5 and 0 kPa O_2 levels (Figure 6.4F). The total amount of ATP produced showed its lowest level at 5 kPa O_2 with 0 kPa being closer to the amount of ATP produced at 8 kPa O_2.

6.4 Discussion

6.4.1 Label substrate for ^{13}C-MFA in plant cells

Selecting an optimal label precursor is important in obtaining precise flux estimates using ^{13}C-MFA. Taking into account that the cells were incubated under low O_2 conditions and that the ^{13}C-label incorporated into free intracellular metabolites was used for flux analysis instead of PAA, the optimal label precursor was selected to ensure accurate flux estimates in the glycolysis, the TCA cycle and the fermentation pathway. In plant tissues, it has been demonstrated that using 1-^{13}C-glucose alone or in combination with unlabelled glucose provides good estimates of the glycolytic pathway and especially the PPP (Williams et al., 2008). With respect to the TCA cycle, using either U-^{13}C glucose alone or by combining with unlabelled glucose gives the best flux estimates (Williams et al., 2008). Considering that the objective of this work was to measure the changes in the glycolysis, the TCA and fermentative metabolism, the fraction of 1-^{13}C-glucose in the substrate mixture was reduced as higher levels are usually needed to properly estimate the PPP. The substrate mixture used for this work was a combination of unlabelled glucose, U-^{13}C-glucose and 1-^{13}C-glucose in a ratio of 10:9:1 resulting in smaller standard errors of the flux estimates as compared to when only unlabelled and U-^{13}C-glucose would have been used.

6.4.2 Incubation times needed to attain steady-state metabolism

The analysis of fluxes using the principle of ^{13}C-MFA requires the realisation of metabolic and isotopic-steady state in the experimental system (Kruger et al., 2012; Ratcliffe and Shachar-Hill, 2006). To determine when the cells reached steady-state, the percentage fractional ^{13}C-label accumulated in the dynamic labelling experiment (*Chapter 3*) was examined. In addition, the fluxes through the central carbon metabolism of tomato cells estimated at different time-points using the principles of dynamic label modelling (*Chapter 5*) was also used to examine steady-state assumptions for the current experiment.

Figure 6.5 show some selected fluxes under 21 and 0 kPa O_2 estimated using the principles of dynamic label modelling. It can be observed that, in the cells incubated at 21 kPa O_2, the glycolytic fluxes v_{3PG_C} and v_{3PG_P}, did not change between 10 and 12 h indicating that they were operating at steady-state conditions. However, various other fluxes (e.g. v_{SUC}, v_{SER}, v_{GLU} and v_{FUM}) still changed between 10 and 12 h, showing they did not reach steady-state yet. At 0 kPa O_2 (Figure 6.5), steady-state metabolism was observed in v_{FUM}, v_{3PG_C} and v_{3PG_P} while

v_{SUC} had not reached steady-state. Also, unsteady-state conditions in other metabolites besides those of the glycolytic pathway were clearly present at both 21 and 0 kPa O_2 even after 12 h of incubation (*Chapter 3*). These results showed that the metabolism of the pathways in the upper part of the central carbon metabolism had reached steady-state after 12 h of incubation while those involved in the TCA cycle and biomass synthesis had not reached steady-state. To ensure isotopic and metabolic steady-state in all the metabolites involved in the central carbon metabolism and the free amino acids used for ^{13}C-MFA, the cells were incubated for a further 12 h, resulting in the total incubation time of 24 h applied in the current work.

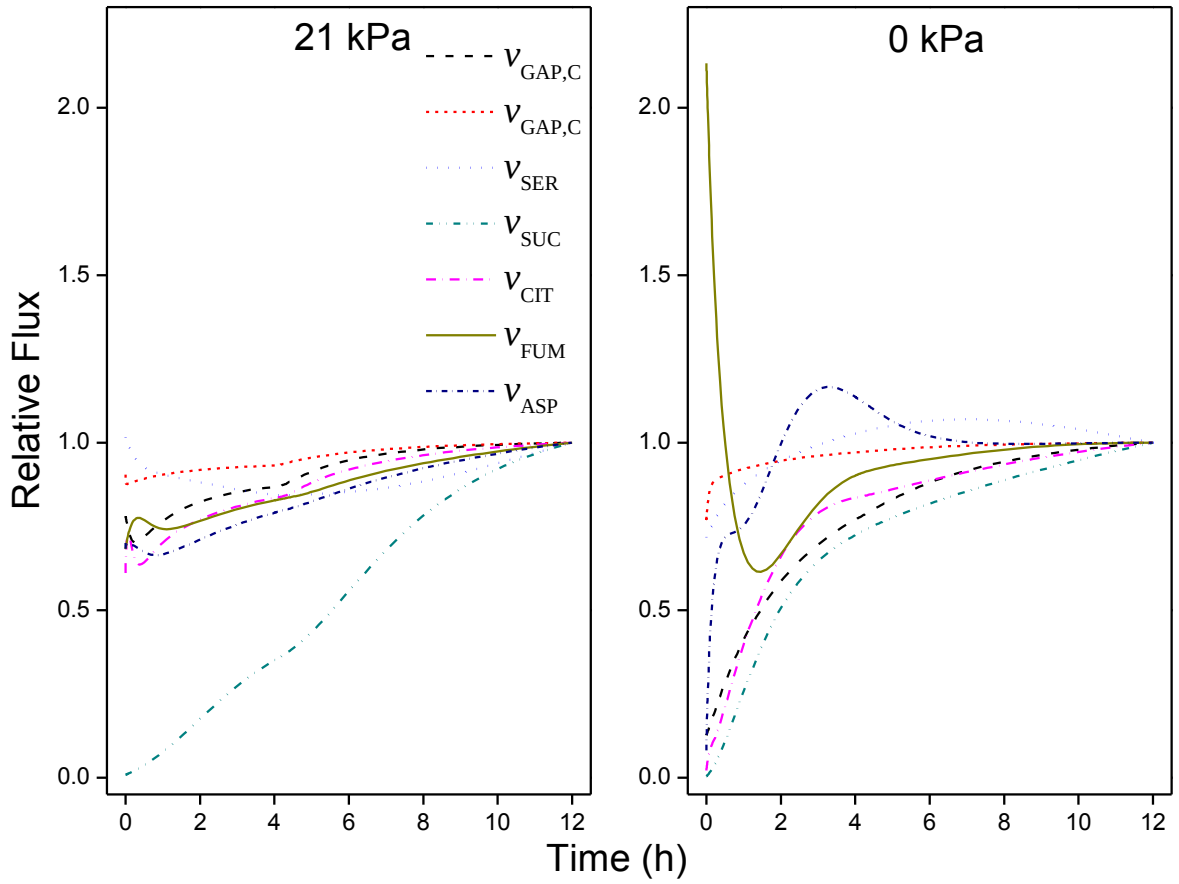

Figure 6.5: An overview of the changes in some selected fluxes through the central carbon metabolism of tomato cell suspension estimated at 21 and 0 kPa O_2 using dynamic label modelling (*Chapter 5*). The fluxes are expressed relative to the final flux at the sampling time point of 12 h. The changes in fluxes with time of v_{SUC}, v_{SER}, v_{GLU}, v_{FUM} at 21 kPa O_2 and v_{SUC} at 0 kPa O_2 show that steady-state metabolism is not reached within the experimental duration.

6.4.3 Low oxygen stress altered the steady-state fluxes through the central carbon metabolism

Low O_2 stress affected the steady-state fluxes through the central carbon metabolism of tomato cells (Figure. 6.3), among others resulting in a decreased uptake of external glucose. Since glucose uptake requires ATP, this decrease in v_{UPT} is important in reducing energy usage by the cells by switching to less ATP costly processes to obtain substrate(s) for glycolysis (Geigenberger et al., 2000). Low O_2 stress resulted furthermore in an increased hydrolysis of stored energy (v_{STA}) and higher fluxes through the cytosolic glycolysis. The increased glycolytic flux is important to ensure a continuous production of ATP. The fate of pyruvate was also affected by the induction of low O_2 stress. At 21 kPa O_2, about 40 % of pyruvate formed in the cytosol was transported to the mitochondria for use in the TCA cycle which reduced to 13, 5 and 2 % at 8, 5 and 0 kPa O_2, respectively. The fraction of pyruvate used for lactate and ethanol (incorporated in v_{EXT}) production, however, significantly increased under the low O_2 conditions (Figure 6.5D), showing the predominant role of fermentation at low O_2 stress conditions.

The effect of low O_2 stress on plant cells could also be assessed by estimating the amount of ATP produced (Figure 6.5E) as well as the ATP/substrate ratio (Figure 6.5F). The ATP/substrate ratio is a measure of the efficiency of substrate utilisation for energy production. The estimated ATP/substrate ratio showed that under the low O_2 conditions less ATP was produced by the cells per substrate utilised as compared to the 21 kPa O_2 level due to the relative inefficiency of fermentative metabolism with regard to energy production. The apparent recovery of the total ATP production at 0 kPa (as compared to 5 kPa) suggests that the cells are at least temporarily able to survive periods of shortage at the cost of exhausting their resources.

The ability of the central carbon metabolism to resist changes in fluxes has been well documented in steady-state MFA of plant tissues under different stress conditions (Rontein et al., 2002; Spielbauer et al., 2006; Williams et al., 2010, 2008). Plant cells have been observed to maintain relatively stable central metabolic fluxes under environmental stress conditions such as increased temperature (Williams et al., 2010) and genetic perturbations in starch production (Spielbauer et al., 2006). The response to low O_2, however, caused a re-programming of the central carbon metabolism. The combined reductions in activity of the TCA cycle, the up-regulation of glycolysis and fermentative metabolism and the low

ATP/substrate ratio observed in the current work are characteristic for plant cells undergoing anaerobic metabolism (Drew, 1997; Geigenberger, 2003). It shows that the relative stability of the central carbon metabolism depends on the type of stress incurred.

In the flux analysis of other plant tissues subject to low O_2 (Grafahrend-Belau et al., 2009b; Lakshmanan et al., 2013), diversion of fluxes and a destabilisation of the central carbon metabolism was observed. The difference in response of the central carbon metabolism between the low O_2 studies and other stress studies could be related to the role O_2 plays in the respiratory metabolism of cells. O_2 serves as an electron acceptor in the re-generation of NADH and $FADH_2$ produced by the TCA cycle. In the presence of O_2, these reducing equivalents are oxidised in the ETC and can be re-used, ensuring the continuous operation of the TCA cycle. Under biotic or abiotic stress conditions not altering the availability of O_2, plant cells remain able to operate the TCA cycle to ensure that the central carbon metabolism remains relatively stable. However, under low O_2 stress plant cells cannot rely on the ETC alone to generate reducing equivalents and therefore, alternative pathways such as fermentation are being utilised.

6.5 Comparative analysis of dynamic and steady-state modelling

One of the objectives of this chapter was to compare steady-state flux models with dynamic label modelling in studying the responses of plant cells to low O_2 stress. The estimation of metabolic fluxes using steady-state ^{13}C-MFA showed flux patterns characteristics of the oxidative and fermentative metabolism at 21 kPa and 0 kPa O_2 levels, respectively. Similar flux patterns were obtained in *Chapter 5* when using dynamic label modelling. Though differences in the estimated absolute fluxes were observed, the overall flux pattern was similar between the two approaches.

The similarity at both 21 and 0 kPa O_2 level can be attributed to the fact that the flux maps in *Chapter 5* were plotted for the 12 h time point. At this time point the metabolism of the cells in the upper part of the central carbon metabolism was in steady-state with most of the fluxes in the lower part of the central carbon metabolism approaching steady-state. Under such conditions when plant metabolism is operating close to steady-state, estimation of fluxes using either steady-state or dynamic analyses are by definition expected to give similar results. Compared to dynamic label modelling, steady-state ^{13}C- MFA is easier to perform

both experimentally and computationally, however, the estimation of fluxes using dynamic label modelling offers several advantages over steady-state analyses.

First, the analysis of fluxes using steady-state ^{13}C-MFA is not applicable to systems where steady-state metabolism cannot be ascertained. Metabolic and isotopic steady-state is reached when the metabolite levels and labelling patterns do no longer change in time. The methods for determining the presence of metabolic steady-state include measuring the rate of substrate uptake, product secretion, changes in intracellular metabolites and biomass. Isotopic steady-state is determined by analysing the time course of label incorporation. This implies that a prior analysis of steady-state must be carried out before performing the actual experiment, doubling the amount of work. While convincing evidence of isotopic steady-state are provided in most flux analysis work on plant (Alonso et al., 2011; Williams et al., 2008) reports of metabolic steady-state are few (Williams et al., 2008). This is related to the difficulty in achieving metabolic steady-state in batch cultures with the changing substrate levels continuously perturbing the cellular metabolism. It must, however, be emphasised that reaching isotopic steady-state is no guarantee for having established metabolic steady-state. Establishing isotopic steady-state in storage polymers and proteins requires extreme long incubation times when working with plant cells under different stress conditions (Williams et al., 2010, 2008). Taking into account that the time to reach such isotopic steady-state is inversely related to the growth rate of cells (Zamboni, 2007), incubation times of more than 5 days are likely to be required. With such long incubation times, changes in biomass and growth can no longer be ignored and requires maintaining plant cells in continuous reactors as used with microorganisms. In addition, under experimental conditions inhibiting cell growth, such as low O_2 stress conditions, reaching true isotopic steady-state requires even longer incubation times. In this work the difficulty in reaching isotopic steady-state was overcome by focusing on the labelling present in free intracellular metabolites ascertaining steady-state in the metabolites of the central carbon metabolism and closely related pathways.

Second, the analyses of fluxes under steady-state conditions require a careful selection of tracer label. Selection of appropriate labelled substrate(s) is important as the ability to estimate certain fluxes and the accuracy of the estimated fluxes is dependent on the labelled substrate(s) fed to the cells (Antoniewicz, 2013; Metallo et al., 2009). Availability and cost are the other factors that influence the choice of labelled substrate(s) in ^{13}C-MFA. For instance, it has been shown in mammalian (Metallo et al., 2009) and plant cells (Nargund and Sriram, 2012) that 1,2-^{13}C-glucose is the appropriate substrate to resolve fluxes though

glycolysis and PPP while a mixture of U-^{13}C-glucose and labelled glutamine provides the best estimate of TCA cycle flux (Metallo et al., 2009). However, the high cost of both 1,2-^{13}C-glucose and labelled glutamine have limited their application in ^{13}C-MFA. When applying dynamic label modelling, even though careful selection of label substrate(s) is required, also a 1:1 combination of unlabelled and U-^{13}C-glucose was already able to accurately resolve the fluxes through the central carbon metabolism of plant cells as described in *Chapter 5*.

Third, extra information can be extracted when using dynamic label modelling compared to steady-state MFA. Besides gaining insight into the eventual metabolic changes in plant cells upon the induction of stress, dynamic label modelling can be used to get a better understanding of the regulatory mechanism underlying the response as this is typically captured by the underlying dynamics of the enzyme kinetics. In addition, the principles of MCA can be applied to determine how the different enzymes and metabolites are involved in the control of metabolic pathways. Further, when using steady-state MFA it is possible to overlook the time resolved response of plant cells to different stress conditions; when the metabolism returns to steady-state conditions similar to that before the perturbation, the metabolic response can only be understood by considering the time dependent fluxes obtained from dynamic analyses. Also, when using dynamic modelling the reaction network and the information that can be obtained are generally more detailed. For instance, in a linear pathway consisting of several reactions, the steady state model is often lumped into few reactions as the consecutive fluxes are by definition the same at steady state. In a dynamic modelling approach the consecutive changes in metabolite levels and the corresponding labelling patterns, including the timing of label arrival, contributes unique information to elucidate the structure and regulation of such pathway.

Even though the analysis of fluxes under dynamic conditions offers several advantages, steady-state ^{13}C-MFA is still useful in obtaining a quick overview of the changes in metabolism of plants upon the induction of stress as long as isotopic and metabolic steady-state can be assured. The lack of dedicated software for performing dynamic label simulations limits its applicability while ^{13}C-MFA steady-state can be readily carried out using freely available software such as 13CFLUX2. Furthermore, interpreting flux maps from dynamic experiments is conceptually more difficult as they have to be interpreted in combination with the changing concentration levels of the involved metabolites.

6.6 Conclusions

Using the ^{13}C-label accumulated in free intracellular metabolites, the steady-state fluxes through the central carbon metabolism of tomato cells under different O_2 levels were estimated. The steady-state response of the tomato cells to low O_2 stress involved a decrease in substrate uptake, a reduction in ATP/substrate ratio and a decreased TCA cycle activity and amino acid synthesis. Contrary to observations made in previous stress studies on the stability of the central carbon metabolism, low O_2 stress caused a re-adjustment of metabolism from oxidative to fermentative metabolism. Comparing the estimated steady-state fluxes to those determined through dynamic label modelling revealed similarities in the overall flux pattern though differences in absolute fluxes were observed. While both techniques can be used to understand plant metabolism, dynamic label modelling offers several advantages including providing more detailed information on the regulation of metabolism under different O_2 stress conditions.

Chapter 7

General Conclusions and Perspectives

7.1 General conclusions

The aim of this thesis was to study the effect of low O_2 stress on plants through metabolome and fluxome analysis with a focus on the response of plant cells to the low O_2 conditions employed during fruit storage. Studying and understanding the response of plant cells to low O_2 stress is important as they serve as an important source of food. Among the sub-objectives of this work was to understand the low O_2 induced changes in the central carbon metabolism of plants due to its role in providing energy and building blocks for the survival and growth of cells.

To measure metabolic fluxes using ^{13}C-MFA, plants have to metabolise a supplied ^{13}C-labelled substrate, with the label incorporated into a metabolite giving an idea of the flux through that pathway. Feeding ^{13}C-labelled substrate to whole plants or tissues is difficult due to the large amount of storage sugars which limits the uptake of external substrate. To ensure that the experimental systems used in this thesis could metabolise the external supplied ^{13}C-labelled substrate, a heterotrophic cell suspension was used as the model system. Cell suspension is a good model system for studying plant metabolism as it can be easily manipulated to grow on a defined substrate.

In this thesis, protocols were developed to establish and maintain cell suspensions from tomato leaves as well as identifying and quantifying the intracellular polar metabolites and ^{13}C-label present in the cells using GC-MS. Subsequently, experiments were performed by incubating the obtained tomato cell suspensions in a bioreactor at different O_2 levels in a medium supplemented with ^{13}C-glucose to determine the effect of low O_2 stress on the

metabolome and fluxome of the cells. As expected, the induction of low O_2 changed the primary metabolome of the cells. The cells accumulated lactate, sugar alcohols such as glycerol and the intermediates of glycolysis. Other metabolites involved in primary metabolism like amino acids, organic acids and nitrogen containing compounds such as GABA were lowered under low O_2 stress. The incorporation of ^{13}C-label showed that, with the exception of lactate, all other primary metabolites accumulated less ^{13}C-label under low O_2 conditions.

To quantitatively interpret the response of plant cells to low O_2 stress, mathematical models of the central carbon metabolism were constructed and calibrated on the experimental data. Both a dynamic kinetic model and a steady state flux model were developed. Both models showed that low O_2 stress caused a reduction in the uptake of external glucose while increasing the hydrolysis of stored energy in the cells. Also, the activity of the TCA cycle and the biosynthesis of amino acids and sugars were reduced under low O_2 stress. However, fluxes towards the synthesis of lactate and ethanol and the transport of glucose-6-phosphate from the plastid to the cytosol increased under low O_2 stress. This activation of fermentative metabolism is important in providing enough energy to the cells under low O_2 stress. Analysis of ATP productions showed that the cells were able to generate the same amount of ATP under all O_2 levels but at an increasing cost of high carbon-usage with lowering O_2 levels. MCA showed that the uptake of extracellular glucose controls most of the fluxes in the central carbon metabolism while the transport of pyruvate from the cytosol to the mitochondria controls the activity of the TCA cycle at low O_2 conditions.

The results obtained using both dynamic and steady-state modelling showed that quantitative information provided by MFA analysis helps to elucidate the intricate regulatory systems that govern the response of the respiration and fermentation pathways to changes in O_2 availability. While similar flux maps were obtained using either dynamic modelling or steady-state flux analysis, the dynamic flux analysis offered several advantages by revealing the time dependent changes to O_2 stress. Steady-state flux analysis, however, can be used to obtain a quick overview of the changes in metabolism upon stress induction assuming careful tracer selection and a system where metabolic and isotopic steady-state can be assured.

7.2 Future perspectives

To shed more light on the adaptive mechanisms plants employ when faced with low O_2 conditions, future research on metabolome and fluxome analyses using plant cells can be extended by elaborating more on the following aspects:

- The non-targeted metabolic profiling of tomato cells using GC-MS can be supplemented with data from other analytical techniques such as LC-MS. Measurements on the intermediates of the PPP and fermentative metabolites such as ethanol and acetylaldehyde can be obtained to provide a complete overview of the changes in primary metabolism upon low O_2 stress induction.

- The kinetic model can be improved by adding measurements from more intermediate O_2 levels, and by adding measurements of currently undetermined metabolites in the central carbon metabolism such as oxaloacetate and ACoA. The rate of respiration can be measured to provide information on O_2 consumption and CO_2 production which can be incorporated into the model. Also, the high energy intermediates, ATP and ADP, as well as the cofactors, NAD^+/NADH and FAD^+/$FADH_2$, can be measured and incorporated into the model. Kinetic models can also be constructed where O_2 is incorporated as an integral part of the modelled kinetics instead of determining the effect of low O_2 stress on the individual kinetic parameters as was done in the current work.

- The estimation of steady-state fluxes can be enhanced by combining GC-MS measurements with data from NMR and other MS approaches such as LC-MS. The estimation of compartmentalised fluxes under steady-state conditions can be improved by using metabolite and ^{13}C-label measurements from different sub-cellular compartments based on non-aqueous cell fractionation techniques.

A reduced central metabolic network was constructed to model the dynamic changes in ^{13}C-label and metabolite concentration in this thesis. However, genome scale models can be constructed to explain the response of the central carbon metabolism to low O_2 stress. To further throw more light on the kinetic response of plant cells to low O_2 stress, genome scale models can be supplemented with full Michaelis-Menten kinetic models based on the underlying biochemistry of effectors and inhibitors of the different pathways of the central carbon metabolism.

To fully comprehend the biochemical response of plant cells to low O_2 stress, metabolic profiling should be supplemented with other profiling data from the transcriptome, proteome and genome. This will offer the opportunity to understand how the different cellular organisational levels are coordinated during the low O_2 stress response of plants. Transcriptome measurements will give insights on how some fluxes are (un)altered by giving information on iso-enzymes that are (de)activated under low O_2 stress. Transcriptome measurements can also be incorporated into the dynamic model to improve its accuracy. Even though this might require additional model parameters, the information gained will provide information on the link between the changes in metabolites and enzymes and how they affect the low O_2 response of plants.

The observed changes in metabolite levels within an hour of incubating cells under low O_2 conditions suggest the presence of an O_2 sensing mechanism in the cell suspension. This sensing mechanism could be due to a direct or an indirect response to low O_2 stress. Although, some components of the indirect sensing mechanism such as changes in metabolites has been modelled dynamically, other indirect sensing agents such as the adenylates (ATP, ADP and/or AMP) could be measured and introduced into the model. Also, the response of the direct O_2 sensing mechanism in plants, which has recently been elucidated, could be measured under different O_2 levels and incorporated into the dynamic model.

To increase our understanding of the response of intact plant organs to low O_2 stress, further research can be carried out on the differentiated cells present in fruit. Differentiated cells can be extracted from fruits and incubated in a bioreactor or very thin slices of tissues can be prepared to overcome the presence of gas diffusion barriers. Working with such material obtained directly from the fruit will require starvation experiments to deplete existing sugar reserves before externally supplied labelled substrates will effectively be taken up by the cells. When working with larger tissue disks or intact fruits, microstructure related gas diffusion barriers that induce additional O_2 gradients have to be considered as they are contributing to the externally applied O_2 stress. Ultimately, to understand the metabolome and fluxome response to low O_2 stress at the whole fruit level, the developed dynamic pathway models can be coupled to existing biophysical models of mass transfer taking into account the actual fruit microstructure. In this way a spatial description can be obtained of the central carbon metabolism in function of the prevalent O_2 gradients in the fruit.

Reference

Affourtit, C., Krab, K., Moore, A.L., 2001. Control of plant mitochondrial respiration. Biochim. Biophys. Acta Bioenerg. 1504, 58–69.

Allen, D.K., Ratcliffe, R.G., 2009. Quantification of Isotope Label, in: Schwender, J. (Ed.), Plant Metabolic Networks. Springer New York, pp. 105–149.

Aloni, B., Rosenshtein, G., 1982. Effect of flooding on tomato cultivars: the relationship between proline accumulation and other morphological and physiological changes. Physiol. Plant. 56, 513–517.

Alonso, A.P., Goffman, F., Ohlrogge, J., Shachar-Hill, Y., 2007a. Carbon conversion efficiency and central metabolic fluxes in developing sunflower (*Helianthus annuus* L.) embrryos. Plant J. 52, 296–308.

Alonso, A.P., Raymond, P., Rolin, D., Dieuaide-Noubhani, M., 2007b. Substrate cycles in the central metabolism of maize root tips under hypoxia. Phytochemistry, 68, 2222–2231.

Alonso, A.P., Val, D.L., Shachar-Hill, Y., 2011. Central metabolic fluxes in the endosperm of developing maize seeds and their implications for metabolic engineering. Metab. Eng. 13, 96–107.

Amoako-Andoh, F.O., Daniëls, B., Keulemans, W., Davey, M.W., 2014. A systematic evaluation of protocols for a proteomics analysis of (lyophilized) fruit tissues. Electrophoresis 35, 1395–1405.

Andrews, D., MacAlpine, D., Johnson, J., Kelley, P., Cobb, B., Drew, M.C, 1994. Differential induction of mRNAs for the glycolytic and ethanolic fermentative pathways by hypoxia and anoxia in maize seedlings. Plant Physiol. 106, 1575–82.

Antoniewicz, M.R., 2013. ^{13}C-metabolic flux analysis: optimal design of isotopic labeling experiments. Curr. Opin. Biotechnol. 24, 1116–1121.

Babcock, G.T., 1999. How oxygen is activated and reduced in respiration. Proc. Natl. Acad. Sci. 96, 12971–12973.

Babushok, V.I., Linstrom, P.J., Reed, J.J., Zenkevich, I.G., Brown, R.L., Mallard, W.G., Stein, S.E., 2007. Development of a database of gas chromatographic retention properties of organic compounds. J. Chromatogr. A 1157, 414–421.

Bailey-Serres, J., Freeling, M., 1990. Hypoxic stress-induced changes in ribosomes of maize seedling roots. Plant Physiol. 94, 1237–43.

Bailey-Serres, J., Fukao, T., Gibbs, D.J., Holdsworth, M.J., Lee, S.C., Licausi, F., Perata, P., Voesenek, L.A.C.J., van Dongen, J.T., 2012. Making sense of low oxygen sensing. Trends Plant Sci. 17, 129–138.

Banti, V., Mafessoni, F., Loreti, E., Alpi, A., Perata, P., 2010. The heat-inducible transcription factor HsfA2 enhances anoxia tolerance in *Arabidopsis*. Plant Physiol. 152, 1471–1483.

Bartram, R.J., 2004. Gas Management Systems for Gas Chromatography, in: Grob, R.L., Barry, E.F. (Eds.), Modern Practice of Gas Chromatography. John Wiley & Sons, Inc., pp. 491–543.

Baxter, C., Redestig, H., Schauer, N., Repsilber, D., Patil, K., Nielsen, J., Selbig, J., Liu, J., Fernie, A.R, Sweetlove, L., 2007. The metabolic response of heterotrophic *Arabidopsis* cells to oxidative stress. Plant Physiol. 143, 312–325.

Biais, B., Beauvoit, B., Allwood, J.W, Deborde, C., Maucourt, M., Goodacre, R., Rolin, D., Moing, A., 2010. Metabolic acclimation to hypoxia revealed by metabolite gradients in melon fruit. J. Plant Physiol. 167, 242–5.

Bino, R.J., de Vos, C.H.R., Lieberman, M., Hall, R.D., Bovy, A., Jonker, H.H., Tikunov, Y., Lommen, A., Moco, S., Levin, I., 2005. The light-hyperresponsive high pigment-2dg mutation of tomato: alterations in the fruit metabolome. New Phytol. 166, 427–438.

Bouvin, J., Cajot, S., 2012. Optimaal ontwerp van ^{13}C gelabelde experimenten voor bepaling van fluxen in het centraal metabolisme. MSc. thesis, KU Leuven, Belgium.

Bowsher, C.G., Tobin, A.K., 2001. Compartmentation of metabolism within mitochondria and plastids. J. Exp. Bot. 52, 513–527.

Branco-Price, C., Kaiser, K.A., Jang, C.J.H., Larive, C.K., Bailey-Serres, J., 2008. Selective mRNA translation coordinates energetic and metabolic adjustments to cellular oxygen deprivation and reoxygenation in *Arabidopsis thaliana*. Plant J. 56, 743–755.

Bylesjö, M., Rantalainen, M., Cloarec, O., Nicholson, J.K., Holmes, E., Trygg, J., 2006. OPLS discriminant analysis: combining the strengths of PLS-DA and SIMCA classification. J. Chemom. 20, 341–351.

Carroll, A.D., Fox, G.G., Laurie, S., Phillips, R., Ratcliffe, R.G., Stewart, G.R., 1994. Ammonium assimilation and the role of γ-aminobutyric acid in pH homeostasis in carrot cell suspensions. Plant Physiol. 106, 513–520.

Cho, K., Shibato, J., Agrawal, G.K., Jung, Y.H., Kubo, A., Jwa, N.S., Tamogami, S., Satoh, K., Kikuchi, S., Higashi, T., Kimura, S., Saji, H., Tanaka, Y., Iwahashi, H., Masuo, Y., Rakwal, R., 2008. Integrated transcriptomics, proteomics, and metabolomics analyses To survey ozone responses in the leaves of rice seedling. J. Proteome Res. 7, 2980–2998.

Cloutier, M., Chen, J., Tatge, F., McMurray-Beaulieu, V., Perrier, M., Jolicoeur, M., 2009. Kinetic metabolic modelling for the control of plant cells cytoplasmic phosphate. J. Theor. Biol. 259, 118–131.

Colón, A.M., Sengupta, N., Rhodes, D., Dudareva, N., Morgan, J., 2010. A kinetic model describes metabolic response to perturbations and distribution of flux control in the benzenoid network of *Petunia hybrida*. Plant J. 62, 64–76.

Cortassa, S., Aon, M.A., 1994. Metabolic control analysis of glycolysis and branching to ethanol production in chemostat cultures of *Saccharomyces cerevisiae* under carbon, nitrogen, or phosphate limitations. Enzyme Microb. Technol. 16, 761–770.

Dauner, M., Sauer, U., 2000. GC-MS analysis of amino acids rapidly provides rich information for isotopomer balancing. Biotechnol. Prog. 16, 642–649.

De Hoffmann, E., Stroobant, V., 2007. Mass Spectrometry: Principles and Applications. John Wiley & Sons.

De Livera, A.M., Dias, D.A., De Souza, D., Rupasinghe, T., Pyke, J., Tull, D., Roessner, U., McConville, M., Speed, T.P., 2012. Normalizing and integrating metabolomics data. Anal. Chem. 84, 10768–10776.

De Vos, R.C.H., Moco, S., Lommen, A., Keurentjes, J.J.B., Bino, R.J., Hall, R.D., 2007. Untargeted large-scale plant metabolomics using liquid chromatography coupled to mass spectrometry. Nat. Protoc. 2, 778–791.

De Wild, H.P.J., Woltering, E.J., Peppelenbos, H.W., 1999. Carbon dioxide and 1-MCP inhibit ethylene production and respiration of pear fruit by different mechanisms. J. Exp. Bot. 50, 837–844.

Dennis, D.T., Huang, Y., Negm, F.B., 1997. Glycolysis, the Pentose Phosphate Pathway and Anaerobic Respiration, in: Dennis, D.T., Turpin, D.H., Lefebvre, D.D., Layzel, B.D. (Eds.), Plant Metabolism. Longman, Singapore, pp. 105–123.

Dettmer, K., Aronov, P.A., Hammock, B.D., 2007. Mass spectrometry-based metabolomics. Mass Spectrom. Rev. 26, 51–78.

Drew, M.C., 1997. Oxygen deficiency and root metabolism: injury and acclimation under hypoxia and anoxia. Annu. Rev. Plant Physiol. Plant Mol. Biol. 48, 223–250.

Dunn, W.B., Ellis, D.I., 2005. Metabolomics: Current analytical platforms and methodologies. Trends Anal. Chem. 24, 285–294.

Edwards, J.M., Roberts, T.H., Atwell, B.J., 2012. Quantifying ATP turnover in anoxic coleoptiles of rice (*Oryza sativa*) demonstrates preferential allocation of energy to protein synthesis. J. Exp. Bot. 63, 4389–4402.

Edwards, J.S., Palsson, B.O., 2000. The *Escherichia coli* MG1655 in silico metabolic genotype: Its definition, characteristics, and capabilities. Proc. Natl. Acad. Sci. 97, 5528–5533.

Evans, D.E., Colemand, J.O.D., Kearns, A., 2003. Cell Suspension Culture, in: Evans, D.E., Colemand, J.O.D., Kearns, A. (Eds.), Plant Cell Culture. Taylor & Francis, London, pp. 63–94.

Fan, T.W., Higashi, R.M., Lane, A.N., 1986. Monitoring of hypoxic metabolism in superfused plant tissues by *in vivo* ^{1}H NMR. Arch. Biochem. Biophys. 251, 674–687.

Felix, G., Grosskopf, D.G., Regenass, M., Basse, C.W., Boller, T., 1991. Elicitor-induced ethylene biosynthesis in tomato cells: characterization and use as a bioassay for elicitor action. Plant Physiol. 97, 19–25.

Fell, D., 1996. Understanding the Control of Metabolism, 1st ed. Portland Pr.

Fell, D.A., Sauro, H.M., 1985. Metabolic control and its analysis. Additional relationships between elasticities and control coefficients. Eur. J. Biochem. 148, 555–561.

Fernie, A.R., Morgan, J.A., 2013. Analysis of metabolic flux using dynamic labelling and metabolic modelling. Plant. Cell Environ. 36, 1738–1750.

Fiehn, O., 2002. Metabolomics--the link between genotypes and phenotypes. Plant Mol. Biol. 48, 155–171.

Fiehn, O., 2006. Metabolite Profiling in *Arabidopsis*, in: Salinas, J., Sanchez-Serrano, J.J. (Eds.), *Arabidopsis* Protocols. Humana Press, pp. 439–447.

Fischer, E., Zamboni, N., Sauer, U., 2004. High-throughput metabolic flux analysis based on gas chromatography–mass spectrometry derived ^{13}C constraints. Anal. Biochem. 325, 308–316.

Fothergill-Gilmore, L.A., Michels, P.A., 1993. Evolution of glycolysis. Prog. Biophys. Mol. Biol. 59, 105–235.

Franck, C., Lammertyn, J., Nicolaï, B.M., 2005. Metabolic profiling using GC-MS to study biochemical changes during long-term storage of pears. Acta Hort. 682, 1991–1998.

Franck, C., Lammertyn, J., Tri, Q., Verboven, P., Verlinden, B., Nicolaï, B.M., Ho, Q.T., 2007. Browning disorders in pear fruit. Postharvest Biol. Technol. 43, 1–13.

Fredlund, E., Blank, L.M., Schnurer, J., Sauer, U., Passoth, V., 2004. Oxygen- and glucose-dependent regulation of central carbon metabolism in *Pichia anomala*. Appl. Environ. Microbiol. 70, 5905–5911.

Fukusaki, E., Jumtee, K., Bamba, T., Yamaji, T., Kobayashi, A., 2006. Metabolic fingerprinting and profiling of *Arabidopsis thaliana* leaf and its cultured cells T87 by GC/MS. Z. Naturforsch. C. 61, 267–272.

Galili, G., 2011. The aspartate-family pathway of plants: linking production of essential amino acids with energy and stress regulation. Plant Signal. Behav. 6, 192–195.

Geigenberger, P., 2003. Response of plant metabolism to too little oxygen. Curr. Opin. Plant Biol. 6, 247–256.

Geigenberger, P., 2011. Regulation of starch biosynthesis in response to a fluctuating environment. Plant Physiol. 155, 1566–77.

Geigenberger, P., A.R., Gibon, Y., Christ, M., Stitt, M., 2000. Metabolic activity decreases as an adaptive response to low internal oxygen in growing potato tubers. Biol. Chem. 381, 723–40.

Geigenberger, P., Stitt, M., Fernie, A.R., 2004. Metabolic control analysis and regulation of the conversion of sucrose to starch in growing potato tubers. Plant. Cell Environ. 27, 655–673.

Gibon, Y., Vigeolas, H., Tiessen, A., Geigenberger, P., Stitt, M., 2002. Sensitive and high throughput metabolite assays for inorganic pyrophosphate, ADPGlc, nucleotide phosphates, and glycolytic intermediates based on a novel enzymic cycling system. Plant J. 30, 221–235.

Gombert, A.K., Nielsen, J., 2000. Mathematical modelling of metabolism. Curr. Opin. Biotechnol. 11, 180–186.

Gout, E., Boisson, A.M., Aubert, S., Douce, R., Bligny, R., 2001. Origin of the cytoplasmic pH changes during anaerobic stress in higher plant cells. Carbon-13 and phosphorous-31 nuclear magnetic resonance studies. Plant Physiol. 125, 912–25.

Grafahrend-Belau, E., Junker, B.H., Klukas, C., Koschützki, D., Schreiber, F., Schwöbbermeyer, H., 2009a. Topology of Plant Metabolic Networks, in: Schwender, J. (Ed.), Plant Metabolic Networks. Springer New York, pp. 173–209.

Grafahrend-Belau, E., Schreiber, F., Koschützki, D., Junker, B.H., 2009b. Flux balance analysis of barley seeds: a computational approach to study systemic properties of central metabolism. Plant Physiol. 149, 585–598.

Green, D.E., Stumpf, P.K., 1942. Starch phosphorylase of potato. J. Biol. Chem. 142, 355–366.

Grob, R.L., 2004. Theory of Gas Chromatography, in: Robert, L.G., Barry, E.F. (Eds.), Modern Practice of Gas Chromatography. John Wiley & Sons, Inc., pp. 23–63.

Gupta, K.J., Zabalza, A., van Dongen, J.T., 2009. Regulation of respiration when the oxygen availability changes. Physiol. Plant. 137, 383–391.

Halket, J.M., Waterman, D., Przyborowska, A.M., Patel, R.K.P., Fraser, P.D., Bramley, P.M., 2005. Chemical derivatization and mass spectral libraries in metabolic profiling by GC/MS and LC/MS/MS. J. Exp. Bot. 56, 219–243.

Hall, R., Beale, M., Fiehn, O., Hardy, N., Sumner, L., Bino, R., 2002. Plant metabolomics: the missing link in functional genomics strategies. Plant Cell 14, 1437–1440.

Han, P.P., Yuan, Y.J., 2009. Metabolic profiling as a tool for understanding defense response of *Taxus cuspidata* cells to shear stress. Biotechnol. Prog. 25, 1244–1253.

Hanes, C.S., 1940. The reversible formation of starch from glucose-1-phosphate catalysed by potato phosphorylase. Proc. R. Soc. B Biol. Sci. 129, 174–208.

Heinrich, R., Rapoport, T.A., 1974. A linear steady-state treatment of enzymatic chains. General properties, control and effector strength. Eur. J. Biochem. 42, 89–95.

Heinzle, E., Matsuda, F., Miyagawa, H., Wakasa, K., Nishioka, T., 2007. Estimation of metabolic fluxes, expression levels and metabolite dynamics of a secondary metabolic pathway in potato using label pulse-feeding experiments combined with kinetic network modelling and simulation. Plant J. 50, 176–87.

Hertog, M.L.A.T.M., Verlinden, B.E., Lammertyn, J., Nicolaï, B.M., 2007. OptiPa, an essential primer to develop models in the postharvest area. Comput. Electron. Agric. 57, 99–106.

Hinshaw, J. V., 2004. Optimization of Separations and Computer Assistance, in: Grob, R.L., Barry, E.F. (Eds.), Modern Practice of Gas Chromatography. John Wiley & Sons, Inc., pp. 193–228.

Ho, Q.T., Buts, K., Herremans, E., Hertog, M.L.A.T.M., Verboven, P., Nicolaï, B.M., 2014. Hypoxic Storage of Fruit, in: van Dongen, J.T., Licausi, F. (Eds.), Low-Oxygen Stress in Plants, Plant Cell Monographs. Springer Vienna, pp. 353–369.

Ho, Q.T., Verboven, P., Verlinden, B.E., Lammertyn, J., Vandewalle, S., Nicolai, B.M., 2008. A continuum model for metabolic gas exchange in pear fruit. PLoS Comput. Biol. 4, 1–13.

Ho, Q.T., Verboven, P., Verlinden, B.E., Schenk, A., Delele, M.A., Rolletschek, H., Vercammen, J., Nicolaï, B.M., 2010. Genotype effects on internal gas gradients in apple fruit. J. Exp. Bot. 61, 2745–2755.

Horchani, F., Khayati, H., Aschi-Smiti, S., 2010. Contrasted responses to root hypoxia in tomato fruit at two stages of development. J. Plant Biol. 54, 15–22.

Huber, S.C., Huber, J.L., 1996. Role and regulation of sucrose-phosphate synthase in higher plants. Annu. Rev. Plant Physiol. Plant Mol. Biol. 47, 431–444.

Hur, M., Campbell, A.A., Almeida-de-Macedo, M., Li, L., Ransom, N., Jose, A., Crispin, M., Nikolau, B.J., Wurtele, E.S., 2013. A global approach to analysis and interpretation of metabolic data for plant natural product discovery. Nat. Prod. Rep. 30, 565.

Ishikawa, T., Takahara, K., Hirabayashi, T., Matsumura, H., Fujisawa, S., Terauchi, R., Uchimiya, H., Kawai-Yamada, M., 2010. Metabolome analysis of response to oxidative stress in rice suspension cells overexpressing cell death suppressor Bax inhibitor-1. Plant Cell Physiol. 51, 9–20.

Kacser, H., Burns, J.A., 1995. The control of flux. Biochem. Soc. Trans. 23, 341–66.

Kader, A.A., Ben-Yehoshua, S., 2000. Effects of superatmospheric oxygen levels on postharvest physiology and quality of fresh fruits and vegetables. Postharvest Biol. Technol. 20, 1–13.

Kanabus, J., Bressan, R.A., Carpita, N.C., 1986. Carbon assimilation in carrot cells in liquid culture. Plant Physiol. 82, 363–368.

Kim, H.K., Choi, Y.H., Verpoorte, R., 2010. NMR-based metabolomic analysis of plants. Nat. Protoc. 5, 536–549.

Kim, H.K., Choi, Y.H., Verpoorte, R., 2011. NMR-based plant metabolomics: where do we stand, where do we go? Trends Biotechnol. 29, 267–275.

Kim, H.K., Verpoorte, R., 2010. Sample preparation for plant metabolomics. Phytochem. Anal. 21, 4–13.

Kind, T., Wohlgemuth, G., Lee, D.Y., Lu, Y., Palazoglu, M., Shahbaz, S., Fiehn, O., 2009. FiehnLib: mass spectral and retention index libraries for metabolomics based on quadrupole and time-of-flight gas chromatography/mass spectrometry. Anal. Chem. 81, 10038–10048.

Klok, E.J., Wilson, I.W., Wilson, D., Chapman, S.C., Ewing, R.M., Somerville, S.C., Peacock, W.J., Dolferus, R., Dennis, E.S., 2002. Expression profile analysis of the low-oxygen response in *Arabidopsis* root cultures. Plant Cell 14, 2481–2494.

Kohlstedt, M., Becker, J., Wittmann, C., 2010. Metabolic fluxes and beyond-systems biology understanding and engineering of microbial metabolism. Appl. Microbiol. Biotechnol. 88, 1065–1075.

Komatsu, S., Yamamoto, A., Nakamura, T., Nouri, M.Z., Nanjo, Y., Nishizawa, K., Furukawa, K., 2011. Comprehensive analysis of mitochondria in roots and hypocotyls of soybean under flooding stress using proteomics and metabolomics techniques. J. Proteome Res. 10, 3993–4004.

Kontunen-Soppela, S., Ossipov, V., Ossipova, S., Oksanen, E., 2007. Shift in birch leaf metabolome and carbon allocation during long-term open-field ozone exposure. Glob. Chang. Biol. 13, 1053–1067.

Kopka, J., Fernie, A.R, Weckwerth, W., Gibon, Y., Stitt, M., 2004. Metabolite profiling in plant biology: platforms and destinations. Genome Biol. 5, 109.

Kreuzwieser, J., Hauberg, J., Howell, K.A., Carroll, A., Rennenberg, H., Millar, A.H., Whelan, J., 2009. Differential response of gray poplar leaves and roots underpins stress adaptation during hypoxia. Plant Physiol. 149, 461–473.

Krook, J., Vreugdenhil, D., van der Plas, L.H.W., 2000. Uptake and phosphorylation of glucose and fructose in *Daucus carota* cell suspensions are differently regulated. Plant Physiol. Biochem. 38, 603–612.

Kruger, N.J., Masakapalli, S.K., Ratcliffe, R.G., 2012. Strategies for investigating the plant metabolic network with steady-state metabolic flux analysis: lessons from an *Arabidopsis* cell culture and other systems. J. Exp. Bot. 63, 2309–2323.

Kruger, N.J., Ratcliffe, R.G., 2009. Insights into plant metabolic networks from steady-state metabolic flux analysis. Biochimie 91, 697–702.

Lakshmanan, M., Zhang, Z., Mohanty, B., Kwon, J.Y., Choi, H.Y., Nam, H.J., Kim, D.I., Lee, D.Y., 2013. Elucidating rice cell metabolism under flooding and drought stresses using flux-based modeling and analysis. Plant Physiol. 162, 2140–2150.

Langbecker, C.L., Ye, G.N., Broyles, D.L., Duggan, L.L., Xu, C.W., Hajdukiewicz, P.T.J., Armstrong, C.L., Staub, J.M., 2004. High-frequency transformation of undeveloped plastids in tobacco suspension cells. Plant Physiol. 135, 39–46.

Lara, M. V., Budde, C.O., Porrini, L., Borsani, J., Murray, R., Andreo, C.S., Drincovich, M.F., 2010. Peach (*Prunus persica*) fruit response to anoxia: reversible ripening delay and biochemical changes. Plant Cell Physiol. 52, 392–403.

Lasanthi-Kudahettige, R., Magneschi, L., Loreti, E., Gonzali, S., Licausi, F., Novi, G., Beretta, O., Vitulli, F., Alpi, A., Perata, P., 2007. Transcript profiling of the anoxic rice coleoptile. Plant Physiol. 144, 218–31.

Lee, J., Rudell, D.R., Davies, P.J., Watkins, C.B., 2012. Metabolic changes in 1-methylcyclopropene (1-MCP)-treated "Empire" apple fruit during storage. Metabolomics 8, 742–753.

Lee, K.W., Chen, P.W., Yu, S.M., 2014. Metabolic adaptation to sugar/O_2 deficiency for anaerobic germination and seedling growth in rice. Plant. Cell Environ.

Lehmann, M., Schwarzländer, M., Obata, T., Sirikantaramas, S., Burow, M., Olsen, C.E., Tohge, T., Fricker, M.D., Møller, B.L., Fernie, A.R., Sweetlove, L.J., Laxa, M., 2009. The metabolic response of *Arabidopsis* roots to oxidative stress is distinct from that of heterotrophic cells in culture and highlights a complex relationship between the levels of transcripts, metabolites, and flux. Mol. Plant 2, 390–406.

Lei, Z., Huhman, D. V., Sumner, L.W., 2011. Mass spectrometry strategies in metabolomics. J. Biol. Chem. 286, 25435–25442.

Libourel, I.G.L., Shachar-Hill, Y., 2008. Metabolic flux analysis in plants: from intelligent design to rational engineering. Annu. Rev. Plant Biol. 59, 625–650.

Licausi, F., van Dongen, J.T., Giuntoli, B., Novi, G., Santaniello, A., Geigenberger, P., Perata, P., 2010. HRE1 and HRE2, two hypoxia-inducible ethylene response factors, affect anaerobic responses in *Arabidopsis thaliana*. Plant J. 62, 302–315.

Lisec, J., Schauer, N., Kopka, J., Willmitzer, L., Fernie, A.R., 2006. Gas chromatography mass spectrometry–based metabolite profiling in plants. Nat. Protoc. 1, 387–396.

Loescher, W.H., 1987. Physiology and metabolism of sugar alcohols in higher plants. Physiol. Plant. 70, 553–557.

Lunn, J.E., 2007. Compartmentation in plant metabolism. J. Exp. Bot. 58, 35–47.

Lunn, J.E., MacRae, E., 2003. New complexities in the synthesis of sucrose. Curr. Opin. Plant Biol. 6, 208–214.

Lytovchenko, A., Beleggia, R., Schauer, N., Isaacson, T., Leuendorf, J.E., Hellmann, H., Rose, J.K., Fernie, A.R., 2009. Application of GC-MS for the detection of lipophilic compounds in diverse plant tissues. Plant Methods 5, 4.

Magneschi, L., Perata, P., 2009. Rice germination and seedling growth in the absence of oxygen. Ann. Bot. 103, 181–196.

Marty, F., 1999. Plant vacuoles. Plant Cell 11, 587–599.

Masakapalli, S.K., Lay, P. Le, Huddleston, J.E., Pollock, N.L., Kruger, N.J., Ratcliffe, R.G., 2010. Subcellular flux analysis of central metabolism in a heterotrophic *Arabidopsis* cell suspension using steady-state stable isotope labeling. Plant Physiol. 152, 602–619.

Martin, C., Smith, M., 1995. Starch biosynthesis. Plant Cell 7, 971–985.

Mathur, J., Koncz, C., 1998. Establishment and Maintenance of Cell Suspension Cultures, in: Martinez-Zapater, J.M., Salinas, J. (Eds.), *Arabidopsis* Protocols. Humana Press, Totowa, NJ, pp. 27–30.

Mcfarlane, N.M., Ciavarella, T.A., Smith, K.F., 2003. The effects of waterlogging on growth, photosynthesis and biomass allocation in perennial ryegrass (*Lolium perenne* L.) genotypes with contrasting root development. J. Agric. Sci. 141, 2003.

Metallo, C.M., Walther, J.L., Stephanopoulos, G., 2009. Evaluation of ^{13}C isotopic tracers for metabolic flux analysis in mammalian cells. J. Biotechnol. 144, 167–174.

Miyashita, Y., Dolferus, R., Ismond, K.P., Good, A.G., 2007. Alanine aminotransferase catalyses the breakdown of alanine after hypoxia in *Arabidopsis thaliana*. Plant J. cell Mol. Biol. 49, 1108–1121.

Miyashita, Y., Good, A.G., 2008a. Glutamate deamination by glutamate dehydrogenase plays a central role in amino acid catabolism in plants. Plant Signal. Behav. 3, 842–843.

Miyashita, Y., Good, A.G., 2008b. Contribution of the GABA shunt to hypoxia-induced alanine accumulation in roots of *Arabidopsis thaliana*. Plant Cell Physiol. 49, 92–102.

Moco, S., Bino, R.J., Vorst, O., Verhoeven, H.A., de Groot, J., van Beek, T.A., Vervoort, J., de Vos, C.H.R., 2006. A liquid chromatography-mass spectrometry-based metabolome database for tomato. Plant Physiol. 141, 1205–1218.

Moing, A., 2000. Sugar Alcohols as Carbohydrate Reserves in Some Higher Plants, in: Gupta A. K., Kaur, K. (Eds.), Developments in Crop Science. Elsevier, pp. 337–358.

Morgan, J.A., Rhodes, D., 2002. Mathematical modeling of plant metabolic pathways. Metab. Eng. 4, 80–9.

Mori, E., Furusawa, C., Kajihata, S., Shirai, T., Shimizu, H., 2011. Evaluating ^{13}C enrichment data of free amino acids for precise metabolic flux analysis. Biotechnol. J. 6, 1377–1387.

Murashige, T., Skoog, F., 1962. A revised medium for rapid growth and bio assays with tobacco tissue cultures. Physiol. Plant. 15, 473–497.

Mustafa, N.R., de Winter, W., van Iren, F., Verpoorte, R., 2011. Initiation, growth and cryopreservation of plant cell suspension cultures. Nat. Protoc. 6, 715–742.

Mustroph, A., Albrecht, G., 2003. Tolerance of crop plants to oxygen deficiency stress: fermentative activity and photosynthetic capacity of entire seedlings under hypoxia and anoxia. Physiol. Plant. 117, 508–520.

Nanchen, A., Fuhrer, T., Sauer, U., 2007. Determination of metabolic flux ratios from ^{13}C-experiments and gas chromatography-mass spectrometry data: protocol and principles. Methods Mol. Biol. 358, 177–197.

Nargund, S., Sriram, G., 2012. Designer labels for plant metabolism: statistical design of isotope labeling experiments for improved quantification of flux in complex plant metabolic networks. Mol. Biosyst. 9, 99–112.

Narsai, R., Howell, K.A., Carroll, A., Ivanova, A., Millar, A.H., Whelan, J., 2009. Defining core metabolic and transcriptomic responses to oxygen availability in rice embryos and young seedlings. Plant Physiol. 151, 306–322.

Narsai, R., Rocha, M., Geigenberger, P., Whelan, J., van Dongen, J.T., 2011. Comparative analysis between plant species of transcriptional and metabolic responses to hypoxia. New Phytol. 190, 472–87.

Nascimento, N.C., Fett-Neto, A.G., 2010. Plant secondary metabolism and challenges in modifying its operation: an overview. Methods Mol. Biol. 643, 1–13.

Nguyen-Quoc, B., Foyer, C.H., 2001. A role for "futile cycles" involving invertase and sucrose synthase in sucrose metabolism of tomato fruit. J. Exp. Bot. 52, 881–9.

Nielsen, J., Oliver, S., 2005. The next wave in metabolome analysis. Trends Biotechnol. 23, 544–546.

O'Carra, P., Mulcahy, P., 1997. Plant lactate dehydrogenase: NADH kinetics and inhibition by ATP. Phytochemistry 45, 897–902.

Oliveira, J., Tavares, R.M., Gerós, H., 2002. Utilization and transport of glucose in *Olea europaea* cell suspensions. Plant Cell Physiol. 43, 1510–7.

Oms-Oliu, G., Hertog, M.L.A.T.M., Van de Poel, B., Ampofo-Asiama, J., Geeraerd, A.H., Nicolaï, B.M., 2011. Metabolic characterization of tomato fruit during preharvest development, ripening, and postharvest shelf-life. Postharvest Biol. Technol. 62, 7–16.

Owens, T., Poole, R.J., 1979. Regulation of cytoplasmic and vacuolar volumes by plant cells in suspension culture. Plant Physiol. 64, 900–904.

Pedreschi, R., Franck, C., Lammertyn, J., Erban, A., Kopka, J., Hertog, M., Verlinden, B., Nicolaï, B., 2009. Metabolic profiling of "Conference" pears under low oxygen stress. Postharvest Biol. Technol. 51, 123–130.

Pedreschi, R., Vanstreels, E., Carpentier, S., Hertog, M., Lammertyn, J., Robben, J., Noben, J.P., Swennen, R., Vanderleyden, J., Nicolaï, B.M., 2007. Proteomic analysis of core breakdown disorder in Conference pears (*Pyrus communis* L.). Proteomics 7, 2083–2099.

Perata, P., Pozueta-Romero, J., Akazawa, T., Yamaguchi, J., 1992. Effect of anoxia on starch breakdown in rice and wheat seeds. Planta 188, 611–618.

Peshev, D., Vergauwen, R., Moglia, A., Hideg, E., Van den Ende, W., 2013. Towards understanding vacuolar antioxidant mechanisms: a role for fructans? J. Exp. Bot. 64, 1025–38.

Plaxton, W.C., 1996. The regulation and organization of plant glycolysis. Annu. Rev. Plant Physiol. Plant Mol. Biol. 47, 185–214.

Quek, L.E., Wittmann, C., Nielsen, L.K., Krömer, J.O., 2009. OpenFLUX: efficient modelling software for ^{13}C-based metabolic flux analysis. Microb. Cell Fact. 8, 25.

Ramautar, R., Demirci, A., de Jong, G.J., 2006. Capillary electrophoresis in metabolomics. Trends Anal. Chem. 25, 455–466.

Ratcliffe, R.G., 1997. *In vivo* NMR studies of the metabolic response of plant tissues to anoxia. Ann. Bot. 79, 39–48.

Ratcliffe, R.G., Shachar-Hill, Y., 2001. Probing plant metabolism with NMR. Annu. Rev. Plant Physiol. Plant Mol. Biol. 52, 499–526.

Ratcliffe, R.G., Shachar-Hill, Y., 2005. Revealing metabolic phenotypes in plants: inputs from NMR analysis. Biol. Rev. Camb. Philos. Soc. 80, 27–43.

Ratcliffe, R.G., Shachar-Hill, Y., 2006. Measuring multiple fluxes through plant metabolic networks. Plant J. cell Mol. Biol. 45, 490–511.

Rebeille, F., Bligny, R., Douce, R., 1980. Oxygen and temperature effects on the fatty acid composition in sycamore cells (*Acer pseudoplatanus* L.). Biochim. Biophys. Acta 620, 1–9.

Reed, J.L., Palsson, B.Ø., 2003. Thirteen years of building constraint-based in silico models of *Escherichia coli*. J. Bacteriol. 185, 2692–2699.

ap Rees, T., 1980. Assessment of the Contributions of Metabolic Pathways to Plant Respiration, in: Davies, D.D. (Ed.), The Biochemistry of Plants. Academic Press, New York, pp. 1–29.

ap Rees, T., Hill, S.A., 1994. Metabolic control analysis of plant metabolism. Plant. Cell Environ. 17, 587–599.

Reggiani, R., Aurisano, N., Mattana, M., Bertani, A., 1993. Influence of K^+ ions on polyamine level in wheat seedlings. J. Plant Physiol. 141, 136–140.

Rios-Estepa, R., Lange, B.M., 2007. Experimental and mathematical approaches to modeling plant metabolic networks. Phytochemistry 68, 2351–2374.

Rischer, H., Orešič, M., Seppänen-Laakso, T., Katajamaa, M., Lammertyn, F., Ardiles-Diaz, W., Van Montagu, M.C.E., Inzé, D., Oksman-Caldentey, K.M., Goossens, A., 2006. Gene-to-metabolite networks for terpenoid indole alkaloid biosynthesis in *Catharanthus roseus* cells. Proc. Natl. Acad. Sci. 103, 5614–5619.

Ritte, G., Rosenfeld, J., Rohrig, K., Raschke, K., 1999. Rates of sugar uptake by guard cell protoplasts of *Pisum sativum* L. related to the solute requirement for stomatal opening. Plant Physiol. 121, 647–56.

Rivoal, J., Hanson, A.D., 1994. Metabolic control of anaerobic glycolysis (overexpression of lactate dehydrogenase in transgenic tomato roots supports the Davies-Roberts hypothesis and points to a critical Role for lactate secretion). Plant Physiol. 106, 1179–1185.

Roberts, J.K.M., Chang, K., Webster, C., Callis, J., Walbot, V., 1989. Dependence of ethanolic fermentation, cytoplasmic pH regulation, and viability on the activity of alcohol dehydrogenase in hypoxic maize root tips. Plant Physiol. 89, 1275–1278.

Robertson, G.H., Mahoney, N.E., Goodman, N., Pavlath, A.E., 1995. Regulation of lycopene formation in cell suspension culture of VFNT tomato (*Lycopersicon esculentum*) by CPTA, growth regulators, sucrose, and temperature. J. Exp. Bot. 46, 667–673.

Rocha, M., Licausi, F., Araújo, W.L., Nunes-Nesi, A., Sodek, L., Fernie, A.R., van Dongen, J.T., 2010. Glycolysis and the tricarboxylic acid cycle are linked by alanine aminotransferase during hypoxia induced by zaterlogging of *Lotus japonicus*. Plant Physiol. 152, 1501–1513.

Roessner, U., Wagner, C., Kopka, J., Trethewey, R.N., Willmitzer, L., 2000. Simultaneous analysis of metabolites in potato tuber by gas chromatography-mass spectrometry. Plant J. 23, 131–42.

Rontein, D., Dieuaide-Noubhani, M., Dufourc, E.J., Raymond, P., Rolin, D., 2002. The metabolic architecture of plant cells. Stability of central metabolism and flexibility of anabolic pathways during the growth cycle of tomato cells. J. Biol. Chem. 277, 43948 – 43960.

Roscher, A., Emsley, L., Raymond, P., Roby, C., 1998. Unidirectional steady state rates of central metabolism enzymes measured simultaneously in a living plant tissue. J. Biol. Chem. 273, 25053–25061.

Ruan, Y.L., 2014. Sucrose metabolism: gateway to diverse carbon use and sugar signaling. Annu. Rev. Plant Biol. 65, 33–67.

Sachs, M.M., Subbaiah, C.C., Saab, I.N., 1996. Anaerobic gene expression and flooding tolerance in maize. J. Exp. Bot. 47, 1–15.

Sauro, H.M., Small, J.R., Fell, D.A., 1987. Metabolic control and its analysis. Extensions to the theory and matrix method. Eur. J. Biochem. 165, 215–221.

Schallau, K., Junker, B.H., 2010. Simulating plant metabolic pathways with enzyme-kinetic models. Plant Physiol. 152, 1763–71.

Schauer, N., Zamir, D., Fernie, A.R., 2005. Metabolic profiling of leaves and fruit of wild species tomato: a survey of the *Solanum lycopersicum* complex. J. Exp. Bot. 56, 297–307.

Schupp, N., Ziegler, P., 2004. The relation of starch phosphorylases to starch metabolism in wheat. Plant Cell Physiol. 45, 1471–84.

Schwender, J., 2009. Isotopic Steady-State Flux Analysis, in: Schwender, J. (Ed.), Plant Metabolic Networks. Springer New York, pp. 245–284.

Schwender, J., Ohlrogge, J.B., 2002. Probing *in vivo* metabolism by stable isotope labeling of storage lipids and proteins in developing *Brassica napus* embryos. Plant Physiol. 130, 347–361.

Shepherd, T., Dobson, G., Verrall, S.R., Conner, S., Griffiths, D.W., McNicol, J.W., Davies, H. V., Stewart, D., 2007. Potato metabolomics by GC–MS: what are the limiting factors? Metabolomics 3, 475–488.

Shingaki-Wells, R.N., Huang, S., Taylor, N.L., Carroll, A.J., Zhou, W., Millar, A.H., 2011. Differential molecular responses of rice and wheat coleoptiles to anoxia reveal novel metabolic adaptations in amino acid metabolism for tissue tolerance. Plant Physiol. 156, 1706–1724.

Simova-Stoilova, L., Demirevska, K., Kingston-Smith, A., Feller, U., 2012. Involvement of the leaf antioxidant system in the response to soil flooding in two *Trifolium* genotypes differing in their tolerance to waterlogging. Plant Sci. 183, 43–49.

Smith, A.M., Denyer, K., Martin, C., 1997. The synthesis of the starch granule. Annu. Rev. Plant Physiol. Plant Mol. Biol. 48, 67–87.

Snow, N.H., 2004. Inlet Systems for Gas Chromatography, in: Grob, R.L., Barry, E.F. (Eds.), Modern Practice of Gas Chromatography. John Wiley & Sons, Inc., pp. 461–489.

Sokol, S., Millard, P., Portais, J.C., 2012. *influx_s*: increasing numerical stability and precision for metabolic flux analysis in isotope labelling experiments. Bioinformatics 28, 687–693.

Spielbauer, G., Margl, L., Hannah, L.C., Römisch, W., Ettenhuber, C., Bacher, A., Gierl, A., Eisenreich, W., Genschel, U., 2006. Robustness of central carbohydrate metabolism in developing maize kernels. Phytochemistry 67, 1460–1475.

Sriram, G., González-Rivera, O., Shanks, J. V, 2006. Determination of biomass composition of *Catharanthus roseus* hairy roots for metabolic flux analysis. Biotechnol. Prog. 22, 1659–63.

St Cyr, J.A., Bianco, R.W., Schneider, J.R., Mahoney, J R, J., Tveter, K., Einzig, S., Foker, J.E., 1989. Enhanced high energy phosphate recovery with ribose infusion after global myocardial ischemia in a canine model. J. Surg. Res. 46, 157–162.

Stephanopoulos, G., 1999. Metabolic fluxes and metabolic engineering. Metab. Eng. 1, 1–11.

Stephanopoulos, G., Aristidou, A.A., Nielsen, J., 1998. Metabolic Engineering: Principles and Methodologies. Academic Press, San Diego, California.

Steuer, R., 2006. Review: On the analysis and interpretation of correlations in metabolomic data. Brief. Bioinform. 7, 151–158.

Stitt, M., Quick, W.P., Schurr, U., Schulze, E.D., Rodermel, S.R., Bogorad, L., 1991. Decreased ribulose-1,5-bisphosphate carboxylase-oxygenase in transgenic tobacco transformed with “antisense” rbcS. Planta 183.

Stoyanova, S., Geuns, J., Hideg, E., Van Den Ende, W., 2011. The food additives inulin and stevioside counteract oxidative stress. Int. J. Food Sci. Nutr. 62, 207–14.

Sweetlove, L.J., Ratcliffe, R.G., 2011. Flux-balance modeling of plant metabolism. Front. Plant Sci. 2, 1–10.

Sysi-Aho, M., Katajamaa, M., Yetukuri, L., Orešič, M., 2007. Normalization method for metabolomics data using optimal selection of multiple internal standards. BMC Bioinformatics 8, 93.

Szecowka, M., Heise, R., Tohge, T., Nunes-Nesi, A., Vosloh, D., Huege, J., Feil, R., Lunn, J., Nikoloski, Z., Stitt, M., Fernie, A.R., Arrivault, S., 2013. Metabolic fluxes in an illuminated *Arabidopsis* rosette. Plant Cell 25, 694–714.

Szyperski, T., 1998. ^{13}C-NMR, MS and metabolic flux balancing in biotechnology research. Q. Rev. Biophys. 31, 41–106.

Tang, Y.J., Martin, H.G., Myers, S., Rodriguez, S., Baidoo, E.E.K., Keasling, J.D., 2009. Advances in analysis of microbial metabolic fluxes via ^{13}C isotopic labeling. Mass Spectrom. Rev. 28, 362–375.

Terzer, M., Maynard, N.D., Covert, M.W., Stelling, J., 2009. Genome-scale metabolic networks. Wiley Interdiscip. Rev. Syst. Biol. Med. 1, 285–297.

Thomas, S., Mooney, P.J., Burrell, M.M., Fell, D.A., S, T., P, M., M, B., D, F., 1997. Finite change analysis of glycolytic intermediates in tuber tissue of lines of transgenic potato (*Solanum tuberosum*) overexpressing phosphofructokinase. Biochem. J. 322, 111–117.

Thomson, C.J., Greenway, H., 1991. Metabolic evidence for stelar anoxia in maize roots exposed to low O_2 concentrations. Plant Physiol. 96, 1294–301.

Tjellström, H., Yang, Z., Allen, D.K., Ohlrogge, J.B., 2012. Rapid kinetic labeling of *Arabidopsis* cell suspension cultures: implications for models of lipid export from plastids. Plant Physiol. 158, 601–611.

Trygg, J., Wold, S., 2002. Orthogonal projections to latent structures (O-PLS). J. Chemom. 16, 119–128.

Umbarger, H.E., 1978. Amino acid biosynthesis and its regulation. Annu. Rev. Biochem. 47, 532–606.

Van de Poel, B., Bulens, I., Oppermann, Y., Hertog, M.L.A.T.M., Nicolai, B.M., Sauter, M., Geeraerd, A.H., 2013. S-adenosyl-L-methionine usage during climacteric ripening of tomato in relation to ethylene and polyamine biosynthesis and transmethylation capacity. Physiol. Plant. 148, 176–188.

Van den Berg, R.A., Hoefsloot, H.C., Westerhuis, J.A., Smilde, A.K., van der Werf, M.J., 2006. Centering, scaling, and transformations: improving the biological information content of metabolomics data. BMC Genomics 7, 142.

Van Dongen, J.T., Roeb, G.W., Dautzenberg, M., Froehlich, A., Vigeolas, H., Minchin, P.E.H., Geigenberger, P., 2004. Phloem import and storage metabolism are highly

coordinated by the low oxygen concentrations within developing wheat seeds. Plant Physiol. 135, 1809–1821.

Van Dongen, J.T., Schurr, U., Pfister, M., Geigenberger, P., 2003. Phloem metabolism and function have to cope with low internal oxygen. Plant Physiol. 131, 1529–1543.

Van Dongen, J.T.T., Fröhlich, A., Ramírez-Aguilar, S.J., Schauer, N., Fernie, A.R., Erban, A., Kopka, J., Clark, J., Langer, A., Geigenberger, P., Frohlich, A., Ramırez-Aquilar, S.J., 2009. Transcript and metabolite profiling of the adaptive response to mild decreases in oxygen concentration in the roots of *Arabidopsis* plants. Ann. Bot. 103, 269–280.

Van Gestel, K., Verbelen, J.P., 2002. Giant mitochondria are a response to low oxygen pressure in cells of tobacco (*Nicotiana tabacum* L.). J. Exp. Bot. 53, 1215–1218.

Van Winden, W.A., Heijnen, J.J., Verheijen, P.J.T., 2002a. Cumulative bondomers: a new concept in flux analysis from 2D [^{13}C,^{1}H] COSY NMR data. Biotechnol. Bioeng. 80, 731–45.

Van Winden, W.A., Wittmann, C., Heinzle, E., Heijnen, J.J., 2002b. Correcting mass isotopomer distributions for naturally occurring isotopes. Biotechnol. Bioeng. 80, 477–479.

Vandendriessche, T., Schäfer, H., Verlinden, B.E., Humpfer, E., Hertog, M.L.A.T.M., Nicolaï, B.M., 2013. High-throughput NMR based metabolic profiling of Braeburn apple in relation to internal browning. Postharvest Biol. Technol. 80, 18–24.

Vanlerberghe, G.C., Yip, J.Y.H., Parsons, H.L., 1999. In organello and *in vivo* evidence of the importance of the regulatory sulfhydryl/disulfide system and pyruvate for alternative oxidase activity in tobacco. Plant Physiol. 121, 793–803.

VCBT, 2012. Vlaams Centrum voor Bewaring van Tuinbouwproducten. Year Report www.vcbt.be (01.09.12).

Verstappen, R., Ranostaj, S., Rausch, T., 1991. The hexose transporters at the plasma membrane and the tonoplast of transformed plant cells: kinetic characterization of two distinct carriers. Biochim. Biophys. Acta Bioenerg. 1073, 366–73.

Villas-Bôas, S.G., Mas, S., Akesson, M., Smedsgaard, J., Nielsen, J., 2005. Mass spectrometry in metabolome analysis. Mass Spectrom. Rev. 24, 613–646.

Voit, E.O., Alvarez-Vasquez, F., Sims, K.J., 2004. Analysis of dynamic labeling data. Math. Biosci. 191, 83–99.

Von Roepenack-Lahaye, E., Degenkolb, T., Zerjeski, M., Franz, M., Roth, U., Wessjohann, L., Schmidt, J., Scheel, D., Clemens, S., 2004. Profiling of *Arabidopsis* secondary

metabolites by capillary liquid chromatography coupled to electrospray ionization quadrupole time-of-flight mass spectrometry. Plant Physiol. 134, 548–559.

Vorst, O., de Vos, C.H.R., Lommen, A., Staps, R. V., Visser, R.G.F., Bino, R.J., Hall, R.D., 2005. A non-directed approach to the differential analysis of multiple LC–MS-derived metabolic profiles. Metabolomics 1, 169–180.

Wahl, S.A., Dauner, M., Wiechert, W., 2004. New tools for mass isotopomer data evaluation in ^{13}C flux analysis: mass isotope correction, data consistency checking, and precursor relationships. Biotechnol. Bioeng. 85, 259–68.

Wang, D.Y., Zhang, Q., Liu, Y., Lin, Z.F., Zhang, S.X., Sun, M.X., Sodmergen, 2010. The levels of male gametic mitochondrial DNA are highly regulated in angiosperms with regard to mitochondrial inheritance. Plant Cell 22, 2402–2416.

Weber, A.P.M., Bräutigam, A., 2013. The role of membrane transport in metabolic engineering of plant primary metabolism. Curr. Opin. Biotechnol. 24, 256–62.

Weitzel, M., Nöh, K., Dalman, T., Niedenführ, S., Stute, B., Wiechert, W., 2013. 13CFLUX2--high-performance software suite for ^{13}C-metabolic flux analysis. Bioinformatics 29, 143–145.

Wiechert, W., Michael, M., Isermann, N., Wurzel, M., de Graaf, A.A., 1999. Bidirectional reaction steps in metabolic networks part III : explicit solution and analysis of isotopomer labeling systems. Biotechnol. Bioeng. 66.

Wiechert, W., Schweissgut, O., Takanaga, H., Frommer, W.B., 2007. Fluxomics: mass spectrometry versus quantitative imaging. Curr. Opin. Plant Biol. 10, 323–330.

Williams, T.C.R., Miguet, L., Masakapalli, S.K., Kruger, N.J., Sweetlove, L.J., Ratcliffe, R.G., 2008. Metabolic network fluxes in heterotrophic *Arabidopsis* cells: stability of the flux distribution under different oxygenation conditions. Plant Physiol. 148, 704–18.

Williams, T.C.R., Poolman, M.G., Howden, A.J.M., Schwarzlander, M., Fell, D.A., Ratcliffe, R.G., Sweetlove, L.J., 2010. A genome-scale metabolic model accurately predicts fluxes in central carbon metabolism under stress conditions. Plant Physiol. 154, 311–23.

Williamson, J.D., Jennings, D.B., Guo, W., Pharr, D.M., 2002. Sugar alcohols, salt stress, and fungal resistance: polyols- multifunctional plant protection? J. Am. Soc. Hortic. Sci. 127, 467–473.

Wittmann, C., 2007. Fluxome analysis using GC-MS. Microb. Cell Fact. 6, 6.

Wittmann, Heinzle, 1999. Mass spectrometry for metabolic flux analysis. Biotechnol. Bioeng. 62, 739–750.

Wolfgang, W., Wiechert, W., 2001. ^{13}C metabolic flux analysis. Metab. Eng. 3, 195–206.

Xiang, L., Le Roy, K., Bolouri-Moghaddam, M.R., Vanhaecke, M., Lammens, W., Rolland, F., Van den Ende, W., 2011. Exploring the neutral invertase-oxidative stress defence connection in *Arabidopsis thaliana*. J. Exp. Bot. 62, 3849–62.

Ye, B., Muller, H.H., Zhang, J., Gressel, J., 1997. Constitutively elevated levels of putrescine and putrescine-generating enzymes correlated with oxidant stress resistance in *Conyza bonariensis* and wheat. Plant Physiol. 115, 1443–1451.

Zamboni, N., 2007. Toward Metabolome-Based ^{13}C Flux Analysis: A Universal Tool for Measuring *In Vivo* Metabolic Activity, in: Nielsen, J., Jewett, M.C. (Eds.), Topics in Current Genetics. Springer-Verlag, Berlin, pp. 129–157.

Zamboni, N., Fendt, S.M., Rühl, M., Sauer, U., 2009. ^{13}C-based metabolic flux analysis. Nat. Protoc. 4, 878–892.

Zamboni, N., Fischer, E., Sauer, U., 2005. FiatFlux – a software for metabolic flux analysis from ^{13}C-glucose experiments. BMC Bioinformatics 6, 209.

Zeeman, S.C., Kossmann, J., Smith, A.M., 2010. Starch: its metabolism, evolution, and biotechnological modification in plants. Annu. rreview plant Biol. 61, 209–34.

Zeng, Y., Wu, Y., Avigne, W.T., Koch, K.E., 1999. Rapid repression of maize invertases by low oxygen. Invertase/sucrose synthase balance, sugar signaling potential, and seedling survival. Plant Physiol. 121, 599–608.

Appendix

Appendix 1 – Chapter 3

Calibration graphs used for the quantification of intracellular polar metabolites in tomato cell suspension. The relative response is based on correcting the abundance of each metabolite standard with that of the internal standard (phenyl-β-D-glucopyranoside). Values are the mean of three independent replicate experiments ± sd.

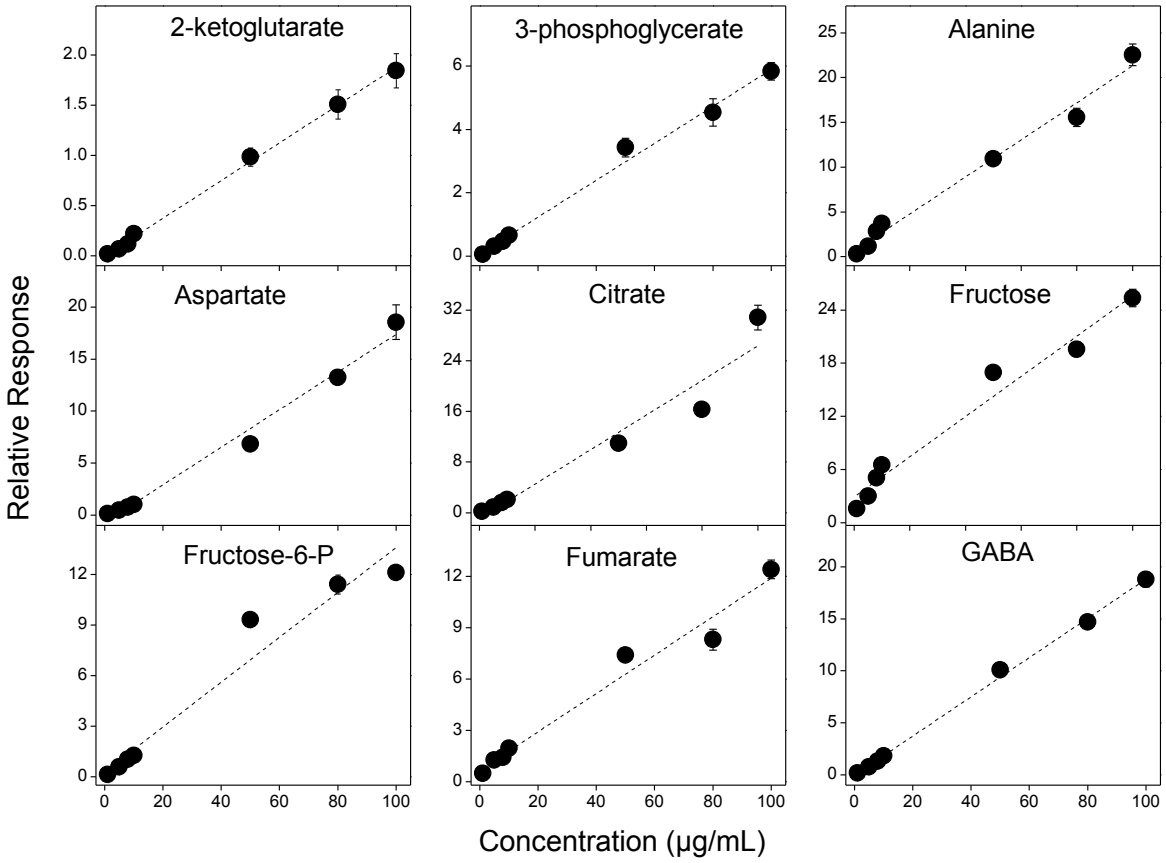

Appendix 1: (continued)

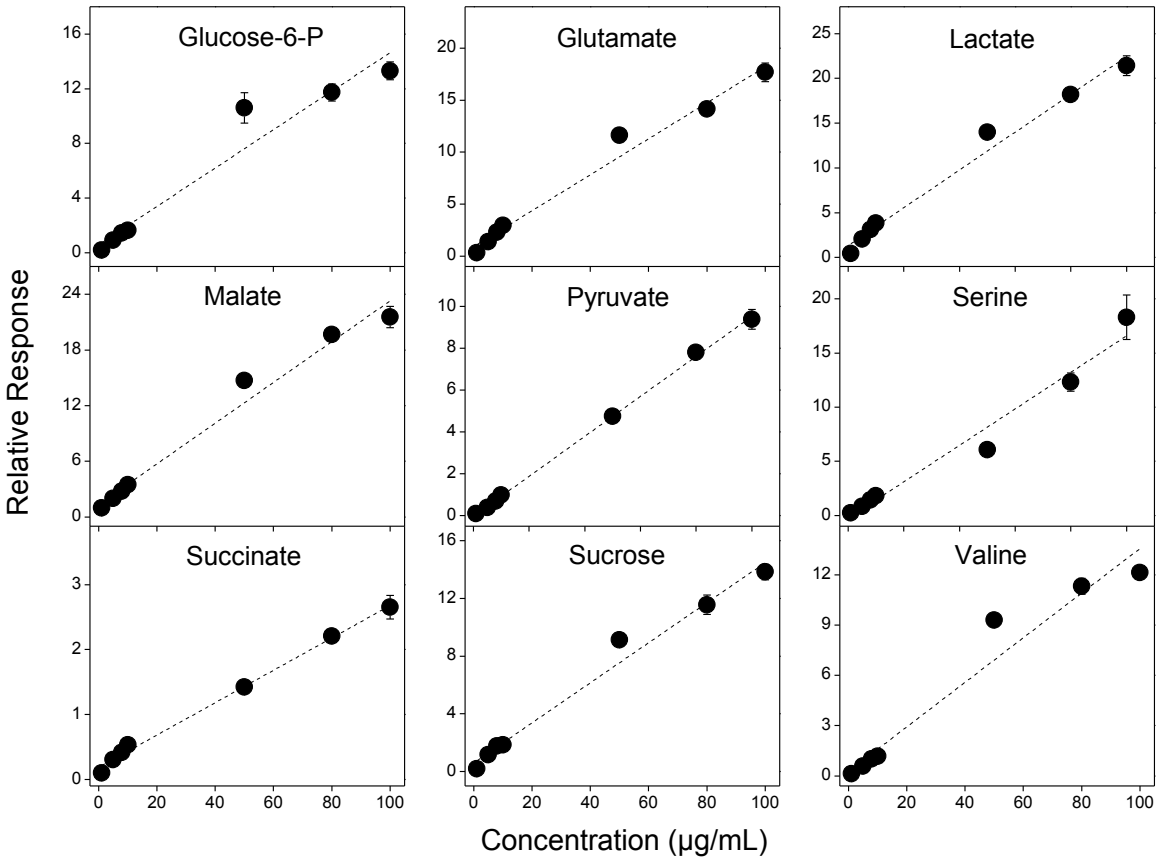

Appendix 2 – Chapter 4

Appendix 2A: Changes in the abundance of metabolites in cultured tomato cells following the induction of low O_2 stress. All values are the average of four independent biological replicates with the error bars indicating the sem. Labels are 21 kPa (●), 1 kPa (x) and 0 kPa (○). Metabolite levels are expressed relative to the starting values.

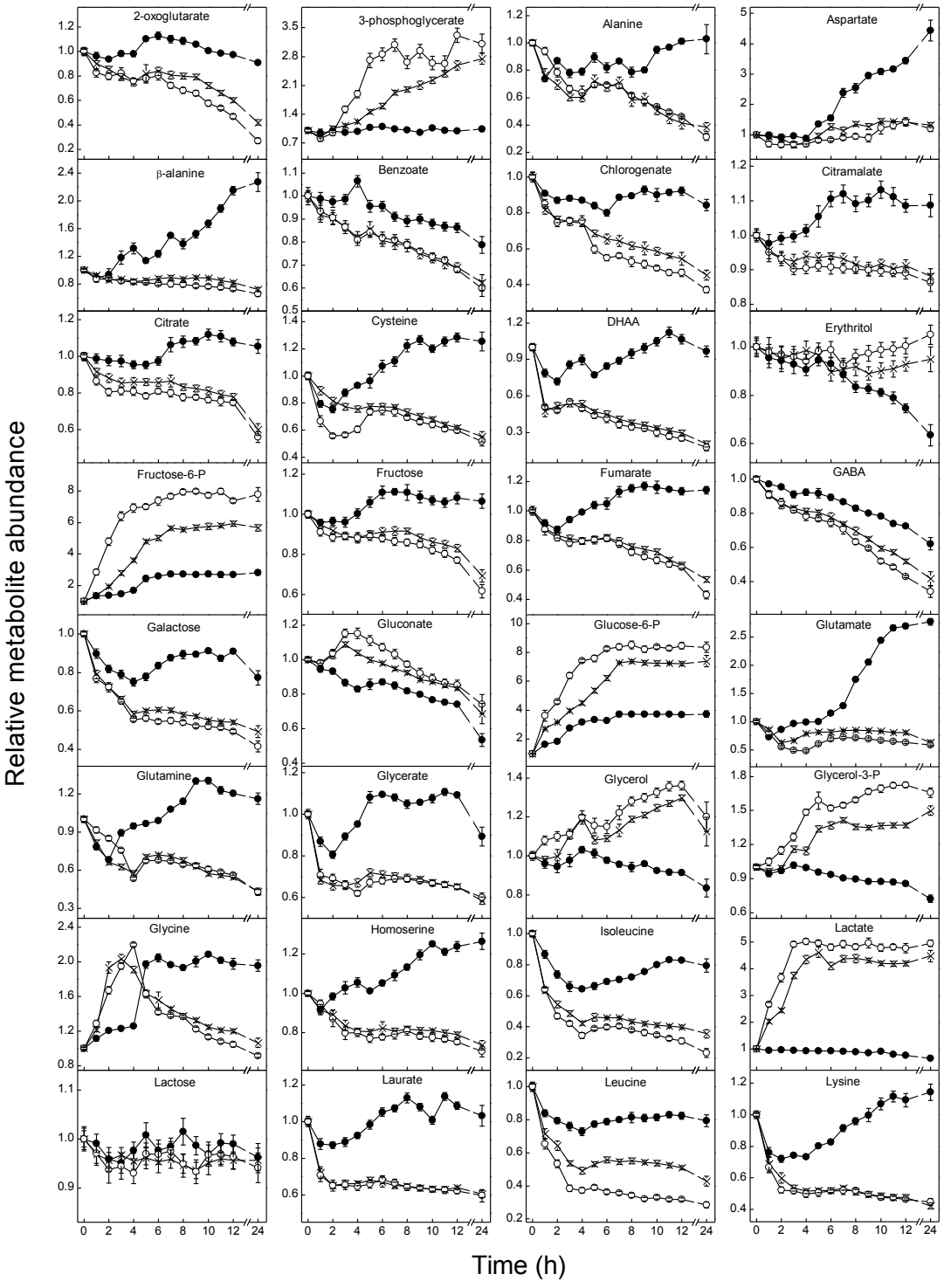

Appendix 2A: (continued).

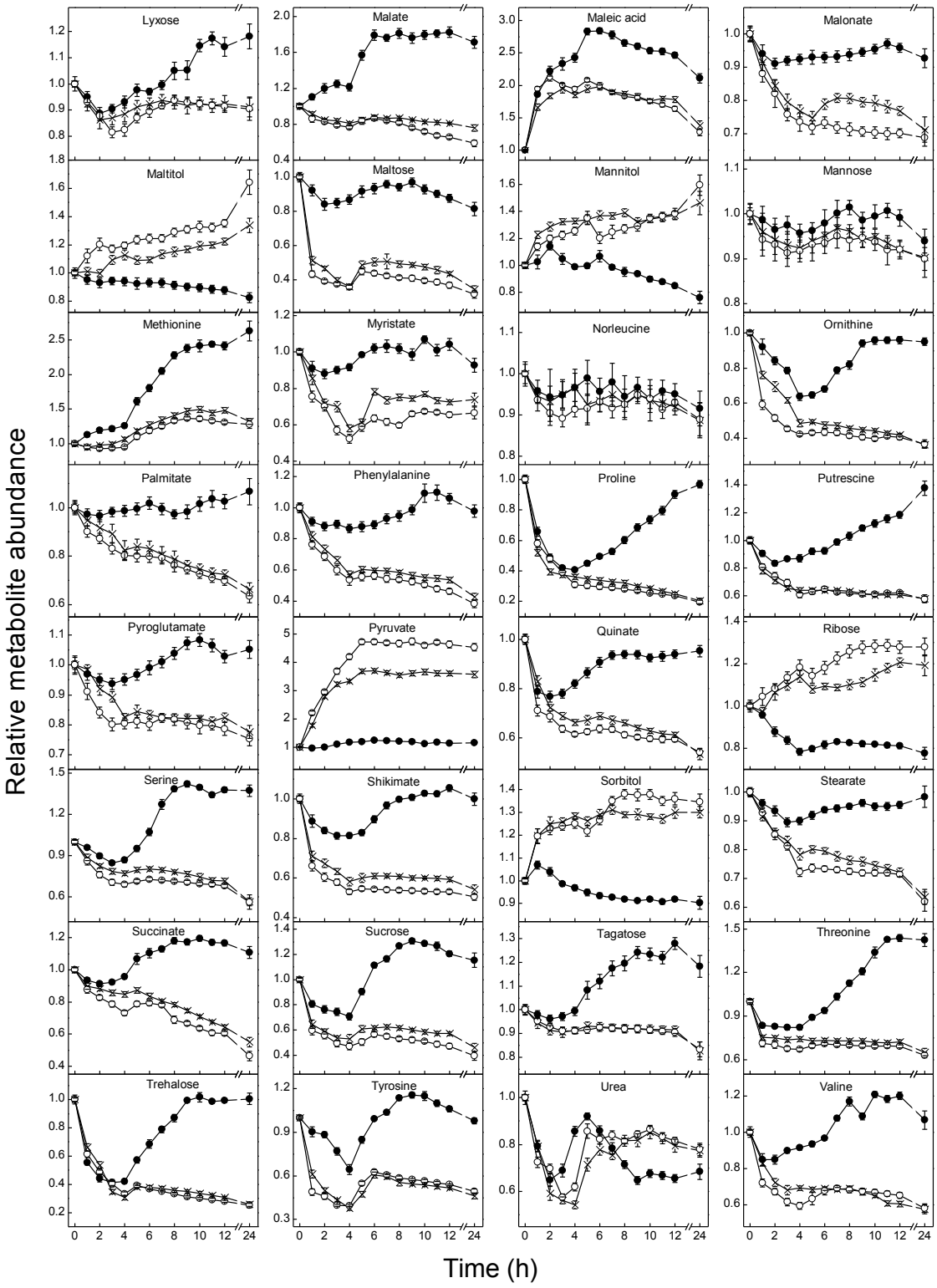

Appendix 2B: Accumulation of ^{13}C-label by primary metabolites as a result of low O_2 stress. Cultured tomato cells were incubated under different O_2 conditions [21 kPa (●), 1 kPa (x) and 0 kPa (o)]. ^{13}C-labelled glucose was added after four hours of incubation. All values are the average of four independent biological replicates with the error bars indicating the sem.

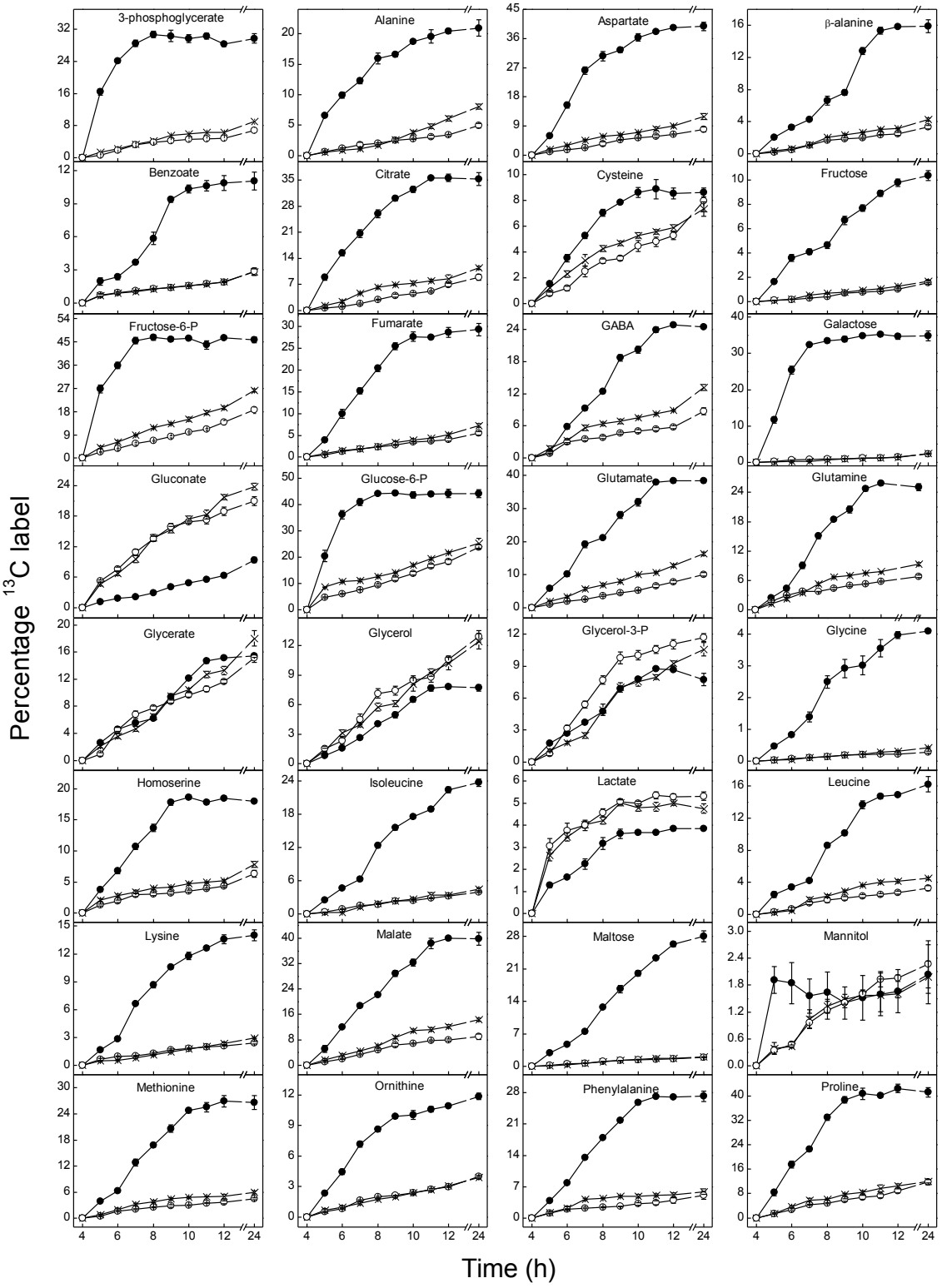

Appendix 2B: (continued)

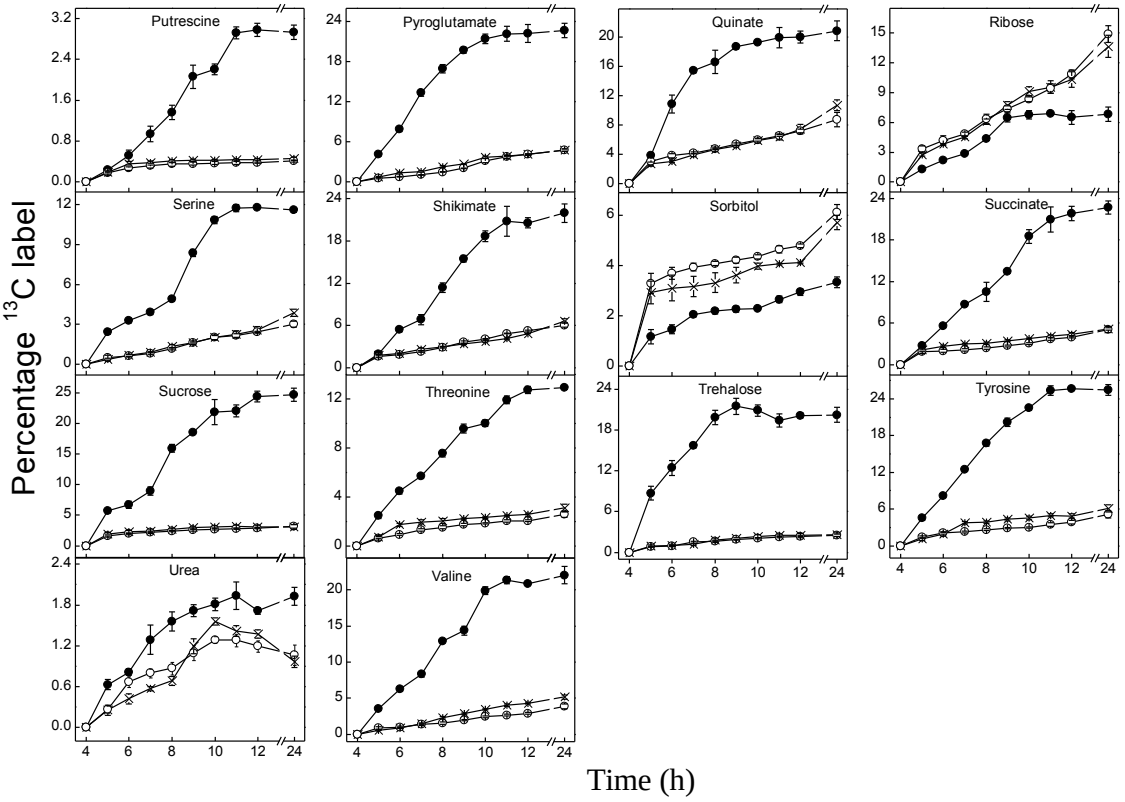

Appendix 3 – Chapter 5

Appendix 3A: The estimated Michaelis-Menten kinetic [K_M (µmol/mg DW) and V_{max} (µmol/(mg DW·h))] parameter values associated with the glycolysis in the cytosol and plastid and the formation of lactate at the different O_2 levels.

Parameter	**21 kPa**			**1 kPa**			**0 kPa**		
	Estimate	**CI**		**Estimate**	**CI**		**Estimate**	**CI**	
$K_{M,\mathrm{G6P},C}$	0.049	0.040	0.052	3.018	2.958	3.051	9.620	9.357	9.815
$K_{M,\mathrm{F6P},P}$	0.756	0.527	0.997	0.052	0.041	0.063	0.125	0.095	0.152
$K_{M,\mathrm{G3P},P}$	0.048	0.022	0.070	0.009	0.006	0.012	0.031	0.023	0.047
$K_{M,\mathrm{PYR},P}$	0.0086	0.0047	0.0115	0.00002	0.00002	0.00002	0.00002	0.00002	0.00002
$K_{M,\mathrm{LAC},C}$				0.0003	0.0003	0.0003	0.0005	0.0005	0.0005
$V_{max,\mathrm{UPT}}$	0.906	0.822	0.999	0.571	0.445	0.725	0.566	0.450	0.674
$V_{max,\mathrm{G6P},C}$	70.792	61.079	77.564	5934.8	5805.1	5978.4	13888.0	13654.0	14176.0
$V_{max,\mathrm{F6P},C}$	1.907	1.440	2.322	1.757	1.359	2.235	2.862	2.224	3.344
$V_{max,\mathrm{G3P},C}$	1.136	0.799	1.425	1.777	1.362	2.233	2.921	2.269	3.390
$V_{max,\mathrm{PYR},C}$	1.879	1.480	2.164	199.6	188.8	204.8	1082.1	956.4	1184.0
$V_{max,\mathrm{F6P},P}$	21.965	14.101	28.408	6.628	5.589	7.566	7.175	6.389	7.877
$V_{max,\mathrm{G3P},P}$	10.444	9.641	11.156	6.967	5.613	8.860	8.672	7.665	9.776
$V_{max,\mathrm{PYR},P}$	37.064	34.222	39.629	71.903	68.929	73.896	77.410	74.254	80.997
K_{P_LAC}				0.00011	0.00010	0.00012	0.00028	0.00026	0.00030
$V_{max,\mathrm{LAC},C}$	3.320	2.880	3.874	8.458	7.711	8.947	11.924	10.909	13.088

Appendix 3B: The estimated rate constants (/h) for the transport reactions under the different O_2 levels.

Parameter	**21 kPa**			**1 kPa**			**0 kPa**		
	Estimate	**CI**		**Estimate**	**CI**		**Estimate**	**CI**	
$k_{G6P,C\rightarrow P}$	0.077	0.066	0.089	0.492	0.375	0.652	1.045	0.618	1.267
$k_{G6P,P\rightarrow C}$	0.141	0.074	0.192	0.308	0.26	0.336	0.173	0.147	0.199
$k_{GLC,C\rightarrow V}$	0.165	0.158	0.169	112.5	110.1	113.6	181.8	179.5	184.6
$k_{FRC,V\rightarrow C}$	0.450	0.450	0.450	0.007	0.003	0.009	0.026	0.016	0.033
$k_{SUC,C\rightarrow V}$	0.104	0.025	0.173	0.262	0.147	0.372	0.312	0.226	0.406
$k_{SUC,V\rightarrow C}$	0.00008	0.00008	0.00008	0.00005	0.00005	0.00005	0.00004	0.00004	0.00004
$k_{PYR,P\rightarrow C}$	0.00005	0.00005	0.00006	0.00001	0.000005	0.00001	0.000005	0.000005	0.000005
$k_{PYR,C\rightarrow M}$	70.859	63.699	82.036	40.914	35.188	48.326	21.663	18.342	25.006
$k_{GLU,M\rightarrow C}$	15.756	11.856	19.770	0.626	0.517	0.728	0.625	0.449	0.740
$k_{GLU,C\rightarrow P}$	0.508	0.399	0.619	27.054	21.397	32.499	19.606	16.962	23.302
$k_{2KG,C\rightarrow M}$	5.506	4.636	6.392	5476.4	5380.0	5565.1	6012.1	5954.3	6052.7
$k_{2KG,P\rightarrow C}$	0.029	0.025	0.034	28.703	26.054	29.768	30.240	28.145	31.404
$k_{GABA,M\rightarrow C}$	0.122	0.113	0.131	0.913	0.583	1.147	0.845	0.637	1.095
$k_{ALA,M\rightarrow C}$	0.0002	0.0001	0.0002	0.0016	0.0005	0.0020	0.0014	0.0009	0.0017

Appendix 3C: The estimated first-order rate constants (µmol/(mg DW·h)) for the synthesis and degradation of amino acids, organic acids and sucrose and the reactions of the TCA cycle at the different O_2 levels.

Parameter	**21 kPa**			**1 kPa**			**0 kPa**		
	Estimate	**CI**		**Estimate**	**CI**		**Estimate**	**CI**	
$v_{STA,P}$	24.30	20.73	27.34	304.97	236.96	369.96	496.60	377.29	588.15
$k_{LAD,C}$	0.018	0.010	0.027	0.069	0.041	0.090	0.246	0.190	0.297
$k_{ALA,C}$	0.027	0.023	0.028	0.002	0.002	0.002	0.003	0.003	0.003
$k_{ALD,C}$	0.429	0.320	0.549	0.430	0.331	0.529	0.274	0.210	0.324
$k_{SUC,C}$	0.563	0.484	0.629	0.059	0.046	0.075	0.035	0.027	0.045
$k_{SUSY,C}$	0.250	0.208	0.288	0.262	0.164	0.376	0.233	0.121	0.350
$k_{GABA,C}$	0.184	0.162	0.213	35.318	29.988	39.136	24.142	19.139	27.320
$k_{GADA,C}$	0.00002	0.00002	0.00003	1.148	0.841	1.472	1.222	0.894	1.558
$k_{FRC,C}$	0.048	0.042	0.051	0.175	0.158	0.195	0.270	0.242	0.297
$k_{INV,V}$	0.0001	0.0001	0.0001	0.098	0.085	0.110	0.147	0.124	0.164
$k_{SER,P}$	0.031	0.026	0.034	0.019	0.014	0.022	0.007	0.005	0.009
$k_{SED,P}$	0.236	0.218	0.254	0.283	0.214	0.340	0.213	0.166	0.258
$k_{VAL,P}$	0.014	0.011	0.017	0.003	0.003	0.004	0.001	0.000	0.001
$k_{VAD,P}$	0.301	0.278	0.324	0.403	0.331	0.481	0.360	0.308	0.402

Appendix 3C: (continued)

Parameter	21 kPa			1 kPa			0 kPa		
	Estimate	CI		Estimate	CI		Estimate	CI	
$k_{CIT,M}$	1.076	0.641	1.429	1.749	1.240	2.260	2.061	1.325	2.828
$k_{2KG,M}$	1.322	1.282	1.364	1.679	1.474	1.840	1.885	1.627	2.076
$k_{SUT,M}$	15.75	8.455	20.29	3.690	3.243	4.023	5.126	4.152	5.709
$k_{FUM,M}$	2.034	1.878	2.169	4.046	3.505	4.622	5.661	4.193	6.934
$k_{MAL,M}$	1.963	1.809	2.093	3.538	3.159	3.929	3.326	2.805	3.788
$k_{OAA,M}$	0.887	0.784	1.014	0.375	0.346	0.398	0.390	0.338	0.427
$k_{AMA,M}$	4.549	3.136	5.930	0.000	0.000	0.000	0.000	0.000	0.000
$k_{ANA1,M}$	117.71	83.13	151.56	9.092	6.403	11.265	9.880	7.032	12.720
$k_{ANA3,M}$	0.0001	0.0001	0.0001	0.00007	0.00006	0.00007	0.00026	0.00025	0.00026
$k_{CLYS,M}$	0.0070	0.0067	0.0073	0.00002	0.00002	0.00002	0.00002	0.00002	0.00002
$k_{GST,M}$	6.261	3.700	8.044	0.040	0.034	0.048	0.033	0.027	0.039
$k_{EXT,C}$	309.7	266.2	351.4	1417.8	1172.8	1735.1	1307.6	1113.0	1602.7
$k_{EXT,P}$	0.218	0.158	0.277	0.001	0.001	0.001	0.183	0.111	0.249
$k_{GLU,M}$	75.939	39.851	99.925	7.242	6.341	8.180	8.887	7.468	10.176
$k_{GLD,M}$	0.003	0.003	0.003	0.090	0.089	0.091	0.093	0.091	0.095
$k_{ASP,M}$	447.5	299.3	528.5	99.1	77.5	115.4	155.2	112.5	196.4
$k_{ASD,M}$	0.965	0.878	1.082	0.779	0.557	0.959	0.924	0.705	1.172

Appendix 3D: The estimated initial concentration (µmol/mg DW) of metabolites in the cytosol, mitochondria, plastid, and vacuole.

Compartment	**Metabolite**	**Concentration**		
		Estimate	**CI**	
Cytosol	2-ketoglutarate	0.006	0.005 -	0.007
	Glutamate	0.012	0.011 -	0.013
Mitochondria	Alanine	0.240	0.238 -	0.242
	GABA	0.071	0.067 -	0.072
	Oxaloacetate	0.348	0.315 -	0.382
	Pyruvate	1.191	1.053 -	1.333
Plastid	2-ketoglutarate	0.288	0.245 -	0.308
	3-phosphoglycerate	4.969	3.863 -	5.864
	Fructose-6-phosphate	0.008	0.007 -	0.009
	Glucose-6-phosphate	0.210	0.194 -	0.222
	Glutamate	22.399	18.231 -	26.241
	Pyruvate	0.156	0.141 -	0.171
Vacuole	Alanine	0.144	0.122 -	0.158
	Citrate	0.207	0.203 -	0.212
	Fructose	0.000	0.000 -	0.000
	Fumarate	0.047	0.044 -	0.049
	Glucose	0.001	0.001 -	0.002
	Succinate	0.100	0.096 -	0.103
	Sucrose	0.207	0.193 -	0.216

Appendix 3E: The estimated 12 h fluxes (µmol/(mg DW·h)) through the central carbon metabolism of tomato cell suspension incubated at different O_2 levels.

Flux	**21 kPa**				**1 kPa**				**0 kPa**			
	Estimate	**CI**			**Estimate**	**CI**			**Estimate**	**CI**		
v_{UPT}	0.421	0.382	-	0.464	0.265	0.206	-	0.337	0.263	0.209	-	0.313
$v_{G6P,C}$	0.421	0.382	-	0.464	0.269	0.210	-	0.340	0.266	0.213	-	0.316
$v_{F6P,C}$	0.462	0.413	-	0.501	1.147	0.879	-	1.429	1.731	1.338	-	2.026
$v_{G3P,C}$	0.904	0.804	-	0.981	2.284	1.743	-	2.854	3.453	2.666	-	4.045
$v_{PYR,C}$	0.904	0.804	-	0.981	2.284	1.743	-	2.854	3.453	2.666	-	4.045
$v_{F6P,P}$	0.028	0.026	-	0.029	0.020	0.017	-	0.022	0.021	0.019	-	0.023
$v_{G3P,P}$	0.055	0.051	-	0.058	0.039	0.033	-	0.045	0.043	0.038	-	0.047
$v_{PYR,C}$	0.031	0.029	-	0.033	0.021	0.017	-	0.027	0.026	0.023	-	0.029
$v_{G6P,C\rightarrow P}$	0.031	0.027	-	0.036	0.384	0.310	-	0.505	0.860	0.537	-	1.021
$v_{G6P,P\rightarrow C}$	0.077	0.062	-	0.089	1.279	1.042	-	1.554	2.329	1.646	-	2.697
$v_{GLC,V\rightarrow C}$	0.0001	0.0001	-	0.0001	0.0033	0.0030	-	0.0035	0.0037	0.0033	-	0.0041
$v_{FRC,V\rightarrow C}$	0.0001	0.0001	-	0.0001	0.0011	0.0005	-	0.0014	0.0037	0.0027	-	0.0044
$v_{SUC,C\rightarrow V}$	0.004	0.001	-	0.005	0.002	0.001	-	0.002	0.002	0.002	-	0.003
$v_{SUC,V\rightarrow C}$	0.0001	0.0001	-	0.0001	0.0001	0.0001	-	0.0001	0.0001	0.0001	-	0.0001

Appendix 3E: (continued)

Flux	21kpa			1 kPa			0 kPa		
	Estimate	**CI**		**Estimate**	**CI**		**Estimate**	**CI**	
$v_{PYR,P\rightarrow C}$	0.0001	0.0001	0.0001	0.0001	0.0001	0.0001	0.0001	0.0001	0.0001
$v_{PYR,C\rightarrow M}$	0.223	0.210	0.233	0.090	0.076	0.099	0.079	0.069	0.089
$v_{GLU,M\rightarrow C}$	0.077	0.073	0.080	0.035	0.031	0.039	0.026	0.021	0.030
$v_{GLU,C\rightarrow P}$	0.061	0.058	0.064	0.018	0.014	0.022	0.014	0.011	0.017
$v_{2KG,P\rightarrow C}$	0.040	0.037	0.042	0.023	0.019	0.026	0.019	0.016	0.022
$v_{2KG,C\rightarrow M}$	0.040	0.037	0.042	0.023	0.019	0.026	0.019	0.016	0.022
$v_{GABA,C\rightarrow M}$	0.014	0.013	0.015	0.009	0.008	0.010	0.006	0.005	0.007
$v_{ALA,M\rightarrow C}$	0.012	0.010	0.013	0.010	0.009	0.011	0.006	0.005	0.007
$v_{SER,C}$	0.025	0.023	0.026	0.013	0.010	0.017	0.011	0.008	0.013
$v_{SED,C}$	0.024	0.022	0.026	0.015	0.011	0.018	0.012	0.009	0.014
$v_{VAL,P}$	0.015	0.014	0.016	0.010	0.007	0.012	0.008	0.006	0.009
$v_{VAD,P}$	0.015	0.014	0.016	0.010	0.008	0.013	0.008	0.007	0.009
$v_{SUC,C}$	0.010	0.010	0.011	0.004	0.002	0.005	0.004	0.003	0.004
$v_{INV,V}$	0.0001	0.0001	0.0001	0.003	0.003	0.003	0.004	0.003	0.004

Appendix 3E: (continued)

Flux	21 kPa		1 kPa		0 kPa	
	Estimate	**CI**	**Estimate**	**CI**	**Estimate**	**CI**
$v_{SUSY,C}$	0.006	0.005 - 0.007	0.001	0.001 - 0.002	0.001	0.000 - 0.002
$v_{FRC,C}$	0.005	0.004 - 0.005	0.004	0.003 - 0.004	0.005	0.005 - 0.006
$v_{ALA,C}$	0.0001	0.0001 - 0.0001	0.0001	0.0001 - 0.0001	0.0001	0.0001 - 0.0001
$v_{ALD,C}$	0.011	0.009 - 0.012	0.010	0.009 - 0.011	0.007	0.006 - 0.008
$v_{LAC,C}$	0.001	0.001 - 0.001	0.018	0.015 - 0.020	0.053	0.042 - 0.063
$v_{LAD,C}$	0.001	0.0001 - 0.001	0.014	0.009 - 0.018	0.053	0.042 - 0.063
$v_{GABA,C}$	0.015	0.014 - 0.017	0.017	0.014 - 0.019	0.012	0.008 - 0.015
$v_{GABA,C}$	0.000	0.000 - 0.000	0.008	0.005 - 0.010	0.006	0.004 - 0.008
$v_{2KG,M}$	0.075	0.072 - 0.078	0.046	0.041 - 0.050	0.041	0.035 - 0.046
$v_{CIT,M}$	0.076	0.073 - 0.078	0.046	0.041 - 0.050	0.041	0.035 - 0.046
$v_{SUT,M}$	0.038	0.036 - 0.041	0.034	0.030 - 0.038	0.034	0.027 - 0.038
$v_{FUM,M}$	0.052	0.049 - 0.056	0.044	0.040 - 0.047	0.040	0.034 - 0.044
$v_{MAL,M}$	0.052	0.049 - 0.056	0.044	0.040 - 0.047	0.040	0.034 - 0.044
$v_{OAA,M}$	0.273	0.244 - 0.316	0.045	0.041 - 0.048	0.041	0.036 - 0.045
$v_{AMA,M}$	0.224	0.194 - 0.265	0.0001	0.0001 - 0.0001	0.0001	0.0001 - 0.0001
$v_{ANA1,M}$	0.134	0.123 - 0.143	0.034	0.023 - 0.044	0.032	0.025 - 0.040

Appendix 3E: (continued)

Flux	21kpa		1 kPa		0 kPa	
	Estimate	**CI**	**Estimate**	**CI**	**Estimate**	**CI**
$v_{ANA3,M}$	0.0001	0.0001 - 0.0001	0.0001	0.0001 - 0.0001	0.0001	0.0001 - 0.0001
$v_{GLU,M}$	0.184	0.171 - 0.195	0.067	0.058 - 0.077	0.058	0.049 - 0.068
$v_{GLD,M}$	0.0001	0.0001 - 0.0001	0.0001	0.0001 - 0.0001	0.0001	0.0001 - 0.0001
$v_{ASP,M}$	0.108	0.097 - 0.118	0.032	0.022 - 0.043	0.032	0.023 - 0.041
$v_{ASD,M}$	0.107	0.096 - 0.118	0.033	0.022 - 0.043	0.033	0.023 - 0.042
$v_{GST,M}$	0.014	0.013 - 0.015	0.010	0.009 - 0.010	0.006	0.005 - 0.007
$v_{CLYS,M}$	0.0004	0.0004 - 0.0004	0.0001	0.0001 - 0.0001	0.0001	0.0001 - 0.0001
$v_{EXT,C}$	0.680	0.584 - 0.770	2.176	1.638 - 2.765	3.321	2.555 - 3.892
$v_{EXP,P}$	0.001	0.001 - 0.002	0.000	0.000 - 0.000	0.009	0.005 - 0.012

Appendix 3F: Model equations used for dynamic modelling of the central carbon metabolism.

```
%----------------------- Volume of subcellular compartments ---------------
      Vp    = 0.003;          % relative volume of Plastid
      Vm    = 0.0008;         % relative volume of Mitochondria
      Vv    = 0.30;           % relative volume of Vacuole
      Vc    = 1-Vp-Vm-Vv;     % relative volume of Cytosol
%--------------------------------------------------------------------------

%----------------------- Modelled Output variables ------------------------
output_var = {'GLC_C_T' 'GLC_C_U' 'GLC_C_L' 'GLC_P_T' 'GLC_P_U' 'GLC_P_L'...
            'FRC_C_T' 'FRC_C_U' 'FRC_C_L' 'FRC_P_T' 'FRC_P_U' 'FRC_P_L'...
            'G6P_C_T' 'G6P_C_U' 'G6P_C_L' 'G6P_P_T' 'G6P_P_U' 'G6P_P_L'...
            'S00_C' 'S10_C' 'S01_C' 'S11_C' 'S00_V' 'S10_V' 'S01_V' 'S11_V'...
            'F6P_C_T' 'F6P_C_U' 'F6P_C_L' 'F6P_P_T' 'F6P_P_U' 'F6P_P_L'...
            '3PG_C_T' '3PG_C_U' '3PG_C_L' '3PG_P_T' '3PG_P_U' '3PG_P_L'...
            'SER_P_T' 'SER_P_U' 'SER_P_L'...
            'PYR_C_T' 'PYR_C_U' 'PYR_C_L' 'PYR_P_T' 'PYR_P_U' 'PYR_P_L' 'PYR_M_T' 'PYR_M_U' 'PYR_M_L'...
            'ALA_C_T' 'ALA_C_U' 'ALA_C_L' 'ALA_M_T' 'ALA_M_U' 'ALA_M_L' ...
            'LAC_C_T' 'LAC_C_U' 'LAC_C_L' ...
            'VAL_P_T' 'VAL_P_U' 'VAL_P_L' ...
            'CIT_00_M' 'CIT_10_M' 'CIT_01_M' 'CIT_11_M'...
            '2KG_M_T' '2KG_M_U' '2KG_M_L' '2KG_C_T' '2KG_C_U' '2KG_C_L' '2KG_P_T' '2KG_P_U' '2KG_P_L'...
            'SUT_M_T' 'SUT_M_U' 'SUT_M_L'...
            'FUM_M_T' 'FUM_M_U' 'FUM_M_L'...
            'MAL_M_T' 'MAL_M_U' 'MAL_M_L'...
            'OAA_M_T' 'OAA_M_U' 'OAA_M_L'...
            'GLU_M_T' 'GLU_M_U' 'GLU_M_L' 'GLU_C_T' 'GLU_C_U' 'GLU_C_L' 'GLU_P_T' 'GLU_P_U' 'GLU_P_L'...
            'ASP_M_T' 'ASP_M_U' 'ASP_M_L' ...
            'GABA_C_T' 'GABA_C_U' 'GABA_C_L' 'GABA_M_T' 'GABA_M_U' 'GABA_M_L' ...
            'G6P_T' 'GLC_T' 'FRC_T' 'SUC_T' 'F6P_T' '3PG_T' 'PYR_T' 'CIT_T' '2KG_T' 'SUT_T' ...
            'FUM_T' 'MAL_T' 'OAA_T' 'SER_T' 'ALA_T' 'LAC_T' 'VAL_T' 'GLU_T' 'ASP_T' 'GABA_T'...
            'G6P_F' 'GLC_F' 'FRC_F' 'SUC_F' 'F6P_F' '3PG_F' 'PYR_F' 'CIT_F' '2KG_F' 'SUT_F' ...
            'FUM_F' 'MAL_F' 'OAA_F' 'SER_F' 'ALA_F' 'LAC_F' 'VAL_F' 'GLU_F' 'ASP_F' 'GABA_F'};
%--------------------------------------------------------------------------
```

```
%------ Declaration of model parameters including initial values assigned ----------
%---- The full set of estimated values for each oxygen level can be found in Appendix 3A-E ---

      param_DEF = {'Km_upt'         83000; ...
                   'Km_G6P_C'       0.795; ...
                   'Km_F6P_P'       0.222; ...
                   'Km_3PG_P'       0.016; ...
                   'Km_PYR_P'       23.24; ...
                   'Vmax_T'         0.228; ...
                   'Vmax_G6P_C_T'   869.5; ...
                   'Vmax_F6P_C_T'   0.440; ...
                   'Vmax_3PG_C_T'   0.302; ...
                   'Vmax_PYR_C_T'   584.7; ...
                   'Vmax_F6P_P_T'   5.889; ...
                   'Vmax_PYR_P_T'   32.87; ...
                   'Vmax_3PG_P_T'   10.07; ...
                   'Kp'             10000; ...
                   'Vmax_LAC_C_T'   4.706; ...
                   'Km_LAC_C'       0.018; ...
                   'k_G6P_CPt'      0.103; ...
                   'k_G6P_PCt'      0.088; ...
                   'k_GLC_VCt'      0.293; ...
                   'k_GLC_CVt'      0.293; ...
                   'k_FRC_CVt'      0.365; ...
                   'k_FRC_VCt'      0.365; ...
                   'k_SUC_CVt'      0.094; ...
                   'k_SUC_VCt'      0.012; ...
                   'k_PYR_PCt'      0.024; ...
                   'k_PYR_CMt'      102.4; ...
                   'k_GLU_MCt'      4.777; ...
                   'k_GLU_CPt'      0.087; ...
                   'k_2KG_CMt'      1.782; ...
                   'k_2KG_PCt'      0.047; ...
                   'k_GABA_CMt'     0.225; ...
                   'k_ALA_MCt'      0.077; ...
                   'V_sta'          11.44; ...
                   'k_LAD_C'        0.033; ...
```

```
'k_ALA_C'          0.036; ...
'k_ALD_C'          0.444; ...
'k_SUC_C'          0.714; ...
'k_SUSY_C'         0.189; ...
'k_SUSR_C'         0.018; ...
'k_INV_C'          0.145; ...
'k_GABA_C'         0.175; ...
'k_GADA_C'         0.114; ...
'k_FRC_C'          0.043; ...
'k_INV_V'          0.012; ...
'k_SER_P'          0.171; ...
'k_SED_P'          0.101; ...
'k_VAL_P'          57.45; ...
'k_VAD_P'          0.135; ...
'k_CIT_M'          24.79; ...
'k_2KG_M'          1.896; ...
'k_SUT_M'          31.05; ...
'k_FUM_M'          5.327; ...
'k_MAL_M'          4.834; ...
'k_OAA_M'          0.332; ...
'k_AMA_M'          0.236; ...
'k_ANA1'           10.21; ...
'k_ANA3'           0.089; ...
'k_CLYS_M'         0.128; ...
'k_GST_M'          31.43; ...
'k_EXT_M'          86.95; ...
'k_EXT_P'          0.235; ...
'k_GLU_M'          46.09; ...
'k_GLD_M'          0.171; ...
'k_ASP_M'          17684; ...
'k_ASD_M'          0.739; ...
'2KG_C_0'          0.012; ...
'GLU_C_0'          0.164; ...
'G6P_P_0'          0.351; ...
'F6P_P_0'          0.115; ...
'3PG_P_0'          1.512; ...
'PYR_P_0'          0.584; ...
```

```
                'GLU_P_0'         7.955; ...
                '2KG_P_0'         0.767; ...
                'PYR_M_0'         9.828; ...
                'ALA_M_0'         0.237; ...
                'GABA_M_0'        0.064; ...
                'GLC_V_0'         0.004; ...
                'FRC_V_0'         0.161; ...
                'SUC_V_0'         0.168; ...
                'CIT_V_0'         0.183; ...
                'SUT_V_0'         0.111; ...
                'FUM_V_0'         0.052; ...
                'ALA_V_0'         0.186; ...
                'GLC_0'           0.083; ...
                'OAA_0'           0.005; ...
                'Km_F6P_C'        0.000; ...
                'Km_3PG_C'        0.000; ...
                'Km_PYR_C'        0.000 };
%-------------------------------------------------------------------------------

%--------- Initial total cellular concentration of metabolites ------------------

                FRC_0 =     0.087554;
                G6P_0 =     0.074043;
                SUC_0 =     0.095476;
                F6P_0 =     0.015668;
                3PG_0 =     0.025537;
                PYR_0 =     0.008917;
                CIT_0 =     0.107239;
                2KG_0 =     0.010622;
                SUT_0 =     0.048651;
                FUM_0 =     0.034384;
                MAL_0 =     0.168591;
                SER_0 =     0.075420;
                ALA_0 =     0.128800;
                LAC_0 =     0.044953;
                VAL_0 =     0.053599;
                GLU_0 =     0.140036;
```

```
                ASP_0 =     0.042297;
                GABA_0 =    0.071943;
%-------------------------------------------------------------------------------


%----- Constraints to prevent zero values in subcellular metabolite levels -------
                GLC_V_0=min(GLC_V_0,GLC_0/Vva);
                FRC_V_0=min(FRC_V_0,FRC_0/Vva);
                G6P_P_0=min(G6P_P_0,G6P_0/Vpl);
                SUC_V_0=min(SUC_V_0,SUC_0/Vva);
                F6P_P_0=min(F6P_P_0,F6P_0/Vpl);
                3PG_P_0=min(3PG_P_0,3PG_0/Vpl);
                GABA_M_0=min(GABA_M_0,GABA_0/Vmi);
                PYR_P_0=min(PYR_P_0*Vpl,PYR_0-PYR_M_0*Vmi)/Vpl;
                2KG_P_0=min(2KG_P_0*Vpl,2KG_0-2KG_C_0*Vcy)/Vpl;
                GLU_P_0=min(GLU_P_0*Vpl,GLU_0-GLU_C_0*Vcy)/Vpl;
%-------------------------------------------------------------------------------

%----------- Assigning initial values for the modelled metabolites ----------------
      y0 = [(GLC_0-GLC_V_0*Vva)/Vcy (GLC_0-GLC_V_0*Vva)/Vcy 0 GLC_V_0 GLC_V_0 0 ...
            (FRC_0-FRC_V_0*Vva)/Vcy (FRC_0-FRC_V_0*Vva)/Vcy 0 FRC_V_0 FRC_V_0 0 ...
            (G6P_0-G6P_P_0*Vpl)/Vcy (G6P_0-G6P_P_0*Vpl)/Vcy 0 G6P_P_0 G6P_P_0 0 ...
            (SUC_0-SUC_V_0*Vva)/Vcy 0 0 0 SUC_V_0 0 0 0 ...
            (F6P_0-F6P_P_0*Vpl)/Vcy (F6P_0-F6P_P_0*Vpl)/Vcy 0 F6P_P_0 F6P_P_0 0 ...
            (3PG_0-3PG_P_0*Vpl-3PG_V_0*Vva)/Vcy (3PG_0-3PG_P_0*Vpl-3PG_V_0*Vva)/Vcy 0 3PG_P_0 3PG_P_0 0 ...
            (SER_0-SER_V_0*Vva)/Vpl (SER_0-SER_V_0*Vva)/Vpl 0 ...
            (PYR_0-PYR_P_0*Vpl-PYR_M_0*Vmi-PYR_V_0*Vva)/Vcy (PYR_0-PYR_P_0*Vpl-PYR_M_0*Vmi-PYR_V_0*Vva)/Vcy 0
                  PYR_P_0 PYR_P_0 0 PYR_M_0 PYR_M_0 0 ...
            (ALA_0-ALA_M_0*Vmi-ALA_V_0*Vva)/Vcy (ALA_0-ALA_M_0*Vmi-ALA_V_0*Vva)/Vcy 0 ALA_M_0 ALA_M_0 0 ...
            (LAC_0-LAC_V_0*Vva)/Vcy (LAC_0-LAC_V_0*Vva)/Vcy 0 ...
            (VAL_0-VAL_V_0*Vva)/Vpl (VAL_0-VAL_V_0*Vva)/Vpl 0 ...
            (CIT_0-CIT_V_0*Vva)/Vmi 0 0 0 ...
            (2KG_0-2KG_C_0*Vcy-2KG_V_0*Vva-2KG_P_0*Vpl)/Vmi (2KG_0-2KG_C_0*Vcy-2KG_V_0*Vva-2KG_P_0*Vpl)/Vmi 0
                  2KG_C_0 2KG_C_0 0 2KG_P_0 2KG_P_0 0 ...
            (SUT_0-SUT_V_0*Vva)/Vmi (SUT_0-SUT_V_0*Vva)/Vmi 0 ...
            (FUM_0-FUM_V_0*Vva)/Vmi (FUM_0-FUM_V_0*Vva)/Vmi 0 ...
            (MAL_0-MAL_V_0*Vva)/Vmi (MAL_0-MAL_V_0*Vva)/Vmi 0 ...
```

```
            (OAA_0-OAA_V_0*Vva)/Vmi (OAA_0-OAA_V_0*Vva)/Vmi 0 ...
            (GLU_0-GLU_C_0*Vcy-GLU_P_0*Vpl-GLU_V_0*Vva)/Vmi (GLU_0-GLU_C_0*Vcy-GLU_P_0*Vpl-GLU_V_0*Vva)/Vmi 0
                 GLU_C_0 GLU_C_0 0 GLU_P_0 GLU_P_0 0 ...
            (ASP_0-ASP_V_0*Vva)/Vmi (ASP_0-ASP_V_0*Vva)/Vmi 0 ...
            (GABA_0-GABA_M_0*Vmi-GABA_V_0*Vva)/Vcy (GABA_0-GABA_M_0*Vmi-GABA_V_0*Vva)/Vcy 0 GABA_M_0 GABA_M_0 0
      ] ;
%-------------------------------------------------------------------------------


%------------- Interpolation to calculate label addition at 4 h ------------
      CLL         = interp1(t_cond,CL,t); % interpolating the changing levels of labelled glucose
      CUU         = 83000;                % the constant level of unlabelled sugar
      R_CUU       = CUU/(CLL+CUU);        % the ration of labelled sugar in the medium
%-------------------------------------------------------------------------------

%----------- Michaelis-Menten kinetics for the uptake of external glucose ---
      V_upt_U     = R_CUU*Vmax_T*(CLL+CUU)/(Km_upt+(CLL+CUU));
      V_upt_T     = Vmax_T*(CLL+CUU)/(Km_upt+(CLL+CUU));
%-------------------------------------------------------------------------------

%-------------------- K_M of glycolysis: cytosol = plastid -------------------
      Km_F6P_C    = Km_F6P_P;
      Km_3PG_C    = Km_3PG_P;
      Km_PYR_C    = Km_PYR_P;
%-------------------------------------------------------------------------------

%--------- Ratio of unlabelled to total metabolite concentrations -----------
      R_GLC_C=GLC_C_U/GLC_C_T;
      R_G6P_C     = G6P_C_U/G6P_C_T;
      R_F6P_C     = F6P_C_U/F6P_C_T;
      R_3PG_C     = 3PG_C_U/3PG_C_T;
      R_PYR_C     = PYR_C_U/PYR_C_T;
      R_G6P_P     = G6P_P_U/G6P_P_T;
      R_F6P_P     = F6P_P_U/F6P_P_T;
      R_3PG_P     = 3PG_P_U/3PG_P_T;
%-------------------------------------------------------------------------------
```

```
%-------------------------------------------------------------------------
%     Differential equations of the metabolites in the different subcellular compartments
%-------------------------------------------------------------------------

%--------- Sucrose and Citrate estimations -----------
                SUC_C_T=S00_C+S10_C+S01_C+S11_C;
                SUC_V_T=S00_V+S10_V+S01_V+S11_V;
                CIT_M_T=CIT_00_M+CIT_10_M+CIT_01_M+CIT_11_M;
%-----------------------------------------------------

%-------- Cytosolic Glucose (GLC_C)-----------------
dGLC_C_Tdt= V_upt_T -         ((Vmax_G6P_C_T*GLC_C_T)/(Km_G6P_C+GLC_C_T)) + GLC_V_T*k_GLC_VCt/Vcy ;
dGLC_C_Udt= V_upt_U - (R_GLC_C*(Vmax_G6P_C_T*GLC_C_T)/(Km_G6P_C+GLC_C_T)) + GLC_V_U*k_GLC_VCt/Vcy ;
dGLC_C_Ldt=dGLC_C_Tdt-dGLC_C_Udt;
%-----------------------------------------------------

%-------- Vacuolar Glucose (GLC_V)------------------
dGLC_V_Tdt=  SUC_V_T*k_INV_V               - GLC_V_T*k_GLC_VCt/Vva ;
dGLC_V_Udt=  S00_V*k_INV_V + S01_V*k_INV_V - GLC_V_U*k_GLC_VCt/Vva ;
dGLC_V_Ldt=dGLC_V_Tdt-dGLC_V_Udt;
%-----------------------------------------------------

%-------- Cytosol Fructose (FRC_C)------------------
dFRC_C_Tdt= SUC_C_T*k_SUSY_C                  + FRC_V_T*k_FRC_VCt/Vcy - FRC_C_T*k_FRC_C ;
dFRC_C_Udt= S00_C*k_SUSY_C  +  S10_C*k_SUSY_C + FRC_V_U*k_FRC_VCt/Vcy - FRC_C_U*k_FRC_C ;
dFRC_C_Ldt=dFRC_C_Tdt-dFRC_C_Udt;
%-----------------------------------------------------

%-------- Vacuolar Fructose (FRC_C)-----------------
dFRC_V_Tdt= SUC_V_T*k_INV_V                    - FRC_V_T*k_FRC_VCt/Vva ;
dFRC_V_Udt= S00_V*k_INV_V  +  S10_V*k_INV_V    - FRC_V_U*k_FRC_VCt/Vva ;
dFRC_V_Ldt=dFRC_V_Tdt-dFRC_V_Udt;
%-----------------------------------------------------

%------Cytosolic Glucose-6-phosphate (G6P_C) --------
dG6P_C_Tdt= ((Vmax_G6P_C_T*GLC_C_T)/(Km_G6P_C+GLC_C_T)) - ((Vmax_F6P_C_T*G6P_C_T)/(Km_F6P_C+G6P_C_T))-
            G6P_C_T*k_G6P_CPt/Vcy + G6P_P_T*k_G6P_PCt/Vcy - G6P_C_T*F6P_C_T*k_SUC_C + SUC_C_T*k_SUSY_C;
```

```
dG6P_C_Udt= (R_GLC_C*(Vmax_G6P_C_T*GLC_C_T)/(Km_G6P_C+GLC_C_T) -
            (R_G6P_C*(Vmax_F6P_C_T*G6P_C_T)/(Km_F6P_C+G6P_C_T))- G6P_C_U*k_G6P_CPt/Vcy + G6P_P_U*k_G6P_PCt/Vcy -
            G6P_C_U*F6P_C_T*k_SUC_C + S00_C*k_SUSY_C  +  S01_C*k_SUSY_C ;
dG6P_C_Ldt=dG6P_C_Tdt-dG6P_C_Udt;
%-----------------------------------------------------

%-------- Plastidial Glucose-6-phosphate (F6P_P) ----
dG6P_P_Tdt= V_sta - ((Vmax_F6P_P_T*G6P_P_T)/(Km_F6P_P+G6P_P_T))        + G6P_C_T*k_G6P_CPt/Vpl -
            G6P_P_T*k_PPP - G6P_P_T*k_G6P_PCt/Vpl ;
dG6P_P_Udt= V_sta -(R_G6P_P*(Vmax_F6P_P_T*G6P_P_T)/(Km_F6P_P+G6P_P_T)) + G6P_C_U*k_G6P_CPt/Vpl -
            G6P_P_U*k_PPP - G6P_P_U*k_G6P_PCt/Vpl ;
dG6P_P_Ldt=dG6P_P_Tdt-dG6P_P_Udt;
%-----------------------------------------------------
%-------- Cytosolic Fructose-6-phosphate (F6P_C)-----
dF6P_C_Tdt=        ((Vmax_F6P_C_T*G6P_C_T)/(Km_F6P_C+G6P_C_T))-
((Vmax_3PG_C_T*F6P_C_T)/(Km_3PG_C+F6P_C_T)) -
            G6P_C_T*F6P_C_T*k_SUC_C ;
dF6P_C_Udt=(R_G6P_C*(Vmax_F6P_C_T*G6P_C_T)/(Km_F6P_C+G6P_C_T))-
(R_F6P_C*(Vmax_3PG_C_T*F6P_C_T)/(Km_3PG_C+F6P_C_T)) -
            G6P_C_T*F6P_C_U*k_SUC_C ;
dF6P_C_Ldt=dF6P_C_Tdt-dF6P_C_Udt;
%-----------------------------------------------------

%-------- Plastidial Fructose-6-phosphate (F6P_P) ---
dF6P_P_Tdt=       ((Vmax_F6P_P_T*G6P_P_T)/(Km_F6P_P+G6P_P_T)) -
((Vmax_3PG_P_T*F6P_P_T)/(Km_3PG_P+F6P_P_T));
dF6P_P_Udt=(R_G6P_P*(Vmax_F6P_P_T*G6P_P_T)/(Km_F6P_P+G6P_P_T))-
(R_F6P_P*(Vmax_3PG_P_T*F6P_P_T)/(Km_3PG_P+F6P_P_T));
dF6P_P_Ldt=dF6P_P_Tdt-dF6P_P_Udt;
%-----------------------------------------------------

%-------- Cytosolic Sucrose (SUC_C)------------------
dS00_Cdt= G6P_C_U*F6P_C_U*k_SUC_C - S00_C*k_SUC_CVt/Vcy + S00_V*k_SUC_VCt/Vcy - S00_C*k_SUSY_C ;
dS10_Cdt= G6P_C_L*F6P_C_U*k_SUC_C - S10_C*k_SUC_CVt/Vcy + S10_V*k_SUC_VCt/Vcy - S10_C*k_SUSY_C ;
dS01_Cdt= G6P_C_U*F6P_C_L*k_SUC_C - S01_C*k_SUC_CVt/Vcy + S01_V*k_SUC_VCt/Vcy - S01_C*k_SUSY_C ;
dS11_Cdt= G6P_C_L*F6P_C_L*k_SUC_C - S11_C*k_SUC_CVt/Vcy + S11_V*k_SUC_VCt/Vcy - S11_C*k_SUSY_C ;
%-----------------------------------------------------
```

```
%-------- Vacuolar Sucrose (SUC_C)-------------------
dS00_Vdt= S00_C*k_SUC_CVt/Vva - S00_V*k_SUC_VCt/Vva - S00_V*k_INV_V ;
dS10_Vdt= S10_C*k_SUC_CVt/Vva - S10_V*k_SUC_VCt/Vva - S10_V*k_INV_V ;
dS01_Vdt= S01_C*k_SUC_CVt/Vva - S01_V*k_SUC_VCt/Vva - S01_V*k_INV_V ;
dS11_Vdt= S11_C*k_SUC_CVt/Vva - S11_V*k_SUC_VCt/Vva - S11_V*k_INV_V ;
%-----------------------------------------------------

%--------- Cytosolic 3-phosphoglycerate (3PG_C) -----
d3PG_C_Tdt  = 2*((Vmax_3PG_C_T*F6P_C_T)/(Km_3PG_C+F6P_C_T)) - ((Vmax_PYR_C_T*3PG_C_T)/(Km_PYR_C+3PG_C_T)) -
              k_ANA2*3PG_C_T;
d3PG_C_Udt=2*(R_F6P_C*(Vmax_3PG_C_T*F6P_C_T)/(Km_3PG_C+F6P_C_T))-
            (R_3PG_C*(Vmax_PYR_C_T*3PG_C_T)/(Km_PYR_C+3PG_C_T))- k_ANA2*3PG_C_U;
d3PG_C_Ldt  = d3PG_C_Tdt - d3PG_C_Udt;
%-----------------------------------------------------



%-----------Plastidial 3-phosphoglycerate (3PG_P) ---
d3PG_P_Tdt  = 2*((Vmax_3PG_P_T*F6P_P_T)/(Km_3PG_P+F6P_P_T)) -
            ((Vmax_PYR_P_T*3PG_P_T)/(Km_PYR_P+3PG_P_T))-3PG_P_T*GLU_P_T*k_SER_P;
d3PG_P_Udt  = 2*(R_F6P_P*(Vmax_3PG_P_T*F6P_P_T)/(Km_3PG_P+F6P_P_T))-
            (R_3PG_P*(Vmax_PYR_P_T*3PG_P_T)/(Km_PYR_P+3PG_P_T)) - 3PG_P_U*GLU_P_T*k_SER_P;
d3PG_P_Ldt  = d3PG_P_Tdt - d3PG_P_Udt;
%-----------------------------------------------------

%----------- Cytosolic Serine (SER_C) ---------------
dSER_P_Tdt  = 3PG_P_T*GLU_P_T*k_SER_P - SER_P_T*k_SED_P;
dSER_P_Udt  = 3PG_P_U*GLU_P_T*k_SER_P - SER_P_U*k_SED_P;
dSER_P_Ldt  = dSER_P_Tdt - dSER_P_Udt;
%-----------------------------------------------------

%---------- Cytosolic Pyruvate (PYR_C) --------------
dPYR_C_Tdt  = ((Vmax_PYR_C_T*3PG_C_T)/(Km_PYR_C+3PG_C_T)) - k_LAC_C*PYR_C_T -
            PYR_C_T*GLU_C_T*k_ALA_C - PYR_C_T*k_PYR_CMt/Vc + PYR_P_T*k_PYR_PCt/Vc - PYR_C_T*k_EXT_M;
dPYR_C_Udt  = (R_3PG_C*(Vmax_PYR_C_T*3PG_C_T)/(Km_PYR_C+3PG_C_T)) - k_LAC_C*PYR_C_U -
            PYR_C_U*GLU_C_T*k_ALA_C - PYR_C_U*k_PYR_CMt/Vc + PYR_P_U*k_PYR_PCt/Vc - PYR_C_U*k_EXT_M;
```

```
dPYR_C_Ldt  = dPYR_C_Tdt - dPYR_C_Udt;
%-------------------------------------------------

%----------- Plastidial Pyruvate (PYR_P) ------------
dPYR_P_Tdt  = ((Vmax_PYR_P_T*3PG_P_T)/(Km_PYR_P+3PG_P_T)) - 2*PYR_P_T*PYR_P_T*GLU_P_T*k_VAL_P -
            PYR_P_T*k_EXT_P - PYR_P_T*k_PYR_PCt/Vp;
dPYR_P_Udt  = (R_3PG_P*(Vmax_PYR_P_T*3PG_P_T)/(Km_PYR_P+3PG_P_T)) - 2*PYR_P_U*PYR_P_U*GLU_P_T*k_VAL_P -
            2*PYR_P_U*PYR_P_L*GLU_P_T*k_VAL_P - PYR_P_U*k_EXT_P - PYR_P_U*k_PYR_PCt/Vp;
dPYR_P_Ldt  = dPYR_P_Tdt - dPYR_P_Udt;
%-------------------------------------------------

%---------------- Mitochondrial Pyruvate (PYR_M) ----
dPYR_M_Tdt  = PYR_C_T*k_PYR_CMt/Vm - PYR_M_T*OAA_M_T*k_CIT_M  - PYR_M_T*k_ANA1 + MAL_M_T*k_ANA3 +
            CIT_M_T*k_CLYS_M - GABA_M_T*PYR_M_T*k_GST_M;
dPYR_M_Udt  = PYR_C_U*k_PYR_CMt/Vm - PYR_M_U*OAA_M_T*k_CIT_M  - PYR_M_U*k_ANA1 + MAL_M_U*k_ANA3 +
            CIT_00_M*k_CLYS_M+ CIT_01_M*k_CLYS_M  - GABA_M_T*PYR_M_U*k_GST_M;
dPYR_M_Ldt  = dPYR_M_Tdt - dPYR_M_Udt;
%-------------------------------------------------



%-------------- Cytosolic Alanine (ALA_C) -----------
dALA_C_Tdt  = PYR_C_T*GLU_C_T*k_ALA_C - ALA_C_T*k_ALD_C + ALA_M_T*k_ALA_MCt/Vc;
dALA_C_Udt  = PYR_C_U*GLU_C_T*k_ALA_C - ALA_C_U*k_ALD_C + ALA_M_U*k_ALA_MCt/Vc;
dALA_C_Ldt  = dALA_C_Tdt - dALA_C_Udt;
%-------------------------------------------------

%------------- Mitochondrial Alanine (ALA_M) --------
dALA_M_Tdt  = GABA_M_T*PYR_M_T*k_GST_M - ALA_M_T*k_ALA_MCt/Vm;
dALA_M_Udt  = GABA_M_T*PYR_M_U*k_GST_M - ALA_M_U*k_ALA_MCt/Vm;
dALA_M_Ldt  = dALA_M_Tdt - dALA_M_Udt;
%-------------------------------------------------

%------------- Cytosolic Lactate (LAC_C) ------------
dLAC_C_Tdt  = k_LAC_C*PYR_C_T - LAC_C_T*k_LAD_C;
dLAC_C_Udt  = k_LAC_C*PYR_C_U - LAC_C_U*k_LAD_C;
dLAC_C_Ldt  = dLAC_C_Tdt - dLAC_C_Udt;
```

```
%-----------------------------------------------------

%------------- Plastidial Valine (VAL_P) ------------
dVAL_P_Tdt  = PYR_P_T*PYR_P_T*GLU_P_T*k_VAL_P - VAL_P_T*k_VAD_P;
dVAL_P_Udt  = PYR_P_U*PYR_P_U*GLU_P_T*k_VAL_P - VAL_P_U*k_VAD_P;
dVAL_P_Ldt  = dVAL_P_Tdt - dVAL_P_Udt;
%-----------------------------------------------------

%-------------- Mitochondrial Citrate (CIT_M) -------
CIT_M_T     = CIT_00_M + CIT_10_M + CIT_01_M + CIT_11_M;
dCIT_00_Mdt = PYR_M_U*OAA_M_U*k_CIT_M - CIT_00_M*k_CLYS_M - CIT_00_M*k_2KG_M;
dCIT_10_Mdt = PYR_M_L*OAA_M_U*k_CIT_M - CIT_10_M*k_CLYS_M - CIT_10_M*k_2KG_M;
dCIT_01_Mdt = PYR_M_U*OAA_M_L*k_CIT_M - CIT_01_M*k_CLYS_M - CIT_01_M*k_2KG_M;
dCIT_11_Mdt = PYR_M_L*OAA_M_L*k_CIT_M - CIT_11_M*k_CLYS_M - CIT_11_M*k_2KG_M;
%-----------------------------------------------------

%------------ Mitochondrial 2-ketoglutarate (2KG_M) --
d2KG_M_Tdt  = CIT_M_T*k_2KG_M - 2KG_M_T*k_SUT_M - 2KG_M_T*k_GLU_M + 2KG_C_T*k_2KG_CMt/Vm +
OAA_M_T*GLU_M_T*k_ASP_M;
d2KG_M_Udt  = CIT_00_M*k_2KG_M- 2KG_M_U*k_SUT_M - 2KG_M_U*k_GLU_M + 2KG_C_U*k_2KG_CMt/Vm +
OAA_M_T*GLU_M_U*k_ASP_M;
d2KG_M_Ldt  = d2KG_M_Tdt - d2KG_M_Udt;
%-----------------------------------------------------

%------------ Cytosolic 2-ketoglutarate (2KG_C) ------
d2KG_C_Tdt  = PYR_C_T*GLU_C_T*k_ALA_C - 2KG_C_T*k_2KG_CMt/Vc + 2KG_P_T*k_2KG_PCt/Vc;
d2KG_C_Udt  = PYR_C_T*GLU_C_U*k_ALA_C - 2KG_C_U*k_2KG_CMt/Vc + 2KG_P_U*k_2KG_PCt/Vc;
d2KG_C_Ldt  = d2KG_C_Tdt - d2KG_C_Udt;
%-----------------------------------------------------

%------------ Plastidial 2-ketoglutarate (2KG_P) -----
d2KG_P_Tdt  = PYR_P_T*PYR_P_T*GLU_P_T*k_VAL_P + 3PG_P_T*GLU_P_T*k_SER_P - 2KG_P_T*k_2KG_PCt/Vp;
d2KG_P_Udt  = PYR_P_T*PYR_P_T*GLU_P_U*k_VAL_P + 3PG_P_T*GLU_P_U*k_SER_P - 2KG_P_U*k_2KG_PCt/Vp;
d2KG_P_Ldt  = d2KG_P_Tdt - d2KG_P_Udt;
%-----------------------------------------------------

%------------ Mitochondrial Succinate (SUT_M) --------
```

```
dSUT_M_Tdt  = 2KG_M_T*k_SUT_M - SUT_M_T*k_FUM_M + GABA_M_T*PYR_M_T*k_GST_M;
dSUT_M_Udt  = 2KG_M_U*k_SUT_M - SUT_M_U*k_FUM_M + GABA_M_U*PYR_M_T*k_GST_M;
dSUT_M_Ldt  = dSUT_M_Tdt - SUT_M_Udt;
%-------------------------------------------------------

%------------ Mitochondrial Fumarate (FUM_M) ---------
dFUM_M_Tdt  = SUT_M_T*k_FUM_M - FUM_M_T*k_MAL_M;
dFUM_M_Udt  = SUT_M_U*k_FUM_M - FUM_M_U*k_MAL_M;
dFUM_M_Ldt  = dFUM_M_Tdt - dFUM_M_Udt;
%-------------------------------------------------------

%------------ Mitochondrial Malate (MAL_M) -----------
dMAL_M_Tdt  = FUM_M_T*k_MAL_M - MAL_M_T*k_OAA_M + OAA_M_T*k_AMA_M - MAL_M_T*k_ANA3;
dMAL_M_Udt  = FUM_M_U*k_MAL_M - MAL_M_U*k_OAA_M + OAA_M_U*k_AMA_M - MAL_M_U*k_ANA3;
dMAL_M_Ldt  = dMAL_M_Tdt - dMAL_M_Udt;
%-------------------------------------------------------

%------------ Mitochondrial Oxaloacetate (OAA_M) -----
dOAA_M_Tdt  = MAL_M_T*k_OAA_M - PYR_M_T*OAA_M_T*k_CIT_M - OAA_M_T*k_AMA_M + PYR_M_T*k_ANA1 -
            OAA_M_T*GLU_M_T*k_ASP_M + CIT_M_T*k_CLYS_M;
dOAA_M_Udt  = MAL_M_U*k_OAA_M - PYR_M_T*OAA_M_U*k_CIT_M - OAA_M_U*k_AMA_M + PYR_M_U*k_ANA1 -
            OAA_M_U*GLU_M_T*k_ASP_M + CIT_00_M*k_CLYS_M + CIT_10_M*k_CLYS_M;
dOAA_M_Ldt  = dOAA_M_Tdt - dOAA_M_Udt;
%-------------------------------------------------------



%------------ Mitochondrial Glutamate (GLU_M) --------
dGLU_M_Tdt  = 2KG_M_T*k_GLU_M - GLU_M_T*k_GLD_M - GLU_M_T*k_GLU_MCt/Vm – OAA_M_T*GLU_M_T*k_ASP_M;
dGLU_M_Udt  = 2KG_M_U*k_GLU_M - GLU_M_U*k_GLD_M - GLU_M_U*k_GLU_MCt/Vm – OAA_M_T*GLU_M_U*k_ASP_M;
dGLU_M_Ldt  = dGLU_M_Tdt - dGLU_M_Udt;
%-------------------------------------------------------

%------------ Cytosolic Glutamate (GLU_C) ------------
dGLU_C_Tdt  = GLU_M_T*k_GLU_MCt/Vc - PYR_C_T*GLU_C_T*k_ALA_C - GLU_C_T*k_GLU_CPt/Vc – GLU_C_T*k_GABA_C;
dGLU_C_Udt  = GLU_M_U*k_GLU_MCt/Vc - PYR_C_T*GLU_C_U*k_ALA_C - GLU_C_U*k_GLU_CPt/Vc – GLU_C_U*k_GABA_C;
dGLU_C_Ldt  = dGLU_C_Tdt - dGLU_C_Udt;
```

```
%-----------------------------------------------------

%------------ Plastidial Glutamate (GLU_P) -----------
dGLU_P_Tdt  = GLU_C_T*k_GLU_CPt/Vp - 3PG_P_T*GLU_P_T*k_SER_P - PYR_P_T*PYR_P_T*GLU_P_T*k_VAL_P;
dGLU_P_Udt  = GLU_C_U*k_GLU_CPt/Vp - 3PG_P_T*GLU_P_U*k_SER_P - PYR_P_T*PYR_P_T*GLU_P_U*k_VAL_P;
dGLU_P_Ldt  = dGLU_P_Tdt - dGLU_P_Udt;
%-----------------------------------------------------

%------------ Mitochondrial Aspartate (ASP_M) --------
dASP_M_Tdt  = OAA_M_T*GLU_M_T*k_ASP_M - ASP_M_T*k_ASD_M;
dASP_M_Udt  = OAA_M_U*GLU_M_T*k_ASP_M - ASP_M_U*k_ASD_M;
dASP_M_Ldt  = dASP_M_Tdt - dASP_M_Udt;
%-----------------------------------------------------

%------------ Cytosolic GABA (GABA_C) ----------------
dGABA_C_Tdt = GLU_C_T*k_GABA_C - GABA_C_T*k_GABA_CMt/Vc - GABA_C_T*k_GADA_C
dGABA_C_Udt = GLU_C_U*k_GABA_C - GABA_C_U*k_GABA_CMt/Vc - GABA_C_U*k_GADA_C;
dGABA_C_Ldt = dGABA_C_Tdt - dGABA_C_Udt;
%-----------------------------------------------------

%------------ Mitochondrial GABA (GABA_M) ------------
dGABA_M_Tdt = GABA_C_T*k_GABA_CMt/Vm - GABA_M_T*PYR_M_T*k_GST_M;
dGABA_M_Udt = GABA_C_U*k_GABA_CMt/Vm - GABA_M_U*PYR_M_T*k_GST_M;
dGABA_M_Ldt = dGABA_M_Tdt - dGABA_M_Udt;
%-----------------------------------------------------



%-----------  Returning all ODE's together as dydt----

dydt = [dGLC_C_Tdt dGLC_C_Udt dGLC_C_Ldt dGLC_V_Tdt dGLC_V_Udt dGLC_V_Ldt ...
      dFRC_C_Tdt dFRC_C_Udt dFRC_C_Ldt dFRC_V_Tdt dFRC_V_Udt dFRC_V_Ldt ...
      dG6P_C_Tdt dG6P_C_Udt dG6P_C_Ldt dG6P_P_Tdt dG6P_P_Udt dG6P_P_Ldt ...
      dS00_Cdt dS10_Cdt dS01_Cdt dS11_Cdt dS00_Vdt dS10_Vdt dS01_Vdt dS11_Vdt ...
      dF6P_C_Tdt dF6P_C_Udt dF6P_C_Ldt dF6P_P_Tdt dF6P_P_Udt dF6P_P_Ldt ...
      d3PG_C_Tdt d3PG_C_Udt d3PG_C_Ldt d3PG_P_Tdt d3PG_P_Udt d3PG_P_Ldt ...
      dSER_P_Tdt dSER_P_Udt dSER_P_Ldt ...
```

```
      dPYR_C_Tdt dPYR_C_Udt dPYR_C_Ldt dPYR_P_Tdt dPYR_P_Udt dPYR_P_Ldt dPYR_M_Tdt dPYR_M_Udt dPYR_M_Ldt ...
      dALA_C_Tdt dALA_C_Udt dALA_C_Ldt dALA_M_Tdt dALA_M_Udt dALA_M_Ldt ...
      dLAC_C_Tdt dLAC_C_Udt dLAC_C_Ldt ...
      dVAL_P_Tdt dVAL_P_Udt dVAL_P_Ldt ...
      dCIT_00_Mdt dCIT_10_Mdt dCIT_01_Mdt dCIT_11_Mdt...
      d2KG_M_Tdt d2KG_M_Udt d2KG_M_Ldt d2KG_C_Tdt d2KG_C_Udt d2KG_C_Ldt d2KG_P_Tdt d2KG_P_Udt d2KG_P_Ldt ....
      dSUT_M_Tdt dSUT_M_Udt dSUT_M_Ldt ...
      dFUM_M_Tdt dFUM_M_Udt dFUM_M_Ldt ...
      dMAL_M_Tdt dMAL_M_Udt dMAL_M_Ldt ...
      dOAA_M_Tdt dOAA_M_Udt dOAA_M_Ldt ...
      dGLU_M_Tdt dGLU_M_Udt dGLU_M_Ldt dGLU_C_Tdt dGLU_C_Udt dGLU_C_Ldt dGLU_P_Tdt dGLU_P_Udt dGLU_P_Ldt ...
            dASP_M_Tdt dASP_M_Udt dASP_M_Ldt ...
      dGABA_C_Tdt dGABA_C_Udt dGABA_C_Ldt dGABA_M_Tdt dGABA_M_Udt dGABA_M_Ldt]';
%-----------------------------------------------------

%---- Combining isoforms into labelled and total ----
      SUC_C_T     =     S00_C    +  S10_C    +  S01_C    + S11_C;
      SUC_V_T     =     S00_V    +  S10_V    +  S01_V    + S11_V;
      CIT_M_T     =     CIT_00_M +  CIT_10_M +  CIT_01_M + CIT_11_M;
      SUC_C_L     =     S10_C    +  S01_C    +  S11_C;
      SUC_V_L     =     S10_V    +  S01_V    +  S11_V;
      CIT_M_L     =     CIT_10_M +  CIT_01_M +  CIT_11_M;
%-----------------------------------------------------




%------ Calculating cellular total concentration of metabolites ----------

      GLC_T =     Vcy*GLC_C_T  +    Vpl*0        +    Vmi*0        +    Vva*GLC_V_T ;
      FRC_T =     Vcy*FRC_C_T  +    Vpl*0        +    Vmi*0        +    Vva*FRC_V_T ;
      G6P_T =     Vcy*G6P_C_T  +    Vpl*G6P_P_T  +    Vmi*0        +    Vva*0 ;
      SUC_T =     Vcy*SUC_C_T  +    Vpl*0        +    Vmi*0        +    Vva*SUC_V_T;
```

```
      F6P_T =     Vcy*F6P_C_T  +    Vpl*F6P_P_T  +    Vmi*0        +    Vva*0;
      3PG_T =     Vcy*3PG_C_T  +    Vpl*3PG_P_T  +    Vmi*0        +    Vva*3PG_V_0;
      SER_T =     Vcy*0        +    Vpl*SER_P_T  +    Vmi*0        +    Vva*SER_V_0;
      PYR_T =     Vcy*PYR_C_T  +    Vpl*PYR_P_T  +    Vmi*PYR_M_T  +    Vva*PYR_V_0;
      ALA_T =     Vcy*ALA_C_T  +    Vpl*0      +      Vmi*ALA_M_T  +    Vva*ALA_V_0;
      LAC_T =     Vcy*LAC_C_T  +    Vpl*0        +    Vmi*0        +    Vva*LAC_V_0;
      VAL_T =     Vcy*0        +    Vpl*VAL_P_T  +    Vmi*0        +    Vva*VAL_V_0;
      CIT_T =     Vcy*0        +    Vpl*0        +    Vmi*CIT_M_T  +    Vva*CIT_V_0;
      2KG_T =     Vcy*2KG_C_T  +    Vpl*2KG_P_T  +    Vmi*2KG_M_T  +    Vva*2KG_V_0;
      SUT_T =     Vcy*0        +    Vpl*0        +    Vmi*SUT_M_T  +    Vva*SUT_V_0;
      FUM_T =     Vcy*0        +    Vpl*0        +    Vmi*FUM_M_T  +    Vva*FUM_V_0;
      MAL_T =     Vcy*0        +    Vpl*0        +    Vmi*MAL_M_T  +    Vva*MAL_V_0;
      OAA_T =     Vcy*0        +    Vpl*0        +    Vmi*OAA_M_T  +    Vva*OAA_V_0;
      GLU_T =     Vcy*GLU_C_T  +    Vpl*GLU_P_T  +    Vmi*GLU_M_T  +    Vva*GLU_V_0;
      ASP_T =     Vcy*0        +    Vpl*0        +    Vmi*ASP_M_T  +    Vva*ASP_V_0;
      GABA_T=     Vcy*GABA_C_T +    Vpl*0        +    Vmi*GABA_M_T +    Vva*GABA_V_0;
%-------------------------------------------------------------------------

%------ Calculating cellular labelled concentration of metabolites ---------

      GLC_L =     Vcy*GLC_C_L  +    Vpl*0        +    Vmi*0        +    Vva*GLC_V_L ;
      FRC_L =     Vcy*FRC_C_L  +    Vpl*0        +    Vmi*0        +    Vva*FRC_V_L ;
      G6P_L =     Vcy*G6P_C_L  +    Vpl*G6P_P_L  +    Vmi*0        +    Vva*0;
      SUC_L =     Vcy*SUC_C_L  +    Vpl*0        +    Vmi*0        +    Vva*SUC_V_L;
      F6P_L =     Vcy*F6P_C_L  +    Vpl*F6P_P_L  +    Vmi*0        +    Vva*0 ;
      3PG_L =     Vcy*3PG_C_L  +    Vpl*3PG_P_L  +    Vmi*0        +    Vva*0;
      SER_L =     Vcy*0        +    Vpl*SER_P_L  +    Vmi*0        +    Vva*0;
      PYR_L =     Vcy*PYR_C_L  +    Vpl*PYR_P_L  +    Vmi*PYR_M_L  +    Vva*0;
      ALA_L =     Vcy*ALA_C_L  +    Vpl*0        +    Vmi*ALA_M_L  +    Vva*0;
      LAC_L =     Vcy*LAC_C_L  +    Vpl*0        +    Vmi*0        +    Vva*0;
      VAL_L =     Vcy*0        +    Vpl*VAL_P_L  +    Vmi*0        +    Vva*0;
      CIT_L =     Vcy*0        +    Vpl*0        +    Vmi*CIT_M_L  +    Vva*0;
      2KG_L =     Vcy*2KG_C_L  +    Vpl*2KG_P_L  +    Vmi*2KG_M_L  +    Vva*0;
      SUT_L =     Vcy*0        +    Vpl*0        +    Vmi*SUT_M_L  +    Vva*0;
      FUM_L =     Vcy*0        +    Vpl*0        +    Vmi*FUM_M_L  +    Vva*0;
      MAL_L =     Vcy*         +    Vpl*0        +    Vmi*MAL_M_L  +    Vva*0;
      OAA_L =     Vcy*0        +    Vpl*0        +    Vmi*OAA_M_L  +    Vva*0;
```

```
      GLU_L =     Vcy*GLU_C_L  +    Vpl*GLU_P_L  +    Vmi*GLU_M_L  +    Vva*0;
      ASP_L =     Vcy*0        +    Vpl*0        +    Vmi*ASP_M_L  +    Vva*0;
      GABA_L=     Vcy*GABA_C_L +    Vpl*0        +    Vmi*GABA_M_L +    Vva*0;
%-------------------------------------------------------------------------------

%----- Calculating the fraction of labelled metabolite in the whole cell ------
      GLC_F =     GLC_L/GLC_T;
      FRC_F =     FRC_L/FRC_T;
      G6P_F =     G6P_L/G6P_T;
      F6P_F =     F6P_L/F6P_T;
      3PG_F =     3PG_L/3PG_T;
      PYR_F =     PYR_L/PYR_T;
      CIT_F =     CIT_L/CIT_T;
      2KG_F =     2KG_L/2KG_T;
      SUT_F =     SUT_L/SUT_T;
      FUM_F =     FUM_L/FUM_T;
      MAL_F =     MAL_L/MAL_T;
      OAA_F =     OAA_L/OAA_T;
      SER_F =     SER_L/SER_T;
      SUC_F =     SUC_L/SUC_T;
      ALA_F =     ALA_L/ALA_T;
      LAC_F =     LAC_L/LAC_T;
      VAL_F =     VAL_L/VAL_T;
      GLU_F =     GLU_L/GLU_T;
      ASP_F =     ASP_L/ASP_T;
      GABA_F=     GABA_L/GABA_T;
%-------------------------------------------------------------------------------

end
```

Appendix 4 - Chapter 6

Appendix 4A: ^{13}C-MFA metabolic reactions and carbon transitions implemented in 13CFLUX2

Cytosolic glycolysis

v_{UPT}	$Gluc_{ext}$ (abcdef)	→	cG6P (abcdef)		
v_{3PG_C}	cG6P (abcdef)	→	c3PG (cba)	+	c3PG (def)
v_{PYR_C}	c3PG (abc)	→	cPYR (abc)		

Plastidial glycolysis

$v_{G6P\_C \rightarrow P}$	cG6P (abcdef)	→	pG6P (abcdef)		
v_{STA}	STARCH (abcdef)	→	pG6P (abcdef)		
v_{3PG_P}	pG6P (abcdef)	→	p3PG (cba)	+	p3PG (def)
v_{PYR_P}	p3PG (abc)	→	pPYR (abc)		
v_{PPP}	pG6P (abcdef)	→	R5P (bcdef)	+	CO_2 (a)
$v_{PYR\_P \rightarrow C}$	pPYR (abc)	→	cPYR (abc)		

TCA cycle

$v_{PYRP\_C \rightarrow M}$	cPYR (abc)	→	mPYR (abc)		
v_{CIT}	mPYR (abc) + mOAA (ABCD)	→	mCIT (DCBAcb)	+	CO_2 (a)
v_{2KG}	mCIT (abcdef)	→	m2KG (abcde)	+	CO_2 (f)
v_{SUT}	m2KG (abcde)	→	mSUT (bcde)	+	CO_2 (a)
v_{MAL}	mSUT (abcd)	→	mMAL (abcd)		
v_{OAA}	mMAL (abcd)	→	mOAA (abcd)		
v_{ANA1}	mPYR (abc) + CO_2 (A)	→	mOAA (abcA)		

Anabolic pathways

v_{SUC}	cG6P (abcdef)	→	vSUC (abcdef)		
v_{GLU}	m2KG (abcde)	→	mGLU (abcde)		
v_{ASP}	mOAA (abcd)	→	mASP (abcd)		
v_{LAC}	cPYR (abc)	→	cLAC (abc)		
v_{ALA}	cPYR (abc)	→	cALA (abc)		
v_{EXT}	cPYR (abc)	→	cEXT (abc)		
v_{SER}	p3PG (abc)	→	pSER (abc)		

v_{VAL}	pPYR (abc) + pPYR (ABC)	→	pVAL (ABbcC)	+	CO_2(A)
v_{HIS}	pR5P (abcde)	→	pHIS (abcde)		
v_{SUC_OUT}	vSUC (abcdef)	→	vSUC_OUT (abcdef)		
v_{GLU_OUT}	mGLU (abcde)	→	mGLU_OUT (abcde)		
v_{ASP_OUT}	mASP (abcd)	→	mASP_OUT (abcd)		
v_{LAC_OUT}	cLAC (abc)	→	cLAC_OUT (abc)		
v_{ALA_OUT}	cALA (abc)	→	cALA_OUT (abc)		
v_{EXT_OUT}	cEXT (abc)	→	cEXT_OUT (abc)		
v_{SER_OUT}	pSER (abc)	→	pSER_OUT (abc)		
v_{VAL_OUT}	pVAL (abcde)	→	pVAL_OUT (abcde)		
v_{HIS_OUT}	pHIS (abcde)	→	pHIS_OUT (abcde)		

Appendix 4B: Relative steady-state fluxes through the central carbon metabolism of tomato cell suspension incubated at different O_2 levels. All fluxes are expressed relative to the glucose uptake rate (v_{UPT}) under each O_2 condition.

Flux	**21 kPa**	**8 kPa**	**5 kPa**	**0kPa**
v_{ALA}	0.0330	0.0227	0.0264	0.0138
v_{ANA1}	0.1219	0.0773	0.0682	0.0564
v_{ASP}	0.0391	0.0265	0.0218	0.0173
v_{CIT}	0.8862	0.3935	0.0965	0.0783
v_{EXT}	1.3966	3.1630	3.3294	6.6755
$v_{G6P\_C\rightarrow P}$	0.2404	0.8431	0.7798	2.4281
v_{3PG_C}	1.2323	1.8347	1.7725	3.4212
v_{3PG_P}	0.0303	0.0258	0.0146	0.0092
v_{GLU}	0.0828	0.0508	0.0473	0.0391
v_{HIS}	0.0088	0.0061	0.0064	0.0023
v_{LAC}	0.0027	0.0053	0.0082	0.0104
v_{MAL}	0.8040	0.3427	0.0491	0.0391
v_{OAA}	0.8040	0.3427	0.0491	0.0391
v_{PPP}	0.0088	0.0061	0.0064	0.0023
v_{PYR_C}	2.4646	3.6702	3.5450	6.8435
$v_{PYR\_C\rightarrow M}$	1.0081	0.4708	0.1647	0.1346
v_{PYR_P}	0.0236	0.0265	0.0118	0.0081
v_{PYR_PC}	0.0249	0.0083	0.0164	0.0081
v_{SER}	0.0370	0.0243	0.0173	0.0104
v_{STA}	0.2795	0.8749	0.7998	2.4407
v_{SUC}	0.0081	0.0076	0.0073	0.0058
v_{SUT}	0.8040	0.3427	0.0491	0.0391
v_{2KG}	0.8862	0.3935	0.0965	0.0783
v_{UPT}	1.0000	1.0000	1.0000	1.0000
v_{VAL}	0.0242	0.0174	0.0136	0.0081

List of Publications

Articles in international peer-reviewed journals

- Ampofo-Asiama, J., Baiye, V.M.., Hertog, M.L.A.T.M., Waelkens, E., Geeraerd, A.H., Nicolai, B.M., 2014. The metabolic response of cultured tomato cells to low oxygen stress. Plant Biology, 16, 594–606.
- Ampofo-Asiama, J., Baiye, V.M.M., Hertog, M.L.A.T.M., Waelkens, E., Geeraerd, A.H., Nicolai, B.M., 2014. Analysing the steady-state fluxes in the central metabolism of *Lycopersicum esculentum* cell suspension at different oxygen conditions. In preparation.
- Ampofo-Asiama, J., Baiye, V.M.M., van Dongen, J.T., Waelkens, E., Geeraerd, A.H., Nicolai, B.M., Hertog, M.L.A.T.M., 2014. Kinetic modelling of the central metabolism of *Lycopersicum esculentum* cell suspension incubated at different oxygen levels. In preparation.
- Bouvin, J., Cajot, S., Huys, P.D., Ampofo-Asiama, J., Anne, J., Van Impe, J., Geeraerd, A., Bernaerts, K., 2014. Cost-effective experimental design for ^{13}C-based metabolic flux analysis. In preparation.
- Cantre, D., Herremans, E., Verboven, P., Ampofo-Asiama, J., Nicolaï, B., 2014. Characterization of the 3-D microstructure of mango (*Mangifera indica* L. cv. Carabao) during ripening using X-ray computed microtomography. Innovative Food Science and Emerging Technologies, doi:10.1016/j.ifset.2013.12.008.
- Oms-Oliu, G., Hertog, M.L.A.T.M., Van de Poel, B., Ampofo-Asiama, J., Geeraerd, A.H., Nicolaï, B.M., 2011. Metabolic characterization of tomato fruit during preharvest development, ripening, and postharvest shelf-life. Postharvest Biology and Technology, 62, 7–16.
- Samapundo, S., Ampofo-Asiama, J., Anthierens, T., Xhaferi, R., Van Bree, I., Szczepaniak, S., Goemaere, O., Steen, L., Dhooge, M., Paelinck, H., Dewettinck, K.,

Devlieghere, F., 2010. Influence of NaCl reduction and replacement on the growth of *Lactobacillus sakei* in broth, cooked ham and white sauce. International Journal of Food Microbiology, 143, 9–16.

- Samapundo, S., Anthierens, T., Ampofo-Asiama, J., Xhaferi, R., Van Bree, I., Szczepaniak, S., Goemaere, O., Steen, L., Dhooge, M., Paelinck, H., Devlieghere, F., 2013. The effect of NaCl reduction and replacement on the growth of *Listeria Monocytogenes* in broth, cooked ham and white sauce. Journal of Food Safety, 33, 59–70.

Articles in international non-peer reviewed journals

- Ampofo-Asiama, J., Hertog, M.L.A.T.M., Geeraerd, A.H., Nicolaï, B.M., Waelkens, E., 2012. Metabolic profiling of the response of tomato cells to oxygen stress. Acta Horticulturae (ISHS) 945, 391–396.

Abstracts presented at conferences

- Ampofo-Asiama, J., Baiye V.M.M., Hertog, M.L.A.T.M, Geeraerd, A.H, Nicolai, B.M, 2013. Unraveling the adaptive response of *Lycopersicum esculentum* cell suspension culture to low-O_2 stress anoxia through metabolome and fluxome analysis. 11th Conference of the International Society for Plant Anaerobiosis. Laguna Philppines, 6-11 October.

- Ampofo-Asiama, J., Hertog, M.L.A.T.M, Waelkens, E., Geeraerd, A.H, Nicolai, B.M., 2013. The control of metabolism in plant cells under oxygen deficiency. 18th National Symposium on Applied Biological Sciences. Ghent University, Belgium, 8 February.

- Ampofo-Asiama, J., Hertog, M.L.A.T.M, Waelkens, E., Geeraerd, A., Nicolai, B.M., 2011. Metabolic profiling of the response of tomato cells to oxygen stress. Advances in Metabolic Profiling. Dublin Ireland, 8-9 November.

- Ampofo-Asiama, J., Hertog, M.L.A.T.M., Geeraerd, A.H., Waelkens, E., Nicolaï, B.M., 2011. Metabolic profiling of the response of tomato cells to oxygen stress. International Conference Postharvest Unlimited. Leavenworth, WA, USA, 23-26 May.

- Bouvin, J., Cajot, S., D'Huys, P.J., Ampofo-Asiama, J., Anné, J., Van Impe, J., Geeraerd, A.H, Bernaerts, K., 2013. Optimal experimental design for ^{13}C-based

metabolic flux analysis: a multi-objective approach ICSB-2013 - The 14th international conference on Systems Biology, Copenhagen, Denmark, August 30 - September 3.